IChF
Institute of Physical Chemistry PAS

PhD Dissertation

Novel photoluminescence-based physicochemical methods for latent fingermarks development

Izabela Olszowska-Łoś

IChF
Institute of Physical Chemistry PAS

PhD Thesis

Novel photoluminescence-based physicochemical methods for latent fingermarks development

Izabela Olszowska-Łoś

Supervisor:
Prof. dr hab. inż. Joanna Niedziółka-Jönsson
Auxiliary supervisor:
Dr Adam Leśniewski

The dissertation was prepared within
the International Doctoral Studies at the
Institute of Physical Chemistry of the Polish Academy of Sciences
Kasprzaka 44/52, 01-224 Warsaw

Warsaw, May 2021

Acknowledgements

First and foremost, I would like to thank my supervisors:

Prof. dr hab. inż. **Joanna Niedziółka-Jönsson** for her excellent supervision, precious advice, encouragement, and kind support with various aspects of my study

Dr **Adam Leśniewski** for his excellent guidance, invaluable help, patient assistance during the whole project, and all good ideas for the experiments he has shared with me

I am profoundly grateful to my co-workers, who have been involved in the work on the luminescent material for forensic application. Especially I thank Dr Fehmida Kanodarwala and Dr Sebastien Moret from the University of Technology Sydney for our successful cooperation in the synthesis and application of upconverting particles to fingermark development and imaging. I am also grateful to Antoni Siejca from Lasar – Elektronika for technical support in using the time-gated imaging setup for fingermark visualisation, Dr inż. Izabela Stefanowicz-Pięta for her assistance with the IR spectra of all synthesised materials, Anna Kelm for cooperation in the characterisation of luminescent properties of zinc oxide quantum dots embedded in silica matrix, Dr Tomasz Ratajczyk for NMR measurements and his support in spectra interpretation of europium complexes, and Dr inż. Maciej Zieliński for providing the XRD spectra of upconverting particles.

I would like to specially acknowledge Dr Kevin Farrugia for giving me the opportunity to participate in his project at Abertay University and for sharing with me his extensive knowledge in the field of fingermark visualisation.

I want to take this opportunity to thank the members of the Surface Nanoengineering Group and other IPC PAS scientists for any support and scientific ideas sharing with me. A particular thanks go to my roommates for their physical support when the experiments failed and for celebrating together when the experiments were successful.

Finally, I want to thank my Husband for his love, tremendous faith in me, understanding, and infinite source of support.

This research was financially supported by the
National Science Centre
within the SONATA 9 Grant 2015/17/D/ST5/01320

Abstract

Fingermarks, as important evidence confirming the presence of a given person at the crime scene, are often invisible to the naked eye. Hence their visualisation requires particular development methods depending on the surface type on which the fingermark is deposited. A broad range of optical methods for latent fingermark visualisation has been developed over the years. These methods are based on the photoluminescence phenomenon, where the luminescent developing agent selectively interacts with fingermark residue and emits visible light upon the irradiation. However, these methods sometimes fail when latent fingermarks are deposited on porous, glossy, reflective, colourful, patterned or immensely luminescent surfaces. The goal of this thesis was to develop an effective optical method of detection fingermarks deposited on porous and non-porous, patterned, coloured surfaces or those exhibiting its own luminescence with the use of composite materials which have particular optical properties such as long-lived luminescence or upconversion, and which selectively interact with fingermark residue.

The first part of my thesis involves the study of the potential application of silica particles as a host for luminophores applied for fingermark visualisation. Silica particles have been surface-modified with a variety of organic moieties to enhance the affinity to the fingermark secretion. Several possible interactions between the fingermark components and surface-modified silica particles have been investigated, including thiol-gold interactions between gold nanoparticles deposited on the fingermark within the Single Metal Deposition technique (SMD) and thiol-modified silica particles, lipophilic interactions between sebaceous components of the fingermark (free fatty acids, triglycerides, waxes, squalenes etc.) and silica particles modified with lipophilic moieties like phenyl groups or long hydrocarbon chains, and amide bond formation between the amine groups present in the fingermark secretions and carboxyl-modified silica nanoparticles. Since silica particles modified with lipophilic groups have shown the highest potential for fingermark development, these moieties were chosen for further research on the luminescent fingermark developer.

In the next part of the thesis, a detailed study of the properties and potential forensic applications of surface-modified silica particles with encapsulated

luminophore is described. Two various luminescent developing materials, such as zinc oxide quantum dots encapsulated in a silica matrix and silica-coated upconverting crystals based on sodium yttrium fluoride doped with ytterbium and erbium ions, have been synthesised. Both these materials were surface-modified with lipophilic moieties to provide desirable selectivity to fingermark ridges. Due to the relatively long luminescence lifetime equal to 0.5 ms, zinc oxide quantum dots in the silica matrix have been investigated as a latent fingermark enhancement agent on reflective, colourful, adhesive or luminescent surfaces such as aluminium foil, magazine paper, sticky side of the tape, beverage cans, or copy paper. Utilising a time-gated imaging method for fingermark visualisation, it was possible to separate the fingermark luminescence from the background interference for most investigated substrates.

Silica-coated upconverting particles have been studied in terms of fingermark visualisation on reflective, patterned, or colourful surfaces. Due to the large anti-Stokes shift, the upconverting particles emit strong luminescence when irradiated with infrared light. Since in most natural surfaces or consumer products the upconversion is rare, the upconverting particles can be advantageous in fingermark detection on multicoloured surfaces, leading to background interference or autofluorescence elimination. The upconverting crystals were synthesised either in the hydrothermal synthesis or solid-liquid-thermal-decomposition process and further coated with a silica layer and surface-modified with lipophilic moieties. Upconverting crystals were involved in the systematic evaluation of fingermarks deposited on several surfaces such as aluminium foil, glass, polymer foils. Fingermarks developed by modified upconverting particles have been compared to fingermarks enhanced by cyanoacrylate fuming followed by Rhodamine 6G staining to examine their potential to suppress background interference. Although the benchmark method of cyanoacrylate fuming with rhodamine staining performed better on most of the investigated fingermarks and surfaces, the upconverting particles may be a promising candidate for fingermark visualisation on highly luminescent or multicoloured surfaces like beverage cans where the conventional method is less efficient due to the background interference.

The last thesis part describes the study of the interactions between the europium complex and oleic acid, L-serine and squalene as the representative fingermark components. Fingermarks in this study were deposited on highly luminescent surfaces like copy or notebook paper. The complex of europium and thenoyltrifluoroacetone ($[Eu(TTA)_3(H_2O)_2]$) exhibits *in situ* changes in the luminescence properties when interacts with fingermark residue. Europium

complex, distributed over the entire sample, reacts only with fingermark components generating locally new compounds with a longer luminescence lifetime than the initial complex. Thus, this phenomenon facilitates the fingermark enhancement by time-gated visualisation with no need for selective deposition of the developing agent on fingermarks and regardless of the background interferences because the difference in the luminescence decay times of the complex on the fingermark and beyond is large enough. Commonly used amino acid reagents such as ninhydrin and 1,2-indanedione were applied for fingermark enhancement on paper substrates as the benchmark methods. It was found that the europium complex developed fingermarks with significantly better quality and higher contrast than ninhydrin and comparable quality and contrast than 1,2-indanedione. However, in samples exposed to water, only the europium complex enhanced the fingermark due to interactions with fingermark components that are hardly soluble or insoluble in water, unlike ninhydrin or 1,2-indanedione.

The results of the research and general conclusions were finally summarised. Furthermore, the possible future directions for optical imaging methods using luminescent sensitisers were also presented.

Streszczenie

Ślady daktyloskopijne, będące ważnym materiałem dowodowym mogącym potwierdzić obecność danej osoby w miejscu przestępstwa, są często niewidzialne gołym okiem. Zatem by móc je zidentyfikować należy zastosować konkretną metodę ujawniania, zależną od podłoża, na którym się znajdują. Na przestrzeni lat opracowano wiele optycznych metod ujawniania śladów opartych o zjawisko fotoluminescencji. W procesie ujawniania luminescencyjny preparat wizualizacyjny selektywnie oddziałuje ze śladem i wzbudzony emituje światło widzialne. Niestety zastosowanie tych metod czasami zawodzi, gdy ślady pozostawione są na podłożach chłonnych, powierzchniach błyszczących, odbijających, kolorowych, wzorzystych lub fluorescencyjnych. Celem niniejszej rozprawy było opracowanie efektywnej optycznej metody ujawniania śladów linii papilarnych na podłożach chłonnych i niechłonnych, wzorzystych, kolorowych i wykazujących własną luminescencję, z wykorzystaniem materiałów kompozytowych, które posiadają właściwości optyczne takie jak długożyciowa luminescencja lub up-konwersja, a także, które selektywnie oddziałują tylko z substancją potowo-tłuszczową śladu.

Pierwsza część rozprawy poświęcona została badaniu potencjalnego zastosowania cząstek polikrzemianowych jako nośnika dla luminoforów do obrazowania śladu linii papilarnych. Powierzchnia cząstek polikrzemianowych została zmodyfikowana różnymi, organicznymi grupami funkcyjnymi w celu zwiększenia ich oddziaływania ze śladem. Dokonano analizy kilku możliwych oddziaływań pomiędzy składnikami substancji potowo-tłuszczowej śladu a powierzchniowo-zmodyfikowanymi cząstkami polikrzemianowymi. Do badanych oddziaływań należą oddziaływania tiol-złoto pomiędzy złotem osadzonym na śladzie techniką osadzania pojedynczego metalu (Single Metal Deposition, SMD) a grupami tiolowymi powierzchniowo-zmodyfikowanych polikrzemianów, oddziaływania lipofilowe pomiędzy składnikami tłuszczowymi śladu (wolne kwasy tłuszczowe, triglicerydy, wosk, skawalen itp.) a grupami fenylowymi lub długimi łańcuchami węglowodorowymi obecnymi na powierzchni cząstek polikrzemianowych oraz oddziaływania związane z tworzeniem wiązań amidowych pomiędzy grupami aminowymi występującymi w substancji potowo-tłuszczowej śladu a grupami karboksylowymi zmodyfikowanych cząstek polikrzemianowych. W związku z tym, że największy potencjał w ujawnianiu śladów linii papilarnych wykazały cząstki polikrzemianowe modyfikowane powierzchniowo grupami lipofilowymi, ten rodzaj

grup funkcyjnych został wybrany do dalszych badań nad luminescencyjnym preparatem wizualizacyjnym.

W dalszej części rozprawy opisano szczegółową analizę właściwości powierzchniowo-modyfikowanych cząstek polikrzemianowych z unieruchomionym luminoforem i ich potencjalnego zastosowania w kryminalistyce. Dokonano syntezy dwóch różnych luminescencyjnych materiałów wizualizacyjnych mianowicie: kropek kwantowych tlenku cynku unieruchomionych w strukturze polikrzemianu oraz kryształów up-konwertujących składających się z fluorku sodu itru domieszkowanego jonami iterbu i erbu, modyfikowanych powierzchniowo polikrzemianem. Powierzchnia obu tych materiałów została w następnej kolejności zmodyfikowana grupami lipofilowymi by zapewnić selektywne oddziaływanie ze śladem. Ze względu na stosunkowo długi czas życia luminescencji kropek kwantowych tlenku cynku unieruchomionych w strukturze polikrzemianu, wynoszący 0.5 ms, materiał ten został poddany analizie zastosowania jako preparat wizualizacyjny śladów na odbijających, kolorowych, lepkich oraz luminescencyjnych powierzchniach takich jak folia aluminiowa, papier używany do druku czasopism, lepka część taśmy klejącej, puszki po napojach lub papier do kopiowania. Wykorzystanie metody obrazowania czasowo-rozdzielczego do ujawniania śladów umożliwiło oddzielenie luminescencji śladów linii papilarnych od interferencji tła dla większości badanych podłoży. Cząstki up-konwertujące pokryte polikrzemianem były badane pod kątem zastosowania do ujawniania śladów daktyloskopijnych na powierzchniach odblaskowych, wzorzystych lub kolorowych. Cząstki te, dzięki emisji antystokesowskiej (up-konwersji), wykazują intensywną luminescencję po wzbudzeniu promieniowaniem w zakresie podczerwonym. Ze względu na to, że zjawisko up-konwersji występuje bardzo rzadko w przypadku większości naturalnych powierzchni i produktów codziennego użytku, badane cząstki mogą być praktyczne w ujawnianiu śladów na kolorowych powierzchniach pozwalając wyeliminować zakłócenia lub fluorescencję tła. Do produkcji kryształów up-konwertujących wykorzystano proces syntezy hydrotermalnej oraz proces termicznego rozkładu w układzie ciało stałe-ciecz. Kryształy te następnie pokryto polikrzemianem, zmodyfikowano ich powierzchnię grupami lipofilowymi i wykorzystano do systematycznej oceny ujawniania śladów linii papilarnych na powierzchniach takich jak folia aluminiowa, szkło czy folie polimerowe. Dokonano również porównania ujawnionych śladów stosując metodę cyjanoakrylową połączoną z barwieniem rodaminą 6G w kontekście zbadania możliwości wyeliminowania zakłóceń tła. Mimo, że ta wzorcowa metoda zadziałała lepiej na większości badanych śladów i podłoży, to cząstki up-konwertujące mogą być obiecującym kandydatem na materiał wizualizacyjny do ujawniania śladów na silnie luminescencyjnych i kolorowych

powierzchniach takich jak np. puszki po napojach, w przypadku których zastosowanie metody konwencjonalnej daje gorszy efekt ujawniania ze względu na zakłócenia tła.

W ostatniej części rozprawy opisano badanie oddziaływań pomiędzy kompleksem europu a reprezentatywnymi składnikami substancji potowo-tłuszczowej śladu tj. kwasem oleinowym, L-seryną oraz skwalenem. W tym badaniu ślady pozostawione były na silnie luminescencyjnych podłożach takich jak papier kserograficzny lub zeszytowy. Kompleks europu i tenoilotrifluoroacetonu ($[Eu(TTA)_3(H_2O)_2]$) reagując ze składnikami substancji potowo-tłuszczowej wykazuje zmianę *in situ* właściwości luminescencyjnych. Rozprowadzony równomiernie na całej próbce, reaguje tylko ze śladem tworząc lokalnie nowe związki o znacznie dłuższym czasie życia luminescencji niż czas życia luminescencji czystego kompleksu. Zjawisko to umożliwia zatem ujawnianie śladów z wykorzystaniem czasowo-rozdzielczego obrazowania bez konieczności selektywnego osadzania preparatu ujawniającego na śladzie i bez względu na zakłócenia tła, gdyż różnica czasów zaniku luminescencji kompleksu na śladzie i poza nim jest wystarczająco duża. Jako metodę porównawczą ujawniania śladów na papierze wybrano ujawnianie ninhydryną i 1,2-indandionem, które są powszechnie stosowanymi odczynnikami reagującymi z aminokwasami. Stwierdzono, że kompleks europu pozwala ujawnić ślady lepszej jakości i uzyskać większy kontrast obrazu niż ślady ujawnione ninhydryną oraz podobnej jakości i z porównywalnym kontrastem do śladów ujawnionych 1,2-indandionem. Natomiast gdy próbki śladu na papierze zostały wystawione na oddziaływanie wody, tylko kompleks europu pozwolił na ujawnienie śladów ze względu na to, że reaguje on z trudno rozpuszczalnymi lub nierozpuszczalnymi w wodzie składnikami śladu, które nie są narażone na wypłukanie, w przeciwieństwie do odczynników reagujących z aminokwasami.

W ostatniej części podsumowano wyniki prowadzonych eksperymentów, przedstawiono ogólne wnioski wynikające z badań i możliwe kierunki rozwoju optycznych technik obrazowania z wykorzystaniem materiałów luminescencyjnych.

List of abbreviations

Abbreviation	Definition
AEAPTMS	N-[3-(Trimethoxysilyl)propyl] ethylenediamine
APTES	(3-Aminopropyl)triethoxysilane
Arg	Arginine
ATR	Attenuated total reflectance
AY7	Acid Yellow 7
BCP	Block Copolymer
BSA	Bovine serum albumin
BV3	Basic Violet 3
CA-R6G	Cyanoacrylate fuming followed by Rhodamine 6G staining
CAST	Centre For Applied Science And Technology
CBA	Cocaine-binding aptamer
CCD	Charge-coupled device
C-dots@SiO₂	Carbon dots dispersed in a silica matrix
CDs	Carbon dots
CDs/SiO₂	Carbon dot silica microspheres
CES	Carboxyethylsilanetriol sodium salt
CET	Cooperative energy transfer
C-SiO₂	Carbogenically coated silica nanoparticles
CTAB	Cetyltrimethylammonium bromide
CVD	Chemical vapour deposition
C_W	Weber contrast
DART-MS	Direct analysis in real-time mass spectrometry
DCCA	Drying control chemical additives
DFO	1,8-Diazafluoren-9-one
DMAB	p-Dimethylaminobenzaldehyde
DMF	N,N-dimethylformamide
DNA	Deoxyribonucleic acid
DOSS	Dioctyl sulfosuccinate
DRIFT	Diffuse Reflectance Infrared Fourier Transform Spectroscopy
EDC	(N-ethyl-N'-(3-dimethylaminopropyl) carbodiimide hydro-chloride
EDTA	Ethylenediaminetetraacetic acid
EDX	Energy-dispersive X-ray Spectroscopy
EGF	Epidermal Growth Factor
EMU	Energy migration-mediated upconversion

ESA	Excited-state absorption
ET	Energy transfer
ETU	Energy transfer upconversion
F-SiNPs	Fluorescein isothiocyanate-encapsulated silica nanoparticles
FTIR	Fourier-transform infrared spectroscopy
GWP	Global warming potential
HDPE	High-density polyethylene
HFE7100	1-Methoxynonafluorobutan
HFE71DE	50% 1-Methoxynonafluorobutane, 50% trans-1,2 Dichloro-ethylene
HLB	Hydrophilic-lipophilic balance
IR	Infrared
IRF	Instrument response function
ITO	Indium tin oxide
LBA	Lysozyme-binding aptamer
LCMDs	Light conversion molecular devices
LDPE	Low-density polyethylene
LED	Light-emitting diode
LFM	Latent fingermark
L-Glu	L-Glutathione
MB	Methylene blue
MBE	Molecular beam epitaxy
MCM-41	Mobil Crystalline Materials
MMD	Multi-Metal Deposition
MMT	Montmorillonite
MPA	Mercaptopropionic acid
MPS	Thiol-functionalised silica gel
MPTMS	3-Mercaptopropyltrimethoxysilane
MSA	Mercaptosuccinic acid
MSNs	Mesoporous silica nanoparticles
MUA	11-Mercaproundecanoic acid
NHS	N-hydroxysuccinimide
NIR	Near-infrared
N-L-Cys	N-Acetylcysteine
NMR	Nuclear Magnetic Resonance
NPs	Nanoparticles
OA	Oleic acid
ODE	1-Octadecene
ODTMS	Octadecyltrimethoxysilane
OLED	Organic light-emitting diode

ORO	Oil Red O
OSiNPs	Organosilicon oxide nanoparticles
p(DMA)	Polydimethylacrylamide
p(DMA-co-MMA)	Poly(dimethylacrylamide-co-methyl methacrylate)
p(DMA-co-Sty)	Poly(dimethylacrylamide-co-styrene)
PA	Photon avalanche
PAA	Polyallylamine
PAMAM	Polyamidoamine
PD	Physical Developer
PE	Polyethylene
PEI	Polyethyleneimine
PET	Polyethylene terephthalate
Phen	1,10-phenanthroline
PP	Polypropylene
PPH	Phosphate heterostructures
PR254	Pigment Red 254
PS	Polystyrene
PSMA-b-PS	Poly-(styrene-alt-maleic anhydride)-b-polystyrene
PTEOS	Triethoxyphenylsilane
PVC	Polyvinyl chloride
PVD	Physical vapour deposition
PVP	Polyvinylpyrrolidone
QDs	Quantum dots
R6G	Rhodamine 6G
RE	Rare earth
RGB	red, green, blue colour
RH	Relative humidity
RO/DI	Reverse osmosis deionisation
rpm	Revolutions per minute
RuBpy	Tris(2,20- bipyridyl)dichlororuthenium (II) hexahydrate
SALDI-MS	Surface-assisted laser desorption/ionisation mass spectroscopy
SALDI-TOF-MS	Surface-assisted laser desorption/ionisation time-of-flight mass spectrometry
SBA-15	Santa Barbara Amorphous
SDS	Sodium dodecyl sulfonate
SEM	Scanning electron microscopy
SERS	Surface-enhanced Raman spectroscopy
SiCNHs	Carbon and silica nanohybrids
SLR	Single-lens reflex
SLTD	Solid-liquid-thermal-decomposition

SMD	Single-Metal Deposition
SND	Single-Metal Nanoparticle Deposition
SPR	Small Particle Reagent
TEOS	Tetraethoxysilane
TES PSA	3-(Triethoxysilyl)propylsuccinic anhydride
TGA	Thioglycolic acid
TMOS	Tetramethoxysilane
TNT	Trinitrotoluene
TTA	2-Thenoyltrifluoroacetone
UC	Upconversion
UCNPs	Upconverting nanoparticles
UCNRs	Upconverting nanorods
UCPs	Upconverting particles
UV	Ultraviolet
VIS	Visible
VMD	Vacuum Metal Deposition
W/O	Water-in-oil
XRD	X-Ray Diffraction

Table of contents

Chapter 1 Introduction

1.1 Fingermarks

Using fingermarks for identification purposes has become the highly important physical evidence and valuable tool in forensic investigations, access control or medical diagnostics [1]. The fingermark is defined as the impressions of friction ridge skin such as a fingertip or palm of uncontrolled quality, left incidentally by the contact with a surface. On the contrary, the fingerprint is a characteristic print created by the friction ridge skin in contact with the plastic surface [2] or the controlled impression of the imprint of the skin ridge made on purpose, i.e. to enter the database [3], [4]. The nature of the fingermark pattern is unique and immutable for each individual throughout their life unless the deep extreme injuries permanently destroy it. The pattern is developed in the embryo between the 9th and 24th week. The diversity of the final ridge skin pattern is due to the fact that each embryo is subjected to different pressure within the womb and different growth rate [5]. The friction ridge skin pattern is a three-dimensional structure. It is formed by the lines of ridges, furrows, and the row of pores along the ridges, and serve three main functions: provide a gripping surface, facilitate an enhanced sense of touch and release perspiration [6]. Due to its unique ridge pattern, the fingermark began to be used to individualise a person in criminal investigations from the end of the 19th century [7]. The crime scenes are usually abundant in traces. According to the Locard's Exchange Principle: "Any action of an individual, and obviously, the violent actions of a crime, cannot occur without leaving a trace " [8].

Several categories of fingermark may be found in the crime scene: visible, latent and plastic fingermarks. The visible fingermarks are easily noticeable with the naked eye without any particular enhancement. These marks are formed when fingertips, palm, foot sole or toes, contaminated with some material such as blood, paint, grease, inks, soot etc., touch the surface, transferring these materials in a pattern corresponding to the friction ridge skin [2]. The vast majority of fingermarks found at a crime scene, and the most challenging ones are so-called latent fingermarks (LFM). These marks are invisible until they are developed and enhanced with an appropriate treatment to achieve a sufficient contrast between the fingermark ridges and the surface [6]. Another category of fingermarks includes plastic marks, which are not related to the deposition of any substance onto

a surface but are formed as a negative ridge pattern when pressed into the soft, plastic and malleable material, for example, paint, clay, wax, chocolate, soap etc. [2].

To enhance the fingermark and make it visible, the appropriate development technique or the sequence of techniques have to be chosen depending on several influencing factors such as the surface structure (porous, non-porous), contaminations (e.g. blood), environmental conditions (temperature, humidity, contact with water), or the fingermark age. There is no single effective technique that would develop each latent fingermark regardless of the factors above-mentioned. Processes of latent fingermark development dedicated to porous surfaces may not work properly on other surfaces [9]. Moreover, there is a variety of enhancement reagents and techniques based on the combination of optical, physical, chemical or physicochemical methods of visualisation, which may be applied under a variety of conditions and surfaces. However, even though a considerable number of development techniques already exist, there is still a strong demand for the development of the reagents and visualisation techniques that would increase the effectiveness of the fingermark development on various specific surfaces [10]. The reasons for searching for novel solutions are problems in enhancement processes, including insufficient sensitivity, problematic surfaces, speed, simplicity, environmental and safety considerations and cost [7], [11].

1.2 Fingermark features

Fingermarks can be used to individualise the unidentified individuals, as well as can be used as evidence of somebody's presence on a crime scene. Thus, it is crucial to know all the fingermark features in the analysis and identification process, especially when the new enhancement and visualisation methods are developed [12]. There are three features of ridge structure: the detail levels, the general pattern, and the minutiae [13].

Levels of ridge details

The friction ridge skin features are generally categorised in a hierarchical order at three levels of detail. Level 1 is relevant to macro details such as the general ridge flow and pattern configuration [13], [14]. This level can only be used for preliminary sorting of data, gathering the information about the delta and core orientation, or excluding the fingermark. Level 2 involves the ridge path, the minutiae points, and the spatial relationship between minutiae clusters, allowing

individualising the fingermark [15], [16]. And finally, Level 3 is related to the ridge contours and width, edge shapes, as well as the position and shape of the pores, breaks, creases, scars and other details [13], [15], [17].

Pattern types of fingermarks

The skin on the palm and sole has a characteristic topographical surface. The general flow of the narrow ridges forms the random patterns. There are four recognisable types of friction ridge patterns: arch, tent, loop, and whorl (Figure 1.1) [6]; however, in some classifications, the arch and tent fall into the one category of the arch as plain arch and tented arch [2], [15], [18]. Moreover, there are several variations of these pattern types.

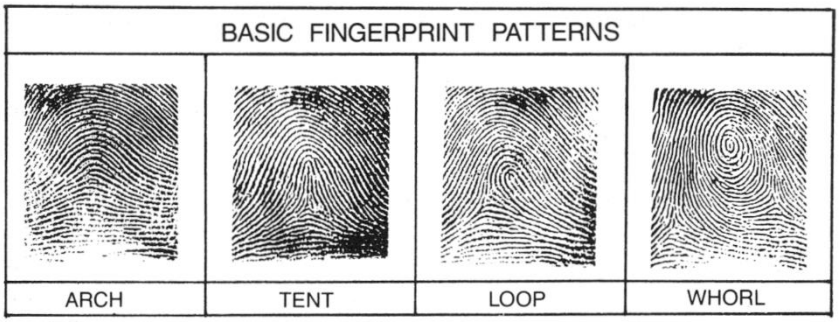

Figure 1.1 Basic friction ridge skin patterns [6]

The arch pattern constitutes only 5 % of all fingermark patterns [2]. In this pattern type, the ridges are continuously flowing from one side of the mark to the other, forming an arch in the centre [15]. However, this pattern does not form a delta, which is the area where three flows of ridges meet, composing a kind of triangular pattern [13]. The arch type can be sub-grouped into a plain arch and tented arch. A gentle and smooth curve in the centre of the mark, which is the pattern's centre characterises the plain arch, whereas, in the tented arch, the curve is steeper and rise sharply, forming some kind of tent [15].

The loop pattern accounts for about 60-65 % of all fingermark patterns [2], [15]. It is a type of pattern in which the ridge curve returns in the direction of the side from which it came from. A loop pattern should have characteristic minutiae such as a single delta, a core, a sufficient recurving ridge that flows between the delta and the core. At least one ridge must come across a looping ridge [2], [18]. Considering the ridge flow direction, two types of loop pattern can be distinguished: the radial loop and the ulnar loop. In the first one, the loop is opening in the direction

of the thumb finger, whereas, in the ulnar loop, the loop opens towards the little finger [2].

The last fingermark pattern is a whorl, which accounts for about 35 % of all fingermark patterns [2]. The ridges in this pattern flow from the side of the finger, forming a full circuit and creating two delta points. The circuit may be formed as a circle or ellipse [19]. In the centre of the circuit, a single ridgeline is located, which is surrounded by the concentric circuits [6]. There are four subcategories of whorl pattern: plain, central pocket loop, double loop and accidental. The plain whorl has two deltas and at least one ridge that encircles the core. The central pocket loop is a combination of whorl and loop patterns. It looks like a loop, but a tiny whorl is located inside the loop ridges [18]. Two loop combination forms a double loop pattern, and the accidental whorl pattern is the combination of more than one pattern types, except plain arch. It may also have more than two deltas [15].

The minutiae features

Galton, the author of the first book on fingermarks published in 1892, also first defined and named the local ridge characteristics, also known as Galton details [20]. Besides the general flow of the ridges in the fingermark, some alternations occur along the papillary ridges, like splitting into more ridges, ending, splitting and then reconnecting or connecting to the other ridges [21]. These recognisable characteristics are called minutiae. The minutiae are usually classified into two types: ridge ending and ridge bifurcation (Figure 1.2 a) [22]. A ridge ending is simply the point of abrupt termination of the ridge, whereas the ridge bifurcation is the point where ridges diverge into more branches [23]. All other ridge minutiae are directly the combination of the ridge ending and ridge bifurcation [13] (Figure 1.2 b). The bifurcation, together with the ending of the short ridge, is called a spur [15]. A ridge limited in length or a dot is seen as two ridge endings, while an enclosure is a structure of two bifurcations [19]. These local characteristics are randomly distributed, and in a good quality fingermark, approximately 40-100 minutiae can be found [23].

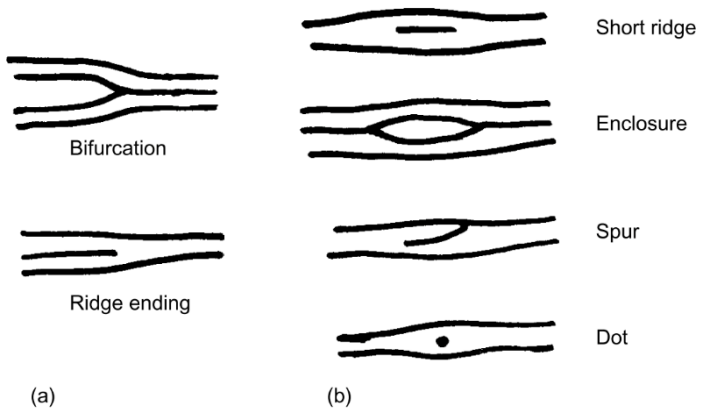

Figure 1.2 Fingermark characteristics called minutiae, employed in the identification process: (a) ridge ending and ridge bifurcation characteristics, (b) configurations of a ridge ending and bifurcation [19]

Composition of fingermark residuals

The fingermarks result from the contact between the finger and the surface. This is due to the transferring of the initial residue formed by the mixture of the natural secretions, the desquamation of the epidermis cells, and environmental contamination from the friction ridge skin to the surface [24].

The natural secretions are produced by the three types of glands: sudoriferous eccrine, apocrine glands, and sebaceous glands. These glands are distributed in the dermis (Figure 1.3), which is the middle layer of the skin, composed of fibro-elastic connective tissue [25]. Each type of gland produces a unique composition of compounds [4]. Between 2 to 4 million eccrine sweat glands are located over the entire body in the dermis [26]. However, in the highest concentration, they are found on the palm side of the hand and the soles of feet [25].

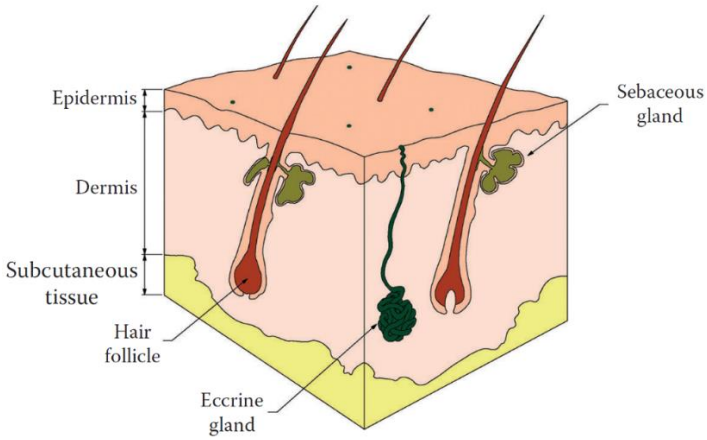

Figure 1.3 The cross-section of the skin illustrating the epidermis and dermis layer, and location of the sebaceous and eccrine glands [27]

The eccrine gland occurs in the form of a tubule with a helically coiled duct located deep in the dermis where reabsorbing sodium, chloride, bicarbonate, and glucose takes place due to minimise the loss of essential solutes from the evaporated water [6]. This gland is responsible for secreting water (approximately 98%) [28] and other waste products such as inorganic and organic components in low quantities [6]. The most abundant bunch of compounds present in the eccrine sweat are proteins and polypeptides [29]. Nonetheless, only a few of the proteins such as lysozyme [6], [30], several glycoproteins, transferrin, γ-globulins, α- and β-lipoproteins [6], keratins 1 and 10 [24], [31], cathepsin D [24], dermcidin, and albumin [31], [32] have been already identified in the fingermark secretion. Amino acids are the second plenteous group of compounds present in eccrine secretions, where serine, glycine, ornithine, alanine, aspartic acid, and histidine are the most frequent [28], [29]. Eccrine sweat is also rich in lactic acid, urea, uric acid, creatinine, B-complex vitamins [28], [29], phenol, choline [29], glucose, pyruvate, creatine, and glycogen [28]. Also, some inorganic compounds are perspired via the eccrine glands, such as chloride, sodium, potassium, calcium [28], [29], iron, bicarbonate, sulphate, phosphate, fluoride, bromide, iodide, and in trace amounts magnesium, zinc, copper [28].

The apocrine sweat glands are distributed in the groin, in the armpits, in the perianal area, on the vagina lips, in the glands of the penis, on the eyelid, and the mammary areolae [4], [33]. The role of these glands is unknown. Probably they act as the scent glands because they become active not until puberty [4]. The apocrine glands secrete substances present in eccrine glands, where water constitute more

than 98 % [3], [25], but they are additionally rich in proteins, carbohydrates, cholesterol [20], [34], lipids [35], and iron [20], [28]. Considering the distribution of apocrine glands, the apocrine sweat plays a minor role in the fingermark deposits, except the sexual assault [3], [34].

The sebaceous glands are located all over the body in the areas containing hair follicles and are not found on the palm and foot sole. They are placed in the epidermis; however, the secretory duct is placed in the dermis. The highest density of sebaceous glands is around the face, forehead and scalp [6]. Sebum is secreted from the sebaceous glands to lubricate the skin and hair, avoid skin desiccation, and prevent bacteria from invading the deeper skin regions [4], [25]. Although the sebaceous glands are not placed on the friction ridge skin area, the sebum-rich secretions are transferring to the fingertips by touching the face, forehead or other parts of the body containing sebaceous glands [27]. The sebum is composed of triglyceride fats, wax esters, fatty acids, squalene, cholesterol esters, cholesterol [28], [36], phospholipids [29], proteins, and salts [25], along with trace compounds such as ketones, aldehydes, amide, tertiary amines, heterocyclic compounds haloalkanes, and mercaptans [34]. In sebaceous secretion, lipids are primary compounds, among which the glycerides accounts for about 30 – 40 %, fatty acids for about 15 – 25 %, wax esters for about 20 – 25 % of all lipids, and squalene for about 10 – 12 % [20], [28]. The majority of free fatty acids present in fingermark residue are derived from the hydrolysis of triglycerides by bacteria [6]. The composition of sebum may be influenced by the age of the donor, gender, diet etc. [37].

Other endogenous components that are present in the fingermark secretion are desquamated cells of the epidermis. The epidermis is the outermost layer of the skin, build mainly from keratinocytes (Figure 1.3). It protects the underlying tissue from infections, dehydration, chemical and mechanical stress [25], [29], [38]. In the permanent process of skin regeneration, the keratinocyte cells are migrating towards the outermost layer, called the stratum corneum, where they are flattening and finally dying [33], [38].

Apart from the natural secretions influencing the fingermark composition, some exogenous substances are also present in the fingermark deposits. Fingermark residue may contain dust, remnant of food, cosmetics [4], explosives [39], drugs [40], [41], bacteria [29], body lotions, and perfumes [42].

Factors affecting fingermark

There are numerous factors that influence the variability of fingermark composition. The changes in the fingermark's initial chemical content can be affected by the donor profile in terms of gender, age, diet, ethnic origin, and medical treatment. Also, external contaminations such as cosmetics, food, drugs may play a role in fingermark composition, the same as environmental conditions such as temperature, humidity, pollution, exposure to dust or bacteria, and light exposure [4], [29]. Moreover, the highly important factors are the deposition conditions such as the nature of the substrate, including porosity [43], [44], adhesion, wetting [3], pH, electrostatic forces [4], and also the age of the fingermark [6], [19], [44].

Age of the fingermark

The initial composition of fingermark residue evolves over time. Some of the compounds may undergo the process of degradation, oxidation, or polymerisation; some may evaporate or migrate. Also, some new products may originate in the deposition material [29], [45]. The recognition of the chemical, physical or biological alterations of the fingermark components in time is important in terms of the fingermark development methods [29].

Considering the eccrine fraction of fingermark residue, the loss of water is the main effect of ageing. The fingermark contains only 20 % of water immediately after the deposition due to the evaporation process. A decrease of up to 98% of the fingermark's original mass may occur in 72 hours after the deposition [46]. Except for water, the eccrine fraction is mainly composed of amino acids, proteins, lactate. The studies showed that both amino acids and proteins are not fully stable in time. However, in the period of 100-200 days, their concentration in the residue deposits on paper is still sufficient to interact with ninhydrin, an amino acid-sensitive developing agent. This stability may be due to the high affinity of amino acids to the cellulose [29], [47].

In the case of the sebaceous fraction of fingermark residue, mainly the degradation of squalene, cholesterol and fatty acids was reported [42], [46], [48]–[51]. The fatty acids do not change significantly in time [42]. According to Archer et al. [49], the levels of fatty acids may vary over the period of ageing. After a rise over the initial quantity in the early stage of ageing (1 month), the fatty acid level may subsequently decrease in time to the initial value. It is worth noting that fatty acids are not secreted by the sebaceous glands, but the bacteria produce them in the process of glyceride degradation. This may be the result of the initial increase in fatty

acid level. The further decrease may be due to the degradation to a shorter chain of fatty acids, especially that their presence was often detected [42], [49]. Squalene, the unsaturated hydrocarbon, undergo degradation due to the microbial processes even in a few days, particularly in the presence of ultraviolet (UV) light. The derivatives of oxidised squalene, such as epoxides, hydroperoxides, ketones, aldehydes [21], and alcohols, are further reacted to fully oxidised forms such as hexanedioic and pentanedioic acids [29], [42], [49], [51]. Cholesterol degrades in time but not rapidly [42]. The possible products of degradation are cholestadienes and cholestenones; however, these compounds were not clearly identified in the deposits [51].

Type of the substrate surface

The substrate upon which the fingermark is deposited can influence the composition of the fingermark, depending on the porosity of the surface [52]. The capacity of the surface to retain the fingermark components highly depends on its texture and physicochemical structure as well as the temperature, electrostatic forces, and surface free energy [29]. The higher is the porosity of the surface, the higher are the adhesion forces, and more compounds migrate into the surface structure [28]. The depth of the penetration of fingermark deposits is proportional to the surface porosity. Three main categories of surfaces are distinguished: porous, non-porous and semi-porous [3], [4].

The porous surface, e.g. paper, untreated wood, cardboard [4], [20], tend to absorb eccrine components such as amino acids, urea, chlorides more rapidly than sebaceous compounds (Figure 1.4) [21], [29]. This resulted in long-lasting impressions, which consist of up to three times more amino acids than residues deposited on the non-porous surface [3]. When the fingermark is deposited on the paper's surface, the water starts to evaporate, and the water-soluble components begin to diffuse into the substrate matrix (Figure 1.4 b). This diffusion's depth depends strongly on the relative humidity (RH) and the degree of porosity. The adsorbed water-soluble components cannot be rubbed away; however, they can be readily washed away with water. After one week, under normal conditions, with the RH < 80 %, the amino acids are well preserved in the porous matrix, while the urea and sodium chloride continuously migrate. Thus, the older fingermarks may produce blurred images when developed with agents which target these compounds (Figure 1.4 c). On the other hand, the water-insoluble components like fatty acids and waxes remain on top of the surface significantly longer due to the inhibited mobility in the

ambient temperature. Moreover, the small amount of the sebaceous fraction remains on the surface, even for years [4].

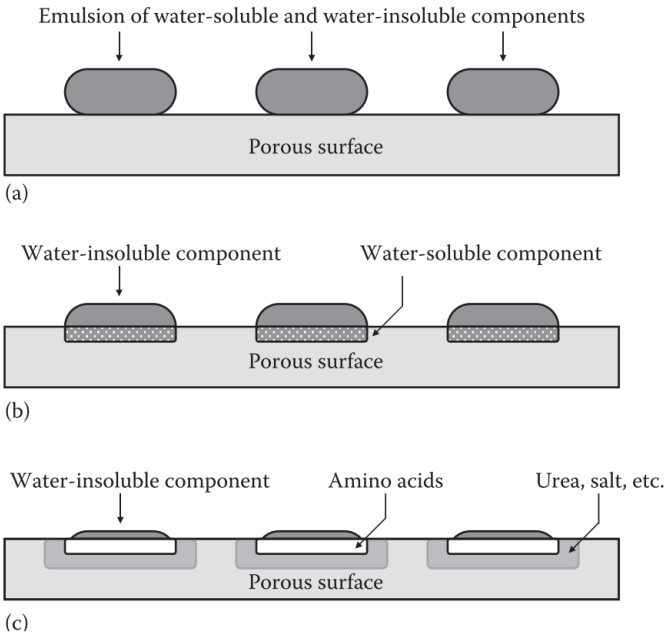

Figure 1.4 A schematic cross-sections of the fingermark deposit on the porous surface at different stages after deposition: (a) right after the deposition, (b) seconds or minutes after deposition, (c) days or weeks after deposition [4]

The surfaces like glass, polished metal surfaces, polyethylene plastic bags, glossy paints, glazed ceramics etc., are all classified as non-porous surfaces [4]. All these substrates do not absorb any compounds of fingermark residue; furthermore, due to the exposure to the environmental factors, the residue is susceptible to degrade or be removed (Figure 1.5 a) [4], [28], [43]. Water from the deposit will evaporate within the first few hours or days, depending on the temperature (Figure 1.5 b) [21]. Both the water-soluble and water-insoluble fingermark components remain on the surface for a very long time, if not damaged, washed with organic solvents or degraded by environmental factors [4].

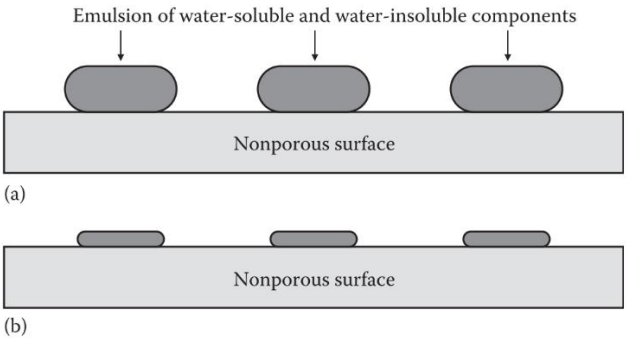

Figure 1.5 A schematic cross-sections of the fingermark deposit on the non-porous surface at different stages after deposition: (a) right after the deposition, (b) days or weeks after deposition [4]

The third category is the semi-porous surface, which may resist or absorb fingermark residue depending on the substrate's properties and the viscous properties of the fingermark residue [20]. This surface absorbs the eccrine and sebaceous components much slower than the porous surface [28]. The water-insoluble components remain on the top of the surface for a long time before some diffusion occurs [4]. The common items with a semi-porous surface are glossy paper, plastics, laminated wood [28], painted surface, polymer banknotes, waxed paper [4], glossy cardboard or magazine cover, or cellophane [20].

1.3 Fingermark detection techniques for porous surfaces

Fingermarks deposited on porous surfaces (e.g. paper or wood) are processed in a different way than on non-porous surfaces (e.g. glass). This is due to the absorption of fingermark residue components, which diffuse into the substrate matrix quickly and become inaccessible for physical interactions, e.g. adhesion of powder developer [4]. The techniques applied for developing latent fingermarks deposited on porous surfaces are mainly based on chemical processes. Friction ridge residue components are dissolved into the surface structure, and the chemicals are able to react with these secretions and not with the surface. [53]

Ninhydrin

Ninhydrin is one of the most advantageous and indispensable reagents applied for the chemical development of latent fingermarks deposited on paper and

other porous surfaces [6], [20]. Ninhydrin reacts with primary and secondary amino acids present in the fingermark residuals resulting in the formation of Ruhemann's purple, which is noticed as purple impressions [27], [47], [54]. The development may take days or even weeks; however, once the heat and steam are applied, the reaction accelerates [6], [27]. When the fingermark is deposited on the porous surface, the aqueous eccrine fraction of the residual starts to diffuse into the surface structure. This fraction contains about 250 ng of amino acids per fingermark [47], which is sufficient to be detected with ninhydrin.

Ninhydrin (2,2-dihydroxy-1,3-indandione) is a colourless to pale yellow crystalline solid soluble in water and other polar solvents, first synthesised in 1910 by Siegfried Ruhemann. [55]. The general mechanism of the reaction between ninhydrin and the amino acid was proposed by Friedman and Williams [56] and modified by Grigg et al. [57] (Figure 1.6). First, ninhydrin (2) tautomerises to 1,2,3-indanetrione (1), which is a dehydrated form of ninhydrin [6]. Both forms are in constant equilibrium. Then, Schiff's base formation takes place in the condensation process between the amine and the central carbonyl of the anhydrous form of ninhydrin [47]. This intermediate imine (5) undergoes then decarboxylation, yielding a resonance-stabilised 1,3-dipolar species (6) (7), confirmed by Grigg et al. [57]. In the process of proton transfer, an intermediate aldimine is forming (8), which then hydrolyses to the aldehyde and an intermediate amine (9). In the further step, the 2-amino intermediate interacts with another molecule of ninhydrin yielding in the deprotonated coloured product, which is Ruhemann's purple (10) [6], [47].

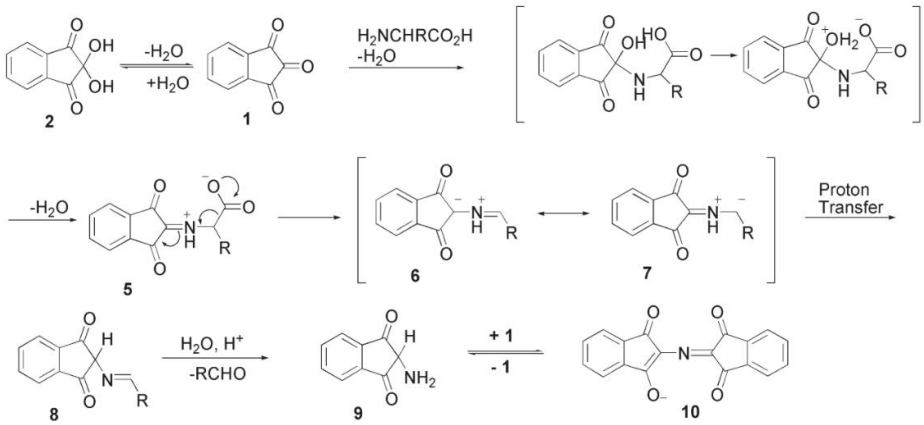

Figure 1.6 The commonly accepted mechanism of the formation of Ruhemann's purple proposed by Friedman and Williams and modified by Grigg et al. [47]

The formulation of ninhydrin developer and the enhancement process conditions such as concentration, temperature, carrier solvent, pH, heating time, and humidity have been changed over the years [58]. Oden's original formulation was based on 0.2 % of ether or acetone ninhydrin solution with the addition of 4 % of acetic acid to keep an acidic environment. The process of fingermark samples treatment was maintained at the temperature of 80-120 °C [59]. Currently, according to the UK Home Office Centre for Applied Science and Technology (CAST), the ninhydrin development procedure recommends a 0.5 $\%_{w/v}$ concentration of ninhydrin in the working solution, based on 1-methoxynonafluorobutan (HFE7100) as a carrier solvent together with the addition of acetic acid, ethanol, and ethyl acetate [60]. The addition of acetic acid provides hydrogen ions and water, which catalyse the reaction of ninhydrin and amines. The application of ninhydrin is performed by immersing the samples in the working solution and drying them in the air to evaporate the solvent before placing in the oven. Heat and high humidity must be maintained during fingermark treatment to increase the reaction rate. The samples should be exposed for 4 to 7 minutes to a temperature of 80 ± 2 °C and relative humidity of 62 ± 5 % to obtain effective enhancement results [54]. HFE7100 is the currently used carrier solvent, which has replaced the CFC-113 (1,1,2-Trichloro-1,2,2-trifluoroethane) several years ago due to its high global warming potential (GWP) value which was equal to 6000. A GWP is a measure of how much energy a unit of greenhouse gas will absorb in the atmosphere over a given time, relative to the energy absorbed by the same amount of carbon dioxide [61]. The research on a new carrier solvent for amino acid reagents, called Solstice PF with a GWP equal to 1, is underway to develop a more environmentally friendly system [62], [63].

Ninhydrin is one of the developing reagents whose effectiveness cannot be questioned. However, some limitations are noted. First of all, ninhydrin cannot be applied to water-soaked surfaces because water is eluting amino acids which are the target for ninhydrin [27], [60]. Also, weak fingermarks and fingermarks deposited on coloured or dark surfaces treated with ninhydrin may result in low contrast [20], [64]. However, this contrast may be enhanced by treating the ninhydrin fingermarks with metal salts like zinc, nickel, or cadmium. The fingermarks then changed the colour and became fluorescent when excited with a 488 nm argon laser [6], [65]. Ninhydrin may undergo uncontrolled reactions with some amine-rich fillers present in the substrate resulting in high background development. The acetic acid present in the working solution may also react with the substrate's thermal layer leading to darkening [54]. Moreover, ninhydrin working solution may cause the ink running or expand the paper fibres damaging the fingermark pattern [53]. Finally, the chemical process is slow, and fingermarks enhanced with ninhydrin are not permanent [6].

DFO and 1,2- Indanedione

Two analogues of ninhydrin, 1,8-diazafluorene-9-on (DFO) and 1,2-indanedione, started to be of broad interest due to their high sensitivity and luminescence intensity in reaction with amino acids in fingermark residue [65], [66].

DFO, proposed by Grigg et al. in 1990, consists of the five-membered ring with one carbonyl group in the centre and two dipoles adjusted on both sides [6] (Figure 1.7 1). DFO reacts with amino acids present in fingermark residue similarly to ninhydrin. However, the reaction yields in a highly luminescent red-coloured product of two DFO molecules linked by a nitrogen atom [67]. The structure of the reaction product is analogous to Ruhemann's purple (Figure 1.7 5) [68]. DFO is also more sensitive than ninhydrin, developing two-and-a-half to three times more latent fingermarks on paper [53]. Latent fingermarks enhanced with DFO provided a faint red fingermark impression, which illuminated with the green light with the excitation between 540 and 570 nm, emit bright luminescence in a broad spectrum of 560-620 nm [4].

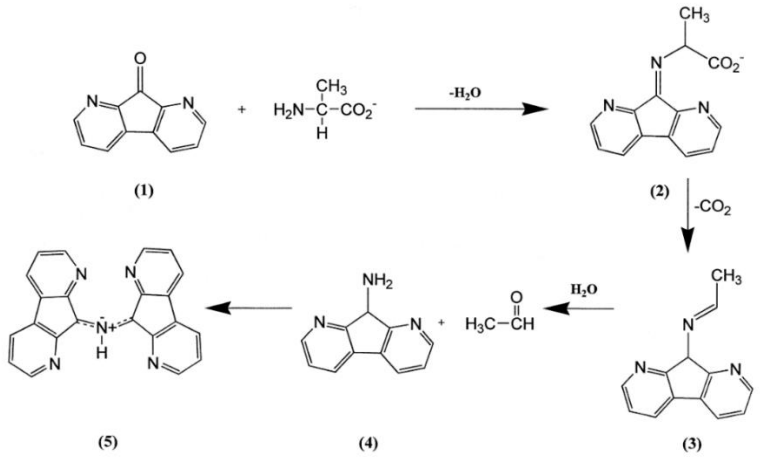

Figure 1.7 The mechanism of the reaction of DFO with an amino acid proposed by Grigg et al. [69]

The possible mechanism of the reaction between DFO and amino acid proposed by Grigg et al. is comparable to the reaction between ninhydrin and amino acids. In the first step, DFO (1) reacts with the solvent forming a hemiketal, a less stable structure and therefore more reactive. Hence, the presence of methanol in the working solution is crucial [20]. The hemiketal favour the attack of the nitrogen in the amino acid at the electron-deficient carbon in the polarised carbonyl group yielding in the loss of water. As a result, an aromatic imine is formed, which then

undergoes decarboxylation to form structure (3). Then acetaldehyde and an aromatic amine are produced (4) by hydrolysis at the nitrogen-carbon double bond (3). The aromatic amine (4) further reacts with a DFO molecule yielding in a red product (5) [69]. Unlike the ninhydrin treatment process, the DFO enhancement procedure must be maintained in a high temperature and a low-humidity environment [65]. The development procedure recommended by the CAST is based on the 0.02 $\%_{w/v}$ of DFO in the working solution. The working solution consists of acetic acid, methanol and the carrier solvent, which is the mixture of HFE71DE (50% 1-Methoxynonafluorobutane, 50% trans-1,2 Dichloroethylene) and HFE7100. DFO treatment is performed by immersing the fingermark samples in the working solution, then drying them in the air and placing the samples in the oven for at least 20 minutes at 100 °C [54]. It was observed that fingermarks developed with DFO followed by the ninhydrin post-treatment did not improve the fingermarks' visualisation; however, additionally developed fingermarks occurred due to the Ruhemann's purple production. Probably the DFO does not react with every amino acid present in the fingermark residue. Thus the combination of DFO and ninhydrin treatment is often applied for porous surface like paper [20], [69], [70].

Some disadvantages of the DFO treatment are related to the reagent formulation and substrate features. Similarly to ninhydrin, the acetic acid present in the working solution and the high temperature in the treatment process may cause the substrate's darkening, especially the thermal paper [54]. Moreover, some highly luminescent inks, paints, and dyes of the substrate may interfere with the fingermark's fluorescence, resulting in a decrease in the contrast between the ridge and the background. The DFO may also stain the substrate a yellow colour. Finally, the DFO process cannot be applied to the wetted surfaces due to the lack of amino acids [27].

1,2-indanedione, proposed and evaluated by Joullié and co-workers in 1997, is a fingermark detection agent which reacts with amino acids present in a fingermark residue, similarly to ninhydrin [71]. The reaction of 1,2-indanedione with amino acids results in a pale pink colour [65], stable and fluorescent product with high quantum yield, and a sufficient Stokes shift to eliminate the background luminescence of most paper surfaces [72]. Latent fingermarks enhanced with 1,2-indanedione excited with the broad spectrum of 490 to 560 nm emit bright luminescence in a broad spectrum covering a region from 550 to 620 nm with a maximum emission peak at 560 nm and 590-600 nm [4].

The reaction mechanism between 1,2-indanedione and amino acid involves the formation of the imine (I), which then undergo decarboxylation to form 1,3-dipolar species existing in equilibrium. The 1,3-dipolar species may then undergo the

Strecker degradation yielding in the formation of 2-amino-1-indanon (II), which in reaction with an excess of 1,2-indanedione produce a coloured and luminescent product – a "Ruhemann's purple"-like dipole [65], [72].

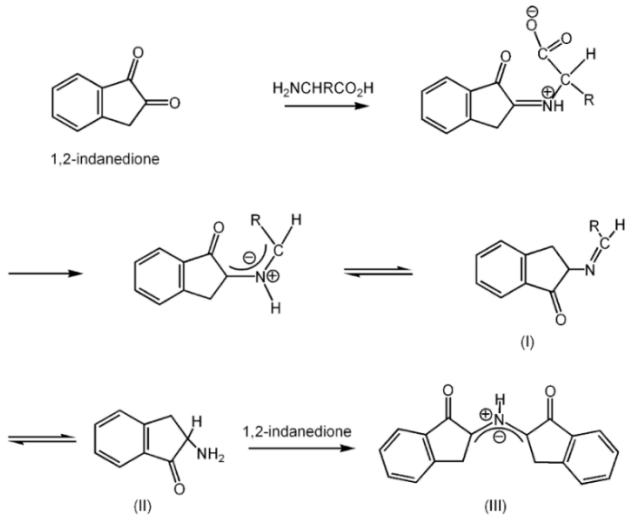

Figure 1.8 The mechanism of the reaction of 1,2-indanedione with an amino acid proposed by Petrovskaia et al. [72]

Various formulations of 1,2-indanedione working solution have been recommended so far. However, most of them consist of 0.02-0.2 $\%_{w/v}$ of 1,2-indanedione, ethyl acetate, acetic acid and HFE7100 as a carrier solvent [73], [74]. The 1,2-indanedione treatment process, unlike the DFO process, does not require a heated environment; however, increased temperature accelerate the reaction process significantly. Similarly to ninhydrin and DFO, the development protocol involves immersing the exhibits in the working solution, drying them in the air and heating them in an oven at the temperature of 100 °C for at least 10 minutes [54]. The application of 1,2-indanedione has been studied in numerous research groups all over the world. There is a wide variety in the results obtained due to the various conditions, environmental factors, substrates and performance of the reagent formulations [65]. Some of the researchers reported the superior results of fingermark detection with 1,2-indanedione comparing to DFO [70], [73], [75]–[77], whereas some groups suggested that 1,2-inanedione was less sensitive to DFO [74], [78]. The research conducted in Australia has shown that the efficiency of the reaction between amino acids and 1,2-indanedione is highly dependent on the relative humidity. For the RH higher than 70 %, the reaction appears to be relatively good, but if the RH was lower than 50 %, the reaction was poor [73], [76]. Due to the regional variations in the above-mentioned environmental factors, humidity, and the

paper's acidity, this formulation is not recommended as the first-choice method in some countries, e.g. the UK [54], [73]. However, the introduction of a catalytic amount of zinc (II) chloride to the working solution before treating the specimen markedly increases the fluorescence of the fingermark and makes the system more resilient to fluctuations of humidity. The zinc (II) ions in the 1,2-indanedione formulation act as a Lewis acid catalyst and stabilise the intermediate product [79]–[81].

Lipid dyes

Lysochrome molecules, widely used in biology, have also found application in fingermark enhancement due to selective staining of the fingermarks residue lipid fraction [82]. Proposed methods such as Oil Red O or Nile Red staining are relatively fast, cost-effective and efficient [3].

Oil Red O

For the first time, Oil Red O (ORO) was introduced for fingermark development on dry or wetted porous surfaces in 2004 by Beaudoin [83]. ORO is a highly lipophilic fat-soluble diazo dye and a lysochrome applied in biology to stain triglycerides and lipoproteins [82], [84]. Its structure is based on two azo groups attached to three aromatic rings (Figure 1.9).

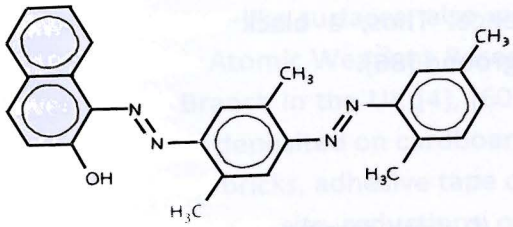

Figure 1.9 Chemical structure of Oil Red O stain [4]

This dye is difficult to ionise what makes ORO highly soluble in lipids [84]. Most of the lysochromes are insoluble in polar solvents such as water or ethanol. In contrast, they are soluble in non-polar solvents, triglycerides and lipids, staining them to a red colour [60]. Latent fingermarks deposited on porous surfaces immersed in the ORO solution undergo visible red impressions due to the dye molecules' accumulation in the lipid fraction of fingermark residue [82]. The background may also be slightly stained in red; however, the contrast between

the fingermark ridges and the substrate remains sufficient for visualisation [85]. ORO interacts with a labile fraction of fingermark, which is the water-insoluble part of the residue rich in components such as saturated and unsaturated fatty acids and triglycerides. These compounds change their structure in the short term due to oxidation when exposed to air, in contrast to the robust fraction, which is composed of proteins and lipoproteins, strongly bound to the cellulose in a paper for a long period of time. Therefore this dye is recommended for fresh fingermarks not older than 28 days [85].

The process of fingermark treatment is completed in three stages. First, the exhibits are immersed for 90 minutes in an Oil Red O staining bath, consists of ORO, methanol, sodium hydroxide and water. The fingermarks are then dipped in a buffer solution of sodium carboxide, nitric acid, and water to neutralise the base side of the staining solution and stabilise the fingermarks. Finally, the fingermark items are rinsed in distilled water [60], [85]. As the effective visualisation of fingermarks developed with ORO is based on the contrast difference between the fingermark ridge and the substrate, this technique may be problematic on dark surfaces. However, the application of rhodamine 6G (R6G) as a luminescent staining post-treatment can induce luminescence in the background. The ORO has a maximum absorption at approximately 518 nm wavelength and produces no emissions. In contrast, Rhodamine 6G has its maximum absorption wavelength of 530 nm and emits high-intensity fluorescence with an emission peak at approximately 553 nm. Illuminating the surface with the light of a 530 nm wavelength will lead the ORO content in the fingermark to absorb the light and Rhodamine 6G in the background to emit fluorescence. Thus, a black fingermark will be visualised against the luminescent background [86].

Nile Red

Nile Red (9-diethylamino-5H-benzo[α]phenoxazine-5-one) is a highly fluorescent, lysochrome dye used to stain lipids in histochemical detection. Nile red is an uncharged heterocyclic molecule (Figure 1.10) that readily dissolves in organic solvents and highly dissolves in lipids but is insoluble in water [84], [87], [88]. Also, Nile Red is solvatochromic, which means that the fluorescence maxima depend on the relative hydrophobicity of the environment [89]. If the dye is dissolved in neutral lipids like triacylglycerols or cholesteryl esters, the fluorescence emission occurs in the yellow region of the light spectrum. On the other side, Nile Red dissolved in more polar solvents like ethanol or phospholipids emits red fluorescence. Moreover, in aqueous media, the Nile Red fluorescence is quenched [87], [90].

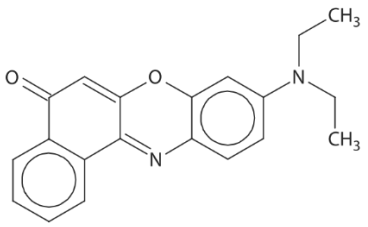

Figure 1.10 Chemical structure of Nile Red stain [4]

Nile Red was first used as a potential luminescent alternative to a physical developer by Saunders in 1993 [3]. The formulation of the staining solution is based on ethanol or methanol solvent with the addition of sodium hydroxide [91], [92]. Due to the photoluminescent properties depending on the solvent's hydrophobicity, Nile Red may provide good results on paper substrates, also wetted [91]–[93]. However, the staining solution requires organic solvents due to the poor solubility in water, affecting the exposed personnel and generating toxic waste. Moreover, the staining solution suffers from Nile Red precipitation when the methanol evaporates from the solution [94]. Nile Red may perform well when applied in the sequence with a physical developer, enhancing fingermarks that were partially developed or not developed in general [4].

Physical developer

Physical Developer (PD) is a chemical procedure of the enhancement of fingermarks deposited on porous, paper-like surfaces, also wetted or soaked in petrol [2], developed in the 1970s by the Atomic Weapons Research Establishment with the Police Scientific Development Branch in the UK [4], [60], [64]. It performs excellent for older marks and fingermarks deposited on cardboard [21], paper bags, currency, rubber or latex gloves, clay-fired bricks, adhesive tape or unfinished wood [53]. The physical developer is based on *in situ* reductions of silver (I) ions to elemental silver, which reacts with the robust fraction of sweat residue consisting of water-insoluble triglycerides, wax esters, hydrocarbon, proteins and lipoproteins [85], to produce visible, grey or black impression along the ridge [64]. The PD enhancement solution consists of silver ions, ferrous/ferric redox couple, a citric acid buffer, a cationic surfactant, and a nonionic surfactant [4], [95]. The silver metal, accumulated on the fingermark ridge, is formed by reducing the silver ions (Ag^+) by the ferrous ions (Fe^{2+}) according to the reaction: $Ag^+ + Fe^{2+} \leftrightarrow Ag^0 \downarrow + Fe^{3+}$. The citric acid buffer maintains the low pH of the process and complexes ferric ions (Fe^{3+}), whereas the surfactant trap the reduced silver particles into the micelles to

avoid premature deposition as well as to inhibit further silver formation. Once the micelles contact the fingermark ridge, they break, and silver is precipitated from the solution [60], [64]. Although the mechanism of the interaction between silver and fingermark components is unclear, one of the hypothesis claims that PD is sensitive not only to a sebaceous fraction of fingermark residue but also may interact with amino acids trapped in the lipid fraction. In the low pH, positively charged amine functional groups of the fingermark components may be electrostatically attracted with negatively charged silver particles, which adhere to the fingermark ridge and starts forming nucleating sites for further growth of silver particles [3], [82].

The PD enhancement procedure is based on the sequence of several treatments. First, the exhibits are immersed in a water bath to remove any dirt and soil. In maleic acid pretreatment, any paper-fillers like calcium carbonate are removed from the alkaline papers due to its neutralisation. The main treatment in silver physical developer lasts from 10 to 30 minutes to obtain a sufficient contrast. Next, the exhibits are rewashed with water to remove the excess of the developer and silver chloride, which may form. The fingermarks are subsequently immersed in the hypochlorite to lighten the background, darken the marks, and then finally be washed with water and air-dried [20]. The application of PD should be the final stage in the sequential processing on porous surfaces with amino acid reagents such as 1,2-indanedione, DFO or ninhydrin. The physical developer is complementary to amino acid-sensitive reagents and tends to target various components of fingermark deposit that DFO or ninhydrin remain undetected [27], [60], [77]. In the case of wetted items, the PD process may be recommended as the first choice due to the lack of amino acids, which were washed from the deposit [96].

The physical developer technique is very effective on porous surfaces [91], [97]–[99]; however, some inconveniences occur during the processing. The PD solution is unstable, can be stored for no longer than two weeks, and the silver ions are sensitive to contaminants that may cause premature silver precipitation [99]–[101]. The PD process is destructive, the developer may react with the paper, so any other enhancement after PD is ineffective [64]. This technique must also be handled carefully because the silver nitrate easily stains everything it contacts [100]. Considering the preparation of the PD and the fingermark treatment procedure consisting of several immersion baths, the PD enhancement is a relatively long process [3], [101]. Moreover, the number of immersion steps may cause the paper to become brittle and damage the marks [98]. Also, PD may be problematic when a fingermark is deposited on a dark surface due to weak contrast between developed ridges and the background.

1.4 Fingermark detection techniques for non-porous surfaces

The type of surface to be examined is one of the most significant factors while choosing the development technique. The non-porous surface is smooth and solid; thus, fingermark retains a sticky deposit on the top of it, which can be developed in the process of powder dusting or some more sensitive techniques like cyanoacrylate fuming or metal deposition [21].

Powders

Fingermark powdering is one of the first technique of fingermark detection used since the nineteenth century [20]. This traditional technique is a simple and widely used procedure for latent fingermark development of nontransportable objects with smooth, non-porous surfaces like glass, metal, glossy or painted material, tiles, mirrors [2], [64], [82]. However, powdering has also been reported as a potential developing method for a bird of prey feathers and eggs, deer antlers or elephant tusk [102]. Powder dusting is a physical method, where the fingermark development occurs by the preferential adhesion of particles to the moist, sticky, and oily fraction of fingermark residue [54], [82]. Powdered fingermarks can be easily lifted off the surface using an adhesive tape [64]. The fingermark powder is commonly applied with a brush made of synthetic material such as polyester or glass fibre, natural bristle (e.g. squirrel) or hairs (e.g. camel). Also, the magnetic brushes called wands, which utilise the ferromagnetic properties of iron powder mixed with a pigment, are widely used, minimising the contact between the fragile fingermark and the applicator [2], [20], [54], [64]. The typical powders consist of two main elements: a binder that provides preferential adhesion to the fingermark ridge and a pigment that provides sufficient contrast between the mark and the background [103]. However, some pigments indicate enough adhesion and can be used individually [20].

In general, there are four generic types of powders: metal flake, granular, magnetic flake and magnetic granular [54]. Metal flakes such as milled aluminium flakes called silver powder, brass flakes called gold powder or aluminium, and kaolin called grey powder have a flat structure [21], [104]. Stearic acid or similar fatty acids are added to this powder as a binder, which provides good sensitivity and makes this powder one of the most effective at developing on smooth and clean surfaces [21]. The black or white granular powders are routinely used as a contrasting agent for fingermark dusting. These powders are mostly suited for smooth, not coloured surfaces; however, they are less sensitive than other powders [54]. The black

powders, composed of graphite, charcoal or molybdenum powder, are applied for light coloured background, whereas white powders, including titanium dioxide, zinc oxide, zinc sulphide, are used on dark surfaces [82]. Also, the bichromatic powders, as a mixture of black and grey powder, can be used for fingermark development on both dark and light substrate [53]. A milled iron mixed with aluminium flakes is a kind of magnetic flake powder, useful for unplasticised polyvinyl chloride window frames [21], [64]. The magnetic powders are the least destructive [9] and suitable for fingermark enhancement on shiny magazine covers, coated surfaces, and plastics such as food storage containers [15]. For multicoloured and reflective substrates, the luminescent granular powders like acridine orange, rhodamine 6G, crystal violet [104], acridine yellow, coumarin 6, or luminescent, magnetic powders with a wide range of colours may be applied depending on the shade of the background [82]. However, some fluorescent powders may indicate less sensitivity than non-fluorescent ones, which may be relevant to their shape and size [21]. Also, magnetic powders are not recommended for ferromagnetic items such as steel or nickel [20]. The visualisation of fingermarks developed with luminescent powders involves particular equipment such as lasers or UV light sources [2].

There is no doubt that powder dusting is a fast, cost-effective and efficient method; however, some drawback must be noted. Firstly, it is not highly sensitive, especially for older fingermarks, which dries and lose stickiness over time. Thou mainly fresh and good quality marks may be fully visualised by powdering [64]. Also, powdering can be applied only on smooth, clean, dry and non-porous surfaces to avoid background interference [54]. Moreover, fingermark ridges may be damaged when in contact with a brush [6]. Some hazards associated with breathing in dust or fibres during the powdering process must be noted [54]. The average size of the metal flakes, granular powder, or non-magnetic carrier particles ranges from 4 to 12 μm [54].

Powders can also be used in the form of suspension for non-porous and semi-porous surfaces, adhesive tapes, and wet or greasy surfaces in particular. The powder suspension consists of an insoluble powder e.g. iron oxide, carbon black, titanium dioxide [21], molybdenum disulphide, cobalt oxide and weak detergent aqueous solution [20], [66], [105]. One of the powder suspension methods is the small particle reagent process (SPR). SPR is effective on wet surfaces since it is sensitive to the sebaceous fraction of fingermark deposit, not soluble in water. The conventional formulation of SPR is based on molybdenum disulphide flake in a detergent solution and is dedicated to the light surfaces due to the grey impressions developed after treatment [2], [4]. However, a few more formulations have been reported, such as charcoal powder or zinc carbonate and titanium dioxide

resulting in black or white fingermark impressions, respectively. Moreover, a fluorescent SPR was also reported based on Basic Yellow 40 or rhodamine 6G to overcome the coloured background interference limitation [105]. In the usual development process, the fingermark samples are dipped in a tank with molybdenum disulphide suspension and then rinsed with water and allowed to dry [21].

Cyanoacrylate fuming

Fuming with cyanoacrylate esters vapour, commercially available as "superglue", is an effective development technique for fingermarks deposited on non-porous surfaces like metals, rubber, electrical tape [2], glass, plastics [64], garbage bags, carbon paper, aluminium foil, wood, cellophane, or smooth rocks. The technique was discovered in the late 1970s in Japan, the United Kingdom and North America at the same time [6]. Cyanoacrylates, mainly methyl or ethyl esters, are colourless, monomeric liquids, which formed hard, white polycyanoacrylate on the fingermark ridge when subjected to heat [19]. The monomeric vapours start to selectively polymerise on the ridges when reacting with some fingermark components but not with the surface. The moisture and ionic material present in the fingermark deposit catalyse the polymerisation; however, the exact components responsible for polymerisation initiation are not fully determined [64]. The main advantage of this enhancement method is the *in situ* polymerisation on fingermark residue ridges without changing the substrate properties. This method is also not destructive to the ridge pattern because neither carrier solvent nor developing agent applicator is necessary for the treatment process [106].

The polymerisation of cyanoacrylate monomers is considered as an anionic polymerisation (Figure 1.11). In the first stage, an A^- nucleophile (e.g. OH–), which acts as an anionic initiator, reacts with the acrylate monomer in the vapour phase, forming a reactive form [107]. However, also amino acids, fatty acids [108], carboxyl groups of lactates [109] or water molecule, present in fingermark secretions, may play the role of initiator of polymerisation due to the two electron-withdrawing groups on the same carbon atom in a monomer and relatively high electron affinity [107], [110]. This reactive form can further react with consecutive monomers (propagation) in the second stage, resulting in a substituted polyethylene-like product [107]. The polymer chain reaction is terminated in the final phase due to the monomer source removal or ending the heating process [82].

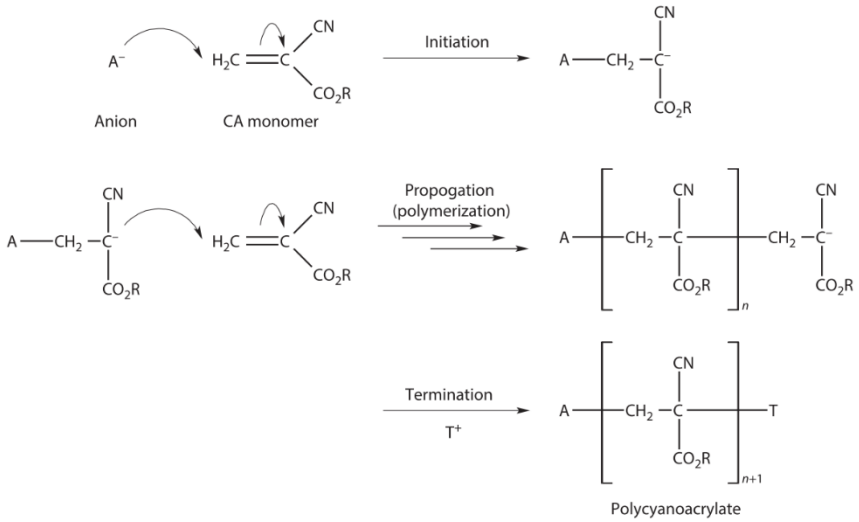

Figure 1.11 The scheme of the cyanoacrylate polymerisation reaction on fingermark deposits resulting in a polycyanoacrylate – a hard, white polymer [4]

Fuming with cyanoacrylate vapour may undergo at room temperature, but it accelerates when heating up to 120 °C [64]. Also, the relative humidity of 80 % during the treatment process is of importance. This is because sodium chloride, present in the fingermark deposit, absorbs moisture increasing the polymerisation reaction, but also maintain the two electron-withdrawing groups in a solvated state facilitating the cyanoacrylate monomers to permeate the fingermark residue [111]. The treatment process is conducted in closed, homemade or commercial chambers with active air circulation [2], [9], or fuming wand [20] until the white polymer on the fingermark deposit is easily observed. However, the contrast between the developed fingermark and the background is often insufficient for identification, e.g. on pale, coloured surfaces. Therefore, the upgrade of the visibility under various wavelengths of light can be introduced by fluorescent or coloured dye staining [112], including Rhodamine 6G [113], [114], Basic Yellow [115], Basic Red, Ardrox, Safranin-O, thenoyl europium chelate [116], Acid Fuchsin, Nile Blue A, Safranin Bluish [117], or Nile Red [92]. The dye post-treatment procedure may cause background staining. To avoid this problem, the vapour-staining process may be introduced to enhance cyanoacrylate-fumed fingermarks by employing p-dimethylaminobenzaldehyde (DMAB), which is a highly volatile fluorescent reagent [118]. Moreover, one-step fluorescent cyanoacrylates are available commercially, including PolyCyano, LumiCyano™, CN Yellow [119], and PECA Multiband [111], which can develop fingermarks in one stage without additional chemical processing. PolyCyano, a solid

cyanoacrylate polymer and dye mixture, requires 60% - 90% of relative humidity and heating at 230 °C [118], producing a toxic hydrogen cyanide gas. Nevertheless, applying PolyCyano for fingermark development on semi-porous surfaces may yield an effective enhancement. On the other hand, Lumicyano™, as a mixture of fluorescent dye incorporated into the cyanoacrylate monomer, does not require specific conditions and may be used in the cabinet for standard cyanoacrylate fuming under the same conditions such as 80 % of relative humidity and temperature 120 °C [120]. The application of one-step fluorescent cyanoacrylates reduces one stage of the process while achieving an effective fingermark development; however, the visualisation examination must be done shortly after fingermark treatment due to the fluorescence decay over time [121].

Vacuum Metal Deposition

Vacuum Metal Deposition (VMD) is one of the most sensitive methods of latent fingermarks development on non-porous surfaces, including glass [122], plastic bags, bottles and packaging, glossy surfaces of cards, photographic paper, magazine covers, also leather handbags or shoes, [20], non-sticky side of adhesive tape [123] or ballistic brass surface [124]. Also, fingermarks deposited on semi-porous surfaces such as certain dark fabrics like polyester [125] or nylon [126], and polymer banknotes, on which other development techniques fail, VMD enhancement yield an effective development [127]. VMD can give excellent fingermark development on both fresh and old, degraded marks [64] and wetted items, making this method superior to cyanoacrylate fuming [20]. This method is based on the deposition of two metals in sequence, first gold or silver and then zinc or cadmium (Figure 1.12). The zinc and cadmium are applied because they do not condense on the grease present in the fingermark residue, but they deposit on small nuclei of metal [20].

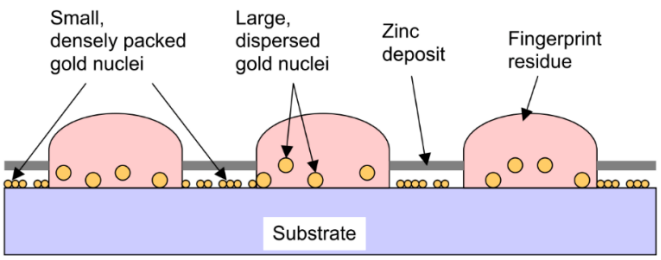

Figure 1.12 The scheme of normal development of fingermark with Vacuum Metal Deposition [60]

The VMD process is conducted under vacuum. In the first stage, a thin layer of gold, invisible to the naked eye, is formed on the whole surface of an examined item due to the metal evaporation. The gold is evenly distributed over the entire surface of the examined item and diffuse into the fingermark residue structure [4]. The morphology of gold nuclei depends on the substrate's surface energy and chemical species deposited on the surface. The layer of gold is several nanometres thin and is not continuous. There are no nuclei present close to the fingermark ridges' surface [60]. In the second stage, a subsequent layer of zinc is formed in the same way; however, the zinc tends to deposit preferentially on the gold nuclei regions but not diffuse into the fatty deposit of fingermark. As a result, the background is plated with the metallic zinc layer, and fingermark ridges are left transparent. The negative marks are being developed in the form of light fingermark impressions on dark background [4]. This type of enhancement is called "normal development" [128]. Nevertheless, as the research has not confirmed the gold nuclei diffusion into the residue matrix, it is also possible that zinc is growing in various regions at different rates. Also, some components of fingermark deposits like palmitic acid, stearic acid, glycerol trioleate, cholesterol oleate, L-arginine, L-leucine, and DL-threonine have been recognised as metal deposition inhibitors. Due to their properties, such as water-insolubility of long-chain fats or low vapour pressure of acids, these components are stable, do not migrate during the VMD process, allowing the development of fingermarks exposed to the aqueous environment [60].

The development process is conducted in a vacuum chamber. The gold and zinc filaments for evaporation are placed at the bottom of the chamber, and the items with deposited fingermarks are clamped above the coating filaments. For gold deposition, the chamber's pressure is lowered to at least 3×10^{-4} mbar, and the current to the gold filament is increased. The deposition is continuing for about 10 seconds. Once the gold is deposited, the pressure in the chamber is increased to 5×10^{-4} mbar to reduce the speed of zinc deposition, and the current starts to flow to the zinc filament. The deposition process is continuing as long as the fingermark impressions become visible on the substrate or the "control" fingermark [20]. During the VMD treatment, some marks may also undergo the "reverse development", which means that zinc is preferentially deposited on fingermark ridges rather than on the background [4], [20]. Moreover, empty prints may occur when zinc is deposited onto the background of the substrate but neither on the ridges nor on the valleys [128]. The reverse development may depend on the polymer substrate category and the amount of gold deposited on the surface. Jones et al. investigated the low-density polyethylene (LDPE), high-density polyethylene (HDPE), polyethylene terephthalate (PET), polyvinyl chloride (PVC) and polypropylene (PP)

within various amounts of deposited gold. The reverse development was observed for the fingermarks deposited on LDPE substrates with a medium amount of gold and PP sheets. Also, for normal development on LDPE, five times less gold was required in comparison to HDPE [129]. In turn, empty fingermarks occur on the fingermarks deposited on PVC and PET substrates [128].

VMD is a sensitive and effective method for various tough surfaces like polymers and aged or wetted fingermarks. Thus, to increase the number of detected fingermarks and improve the ridge details, VMD can be used in a sequence after cyanoacrylate fuming [128], [130]. Nevertheless, this method is still expensive due to specific and costly equipment. Moreover, experience in handling with the detection process is highly required to obtain sufficient development results, especially since the metal deposition time depends on the substrate composition [131].

Multi and Single Metal Deposition

Multi-Metal Deposition (MMD), first proposed by Saunders in the 1980s, is a well-known method for the development of fingermarks deposited on porous, semi-porous and non-porous surfaces, also dry or wet as well as tough wax papers and latex gloves [60], [64]. The two-step treatment process, depicted in the scheme (Figure 1.13), involves the deposition of colloidal gold on the fingermark residue followed by reducing silver on a gold surface to enhance the fingermark ridge impression.

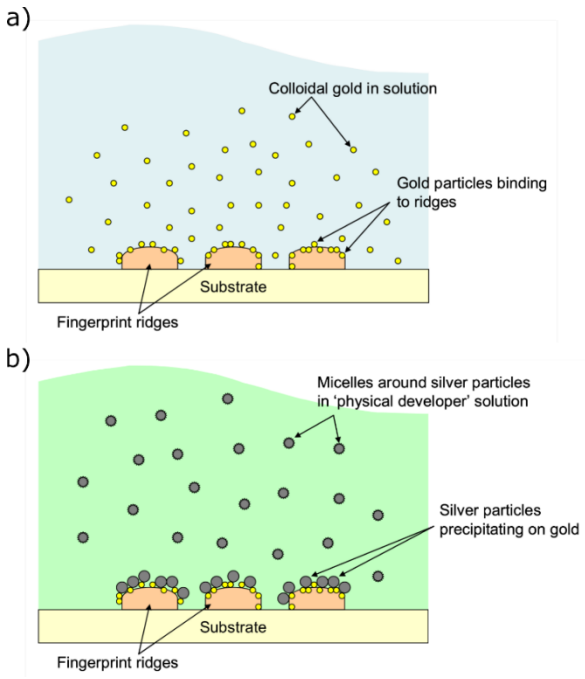

Figure 1.13 A scheme of MMD deposition process steps: a) gold nanoparticles from colloidal solution bind to the fingermark ridges, b) silver precipitates preferentially deposit on pre-existing gold [60]

In the first step, the substrate with deposited fingermarks is immersed in a colloidal gold solution at pH 2.6-3.9 [60]. The colloidal gold binds selectively to protonated amino acids, proteins and peptides present in the fingermark secretions via electrostatic interactions [132]. The colloidal gold is produced in the process of the chemical reduction of tetrachloroauric acid. The gold particles are hydrophobic and negatively charged due to the adsorption of citrate ions, which favours binding to fingermark secretion components [133]. As the binding mechanism alters with the pH, in the acidic environment, electrostatic interactions between negatively charged gold nanoparticles (NPs) and positively charged fingermark components are dominating, in contrast to higher pH where hydrophobic interactions start to dominate [60]. However, the electrostatic mechanism has been recently questioned by Moret and co-workers. In the research, they used carboxyl-functionalised silica nanoparticles to evidence that charged particles in the acidic environment do not play a significant role in the interactions between fingermark deposits and colloidal gold in MMD treatment, but the chemical interactions appear to provide the amide

bond formation between protein-based amino groups in secretion and carboxyl-functionalised gold nanoparticles [134].

The colloidal gold binding to the target species in fingermark deposits provides the catalytic nucleation sites for further silver precipitation [60]. In the second step, the substrate is immersed in a modified physical developer solution, containing silver particles stabilised with a surfactant and the reducing agent. The potential sources of silver ions are based on silver acetate, silver bromide, silver nitrate, or silver lactate. However, the most sensitive reducing system comprises silver acetate and hydroquinone as the reducing agent [133]. Once the silver particles bind to the gold, they start to grow. A dark grey or black fingermark impressions are the silver precipitates deposited around the gold nucleation sites, enhancing the metallic gold image [64].

Several modifications to the original MMD were proposed and evaluated in time. Schnetz and Margot [133] improved the process's effectiveness by increasing the reactivity due to the controlled pH (2.5-2.8) and by enhancing the resolution due to the gold nanoparticle size decrease from 30 nm to approximately 14 nm. Becue et al. [132] simplified the treatment process, reducing the number of immersion baths. He also functionalised gold nanoparticles with thiolated cyclodextrins, which can complex the dye molecules (Acid Blue 25), trapping them in their cavity and thereby improve the contrast of fingermark. Also, the luminescent gold nanoparticles have been proposed by Becue et al. [135] to enhance the method's sensitivity independently from the background colouration. The gold nanoparticles were covered with the zinc oxide layer due to the photoluminescent properties of ZnO nanostructures. On the other hand, Jaber et al. [136], [137] reported “negative” fingermark impressions on paper developed with gold nanoparticles modified with bifunctional agents, followed by conventional silver precipitation. The method was based on the interactions between gold particles and cellulose in the substrate. The modified MMD method was also proposed by Xu et al. [138]. The method combines the immunoassay with multi-metal deposition. Gold nanoparticles were modified with antibodies that bind with the corresponding antigens in fingermark deposit. The deposition of modified gold nanoparticles, followed by silver precipitation, resulted in black fingermark impressions and allowed for recognising the specific components of the fingermark residue like epidermal growth factor polypeptide (EGF) and lysozyme.

Although MMD is a highly sensitive method of fingermark development, some drawbacks also occur. Firstly, when applied to porous surfaces, a thorough rinsing has to be done in the first step to elute unbound gold nanoparticles trapped in the pores and thereafter avoid possible background development [20]. Also, the

reagents are expensive, the silver reagent is delicate, the whole treatment process is time-consuming [96], and the enhanced fingermarks are only black or grey, limiting the application only to transparent, white or light substrates [135]. Also, MMD on dry surfaces is less sensitive than cyanoacrylate fuming or DFO. On the other hand, this method yields good results when applied to plastic, adhesive tape, expanded polystyrene, difficult surfaces such as beer bottle labels, plastic gloves [10], cling films and other types of plasticised vinyl [139], and relatively good results for polymer banknotes [140].

An alternative to MMD, which yields similar results, is the Single-Metal Deposition (SMD) method, first reported by Stauffer et al. [141]. SMD develops fingermarks with comparable sensitivity and selectivity to MMD; however, SMD is less time-consuming, more cost-effective and requires fewer reagents which also have a longer shelf life. In the SMD procedure, the first step, which is colloidal gold deposition, remains unchanged, but instead of silver precipitation, the gold reduction is applied in the second step. The SMD substitutes silver redox agent with gold chloride and reduces hydroquinone and hydroquinone/silver immersion baths to one hydroxylamine/gold chloride bath, which is a more stable solution. Thus, the number of reagents is reduced. The SMD process was further developed by Durussel and co-workers [142], who optimised several parameters such as immersion time, gold/hydroxylamine ratio, gold concentration, and stirring speed. In the range of examined porous and non-porous surfaces such as glass, bleached and unbleached white paper, painting tape (both sides), latex gloves, and polystyrene foam, SMD yielded the same sensitivity and comparable results in comparison to MMD; however, SMD generates fewer costs and labour.

The ongoing investigations have mainly focused on overcoming the need for precise pH control of the colloidal gold solution. The use of aspartic acid conjointly with sodium citrate in the synthesis of colloidal gold nanoparticles allows extending the range of pH up to 6.7, for which the fingermark detection is still effective [143]. Moret and Becue then reported another progress in SMD treatment [144], which optimised the preparation of colloidal gold synthesis, reducing the procedure to one step, as well as change the dilution factor of the working solution and the pH setting. The optimised SMD II method resulted in higher efficiency, yielding 50 % more detected fingermarks than the original SMD. This was also confirmed in subsequent research on SMD efficiency on a wide range of porous, non-porous and semi-porous surfaces such as numerous types of paper, aluminium foil, various kinds of polymer surfaces, cardboard, and glass, reported by Newland and co-workers [145]. SMD II performs excellent also on polyethylene surfaces such as zip-lock bags or calcium carbonate/polyethylene blended papers which were exposed to the dry and wet

environment for a long time [146]. Similarly to MMD, SMD develops fingermarks only in black or dark violet colouration. However, to improve the visual contrast of fingermark impression on dark or coloured surfaces, SMD may be combined with surface-enhanced Raman spectroscopy (SERS). Results reported by Kolhatkar and co-workers have shown that the gold nanoparticles deposited on fingermark ridges provide strong plasmonic resonance and luminescence [147]. This gives the possibility to create a chemical map of the fingermark pattern due to collecting the signal of fingermark components measured using a SERS effect.

1.5 Nanoparticles for latent fingermark enhancement

None of the currently available fingermark development methods is versatile and performs excellently on fingermarks regardless of their age, surface structure on which they are deposited, ambient environment conditions (heat, humidity, light), or colouration of the substrate background. There is still a need to develop new methods or improve the available ones to increase the sensitivity, selectivity and detection success rate. The considerable interest has been directed to nanoparticles or nanocomposites, the matter with a dimension between 1 and 100 nm [134], [148], [149]. Such a small particle size increases the ratio of surface area to volume, which changes the matter's properties compared to the bulk solid. The material dimension decrease influences its structural, thermal, electromagnetic, mechanical and optical properties [150]. The several unique properties of nanoparticles have been recently utilised to develop materials and methods for fingermark detection, which resulted in the improvement of selectivity, sensitivity and contrast of fingermark image [151]. Firstly, nanoparticles' size is 1 000 to 10 000 times smaller than the fingermark friction ridge with an approximate width of 480 µm [152]. Applying such small particles can significantly increase the sensitivity and the resolution of the detection, maximising the contrast between the enhanced fingermark ridge and the substrate [149]. Secondly, the large surface area of nanoparticles, much greater than the bulk material, increases catalytic activity and surface modification capability. Chemical moieties can easily modify nanoparticles' surface to selectively target either the components of the fingermark residue instead of the underlying surface [148] or the background surface, yielding the reversed fingermark enhancement [136]. Finally, due to the nanoparticles' optical properties, the contrast between the fingermark and the background may be significantly enhanced. The optical properties are of great importance when a fingermark is deposited on a luminescent, patterned

or coloured background. Applying, e.g. quantum dots (QDs), intrinsically luminescent nanoparticles, or silica nanoparticles with incorporated luminescent dye in its matrix may successfully suppress the underlying substrate interference [134].

Two distinct features of a developing agent have to be considered while developing the new fingermark enhancement method based on nanomaterial. First, "the marker" has to be selected, e.g. optical properties of the nanoparticle or its atomic composition, which can be optically detected. Secondly, the nanoparticles' surface should be altered with either capping agents or developing conditions like pH of the working solution to selectively interact with fingermark secretions [82], [148]. Numerous nanoparticle types have been developed to enhance fingermarks involving metal NPs, metal oxide NPs, silica NPs, quantum dots, or upconverters.

1.5.1 Metal NPs

Gold

Among all metal nanoparticles employed for fingermark development, gold is one of the most commonly applied material. This is due to the gold usage in the widely researched MMD and SMD processes described in Chapter 1.4. In MMD and SMD treatment, the fingermark development is driven by physicochemical mechanisms like electrostatic interaction, and the gold is used without any surface modification, except stabilising ions. However, various other methods applying gold nanoparticles for fingermark detection have been already reported, especially the gold NPs with a functionalised surface to target the fingermark [82], [148].

Leggett and co-workers [153] reported the approach of conjugating the antibodies to the gold nanoparticle surface, which then bind to an antigen in the sweat, providing information on the presence of drug metabolites. This highly selective antibody-antigen recognition mechanism was based on detecting the cotinine, which is a specific metabolite of nicotine in tobacco smokers' fingermark sweat residue. Anti-cotinine-nanoparticle conjugates deposited on the fingermark ridges were further enhanced with fluorescently tagged secondary antibody fragment, which yielded a fluorescent image of fingermark ridges. Another strategy of application antibody-conjugated gold nanoparticles for fingermark enhancement was proposed by Spindler et al. [154]. In this approach, the rabbit anti-L-amino acid antibodies conjugated to gold NPs were used to detect fingermark on a non-porous surface by interaction with amino acids present in fingermark residue. The anti-

rabbit secondary antibodies labelled with Red 610 fluorescent fluorophore have been deposited on antibody-gold modified fingermark for imaging purposes.

In turn, Sametband et al. [155] applied gold NPs stabilised with long-chain n-alkanethiols for fingermark detection on paper as well as non-porous surfaces. The fingermarks developed with functionalised gold NPs were followed by silver physical developer yielding the dark impressions. The hydrophobic functionalised gold NPs undergo lipophilic interactions between fatty acids present in fingermark secretions and aliphatic chains. The selective interactions improved the intensity and clarity of enhanced fingermarks. Gold nanoparticles functionalised with glucose have been proposed by Gao et al. [156] to one-step single-metal nanoparticle deposition (SND) on non-porous surfaces. The SND process significantly reduces the number of MMD baths to one bath with a working solution and one bath with water. Gold NPs stabilised by glucose were used as the working solution for fingermark enhancement at a wide range of pH compared to the MMD process. The one-step process using gold nanoparticles for fingermark detection has also been investigated by Hussain and co-workers [157]. The process was based on *in situ* reductions of tetrachloroauric acid in the presence of fingermark residue components, yielding the red to purple visible fingermark impressions. The lecithin and its combination with potassium iodide present in fingermark secretion were identified as the reducing agent of gold ions to gold nanoparticles.

Shenawi and co-workers [137] presented gold nanoparticles modified with mercaptocarboxylic acid as the bifunctional developing agent, followed by silver precipitation, for latent fingermarks deposited on the paper. In this approach, the thiol groups of mercaptocarboxylic acid bind to the gold NPs and the carboxylic group interact with cellulose via hydrogen bonding resulting in reverse development of fingermark. The further silver precipitation results in the deposition of silver around the fingermark ridges but not on them. Within this method, an improved yield of latent fingermarks on paper may be obtained; nevertheless, the comparison to benchmark methods have not been made. A high resolution of fingermark and 3rd level of ridge details may be obtained with gold nanoparticles modified with amphiphilic block copolymer (BCP) poly-(styrene-alt-maleic anhydride)-b-polystyrene (PSMA-b-PS). Song et al. [158] reported the strategy of both colourimetric and photoacoustic imaging of latent fingermarks deposited on porous, semi-porous or non-porous surfaces like paper, adhesive tape, plastic, glass, a silicon wafer, and a paper banknote. The gold nanoparticles capped with PSMA-b-PS interacted with proteins, polypeptides and amino acids in fingermark secretions through electrostatic and hydrophobic interactions, yielding a good fingermark ridge enhancement. Another strategy for enhancement of the fingermarks deposited on

a paper substrate, proposed by Lee et al. [159], [160], is based on gold nanoparticles modification with a bifunctional reagent containing 1,2-indanedione moiety to react with amino acids and long alkyl-thiol chain to stabilise the ligand on gold nanoparticle. This bifunctional agent may target both amino acids in eccrine fraction and hydrophobic lipids in sebaceous fraction; thus, followed by MMD processing may result in high sensitivity of fingermark detection. The other fingermark detection method related to gold nanoparticles' use is based on gold seed-mediated growth, which was developed by Su et al. [161]. In this technique, a lysozyme-binding aptamer (LBA) was chosen to conjugate with gold seed by a thiol-gold bonding. This aptamer targets a lysozyme, which is abundantly present in fingermark secretions. Once the gold seeds modified with LBA are deposited on the fingermark ridges, the mark is treated with a gold ion complex solution. The self-catalytic process of the gold ion reduction to metallic gold occurs, introducing gold nanoparticles' growth on Au seeds and resulting in red fingermark impressions. The method was introduced as faster than existing methods and was expected to increase detection efficiency; however, no comparative assessment was reported. Another aptamer-bound gold nanoparticles have been used for the recognition of cocaine in fingermark. In the research of Li et al. [162], gold nanoparticles were modified with cocaine-specific aptamers, which in the case of the cocaine presence in the fingermark, could induce the aggregation of gold nanoparticles on the fingermark ridges, and thus, provide the green-to-red colour change of the scattered light in the dark-field microscope imaging due to localised surface plasmon resonance of gold NPs.

New dusting powders involving gold nanoparticles are another trend in fingermark development. Yan et al. [163] demonstrated nanocomposite powder's application based on gold nanoclusters that were *in situ* grown on the surface and inside the matrix of bovine serum albumin/montmorillonite clay (BSA/MMT) due to the reduction of tetrachloroauric acid by BSA. The gold nanocluster BSA/MMT composite may be applied to multicoloured surfaces since it indicates strong red and infrared (IR) fluorescence. Gold nanoclusters prepared *in situ* on thiol-functionalised silica gel 60 (MPS) for fingermark deposited on non-porous and porous substrates were reported by Andrade and co-workers [164]. The gold-MPS nanocomposites effectively adhere to the fingermark ridges after powder dusting; however, the examined fingermarks were artificially enriched in sebum.

Silver

Besides a physical developer's method, various other fingermark enhancement techniques using silver nanoparticles have been reported. Prasad et

al. [165] analysed the silver nanoparticles to enhance fingermarks deposited on paper substrates. Fingermarks were first immersed in acetic acid to charge the fatty components of fingermark secretion positively. Then fingermarks were exposed to negatively charged silver nanoparticles from the colloidal solution yielding clearly visible fingermark impressions. The stability of latent fingermarks enhanced with silver NPs was compared with the silver nitrate method; however, no comparative assessment to any benchmark method was reported. An immunodetection strategy relying on an antibody conjugated to silver nanoparticles combined with large-area SERS imaging has been proposed by Song and co-workers [166]. The antibody-silver NPs Raman probe interacts specifically with human IgG present in fingermark secretions enabling the ridge pattern visualisation by the SERS imaging technique. Nevertheless, none of the protein types was specified in this research. Souza and co-workers [167] examined the SERS substrate composed of a thin layer of silver nanoparticles in the agar matrix to detect methamphetamine hydrochloride in the deposited latent fingermark. Recorded Raman map images visualised the clear fingermark ridge pattern before and after the development with black powder, indicating ca. 190 μg of methamphetamine hydrochloride in the fingermark secretions.

A different approach was attempted by Qin and co-workers [168]. They developed latent fingermarks deposited on conductive surfaces like indium-tin oxide-coated glass, gold, platinum, or stainless steel coins by the selective electrodeposition of gold or silver nanoparticles. The fingermark secretions acted as an insulator in the electrodeposition process. Silver or gold nanoparticles were deposited on the conductive valley regions resulting in a high contrast reverse development of the fingermark. In turn, Ran et al. [169] used the fluorescent markers based on aptamer-modified silver nanoclusters with the emission regulated by nearby DNA regions to detect exogenous components in the fingermark as well as the latent fingermark itself. The detection of the exogenous fingermark components like explosives was based on the interaction between the silver-DNA aptamer and trinitrotoluene (TNT) present in the fingermark secretions, yielding the coloured image. In the imaging process, the silver-DNA aptamer targeted lysozyme in fingermark secretions resulting in the fluorescent fingermark impression and overall multicoloured image. Another strategy was proposed by Yang and co-workers [170]. This non-destructive process of enhancing the fingermarks deposited on non-porous substrates was based on applying “silver imaging ink” to the fingermark and drying at 90 °C, which resulted in *in situ* generation of silver nanoparticle precipitates and reversed fingermark development. The ink was composed of the silver-amino coordination ions in the water-ethanol solution. Due to the hydrophobic properties

of the fingermark secretions, the ink containing 60% of water adhered preferentially to the furrows, not to the ridge area. After heating to 90 °C, the dark impressions of reduced silver nanoparticles provided the negative fingermark ridge pattern. Cheng et al. [171] reported the use of silver and gold alloy nanoparticles (Ag:Au 60:40 $\%_{wt}$) for fingermark enhancement on porous and non-porous surfaces by argon ion sputtering. The deposition resulted in an amber-colour ridge impression and purple-blue background. Applying silver and gold alloy NPs provided a higher contrast of latent fingermark images due to the enhanced optical absorption efficiency with the presence of silver, and also improved stability due to the presence of gold in the alloy, which suppresses aggregation behaviour. Moreover, with the surface-assisted laser desorption/ionisation mass spectroscopy (SALDI-MS), the spatial distribution of the latent fingermark compounds with better sensitivity was possible in comparison to pure silver or gold nanoparticle deposition.

1.5.2 Metal oxide NPs

Metal oxides are mainly used for fingermark detection in the form of powder; however, the nanosized powder may cause health hazards due to the extremely small particle size [148]. Only a few studies reported the use of metal oxide powder suspension, which is much safer than dry powder due to the lower risk of airborne particles inhalation. The most commonly reported metal oxides for fingermark detection are zinc oxide, iron oxides, titanium oxide, and aluminium oxide.

Zinc oxide

Nanoparticles of zinc oxide (ZnO NPs) are of great interest in applying to fingermark development mainly due to their luminescent properties. Zinc oxide indicates a broad emission band in the visible (VIS) light spectrum region when excited with UV irradiation [172]. Guzman et al. [173] reported using zinc oxide nanoparticles with the mean size from 10 to 30 nm in the form of powder to develop fingermarks deposited on non-porous substrates like steel, aluminium, black glass, black paperboard, and wood surface. The fingermarks were found to be clearly visible on steel and aluminium under UV light illumination; however, barely impressions were found on wood. Also, some reference sample was introduced; nevertheless, no further details related to the benchmark method were given. Choi and co-workers [174] proposed the application of nanostructured zinc oxide particles, pure or lithium-doped, in the form of luminescent powder and powder

suspension to develop latent fingermarks deposited on non-porous surfaces like aluminium foil, glass, and polyethylene. They obtained flower-like zinc oxide particles in a size range of 1-3 µm for pure powder and in the range of 1-2 µm for lithium-doped ZnO. However, the nanostructures in the micron-sized particles have been observed under the scanning electron microscope. The incorporation of lithium ions slightly increased luminescence intensity. Nanostructured ZnO powder developed clear fluorescent fingermarks on each examined surface; nevertheless, ZnO powder suspension performed better on polyethylene substrate and aged fingermarks. It is worth noting that the study was conducted on sebaceous fingermarks. Moreover, in the comparative assessment, the commercial powder produced more intensive fluorescence intensity of developed fingermarks than the proposed ZnO powder, albeit ZnO powder produced less background development.

Several metal oxide nanoparticles for optical imaging of latent fingermarks deposited on non-porous substrates have been examined by Amin et al. [175]. They also determine the small drug molecules like nortriptyline, amitriptyline, imipramine, and promazine in fingermark secretions using the SALDI-MS technique. The sebaceous fingermarks deposited on glass were powder dusted with ZnO nanoparticles and imaged with an optical microscope. The ZnO NPs powder, with an average size of 46 nm, preferentially adhered to the fingermark ridges resulting in a clear white fingermark impression. Also, using ZnO NPs in the SALDI-MS drug molecule recognition lowered the background noise compared to the conventional organic matrix. Similarly, Luthra and Kumar [176] reported the application of zinc oxide nanoparticles of ca. 15 nm size for fingermarks detection on non-porous surfaces such as glossy cardboard, plastic and glass. They obtained clear and of good quality fingermarks on all substrates using the powder dusting method. However, no details have been described related to the type and age of fingermarks. Also, no comparison to benchmark methods has been reported.

To increase zinc oxide nanoparticles' fluorescence intensity and extend the photoluminescent spectra to the blue-green region of the visible light spectrum, Shivananjaiah and co-workers [177] synthesised ZnO NPs doped with lanthanum ions (La^{3+}). They obtained the nanocrystallites with a size ranging from 13 to 20 nm depending on the La^{3+} concentration. The eccrine fingermarks deposited on wood, mobile phone, and bottle were dusted with ZnO NPs doped with 2 $\%_{mol}$ of La^{3+} ions and photographed under 254 nm UV light excitation. All the fingermarks were successfully developed with clearly defined 2nd level ridge details. However, again, no comparison to the benchmark methods have been performed. A different approach to increase the photoluminescence intensity of zinc oxide was proposed by Prabakaran et al. [178]. They coated the zinc oxide nanoparticles (average size of

40-50 nm) with nitrogen-doped carbon dots (N-CDs/ZnONPs) and obtained the composite, which increased the emission intensity in the blue region of the light spectrum. N-CDs/ZnONPs powder has been used for fingermark detection on non-porous substrates such as white marble, a black mat, aluminium foil, aluminium sheets, an aluminium rod, a compact disc, an iron disc, and magazine paper, demonstrating good selectivity and sensitivity. The comparative assessment of fingermark development has been done among composite N-CDs/ZnONPs powder, ZnO NPs, and nitrogen-doped carbon dots for fresh and aged fingermarks. Developed fingermarks were examined under white and UV light. Applying N-CDs/ZnONPs resulted in a higher contrast between the fingermark ridge and the background and visible 2nd level ridge details. N-CDs/ZnONPs composite also performed better than TiO_2 and $ZnSO_4$ commercial powders.

Arshad and co-workers [179] synthesised a nanopowder based on zinc oxide and silicon dioxide (ZnO-SiO_2) as a developing agent for fingermarks deposited on various types of surfaces such as polymer cardboard, metallic can, glass, and some plastic substrates (laptop, calculator, board marker, glazed wrapper). ZnO-SiO_2 nanopowder, with an average size of 32.9 nm, was deposited on sebum-rich fingermark ridges in both ways: by powder dusting and by powder suspension (only glass substrate). In general, ZnO-SiO_2 nanopowder in both application forms performed very well on most examined dark substrates, yielding good quality marks with visible 3rd level ridge details. Also, better visibility without background staining has been noticed compared to commercial powders like zinc stearate or titanium dioxide; however, authors did not explore the material's photoluminescence properties, which could have significantly increase the contrast not only on dark surfaces. An interesting approach was reported by Chadwick and co-workers [180], who coated several metal oxides with a mixture of Rhodamine 6G and the near-infrared (NIR) laser dye Styryl 11 (STaR 11), followed by the mixture with magnetic powder to visualise fingermarks luminescence in the visible and near-infrared spectrum of light as a result of excitation with the visible light. Natural and charged, aged fingermarks have been examined on various substrates such as glass, aluminium beverage cans, polyethylene, or laminate. Also, a comparison of development efficiency to commercial powder Blitz Green have been made. However, zinc oxide nanoparticles with a size less than 100 nm coated with STaR 11 did not perform well, giving weak NIR luminescence and no luminescence in the visible region.

Iron oxide

Diacetylene-magnetite composites consisted of iron (II, III) oxide (Fe_3O_4) nanoparticles (15-40 nm) and diacetylene polymer have been proposed as the fingermark developing powder by Lee et al. [181]. In this study, sebaceous fingermarks deposited on solid surfaces like black or red paper, PET film and aluminium foil have been processed with a magnetic powder, which undergoes colour change from brown to blue upon the UV irradiation, and then from blue to red upon heat treatment at 80 °C what induce the polymerisation of diacetylene. The possibility of tuning the colour depending on the background colouration was advantageous.

Li et al. [182] coated Fe_3O_4 nanoparticles with amino-terminated silane, followed by capping the particles with gold. The obtained Fe_3O_4@SiO_2-Au composite was used to detect fingermarks deposited on paper, glass, polyethylene bags, using both methods: powder dusting and powder suspension. The pH effect of Fe_3O_4@SiO_2-Au powder working suspension on fingermark development was investigated. Good ridge details were obtained for pH lower than 5. Both powder dusting and powder suspension methods yielded good fingermark detection. Also, the performance of Fe_3O_4@SiO_2-Au composite was compared with the commercial copper powder resulting in good ridge details and low background staining on glass and polyethylene for both methods; however, Fe_3O_4@SiO_2-Au composite performed better on paper substrate. Nevertheless, the applied fingermarks were of the sebaceous type, which may boost the interactions between the powder and fingermark constituents. Similarly, Zhang and co-workers [183] coated Fe_3O_4 nanospheres with thiol-terminated silane followed by a silver shell capping to obtain monodisperse, stable and magnetically active nanocomposite (Fe_3O_4@Ag nanoeggs) for the development of fingermarks on non-porous surfaces like paper, ceramic, polyethylene, and glass. With an average size of 300 nm, these core-shell composites can detect fingermarks within powder dusting or powder suspension application. The dependence of the fingermark quality on working suspension pH was examined. At low pH, low background interference has been noticed. Fingermarks developed by powder dusting with Fe_3O_4@Ag nanoeggs gave better overall contrast of the ridges than commercial powders such as magnetic Fe_3O_4, carbon, or aluminium with an average particle size in the range of 1 – 82 μm. However, no details have been given on the type and age of used fingermarks.

Besides the ZnO NPs, Amin et al. [175] also employed iron (III) oxide (Fe_2O_3) nanoparticles (11 nm particle size) for optical imaging of latent fingermarks deposited on non-porous surfaces and for determination of small drug molecules in

fingermark secretions using SALDI-MS. The fingermark ridges have been successfully enhanced with Fe_2O_3 nanoparticles yielding dark brown impressions, contrasting efficiently with light-coloured backgrounds. Moreover, Fe_2O_3 nanoparticles performed the best in the detection of small drug molecules with the SALDI-MS detection method.

Titanium dioxide

Choi and co-workers [184] coated two commercially available types of titanium dioxide particles (TiO_2) with fluorescent perylene diimide dye for fingermark detection on polyethylene, glass, and painted wood. Fingermark developed with fluorescent composite, composed of either small TiO_2 nanoparticles (20 nm size) or bigger TiO_2 particles (size 100-500 nm), resulted in similar performance; however, the TiO_2 nanoparticles produced clearer ridges and less background development. Compared to commercially available fluorescent powders such as Black Emerald and Blitz Green, the fluorescent TiO_2 nanoparticles yielded a weaker fluorescence under the 505 nm light excitation. Still, they demonstrated only minimal background development, whereas commercial luminescent powders were largely found in the background. Both commercial fluorescent powders and TiO_2 particles did not develop fingermarks on painted wood. The processed fingermarks were of the sebaceous type, aged up to 1 month.

TiO_2 nanoparticles as the fingermark development luminescent agent were also considered by Chadwick in the research mentioned above [180]. However, these nanoparticles coated with Rhodamine 6G and Styryl 11 dye emitted very weak NIR luminescence. Luthra and co-workers [176], besides the zinc oxide, also reported above, investigated tin oxide for latent fingermarks development on non-porous surfaces like glass, plastic, and glossy cardboard. However, tin oxide nanoparticles did not show a clear development of the fingermark. Amin et al. [175], who reported the successful application of ZnO and Fe_2O_3 to fingermark enhancement and small drug molecules recognition by SALDI-MS, also considered tin oxide nanoparticles. Applying TiO_2 nanoparticles, with an average size diameter of 4 nm, led to efficient fingermark ridge development, yielding white impressions and successful drug detection in fingermark residue.

A cobalt titanium oxide composite nanopowder (Co_2TiO_4) for the development of latent or blood fingermarks deposited on aluminium foil, ceramic tiles, painted wood, glass, cardboard, plastic, and copy paper has been proposed by Peng and co-workers [185]. The charged, latent and blood fingermarks were enhanced by the powder dusting method and powder suspension, respectively,

yielding green fingermark impressions. The Co_2TiO_4 nanopowders, with an average size of 65 nm, performed with high sensitivity, selectivity and low background staining on fresh and aged fingermarks deposited on all examined surfaces. For the comparative assessment, commercial powders like bronze powder, carbon powder, and magnetic ferric powder have been chosen. The Co_2TiO_4 nanopowders, in contrast to commercial ones, facilitated the recognition of third levels of ridge details like sweat pores.

Aluminium oxide

Fouda-Mbanga et al. [186] proposed the composite of carbon dots and aluminium oxide nanofibers (CDs/Al_2O_3 NFs) as a lead ions absorber for further forensic usage. The examined latent fingermarks, deposited on non-porous substrates like glass or aluminium foil, sheets or rod, were of sebaceous type. The powder dusting resulted in fingermark detection with clear ridge details; however, no comparative assessment have been reported.

The above-mentioned research by Chadwick [180] on metal oxide nanoparticles coated with Styryl 11 dye, Rhodamine 6G and combined with magnetic powder for fingermark enhancement yielded the best results for aluminium oxide nanoparticles. Luminescent Al_2O_3 nanoparticles exhibited high NIR luminescence intensity and stability. Compared with commercial powder Blitz Green, luminescent Al_2O_3 powder performed better for textured surfaces, yielding a background development decrease and greater ridge details. However, for smooth or glossy substrates, applying Blitz Green resulted in slightly better ridge development.

Ceric dioxide

Also, cerium (IV) oxide (CeO_2) have been investigated for fingermark development. Rohini et al. [187] synthesised CeO_2 nanopowders, in a solution combustion technique, for powdering the fingermarks deposited on non-porous surfaces like glass, mobile screen, stainless steel, or aluminium foil. CeO_2 nanopowders, with an average size of 5-40 nm, exhibited excellent adhesion to the fingermark ridges, yielding in 3rd level fingermark details like pores or ridge contours and no background development. However, the examined fingermarks were of sebaceous type. Compared to commercially Fe_2O_3 and TiO_2 powders, CeO_2 nanopowder performed better, yielding clear ridge details and low background development. SALDI-MS technique for small drug molecule recognition in latent fingermarks, reported by Amin et al. [175], was also examined for ceric dioxide

nanoparticles. With an average size of 5.4 nm, this nanopowder has developed sebaceous fingermarks with high detection sensitivity yielding white ridge impressions; however, not higher sensitivity than for Fe_2O_3 nanoparticles was achieved. CeO_2 nanoparticles were found to be efficient as a substrate for small drug molecule recognition by SALD-MS.

1.5.3 Silica NPs

The silicon oxide nanoparticles (SiO_2 NPs), due to their structure, possess several desirable properties crucial for effective fingermark development. SiO_2 NPs are usually synthesised in either Stöber synthesis or reversed microemulsion yielding a controllable and small nanoparticle size. Dye molecules, easily becoming entrapped in the porous SiO_2 NPs matrix, provide diverse optical properties, and silanol groups present in the external layer of the SiO_2 matrix facilitate the surface functionalisation with a variety of organic moieties [188]. Plenty of studies on silica NPs for fingermark detection involve powder dusting as an application technique; however, silica NPs powder suspension has also been reported.

Silica nanoparticles in a carrier solution

The broad research on silica nanoparticles employed for fingermark detection and the reaction mechanism between silica NPs and fingermark deposits was conducted by Moret and co-workers [134], [188]. Silica nanoparticles with an average size of 84 nm were surface-modified with carboxyl groups to increase the affinity to fingermark deposit. Moreover, several dyes such as rhodamine 6G, rhodamine B, and tris(2,20- bipyridyl)dichlororuthenium (II) hexahydrate (RuBpy) were entrapped in the silica matrix to tune the optical properties of the developing agent. The natural fingermarks deposited on non-porous surfaces, e.g. glass, transparent polypropylene, black polyethylene, and aluminium foil, were developed with dye-doped silica NPs aqueous suspension. The luminescent cyanoacrylate fuming by Lumicyano™ was chosen as a benchmark method. Both methods resulted in similar results; however, luminescent silica NPs performed better in terms of homogeneity of the material on the fingermark ridge. Also, the effective interaction of silica NPS with fingermark was less influenced by the donor's variability. On the other hand, in the case of luminescent silica NPs, more quality variations between the substrate types have been noticed. Further optimisation of RuBpy-doped silica NPs modified with carboxyl moieties concerning working suspension concentration, immersion time, the temperature of the treatment process, variability of donors and

comparison to a benchmark method such as cyanoacrylate fuming followed by luminescent dye staining was performed by Lee and co-workers [189], [190].

Alsolmy et al. [191] demonstrated the sebaceous-rich fingermark development with fluorescein isothiocyanate-encapsulated silica nanoparticles (F-SiNPs). The 4 nm fluorescent F-SiNPs modified with phenyl groups were synthesised via water-in-oil microemulsion. The fresh and 1-month-aged fingermarks deposited on glass, aluminium foil and polystyrene were developed in aqueous ethanol working suspension of F-SiNPs. Incorporation of fluorescein isothiocyanate into the silica matrix yielded a good contrast of fingermark ridge and 2nd level details on a glass substrate; however, on aluminium foil and polystyrene, a high background staining was observed. No comparative method of fingermark development has been performed. Similar research was reported by Abdelwahab et al. [192], who encapsulated the butenamine derivative of fluorescein isothiocyanate in silica nanoparticles with a phenyl-functionalised shell. Among all synthesised silica nanoparticles, those with an average size of 30-40 nm resulted in good fingermark enhancement with 2nd levels of ridge detail and high affinity to the fingermark deposit. Guleria et al. [193] examined organosilicon oxide nanoparticles (OSiNPs) modified with L-glutathione (L-Glu) for forensic application. The blue emitting L-Glu@OSiNPs in aqueous solution, with an average size of 3-5 nm, were used to develop the sebaceous-rich fingermarks deposited on glass, aluminium foil, metal sheet, compact disc and its plastic cover. The developed fingermarks observed under UV excitation (365 nm) exhibited a clear ridge pattern on most surfaces.

Small, 50 nm mesoporous silica nanoparticles (MSNs) dye-loaded with methylene blue (MB) for fingermark detection were reported by Zhang et al. [194]. Sebaceous-rich fingermarks deposited on a glass substrate and treated with MSNs@MB aqueous suspension yielded a good fingermark contrast due to the abundant nanoparticles on the ridge and blue dye colouration. However, no other substrates have been reported, and no benchmark assessment has been done to compare the results. Wang et al. [195] loaded mesoporous silica nanoparticles with Nile red dye (MSN@NR) to detect fingermarks deposited on thermal paper, such as market receipts. In their research, charged fingermarks were developed with water suspension of MSN@NR, yielding high-quality fingermark impressions without background staining and retaining the background text, unlike the benchmark methods: ORO or the Nile red performed. The high dispersibility of MSN@NR in water was advantageous; it avoided using methanol as a carrier solvent. Meng and co-workers [196] have also investigated mesoporous silica nanoparticles with a narrow size distribution as a reagent for bloody fingermarks development. The fingermarks deposited on a black non-porous surface were developed by spraying

the samples with an ethanol suspension of MSNs and imaged with a digital camera with a yellow-green filter under white light or monospectral light excitation. The clear ridge impressions were possible to observe due to the photonic crystal structure of MSNs, exhibiting the Bragg diffraction. However, no comparative assessment has been performed. Also, the MSNs were of an average size equal to 240 nm, which does not qualify these particles to the class on nanomaterials. Theaker et al. [197] introduced fluorescent dye-embedded hydrophobic silica nanoparticles aqueous suspension for fingermark development. Several dyes, e.g. crystal violet or rhodamine 6G, incorporated into the silica NPs have been investigated as a developing agent for sebaceous-rich fresh and aged fingermarks deposited on glass slides. The results of fingermark enhancement with both rhodamine 6G and crystal violet doped silica nanoparticles resulted in good quality fingermark enhancement with clear ridge details and slight background staining. However, the reported results of using the benchmark method concerned only powder dusting the fingermarks. Furthermore, the silica particles were of an average size of 400-500 nm.

Silica nanoparticles as dry powders

Zhang et al. [198] reported the small 30 nm silica NPs with non-conjugated siloxane fluorescent molecules incorporated inside the silica matrix. The blue-emitting silica NPs have been employed as a developing agent for fresh and aged sebaceous-rich fingermarks, deposited on stainless steel, glass, wood, and polyethylene film. Good quality of luminescent fingermark impressions, high resolution and contrast between the ridges and the background were observed under 365 nm light excitation on all examined substrates. Up to 16 minutiae have been recognised when compared to the fingerprint made using the red ink pad. Slightly lower quality and coverage of the ridges were observed for 30-days-aged fingermarks, which may happen due to decomposition of oily fraction in fingermark deposits. Divya et al. [199] modified silica nanoparticles with various-length alkyl chains to tune its surface amphiphilicity and improve adherence to fingermark deposits. Then, they modified silica nanoparticles with a π-electron-rich platinum complex luminophore containing a long hydrophobic chain ($–C_{12}H_{25}$) to improve the fingermark contrast. The broad study involved fresh and 45 days-aged fingermarks deposited on notebook paper, steel, wooden surface, and glass. Development of the fingermarks on glass with hydrophobic silica nanopowder and imaging under white light illumination has resulted in obtaining the 3rd level of ridge details. Hydrophobic silica nanopowder performed well on all studied surfaces; however, the platinum

complex-modified hydrophobic silica nanopowder gave superior results in terms of clarity of ridges and an image's resolution. The hydrophobic and luminescent properties of silica nanopowders allowed for obtaining good images of aged fingermarks under UV light excitation. Both hydrophobic silica nanopowder and fluorescent platinum-complex modified silica nanopowder, with an average size of 135 ± 10 nm, gave comparable results of fingermark development to commercial grey or black powder. In addition, lower background staining caused by the examined silica NPs was observed.

The polyvinylpyrrolidone (PVP)-coated silica nanoparticles, with fluorescent Pigment Red 254 (PR254) dye incorporated, for fingermark enhancement have been proposed by Kim and co-workers [200]. In this study, the sebaceous fingermarks deposited on a hydrophilic surface such as glass and hydrophobic surface such as polystyrene were powder dusted by the fluorescent silica nanoparticles (PR254@SiO_2@PVP), with an average size of 95.2 nm. The PVP surface modification was to improve the binding affinity of PR254@SiO_2@PVP to fingermark deposit. Well-defined ridge flow and second level of ridge details have been observed on fingermarks on both substrates. Due to the amphiphilic property of PVP, such as the ability to bind with hydrophilic molecules by polar amide group and interact with proteins by nonpolar methylene and methine groups in the backbone, the PR254@SiO_2@PVP nanoparticles indicated higher sensitivity and developed fingermark with better contrast than those not modified with PVP. Another amphiphilic silica nanoparticles have been introduced by Huang and co-workers [201]. However, obtained silica particles had an average size of 250, 550, 700 nm before further surface modification with 4-(chloromethyl) phenyltrichlorosilane. They investigated the particle size and the mass ratio of SiO_2: 4-(chloromethyl) phenyltrichlorosilane as the factors that affected fingermark detection. Three hundred latent sebaceous-rich fingermarks, fresh and 7-days-aged deposited on glass, were powder dusted with amphiphilic silica particles. The best results were obtained for the largest particles (700 nm) and SiO_2: 4-(chloromethyl) phenyltrichlorosilane mass ratio equal to 50:1. However, only a few images of developed fingermark have been reported (one image for each examined mass ratio of SiO_2 to 4-(chloromethyl) phenyltrichlorosilane), and no statistical analysis was performed on the developed fingermarks.

As a matrix for upconversion luminophore used for fingermark enhancement, silica nanoparticles have been described by Wang et al. [202]. The sodium yttrium fluoride ($NaYF_4$) crystals with the shape of nanodumbbell have been coated with silica and applied as a developing agent for sebaceous-rich fingermarks deposited on coins, plastics, paper and glass. The signal of the $NaYF_4$@SiO_2

nanodumbbells-developed fingermarks has been collected under 980 nm light illumination. The good fingermark images with several ridge details have been obtained for powdering fingermarks on glass, coin and polystyrene. Fingermarks deposited on a white plastic bag and packaging paper have been developed with both $NaYF_4$@SiO_2 nanodumbbells and commercial luminescent fingermark powder. No clear fingermark ridges have been observed, and strong background fluorescence has been noticed for fingermark on paper and plastic bag developed with commercial powder when illuminated with UV light. Whereas, for fingermarks enhanced with $NaYF_4$@SiO_2, the background interference was eliminated due to infrared illumination, which excited neither paper nor white plastic bag.

Yang et al. [203] introduced a red-emissive conjugated oligomer incorporated into the silica nanoparticles with an enhanced affinity toward fingermark deposits due to surface modification with hydroxy, amino or epoxy groups. The fluorescent silica nanopowder developed fingermarks with high resolution and high level of ridge details, yielding an intense red fluorescence under excitation with 365 nm light. Epoxy-modified fluorescent silica nanoparticles, with an average size of 20 nm, show superior affinity to sebaceous-rich fingermarks deposited on each examined surface, e.g. stainless steel, coloured paper, newspaper, glass, package, leaf. The fluorescent silica NPs indicated high sensitivity when applied to overlapped fingermarks deposited on glass resulted in clear ridge impressions. Interesting research on silica nanoparticles' application for fingermark development has been proposed by Aisyiyah and co-workers [204]. With an average diameter of 20-30 nm, silica nanoparticles were recycled from geothermal power plants' wastes and further modified with rhodamine 6G. Sebaceous-rich and fresh fingermarks were involved in the study. Fingermarks deposited on glass, aluminium foil, and polyurethane surface developed with rhodamine-modified silica NPs and imaged under UV light illumination have shown high contrast and distinguishable ridge details; however, development of the fingermark deposited on acrylic surface resulted in low contrast and strong background interference.

A few research on luminescent carbon and silica-based nanomaterials applied for fingermark detection have been reported. Li and co-workers [205] synthesised blue-emitting carbon and silica nanohybrids (SiCNHs) by carbonising sodium citrate and organosilane in hydrothermal method. SiCNHs powder, with an average size of 100 nm, has been applied to develop the sebaceous-rich fingermarks deposited on marbles, painted wood, white ceramic tiles, black plastic bags, stainless steel, transparent tape, fruits and colourful drink bottles. The SiCNHs performed well on each of the examined surfaces; the second level of ridge details have been visualised; however, no comparative assessment has been done involving natural

fingermarks. A carbogenically coated silica nanoparticle powders (C-SiO_2) for fingermark development have been described by Fernandes et al. [206]. The C-SiO_2 nanoparticles, applied as a luminescent developing agent for charged sebaceous fingermarks on non-porous surfaces, yielded a good quality fingermark impression. Compared to standard white fingermark powder, significantly more minutiae were found on fingermarks enhanced with C-SiO_2 nanoparticles, and no background interference was noticed. Also, C-SiO_2 NPs indicated colour-tunability, emitting in a blue, green and red region of the visible light spectrum when illuminated with violet, blue and green light, respectively. Zhao et al. [207] also reported a powder for fingermark detection with tunable fluorescence. The mesoporous carbon dot silica microspheres (CDs/SiO_2), with an average size from 84 to 190 nm, were obtained by a citric acid pyrolysis process. Natural fingermarks, fresh and aged up to 60 days, deposited on aluminium foil, glass, leather, drug packing, and plastic bags developed with CDs/SiO_2 powder yielded a good fingermark contrast, low background staining, and high level of ridge details. Compared with commercial fluorescent powder, CDs/SiO_2 performed more effectively, with minor background staining, higher sensitivity and more ridge details. Moreover, CDs/SiO_2 powder emitted tunable fluorescence, depending on an irradiation wavelength of light, which made this material more advantageous on multicoloured and patterned surfaces in particular. Carbon dots dispersed in a silica matrix (C-dots@SiO_2) synthesised by microwave irradiation were proposed by Chen and Liu [208]. Fingermarks, fresh and aged, deposited on aluminium foil, ceramic tile, glass, coloured leaflet, yuan banknote, envelope and ticket, powdered with C-dots@SiO_2 nanoparticles with an average size of 34 nm, performed good and with low background staining on both porous and non-porous surfaces. Furthermore, on porous surfaces like a banknote, even sweat pores can be visible. C-dots@SiO_2 nanoparticles used for fingermark development on aluminium foil yielded equally high-quality ridge impressions comparing to conventional fluorescent powder. Whereas fingermarks deposited on the colourful leaflet, envelope and ticket have been developed by C-dots@SiO_2 NPs with better contrast, resolution and lower background staining than fingermarks powdered by a conventional fluorescent magnetic powder. Also, many more minutiae have been recognised on the fingermark enhanced by C-dots@SiO_2 NPs.

Some research on nanophosphorous material has been reported by Saif [209]. Eu^{3+} or Tb^{3+} ion-doped yttrium zirconate embedded in a silica matrix (EuYZS and TbYZS) has been considered as a fingermark development agent due to their longest lifetimes and high intense red and green luminescence, respectively. Among the fingermarks deposited on a glass slide, compact disc, plastic bag, aluminium foil and developed with either EuYZS or TbYZS nano-phosphors, only those deposited on

the glass slide exhibited clear ridge details and good contrast under UV light irradiation. Lower contrast of fingermark was observed for the aluminium foil substrate, and EuYZS developed fingermark in particular. The contrast of fingermark and ridge details were of poor quality for fingermarks deposited on compact disk and plastic bag. In another research of nano-phosphors, Saif et al. [210] concentrated on lanthanum titanate doped with europium ions also embedded in a silica matrix. In the case of this nanophosphor, again, the best contrast and ridge clearness under UV light illumination was obtained for fingermarks deposited on glass and aluminium foil, whereas on compact disc or plastic surface, the impressions of fingermarks were weak. Additionally, background staining was observed on plastic substrates.

Bifunctional fluorescent-magnetic nanoparticles of 30 nm size, prepared by linking amino-modified silica-coated iron (II, III) oxide with glutathione-modified CdTe quantum dots (CdTe-GSH QDs) were reported by Wang et al. [211] as a developing agent. The charged sebaceous fingermarks deposited on leather, banknote, black paper, plastic, ceramic and glass were powder dusted with magnetic-fluorescent nanopowder and imaged under 375 nm excitation light. Compared to pure glutathione-modified CdTe QDs or pure Fe_3O_4 NPs, the investigated nanopowder indicated the superior quality of the fingermark with a higher number of ridge details and much less background staining due to the magnetic properties of the nanopowder, which the magnetic wand can easily remove. However, no clear ridges were observed on the developed fingermark deposited on leather. Also, no comparative assessment has been done to a benchmark method on natural fingermarks. Wei and Cui [212] investigated dendritic mesoporous silica nanospheres (KCC-1) as carriers for Au NPs in development powder. The average size of the composite was 315 nm. Au@KCC-1 composites applied to sebaceous fingermarks deposited on paper, cardboard, plastic, glass, compact discs indicated sufficient selectivity and sensitivity due to a good monodispersity of relatively small size of particles. Compared with commercial gold and silver powders, Au@KCC-1 composites yielded a higher contrast of fingermark ridges and significantly lower background staining. Besides, the second and third levels of detail could have been observed on the 6-months-aged fingermark developed with Au@KCC-1 composites.

Previously mentioned mesoporous silica nanoparticles dye-loaded with methylene blue reported by Zhang et al. [194] have also been applied as a powder for fingermark detection. Bare MSNs, MSN@MB, and methyl-coated MSNs-TMS@MB were powder dusted on sebaceous-rich fingermarks deposited on glass, metal surface, plastic and papery shell of a notebook. The results of the powder dusting method were superior to MSN@MB aqueous suspension fingermark

treatment. MSNs surface modification with methyl moieties resulted in worse fingermark development and weaker fingermark impression. On the other side, powder dusting with MSN@MB yielded better contrast, good resolution and selectivity.

The formerly-mentioned research conducted by Abdelwahab et al. [192] concerning the encapsulation of the butenamine derivative of fluorescein isothiocyanate in silica nanoparticles with phenyl-functionalised shell also involved powder dusting fingermarks with fluorescent silica nanoparticles. Applying the developing agent on fingermarks deposited on glass, polystyrene Petri dish, aluminium foil resulted in good fingermark enhancement with the second level of ridge details. Nevertheless, powder dusting failed on porous surfaces like white paper or currency paper, where no clear ridges were obtained.

Silica nanoparticles have also been applied as an enhancing matrix in detecting the illicit drugs in fingermark deposits using surface assisted laser desorption/ionisation time-of-flight mass spectrometry (SALDI-TOF-MS). Rowell and co-workers [213] reported the application of carbon black embedded hydrophobic silica particles to enhance the SALDI signal of illicit drugs like cocaine, diacetylmorphine, codeine or methadone in a fingermark deposited on steel or lifted by a tape. Among 19 commercial dusting powders, only three – black, green, and white powder – rendered to be effective. However, new hydrophobic carbon black-silica particles have shown a superior SALDI performance on codeine recognition in fingermark directly deposited and on diacetylmorphine recognition in lifted fingermark. Furthermore, the excreted drugs can be detected in the pre-dusted lifted mark, and their distribution can be visualised over the surface of the fingermark. Further research in this field was conducted by Lim and Seviour [214]. They analysed the detection of terbinafine – an anti-fungal medicine – in lifted fingermarks of the treated person within 14 days. Fingermarks were enhanced by powder dusting with the magnetic phenyl-functionalised silica nanoparticles with embedded carbon black. SALDI-TOF-MS spectra and images exhibited an increase in terbinafine signal intensity and signal-to-noise ratio from day 0 to day 14. Moreover, the hydrophobic silica nanoparticles performed better than commercially available 2,5-dihydroxybenzoic acid applied as a matrix for terbinafine MS analysis. Lim et al. [215] has also investigated the use of SALDI-MS and direct analysis in real-time mass spectrometry (DART-MS) to recognise several other drugs like heroin, methadone, nicotine, and noscapine in fingermark residue. Fingermarks deposited on ceramic tile, wood laminate, non-sticky side of adhesive tape, glass, and steel were powder dusted with carbon black-silica particles. The signals from illicit drugs, present in lifted fingermarks, were not distinguished from the complex background in

DART-MS; however, the signals of non-lifted fingermarks on the glass probe were successfully detected.

1.5.4 Quantum dots

Strong luminescence at room temperature depending on the size of a nanoparticle, a broad excitation spectrum in the ultraviolet region of light and an easy-tunable surface are the properties that have bought a general interest in quantum dots application for fingermark development [82]. Several of the reported forensic applications of QDs are to deposit the material in powder due to the quick and easy treatment process. However, safety hazards concerning airborne QDs nanoparticles' inhalation have been discussed, involving cadmium QDs in particular. An application of QDs powder as a liquid or even aqueous suspension would have been more secure and eliminate the risk of inhalation of the airborne particles [82], [216], [217].

Quantum dots in a carrier solution

Sametband and co-workers [155] used cadmium selenide quantum dots (CdSe QDs) coated with zinc sulfide (ZnS) shell, stabilised by n-alkeneamine and dispersed in petroleum ether to detect sebaceous fingermarks deposited on silicon wafers and paper. Fingermarks on silicon wafers were successfully developed and visualised under UV light illumination, whereas fingermarks on paper were impossible to image due to the paper background's strong fluorescence. Becue et al. [218] proposed cadmium telluride quantum dots (CdTe QDs), stabilised with thioglycolic acid (TGA) as a highly luminescent and sensitive developing agent for aged bloody fingermarks deposited on non-porous surfaces such as aluminium foil, glass, black and transparent polyethylene. Fingermarks developed in an aqueous suspension of CdTe QDs were successfully enhanced, yielded well-defined green fluorescent ridge impressions without background development. Compared with Acid Yellow 7 dye, an efficient blood reagent, CdTe QDs performed better on fingermarks deposited on aluminium foil and with equal quality on polyethylene, polypropylene and glass surfaces. Instead of toxic cadmium presence in CdTe QDs, Moret et al. [219] reported another luminescent developing agent for bloody fingermarks based on ZnS QDs coated with copper (ZnS:Cu). Fingermarks, also deposited on non-porous surfaces such as aluminium foil, glass, black and transparent polyethylene, were successfully enhanced, resulting in blue-green fluorescent ridge impressions. Compared to Acid Yellow 7, the ZnS:Cu QDs

performed better in terms of ridge quality. Comparing to CdTe QDs previously used as a developer, ZnS:Cu QDs gave comparable results; however, the examined QDs were less toxic than cadmium based ones. Multicoloured CdTe QDs stabilised with thioglycolic acid have also been examined by Liu and co-workers [220] as a potential development agent for latent fingermarks. Applying different refluxing time during the synthesis resulted in a range of CdTe QDs with an average size from 1.5 to 3 nm and thereby with various colours of fluorescence emission under UV excitation (from green to orange). The surface modification of CdTe QDs with TGA, rich in carboxyl groups, enhanced the selective interaction with fingermark. This was due to the presence of amine groups in deposits, yielding a good contrast of fingermark deposited on a transparent adhesive tape placed on a coloured surface. However, no fingermark type and age details have been reported, and no comparative assessment has been done. Other fluorescent CdTe QDs stabilised with TGA for fingermark development have been widely investigated by Yang et al. [221]. They examined the development efficiency of sebaceous fingermarks on adhesive surfaces like cellulose paper, yellow sealing tape and black electrical tape depending on the temperature of processing, pH of the working suspension and deposition time. Compared to the benchmark rhodamine 6G staining method, applying TGA-CdTe QDs for fingermark enhancement resulted in better ridge contrast and greater fluorescence intensity.

Further investigation on CdTe QDs capped with mercaptosuccinic acid (MSA) for superfast fingermark detection on non-porous surfaces such as aluminium foil, stainless steel, transparent tape, and adhesive tape have been studied by Cai and co-workers [222]. The best quality of sebaceous fingermark developed by MSA-CdTe QDs suspension was obtained for optimised pH in the range of 9-10. Compared with benchmark techniques such as methyl violet or rhodamine 6G staining, MSA-CdTe QDs, yielded a high green fluorescence under UV light illumination, performed better sensitivity and quality of the fingermark ridges. This approach was also reported by Yu et al. [223]. They investigated the application of MSA-CdTe QDs, with an average size of 3-4 nm, to detect fingermarks deposited on aluminium alloy, tinfoil, stainless steel, scotch tape, black tape, and the adhesive side of the yellow tape. Compared to cyanoacrylate/rhodamine 6G or gentian violet methods, CdTe/MSA QDs performed better on aluminium alloy and the adhesive side of the tape in terms of a clear ridge contrast and less background interference. Gao et al. [224], in turn, reported positively charged quantum dots CdTe-$COONH_3NH_3^+$ as a fluorescent development agent for sebaceous fingermarks deposited on polymer surfaces, glass, transparent polypropylene, marble or aluminium foil. Due to the electrostatic interactions between positively charged QDs and negatively charged amino acids

present in fingermark deposits, the well-defined fingermark ridges have been obtained in the basic pH of working suspension. However, the quality of developed fingermark has not been compared with benchmark methods.

CdTe QDs capped with N-acetylcysteine (N-L-Cys) for eccrine fingermark detection, and analysis of 2nd and 3rd level ridge details was reported by Li et al. [225]. The red-emitting CdTe QDs capped with N-L-Cys, with an average size of 3.77 nm, to effectively visualising 2nd and 3rd level ridge characteristics proved to be superior to a benchmark cyanoacrylate fuming or ink. Applying the solution of CdTe QDs capped with N-L-Cys for fingermarks indicated higher accuracy for mapping the sweat pores; however, no information on the type of substrates used or fingermarks age has been given. N-acetylcysteine, as a capping ligand, was also investigated by Xu et al. [226] for manganese-doped zinc sulfide quantum dots (Mn-ZnS QDs) surface-modified with amine, carboxyl or acetyl moieties. Similarly, the 2nd and 3rd level of ridge details in fresh and aged eccrine fingermarks have been examined on non-porous surfaces like glass, compact discs, aluminium foil or plastic bags. The good and reproducible quality of fingermark imaging, the 3rd level of details like sweat pores and sufficient contrast between the background and the fingermark was obtained with carboxyl-terminated N-L-Cys Mn-ZnS QDs nanocomposite. Shahbazi et al. [227] proposed core-shell quantum dots composed of copper indium sulfide and zinc sulfide coating ($CuIS_2$/ZnS QDs) stabilised with N-acetylcysteine, indicating red to NIR photoluminescence. Glass, aluminium, black tape, sticky side of adhesive tape, zip-lock bag or highly patterned polymer banknote have been investigated. Natural and charged fingermarks, developed by immersion in the QDs aqueous suspension, yielded a good quality of ridges and high levels of fingermark details. Due to the broad range of excitation wavelengths, resulting in the red to NIR wavelength luminescence emission, some luminescent security features or multicoloured patterns on substrates can be eliminated.

Cui et al. [228] have used the bifunctional nanocomposite consisted of copper sulfide nanoparticles (Cu_7S_4 NPs) and CdSe@ZnS QDs to detect TNT in the latent fingermark deposits on the sticky side of the tape and image the fingermark ridges. The Cu_7S_4-CdSe@ZnS nanocomposite functionalised with amine moieties and deposited on sebaceous fingermarks were able to concurrently image the ridges with the photothermal effect when continuously illuminated with 808 nm wavelength of light and detect TNT molecules leading to the Cu_7S_4-CdSe@ZnS fluorescence quenching. The quenching effect is due to the acid-base pair between the TNT electron-deficient aromatic ring and electron-rich amine moieties on the nanocomposite. Applying the NIR light-responsive photothermal nanocomposite can significantly decrease the background interference yielding a high contrast of latent

fingermark impression. Another approach to TNT detection in fingermark deposits was reported by Wu and co-workers [229]. A dual-emitting nanohybrid consisted of red-emitting zinc cadmium sulfide doped with copper (Cu-ZnCdS), embedded in silica matrix, coated with green-emitting ZnCdS QDs and further functionalised with polyallylamine (PAA), was applied for sebaceous fingermark development and TNT visualisation. The “traffic light” type of nanohybrid performed the red colour fluorescence when PAA form a complex with TNT present in the fingermark. The fluorescence of green-emitting QDs was quenched then. For fingermarks not marked with TNT, the developed ridges performed green fluorescence impressions. CdSe QDS stabilised with TGA and surface coated with cadmium sulfide CdS for sebaceous fingermark detection on adhesive substrates were reported by Wang and co-workers [230]. In the research, several factors influencing the fluorescence intensity, such as pH, the concentration of cadmium ions, shell structure, and stabiliser effect, have been investigated. The CdS shell structure significantly increased the contrast of the fingermark, and less background staining was observed. However, no comparison with benchmark methods of fingermark development has been performed. Another cadmium selenide QDs for a forensic application has been proposed by Na Ayudhaya et al. [231]. CdSe QDs stabilised with starch were synthesised at different pH conditions, resulting in various nanoparticle sizes from 4.6 to 7.5 nm and various maximum fluorescence emission wavelengths associated with the QD size. CdSe QDs enhanced somewhat the sebaceous fingermarks deposited on porous and non-porous surfaces; however, the results were not compared to the well-established techniques.

Chen et al. [232] proposed a ninhydrin-embedded NIR fluorescent semiconducting polymer dots (P dots), functionalised with various moieties like carboxyl, thiol or hydroxyl groups, for sebaceous fingermarks enhancement deposited on non-porous (aluminium foil, glass, acrylic sheet, plastic bag) and porous (coloured and printing paper) substrates. For porous surfaces, the fluorescent P dots suspension in acetone was sprayed over the sample. For non-porous substrates, the water-based suspension was used for immersion of the samples. Due to ninhydrin's presence, the samples had to be heated at 60 °C to be visible by the naked eye under white light excitation. The fluorescent P dots modified with carboxyl groups performed the best on all examined surfaces, yielding a high contrast, high levels of ridge details, low background interference and high fluorescence brightness. The P dots alone emit the NIR light, invisible to the naked eye. Whereas the emission of the P dots deposited on the fingermark ridges was blue-shifted, resulting in a strong red emission, enhancing the fingermark contrast. Jia and co-workers [233] applied quantum dots based on boron carbon oxynitride (BCON) as a luminescent developer

for fingermarks deposited on a banknote. The BCON QDs were synthesised in the template of mesoporous silica SBA-15, which was then removed by hydrofluoric acid. To identify the efficiency in fingermark visualisation, the BCON QDs stabilised by polyvinylpyrrolidone (PVP) in water were smeared on the finger, then touch the banknote to leave the finger' ridge impressions and observe the QDs luminescence under UV excitation. Nevertheless, the developing agent was examined only for one substrate type; no results of comparable methods were presented.

Dilag and co-workers [234] synthesised a fluorescent nanocomposite of cadmium sulfide quantum dots (CdS QDs) in a polymer matrix of polydimethylacrylamide (p(DMA)). They examined QDs as the development agent for fresh and aged latent fingermarks on non-porous surfaces (glass, aluminium foil). As a result, CdS QDs/p(DMA) covered the whole area of fingermark and background in the case of fresh fingermarks, rendering the ridge details impossible to distinguish. Once the fingermark sample was aged, the contrast between the ridges and the substrate has improved due to the degradation and evaporation of some fingermark residue components and make the fingermark less subjected to solubilisation when in contact with water suspension of the nanocomposite. Jin and co-workers reported several applications of CdS QDs embedded inside polyamidoamine dendrimers (PAMAM) for fingermark detection. In the first approach, photoluminescent CdS QDs in the PAMAM structure were applied to enhance sebaceous and fresh fingermarks deposited on tinfoil and priorly fumed with cyanoacrylate esters [235]. Amino-terminated PAMAM dendrimers react with cyanoacrylate-fumed fingermark deposits rich in carboxylic esters, yielding a high selectivity and significant contrast increase between mark and background. In further research, a powder suspension of CdS QDs in PAMAM dendrimers was applied to detect the sebaceous and aged fingermarks deposited on adhesive tape [236]. The yellow-emitting CdS QDs in PAMAM nanocomposite indicated significantly better selectivity, sensitivity and contrast on aged fingermark than commercial TiO_2 powder suspension. The fluorescence of CdS QDs/PAMAM decreased with the increase of ageing time due to degradation and volatilisation of the residue compound by heat and light. Jin and co-workers [237] also investigated the influence of several metallic ions on CdS QDs/PAMAM photoluminescence properties. Sebaceous and fresh fingermarks deposited on tin foil were examined. It was found that both Cd^{2+} and Zn^{2+} ions increase the CdS QDs/PAMAM photoluminescence, increasing the contrast and resolution of the fingermark image. Dong et al. [238] proposed CdTe QDs self-assembled on the silica nanobead carriers covered with SiO_2 shell to avoid the toxic cadmium leakage and further modified with either amine or carboxyl groups to interact preferentially with fingermark deposits. The SiO_2–CdTe@SiO_2–COOH

nanostructures exhibited strong fluorescence in the green to red region of visible light, enabling eliminating background interference by filtering out the luminescence of the fingermark. Unfortunately, no information concerning the type and age of fingermarks have been given in this research, and no benchmark assessment have been included.

Quantum dots powders

Dilag and co-workers [239] reported highly fluorescent CdS QDs embedded in a chitosan matrix employed to develop latent fingermarks deposited on aluminium foil. CdS/chitosan nanocomposite was applied on fingermarks in the form of powder, produced in a freeze-drying process of the nanocomposite, and tergitol suspension. Sebaceous fingermarks, powder dusted with CdS/chitosan, yielded fluorescent fingermark ridge impressions under the illumination of 450 nm light. However, compared to commercial white powder or aluminium powder, less powder adhered to the fingermark ridges resulting in a lower resolution. The reason was found in the size of freeze-dried CdS/chitosan particulates, which was bigger than the size of commercial powders 1-10 μm. The same research group investigated also the fluorescent nanocomposite of CdS QDs in a polymer matrix of poly(dimethylacrylamide-co-methyl methacrylate) (p(DMA-co-MMA)) and poly(dimethyl- acrylamide-co-styrene) (p(DMA-co-Sty) [234]. The examined CdS QDs/p(DMA-co-MMA) and CdS QDs/p(DMA-co-Sty), used for powder-based development for fresh and aged latent fingermarks on glass and aluminium foil, performed significantly better on all fingermark samples than previously-described CdS QDs/p(DMA) aqueous suspension. The powders adhered effectively to the fingermark ridges and could have been successfully visualised under UV illumination.

Another highly fluorescent hybrid composite based on thiol-functionalised CdSe QDs in porous phosphate heterostructures (PPH-S-CdSe) for fingermark detection have been reported by Algarra et al. [240]. Sebaceous fingermarks were deposited on a series of porous and non-porous substrates, e.g. silica gel, wood handle, polymeric credit card, polymeric tweezers, glass screen mobile phone, aluminium foil and crystal glass, have been powder dusted with PPH-S-CdSe composite and imaged under UV light illumination. Good results and clear contrast were obtained for porous surfaces. The recorded fluorescence from the PPH-S-CdSe composite on most substrates was not very high; however, ridge details could have been distinguished. This composite was further optimised by Algarra and co-workers [241] by intercalation CdSe QDs in the PPH modified with amine moieties (PPH-NH_2@CdSe). PPH-NH_2@CdSe was further used for powder dusting the

sebaceous fingermarks deposited on non-porous surfaces (credit card, glass screen of mobile phone, steel tweezers, polymer banknote). The quality of fingermark ridges was high, and most of the details were able to be identified. Moreover, the suitability of 8 to 12 point of correspondences between fingermarks enhanced by PPH-NH_2@CdSe nanocomposite and well-known fingerprints have been evaluated. Applying PPH-NH_2@CdSe as a developing agent and further enhancing contrast resulted in an increasing number of positive matches between the analysed samples.

Cadmium telluride quantum dots intercalated into the montmorillonite clay matrix have been used by Gao et al. [242] as a fluorescent labelling marker for fingermark detection due to the good stability, optical and adhesive properties of this nanocomposite. The sebaceous fingermarks deposited on glass, polymer, painted wood and leather have been powder dusted and imaged under UV irradiation. A good contrast of fingermark has been obtained with well-defined ridge details, and no background development was observed in comparison to the commercial fluorescent labelling marker presented in the research. Gao and co-workers further investigated the potential of CdTe QDs for fingermark detection. They proposed a core-shell structure of CdTe QDs coated with silica (CdTe@SiO_2) [243]. Sebaceous fingermarks deposited on paper, aluminium, glass, polymer, marble and rubber were powder dusted with CdTe@SiO_2 and compared with fingermarks detected with commercial fluorescent powder, silver powder, and ninhydrin powder. CdTe@SiO_2 indicated good sensitivity and strong adhesion to the fingermark deposits resulting in better resolution and contrast of fingermark ridges. Niu et al. [244] also investigated CdTe QDs incorporated into the silica matrix; however, silver nanoparticles were additionally uniformly dispersed on the surface of the nanocomposite (CdTe@SiO_2/Ag) to obtain the antibacterial property of the material in case the need for long-term preservation of fingermark for further identification. The sebaceous fingermarks deposited on white ceramic, agate, plastic film and strip, glass, aluminium foil were investigated. Most of the fingermarks were successfully developed with CdTe@SiO_2/Ag, resulting in well-defined ridge details, highly fluorescent fingermark impressions and low background staining. A better resolution was obtained for CdTe@SiO_2/Ag nanocomposite than commercially available powders such as silver powder. Singh and co-workers [245] proposed CdTe QDs capped with mercaptopropionic acid (MPA) in the microwave irradiation synthesis as a luminescent powder for fingermark detection. The sebaceous fingermarks deposited on glass and black tape have been powdered with MPA capped CdTe QDs resulting in sufficient ridge details; nevertheless, background staining was observed, and no comparative assessment was proposed in the research.

1.5.5 Upconverting nanoparticles

A number of fingermark development and visualisation approaches concern using upconverting nanoparticles (UCNPs) with the optical properties facilitating imaging of the fingermark deposited on patterned and multicoloured substrates. This is due to the fact that not many materials and everyday-use items emit visible light when exposed to infrared or visible light. In contrast, they usually absorb IR light leading to an increase in contrast between the UCNPs developed fingermark and the background [217]. Similarly to quantum dots application, the UCNPs for fingermark development are used mainly in powder form than powder suspension, which may cause severe health and safety risk for a crime scene operator [216].

Powder upconverters

Zhao et al. [246] reported a simultaneous latent fingermark imaging and nicotine traces detection in the fingermark deposits by thulium-doped sodium yttrium fluoride upconverting nanoparticles ($NaYF_4$:Yb/Tm UCNPs) and iodine fuming process. The Tm-doped UCNPs convert NIR light illumination radiation to 345 nm and 361 nm UV light emission and 450 nm and 475 nm blue light emission in the upconversion mechanism. The complexes of nicotine and iodine absorb the blue light, whereas neither nicotine nor iodine itself does. In the presence of nicotine, the fluorescence intensity of the UCNPs-developed fingermarks fumed with iodine decreases and can be quantified by the fluorescence intensity change. The charged sebaceous fingermarks have been collected on a series of substrates such as glass, plastic card, paper, aluminium foil, and porous foam board. The small UCNPs with an average size of 28 nm, powder dusted on the fingermarks, performed best with a good fingermark contrast, high sensitivity and second and third level ridge details, mainly on smooth surfaces. The multicoloured and patterned substrates interfered with the fingermark ridge impressions. Also, no comparative treatment process with a benchmark method has been done. The nicotine traces in fingermark deposits were calculated with the MATLAB software based on the fluorescence intensity change of the fingermark images.

Wang and co-workers [247], [248] proposed the nano-sized $NaYF_4$:Yb,Er UCNPs with strong NIR-induced green fluorescence for fingermark detection on a series of surfaces like glass, marble, leather, ceramic tile, aluminium foil, stainless steel, wood, papers. Sebaceous-rich fingermarks have been powder dusted with $NaYF_4$:Yb,Er UCNPs of average size between 62 and 89 nm. Clear and well-defined fingermark ridges with a high level of ridge details and no observed background

interference have been reported for all kinds of examined surfaces, even on porous paper substrates. However, on colourful and patterned porous surfaces, the background interference was slightly observable. The influence of background interference has also been determined by developing fingermarks deposited on a variety of types of patterned marble. The NIR light illumination of developed fingermarks yielded well-defined fingermark ridges, no background interference or colour disruption. A wide comparative assessment has been done between $NaYF_4$:Yb,Er UCNPs and other developing powders. Fingermarks deposited on marbles were developed either with $NaYF_4$:Yb,Er UCNPs or with magnetic iron oxide powder, TiO_2 powder and commercial fluorescent powder. As a result, more effective enhancement was observed for $NaYF_4$:Yb,Er UCNPs in terms of ridge edge sharpness and high resolution. Additionally, fingermarks were also powdered by micron-size $NaYF_4$:Yb,Er upconverter to determine the sensitivity of examined $NaYF_4$:Yb,Er UCNPs. As a result, more ridge details such as sweat pores have been observed on fingermarks developed with a nano-size $NaYF_4$:Yb,Er powder.

The fluorescent upconversion nanorods of erbium and gadolinium-doped sodium yttrium fluoride NPs ($NaYF_4$:Yb,Er,Gd NPs) for blood fingermarks have been described by Li et al. [249]. Fingermarks deposited on non-porous surfaces like marble, glass, ceramic tile, aluminium foil and steel sheet, and paper porous substrates have been imaged under 980 nm light illumination. To test the sensitivity of the $NaYF_4$:Yb,Er,Gd NPs, a series of fingermark enhancement with various blood dilution have been processed. As a result, for all investigated surfaces, green fluorescent fingermark ridges of blood fingermarks, with no background interference, were observed for most blood dilutions. However, for the 100 times diluted blood, the fingermark on coin and paper ticket was noticeably less enhanced with no clear ridges. The $NaYF_4$:Yb,Er,Gd NPs powdered fingermarks compared to the fingermarks developed with a commercial reagent for blood fingermarks - fluorescent Acid Yellow 7 (AY7) exhibited higher sensitivity, better contrast, and no background interference, in comparison to AY7 enhanced fingermarks deposited on ceramic tile, marble and magazine cover.

Wang and co-workers [250] proposed a thulium-doped $NaYbF_4$:Tm UCNPs for dual-mode fingermark visualisation. $NaYbF_4$:Tm UCNPs excited with 980 nm light showed strong NIR emission of light with a maximum at 800 nm and strong visible light emission with a maximum at 475 nm. The contrast between the fingermark ridges and the background was examined for $NaYbF_4$:Tm UCNPs powdered fingermarks deposited on stainless steel, marble, red fluorescent paper and paper money. The imaging process was taken either under NIR-to-VIS mode using a 750 nm short-pass filter to block 800 nm light emission and enable passing the blue light

emission or under NIR-to-NIR mode using an 800 nm band-pass filter to register the emission of 800 nm light only. High contrast between $NaYbF_4$:Tm UCNPs developed fingermark ridges and the background was obtained for both modes of imaging; however, for NIR-to-VIS mode, no background interference was observed on colourful and pattern substrates, but high excitation power was required. In turn, for NIR-to-NIR mode, the light patterned surfaces interfered with a white impression of fingermark ridges, but the imaging can be conducted with a low excitation power. Xu et al. [251] proposed another dual-mode luminescent nanomaterial, composed of the upconversion fluorescent silica-coated Y_2O_3:Er^{3+},Yb^{3+} core and a down-conversion fluorescent shell based on gadolinium, europium and terbium hydroxides with an interlayer of pyromellitic acid (LGdEuTbH-PMA), which improve the luminescence intensity of the shell. The nanocomposite produced multicoloured fluorescence emission. Illuminated with 980 nm light nanocomposite emitted a bright red upconverted fluorescence. Irradiated with 254 nm UV light, a wide range of colour luminescence from green to red occurred, depending on the ratio of terbium and europium ions in the LGdEuTbH-PMA shell. The sebaceous-rich fingermarks, deposited on glass, plastic Petri dish, plastic bag, aluminium alloy, and ceramic tile, were powder dusted with nanocomposite and then visualised under 980 nm and 254 nm light excitation. No background staining was observed. Clear fingermark ridges and second and third level of details have been identified due to the good selectivity and sensitivity of the nanocomposite with an average size of 130 nm. However, no benchmark method of fingermark enhancement was proposed as well as no multicoloured and pattern surfaces have been investigated to examine the potential of the nanocomposite.

The holmium-activated $NaYF_4$:Ho^{3+} UCNPs have been introduced as a fingermark development powder by Du and co-workers [252]. The $NaYF_4$:Ho^{3+} UCNPs, of average size between 10 and 25 nm, exhibited bright green emission with a maximum at 540 nm and weak red fluorescence emission with a maximum at 646 nm, under 980 nm light excitation. $NaYF_4$:Ho^{3+} UCNPs were used to develop natural fingermarks deposited on glass, plastic and coin. Bright and clear luminescent impressions of fingermark ridges, with no background interference, were observed for examined surfaces; however, the ridge details were not clearly readable. NIR-to-NIR hexagonal thulium and ytterbium-doped sodium yttrium fluoride nanocrystals ($NaYF_4$:2%Tm,48%Yb) for latent fingermark visualisation have been evaluated by Baride and co-workers [253]. The $NaYF_4$:2%Tm,48%Yb nanocrystals demonstrated NIR luminescence emission with a maximum at 800 nm when illuminated with 976 nm light. The $NaYF_4$:2%Tm,48%Yb NPs were used as a developing powder for charged and fresh fingermarks deposited on colourful soft-

drink can. The performance of the $NaYF_4$:2%Tm,48%Yb UCNPs was compared with NIR-to-visible $NaYF_4$:2%Er,18%Yb UCNP of comparable size with a maximum emission at 540 nm. Developed fingermarks were visualised using either 850 nm short-pass filter to block excitation irradiation and 750 nm long-pass filter to collect NIR upconversion emission of the $NaYF_4$:2%Tm,48%Yb UCNPs or 475 nm long-pass and 575 nm short-pass filter to collect the green emission of NaYF4:2%Er,18%Yb UCNP selectively. High sensitivity, good selectivity and high level of ridge details of $NaYF_4$:2%Tm,48%Yb UCNPs have been observed with developed fingermarks. Also, background interference was greatly reduced. On the other hand, a high background interference was observed for fingermarks developed with NIR-to-VIS $NaYF_4$:2%Er,18%Yb UCNPs.

Mahata et al. [254] proposed terbium and erbium-doped yttrium orthovanadate nanocrystals (YVO_4:Er^{3+}/Yb^{3+}) with a potential forensic application. The 17 nm-size nanocrystals, excited with a UV light, have shown a green luminescence emission with a maximum at 527 and 555 nm. When illuminated with 980 nm light, the nanocrystals indicated strong green emission at 525 and 554 nm and weak red luminescence emission at 661 nm. However, as a fingermark development powder, the nanocrystallites were in the form of microdiscs. Only one example of a fingermark deposited on glass has been demonstrated. The first level of ridge details was observed, and no background interference was noticed. Nevertheless, no comparative method of fingermark enhancement was introduced.

Wang et al. [255] reported a core-shell-shell nanostructure to enhance the upconversion luminescence of sodium gadolinium fluoride NPs, with a possible application for fingermark development. The nanostructure was composed of $NaGdF_4$:Yb/Tm core, $NaGdF_4$ energy migratory interlayer to suppress the interfacial quenching between accumulator Tm^{3+} and the lanthanide activators (A), and $NaGdF_4$:A (A = Dy, Sm, Nd, Eu, Tb) as the outermost shell layer. The sebaceous-rich fingermarks were deposited on blank and photo paper, powder dusted with $NaGdF_4$:Yb/Tm@$NaGdF_4$@$NaGdF_4$:A (A = Eu, Tb), and imaged under 980 nm light excitation. The fingermark ridges were clearly visible with the first and second level of ridge details, such as termination or bifurcation. The nanostructures with Eu^{3+} and Tb^{3+} in the outermost layer exhibited longer upconversion luminescence lifetimes than Tm^{3+} in the core; hence, imaging the fingermarks in a time-gated mode, using a chopper with a synchronised speed at a specific frequency, resulted in the colour change of fingermarks. Tunable luminescence emission can be an advantage in the case of a coloured background. However, no fingermark development results on patterned and colourful substrates have been reported to examine the time-gated strategy thoroughly. Singh et al. [256] presented a nanophosphor material based on

gadolinium oxide codoped with ytterbium and erbium ($Gd_2O_3:Er^{3+},Yb^{3+}$) characterised by colour-tunable strong UV/VIS upconversion emission. Fingermarks, deposited on glass, metal surface and fresh leaf, were powder dusted with nanophosphor and imaged under 976 nm light illumination. Fingermark deposited on glass surface exhibited clearly readable first level ridge details with good contrast between the mark and the background. Red and green upconversion luminescence of the same fingermark was registered since the powder's main advantage was the variability in the luminescence emission colour, depending on the illuminating laser power. The low photon density excitation resulted in the domination of the energy transfer (ET) process. In contrast, the increase in photon density leads to excited-state absorption (ESA) process domination. However, no other results involving powder dusting with Gd2O3:Er^{3+},Yb^{3+} nanophosphor have been reported except for one fingermark image.

Zhou and co-workers [257] proposed a core-shell $mCu_{2-x}S@SiO_2@Y_2O_3:Yb^{3+}/Er^{3+}$ nanocomposite based on semi-conductor multi-copper sulfide nanoparticles randomly distributed in the silica matrix and then covered with a layer of $Y_2O_3:Yb^{3+}/Er^{3+}$. The $Cu_{2-x}S$ NPs plasmons enhanced the upconversion of the $mCu_{2-x}S@SiO_2@Y_2O_3:Yb^{3+}/Er^{3+}$ nanocomposite 30-fold in comparison to $SiO_2@Y_2O_3:Yb^{3+}/Er^{3+}$ composite, changing the red-to-green light emission ratio. The fingermark deposited on a paper substrate and developed with $mCu_{2-x}S@SiO_2@Y_2O_3:Yb^{3+}/Er^{3+}$ powder was further imaged under the illumination of 980 nm light. The obtained fingermark impression exhibit good contrast and resolution. The fingermark ridge brightness and luminescence colour were gradually changing from green to orange with an increased power density of the light source. However, no details concerning the type or age of fingermark were given. Only one type of substrate was introduced, and no comparison to benchmark methods have been provided.

Upconverters as a suspension

Wang [258] investigated the sodium yttrium fluorides doped with erbium, thulium or holmium ($NaYF_4$:Yb,Er/Tm/Ho) stabilised with sodium dodecyl sulfonate (SDS) as a NIR-responsive upconversion fluorescent material for sebaceous-rich fingermark detection on a multicoloured background. The comparative assessment has been done on selectivity, sensitivity and practicability between the $NaYF_4$:Yb,Er/Tm/Ho NPs and commercially available zinc oxide, ferric oxide and green fluorescent powder suspensions. Fingermarks deposited on plastic plates, developed with either zinc oxide or ferric oxide and imaged in white light

illumination, were of low contrast due to the multicoloured background. Applying green fluorescent powder suspension, the contrast of the fingermark, observed under 254 nm light illumination, was also disturbed by strong background luminescence. Using $NaYF_4$:Yb,Er/Tm/Ho NPs for fingermark staining allowed for eliminating background interference on several examined surfaces like steel, aluminium, ceramic tile, wood, marble, plastic card, glass, and banknote. Only strong green emission under 980 nm light excitation has been observed, yielding a good contrast of fingermark ridges. Also, due to the small size of $NaYF_4$:Yb,Er/Tm/Ho NPs, with an average diameter of 73 nm, the ridge details like sweat pores were observable, leading to increased sensitivity. Changing the Er, Tm and Ho dopants and their molar ratio in the upconverter structure resulted in a multicolour light emission under 980 nm illumination.

Antibody modified $NaYF_4$:Yb, Er, Gd fluorescent upconversion nanorods (UCNRs/anti-hHb) for specific recognition of haemoglobin in human blood fingermarks have been proposed by Liu et al. [259]. Small UCNRs/anti-hHb, with an average length of 96 nm, were used to develop blood fingermarks deposited on a variety of surfaces, e.g. steel, glass, optical disc, aluminium foil, wood, artificial leather, and magazine cover. The high sensitivity and affinity of the examined material to fingermarks containing human blood was manifested in obtaining second and third levels of ridge detail on most of the investigated substrates. Compared with Acid Yellow 7, stronger luminescence and lower background interference were obtained for fingermarks developed with UCNRs/anti-hHb on all considered surfaces. In the case of aged fingermarks, clear ridge details have been received for fingermarks aged up to 15 days, whereas for older fingermarks, e.g. up to 30 days, the fingermark ridges were noticed not as clear as for fresh fingermarks.

Wang and co-workers [1] have functionalised $NaYF_4$:Yb^{3+}/Er^{3+} UCNPs with lysozyme-binding aptamer (LBA) and cocaine-binding aptamer (CBA) to recognise the molecules of lysozyme or cocaine in the fingermark deposits and visualise mark impression. As a universal compound present in fingermark residue, lysozyme can increase the selectivity of photoluminescent material applied for fingermark detection. The CBA conjugated with UCNPs can improve the detection of cocaine traces in fingermark secretions and enhance the fingermark impressions. The sebaceous-rich fingermarks deposited on marble, glass, plastic, and coin were developed by covering the fingermark area with a drop of UCNPs suspension. Clear ridge details and bright luminescent impression of fingermark has been obtained for glass and a plastic substrate. However, the ridge details on the coin were less clear and readable. Nevertheless, compared to the formerly-mentioned LBA-functionalised CdTe QDs, the UCNPs performed with higher contrast and no

background interference. In the case of UCNPs-CBA, even a 0.1 µg cocaine-doped fingermark can be easily developed and recognised in the fingermark ridges.

Wang et al. [260] reported the application of europium, samarium, and manganese-doped calcium sulfide nanoparticles (ESM-CaS NPs), with an average size of 30 nm, as a luminescent developing agent for fingermark detection. Due to improved stability of dispersion in aqueous solution, suppress the fluorescence quenching, and support interactions with fingermark residue, the ESM-CaS NPs have been encapsulated by a 1-dodecanethiol (DT) and 11-mercaptoundecanoic acid (MUA), and then surface modified with arginine (Arg) to target amino acids in fingermark residue. For comparative purposes, the Yb, Er, Mn-doped sodium yttrium fluoride nanoparticles ($NaYF_4$:Yb,Er,Mn NPs) modified with 3-mercaptopropionic acid (MPA) and arginine have been developed. Fingermarks deposited on plastic, ceramic tile, and glass have been developed in an aqueous suspension of either Arg-DT/MUA@ESM-CaS NPs or Arg-MPA-$NaYF_4$:Yb,Er,Mn NPs. As a result, Arg-DT/MUA@ESM-CaS NPs developed fingermarks with higher contrast between ridges and substrate, higher selectivity and no background interference when imaged under 980 nm light excitation. In contrast, the image of fingermark developed with Arg-MPA-$NaYF_4$:Yb,Er,Mn NPs displayed a very weak upconversion luminescence and made the fingermark almost invisible.

Li et al. [261] described a latent and bloody fingermark development agent based on hierarchically structured citrate coated $NaYbF_4$:Tm@$NaYF_4$:Yb@$NaNdF_4$:Yb nanoparticles indicating dual modes of near-infrared emission (980 nm and 696 nm) under 808 nm excitation. $NaYbF_4$ host acted as a core to promote energy transfer to Tm^{3+}. The $NaYF_4$ shell doped with Yb^{3+} was to block the energy relaxation process from Tm^{3+} to Nd^{3+}. Finally, the second shell of $NaNdF_4$:Yb promoted energy transfer from Nd^{3+} to Yb^{3+}. Charged sebaceous latent and bloody fingermarks have been deposited on soft-drink labels as semi-porous substrates and polyethylene bags as non-porous substrate. For developed fingermarks on both substrates, the well-defined first and second level of ridge details have been observed for the Tm^{3+} upconversion luminescence at 696 nm and the Yb^{3+} Stokes emission at 980 nm under 808 nm excitation. In the case of blood fingermarks, the quenched upconversion emission at 696 nm in imaging mode was observed, while in Stokes emission imaging mode, the well-defined fingermark ridge details have been noticed. Blood fingermarks developed with a commercial reagent, Acid Yellow 7, yielded an inferior quality of fingermark image.

Infrared to visible upconversion fluorescence was also reported by Kumar and co-workers [262], who proposed gadolinium (III) oxide doped with holmium and ytterbium ions (Gd_2O_3:Ho^{3+}/Yb^{3+}) as a development agent. Gd_2O_3:Ho^{3+}/Yb^{3+}

nanoparticles, with an average size of 40 nm, were prepared in the form of powder suspension in hexane and sprayed upon the charged sebaceous fingermarks deposited on glass and aluminium foil. The examined phosphor exhibited strong green luminescence under 980 nm light illumination. A commercial green luminescent powder has been applied under 380 nm light excitation as a comparative developing agent. Fingermark developed with Gd_2O_3:Ho^{3+}/Yb^{3+} NPs and imaged under upconversion emission mode resulted in good contrast between the mark ridges and surface and clear and readable ridge pattern. On the other hand, fingermarks developed with commercial luminescent powder has shown lower contrast and less clear ridge flow. A strong background luminescence has been noticed on both surfaces, which significantly reduced the fingermark contrast.

1.6 Silicon dioxide nanoparticles

Silicon, one of the most abundant elements on earth, forms with an oxygen a water-insoluble silicon dioxide (SiO_2, silica), naturally existed in several polymorphic forms such as quartz, tridymite, cristobalite [263], coesite, stishovite or amorphous like opal [264] and exhibiting different characteristics and properties depending on its structure, composition, impurities and preparation [265]. The natural mineral silica occurs in crystalline form with metal impurities. Pure, nanosized silica for industrial or scientific applications, is produced in a synthetic way mostly as an amorphous powder in the form of silica gels, silica colloids, precipitated silica, or pyrogenic silica [263]. Common amorphous silica, in the form of gel, sol, powder or porous glass, mainly consists of spherical, less than micron size SiO_2 particles with a specific surface area greater than 3 m^2 g^{-1}. The particle surface consists of anhydrous SiO_2 or silanol groups (Si-OH) [266]. The structure of silica particles is based on randomly distributed tetrahedrons (SiO_4) with four oxygen atoms placed at the corners and silicon ion located in the centre of the cavity [264]. Each atom of oxygen is shared by two tetrahedra in silica [267], [268].

The use of silica nanoparticles (SiO_2 NPs) for forensic application has been widely studied in recent years. It has shown great potential as a developing agent for the detection of latent fingermarks [151]. The effectiveness of latent fingermark development with silica nanoparticles is due to its properties. The synthesis of silica particles is relatively easy. Organic dye molecules, luminescent metal, quantum dots can be entrapped within the silica matrix resulting in a broad range of optical properties [188], [269]. Also, the particles' surface can be functionalised due to the

presence of silanol groups on the outer shell of the particle, which may yield the interactions between the silica NPs and the fingermark constituents. This also may prevent the photo-decomposition of the dye-loaded particle [151].

Two main types of silicon dioxide nanoparticles can be distinguished: the solid silica NPs and mesoporous silica nanoparticles (MSNs). Both these types have the properties mentioned above; furthermore, solid SiO_2 NPs are photochemically stable, biocompatible and indicate colloidal properties. MSNs, in turn, have large pore volumes, adjustable pore sizes, and high surface area [265].

1.6.1 Synthesis processes

Silica nanoparticles can be synthesised by several methods, including hydrothermal method, chemical vapour deposition, plasma and combustion synthesis, sol-gel process [270], [271], or flame synthesis. The sol-gel method is broadly used to obtain the particles with controllable particle size, morphology, and size distribution due to the monitoring of the reaction parameters [263] such as temperature, pH, synthesis duration, surfactant addition, washing and drying operation [270]. The Stöber synthesis and the reversed micro-emulsion are the most commonly used procedures in the sol-gel silica NPs production [188], [265].

The sol-gel process involves the formation of colloidal suspension – sol, which is then transformed to viscous gel and then to solid material. Sol is a dispersion of particles with dimensions between 1 and 1000 nm, suspended in Brownian motion within a fluid matrix. The stability of the suspension depends on the resistance of the particles to agglomerate. The sol-gel process is advantageous due to mild chemical process condition, low temperature of the synthesis (usually close to room temperature), possibility to obtain a pure and homogenous product since the precursors of the synthesis are mostly volatile and easy to purify [263], [272]. As the source of “inorganic” monomers, the metal alkoxides are mainly applied precursors in the sol-gel process because they are well soluble in organic solvents. It is also possible to control their hydrolysis and condensation kinetics by solution chemistry [273]. The sol-gel process consists of several steps, starting with hydrolysis and condensation of the reaction precursors through gelation, ageing, drying to densification.

The hydrolysis process of metal alkoxide ($Si(OR)_4$) lead to a transformation of the Si–OR-terminated species to Si–OH-terminated ones. The metal alkoxides like tetraethoxysilane (TEOS) and tetramethoxysilane (TMOS), or inorganic silicates, are mostly used precursors [263], [274]. The process may be catalysed by acid (e.g. HCl)

or base (e.g. NH_3) (Figure 1.14). The pH value of the reaction influences the rate effect of catalysis. For silica, the isoelectric point is at pH 2.2. In the acidic environment, below the point of zero charge, the oxygen in ≡Si–OR group is protonated. The central silicon atom starts to be more electrophilic and susceptible to attack by water due to the electron-withdrawing. As a result, a good leaving group (e.g. water) is formed. In the basic environment, in turn, the nucleophilic attack of a hydroxyl group to the silicon atom occurs with an S_N2 type mechanism [274].

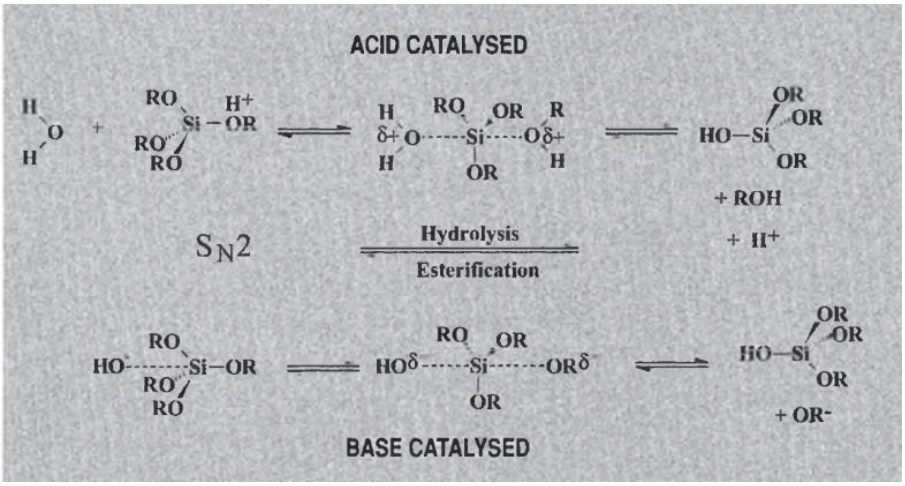

Figure 1.14 The mechanism of the hydrolysis process of metal alkoxide ($Si(OR)_4$) in the acidic and base environment [272]

Following the hydrolysis, the condensation reaction occurs, generating siloxane bond units and eliminating water or alcohol product:

$$\equiv Si–OH + \equiv Si–OH \rightleftarrows \equiv Si–O–Si\equiv + H_2O$$
$$\equiv Si–OH + \equiv Si–OR \rightleftarrows \equiv Si–O–Si\equiv + ROH$$

Similarly to the hydrolysis process, at pH below the point of zero charge, the oxygen atom of ≡Si–OH or ≡Si–OR group undergoes fast protonation (Figure 1.15). It generates a leaving group in the form of water or alcohol and makes the silicon atom susceptible to a slow attack by silanol groups. In the basic environment, a nucleophilic attack of $\equiv Si–O^-$ ion to the neutral silicon species takes place with an S_N2 type mechanism. It is worth noting that hydrolysis and condensation reactions of alkoxides compete with each other in the sol-gel process [272], [274].

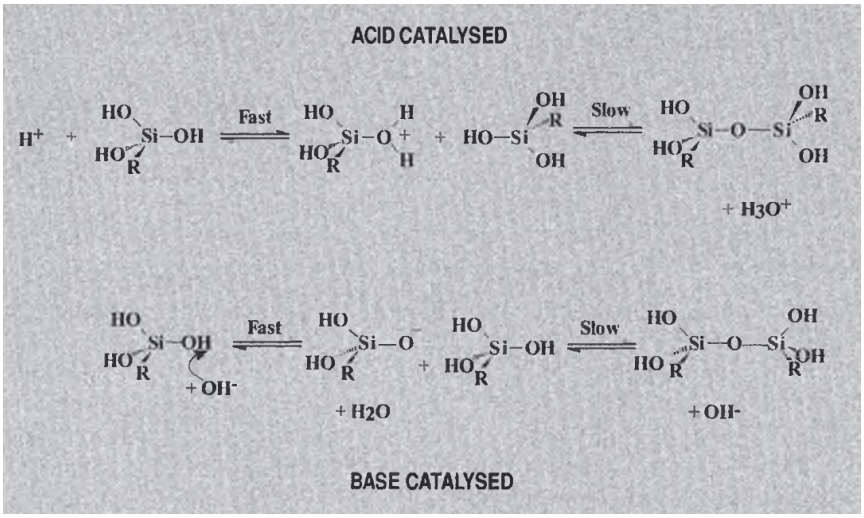

Figure 1.15 The mechanism of the condensation process in the acidic and base environment [272]

The stabilisation of the intermediates and relative rates of reaction during the hydrolysis and condensation process depends on the inductive effect of the silicon atom substituents and steric effects. Hence, the pH at which hydrolysis and condensation occur strongly influence the final gel structure. The ≡Si–R' species (R' - any hydrolytically stable organic moiety) has the highest electron density; then the density is lower for ≡Si–OR and ≡Si–OH, and finally, ≡Si–O–Si has the lowest electron density at the silicon atom [274]. Thus, in acidic conditions, with positively charged intermediates stabilised by electron-donating groups, the condensation of $(RO)_3SiOH$ undergoes faster than $(RO)_2Si(OH)_2$, and $(RO)_2Si(OH)_2$ is faster than $(RO)Si(OH)_3$. Consequently, for acidic catalysis, the first step of hydrolysis is the fastest, and its product also condenses the fastest. As a result, a chain-like network is forming, and then further hydrolysis and cross-condensation occur. On the other hand, in a basic environment, the hydrolysis steps undergo increasingly fast and completely hydrolysed species start to condense rapidly. Hence, big and crosslinked sol particles are initially formed, which then transform into branched networks with large pores between the particles [272].

Gelation is the next step of silica gel-forming. It occurs when the particles are connected together in branched chains to the extent that they fill the whole volume of sol. The initial gelling mixture is viscous and starts to solidify; however, some sol particles are still entrapped in the chain network, influencing the low elasticity. During the gelling process, further cross-linking of trapped sol particles occurs, resulting in both an elasticity and viscosity increase [266], [272]. Sol may also

undergo coagulation and form a precipitate [264]. Coagulation exhibits when the particles are joined together, forming dense aggregates in which silica is more concentrated than in the initial sol [266]. Several factors influence the process of gelation. The rate of gelling depends on the pH of the reaction environment and is proportional to the hydroxyl ion concentration because particle linkage is formed in the catalytic process in the presence of hydroxyl ions. The rate of gel formation increases with the pH increase in the range of 3 - 5. For higher pH, the concentration of hydroxyl ions does not influence the gelling rate. Due to the increasing particles' charge and fewer collisions between particles, the particle' aggregation rate decreases. Furthermore, also concentration and particle's size influence the process of gelling. The gelling rate is proportional to the total surface area of silica in a given sol volume. Particles undergo gelling at the same rate when the ratio of sol concentration to particle' diameter is the same in equivalent conditions. The gelling rate increases also with temperature. Electrolytes and organic liquids may influence the rate of gelling as well. Silica starts to be negatively charged above the pH of 3.5. In the presence of salts, the overall net repulsion is then reduced, so gelling and coagulation accelerate [266]. Polar protic solvents and alcohols may lower the reactivity of the $Si–O^-$ group in the neutral pH by forming the hydrogen bonds, decreasing the efficiency of condensation as a result. This may lead to form more branched structures and reduce gelling time. On the other hand, aprotic dimethylformamide, an acceptor of hydrogen bonds, leads to a decrease in the reaction environment's acidity, thus decreasing the rate of hydrolysis in acidic catalysed reaction [272].

Silica network formation in chemical reactions is not related to the gelation process only, but further structural rearrangements occur in the wet gel in the ageing process, yielding a higher gel's stiffness [274]. The ageing process consists of several steps, including further polymerisation, syneresis, coarsening, phase separation, and in some cases, hydrolysis and esterification [264]. During the ageing process, the gradual changes in the gel's structure and properties occur due to the pore liquid being still a sol that contains monomers, polymers or particles which further condense. Initially, the flexible gel network starts to be more contracted due to subsequent condensation of neighbouring pore-surface –OH and –OR groups and pore liquid expulsion occurrence. This shrinking process, called syneresis, continue as long as the flexibility of the gel structure is sufficient [264], [274]. Two mechanisms influence the structure and properties of a gel during the ageing process: a neck growth, which is a region where two particles join to each other, and a dissolution of smaller particles, which further precipitate on the larger particles according to the Ostwald ripening mechanism [275]. In the coarsening and ripening processes, the

material dissolves from thermodynamically unfavourable regions, which are mostly surface or particle with high positive curvature or small particles. The dissolved species condense then in the favourable regions including, crevices, pores, or narrow particle necks, with a smaller negative radius of curvature. These processes, influenced by temperature, pH, ageing medium, or pressure, reduce the solid-liquid interfacial energy and the net curvature, change the pore size and shape, and strengthen the solid [272], [274]. The last ageing process is associated with phase transformation. During a quick gelation process or when various precursors of different miscibility with water were applied, the unreacted chemicals may remain in the isolated porous regions of the silica matrix. When the silica is aged in water, the remaining unreacted monomers or oligomers may react, yielding inclusions with different refractive index, structure and composition of silica. This leads to phase separation of unreacted silica species and turns the gel to opaque due to the different refractive index comparing to the host matrix. To avoid turning to opaque, washing with ethanol lead to remove the unreacted precursors and low molecular weight products. The silica structure may be altered by ageing in solutions or solvents different from the initial solvent. Using ethanol for ageing conduce to partial esterification of the silica surface, leading to an increase of surface roughness and depolymerisation of the silica network, breaking the Si–O–Si bonds providing new surfaces [272].

The conventional drying process, conducted with either temperature increase or pressure decrease, involves three stages. In the first stage, also called the constant rate period, the gel starts to contract by the volume of liquid that priorly existed in the pores. The liquid undergoes evaporation. The direction of the liquid flow is from the interior of the gel to the surface. Not stiffed gel network undergoes deformations, which further result in new Si–O–Si bond formation since –OH groups at the inner surface come closer and can react with each other. The network rigidity increases with drying duration and the surface tension of the liquid; hence, the pore volume becomes smaller. The liquid/vapour interface is at the exterior surface. In the next stage, called the first falling rate period, at the critical point, the gel structure starts to be too rigid for further shrinking as the liquid continues to evaporate. The surface tension increase to such an extent that cracking is the most likely to occur. The liquid/gas interface draws back to the gel body; however, due to the pores' capillary forces and hydrophilic nature, a thin film of liquid stays at the pore walls and continues to move to the exterior surface, followed by evaporation. In the third stage of drying, called the second falling rate period, the liquid film is ruptured. The liquid, isolated in droplets, can evaporate from the gel network only by diffusion through the gas phase to the exterior [264], [274]. Several methods have

been developed to minimise gel cracking and fracturing during the drying process. First of all, when the gel is drying very slowly, the shrinking rates of gel interior and surface are comparable, and the gradient in the strain is reduced. Also, the network is strengthened during the ageing process, which may result in the pore radius increase and capillary tension decrease [264]. Another method to reduce cracking is the application of drying control chemical additives (DCCA), like dimethylformamide, acetonitrile, formamide, oxalic acid. DCCA influence the larger pore-forming, where capillary forces are weaker, and the stress toward the gel network is smaller during drying. The solvent evaporation is favoured due to the higher vapour pressure in the larger pores. DCCA interacts with the silica surface via hydrogen bonds, which prevent the interactions between silanol groups in the pore walls and water molecules, facilitating the removal of the aqueous solvent. Also, the addition of surfactants can facilitate the removal of aqueous solvent from the pores by modification of the silica inner pore surface by alkyl chains, making the surface hydrophobic and reducing water interactions with the pore walls. However, DCCA modifies the properties of the gel to the undesirable ones and may be tough to remove [272]. The capillary pressure and cracking can also be reduced in the process of supercritical drying, where no distinction between liquid and vapour exists. The process requires the alcohol as a solvent instead of water, which is then extracted above its critical point. The liquid/vapour interfacial energy is equal to 0 (γ_{LV}=0), so no capillary tension occurs during the drying process. The supercritical drying silica gel product is called aerogel since it is composed of more than 99% of air. The gels conventionally dried are known as cracked material called xerogel [264]. Finally, freeze-drying is also a process of drying, in which the solvent is frozen inside the pores and sublimed under vacuum, yielding a product with large pores called a cryogel. However, solvent crystallisation in the pores produces cracking and shrinkage of the gel [275].

Silica nanoparticles are commonly synthesised in either the Stöber synthesis or the reverse microemulsion [265]. Stöber method, as an important example of the sol-gel process, was first described by Stöber and Fink in 1968. Monodispersed silica particle suspensions were obtained in the controlled hydrolysis and condensation process, and in the colloidal size range from 0.05 to 2 μm, depending on the synthesis conditions such as type of alcohol solvent, alkyl silicate precursor, catalyst and water concentration, reaction time [276], ethanol-to-water ratio, and reaction temperature [269]. Another method to obtain the monodisperse silica particles is the reverse microemulsion synthesis [265], [268]. According to Winsor microemulsion classification [277], the water-in-oil (W/O) is a type II system that involves the presence of small droplets of water dispersed in a large volume of

organic (oil) continuous phase and stabilised with an amphiphilic surfactant and co-surfactant, whereby the surfactant is mainly in the oil phase. Microemulsions are thermodynamically stable with potentially infinite lifetimes and a droplet size between 3 to 50 nm. Due to the small size of droplets, microemulsion stays transparent or have a slightly bluish shade [268], [278]. The microdroplets formation depends on the proportion of microemulsion components involving water-to-surfactant ratio (W), hydrophilic-lipophilic balance value (HLB) of the surfactant used or co-surfactant application. The amphiphilic surfactant molecules consist of a hydrophilic region with a small ionic or polar head and a lipophilic region with a long hydrocarbon tail. The co-surfactant such as medium chain-length alcohols are applied frequently in conjunction with an ionic surfactant to lower the interfacial tension. The spherical microdroplets, commonly reverse micelles, are generated due to the thermodynamically driven surfactant self-assembly. With the various W value, the size and shape of the aqueous core, formed by a surfactant, can be controlled, yielding the uniform, nanometer-sized water droplets. In the dynamic microemulsion system, the micelles are in a random Brownian motion, colliding regularly. Due to the feasible coalescence, the micelles form dimers, exchange the reaction components and break apart further. Micelles form a kind of "nanoreactors", where controlled nucleation and growth occurs [279].

The standard reverse microemulsion synthesis of spherical silica nanoparticles involves cyclohexane, alkylphenol ethoxylate as a surfactant, water, a silicate precursor, e.g. tetraethylorthosilicate (TEOS), a small amount of aqueous ammonium hydroxide as a catalyst, and very often medium-chain alkyl alcohol like pentanol or hexanol acting as a cosurfactant [268]. TEOS diffuses into the water droplet "nanoreactors", where undergoes hydrolysis with an alcohol forming [280]. The water droplets control the kinetics of the nucleation and growth of silica nanoparticles. Therefore, the water-to-surfactant ratio has to be carefully adjusted to control the size and polydispersity of the nanoparticles [265]. However, water may be partially expulsed from the microemulsion phase, producing the second water phase and further resulting in the bimodal silica particle size distribution [268]. In general, the microemulsion reaction needs a longer time. Still, this method precisely controls the size of the particles yielding monodisperse silica NPs with a size smaller than 100 nm. Whereas the Stöber synthesis is a relatively shorter reaction with a higher yield; however, larger and non-uniform particles are obtained [188], [265].

The sol-gel process can be modified with an addition of organic surfactant as a structuring agent to obtain the mesoporous solid silica with desired properties such as internal and external pores, a uniform and tunable pore size, gating mechanism

of the pore opening, or a carrier for loading a variety of molecules, e.g. drugs [264], [274], [281]. According to IUPAC, the mesoporous material has a pore size in a range of 2 to 50 nm, an ordered pore structure with the amorphous walls of the pores [274], [281]. Among several methods of mesoporous silica preparation, a modified Stöber synthesis is the most commonly used [282]. The widely known commercial mesoporous silica particles are Mobil Crystalline Materials (MCM-41) and Santa Barbara Amorphous (SBA-15). The MCM-41 is a hexagonal material with pores in the size range of 2.5 to 6 nm, synthesised with a template of cationic surfactant. SBA-15, in turn, is a material with a highly ordered structure, pore size in the range of 4.6 to 30 nm and thick silica walls [281]. The synthesis of mesoporous silica particles includes cationic, anionic or nonionic surfactant as a structuring agent, which acts as a template of solid porous structure construction. Cetyltrimethylammonium bromide (CTAB), 1,2 bis (2-ethylhexyloxycarbonyl)-1-ethanesulfonate, polyvinylpyrrolidone, polystyrene, polyresorcinol, or polymethylmethacrylate are only some of the surfactants used as the structure templates [283]. The silicate precursor interacts with the surfactant aggregates in the condensation process, yielding a solid containing surfactant. In the process of extraction or calcination, the surfactant is then removed, forming a mesoporous solid material. The formation of the porous structure is controlled by weak noncovalent interactions like van der Waals forces, electrostatic interactions, or hydrogen bonds between the organic template and inorganic particles [274]. Due to the controllable pore size, shape and volume, high loading capacity, and high specific surface, mesoporous silica particles can be widely applied for bioapplications like nano-carriers in drug delivery [284], [285], dye-doped material in cell imaging [286], the intracellular drug delivery [287], extracellular delivery of a small protein, enzyme immobilisation and catalysis [288].

The modification of a sol-gel synthesis precursor, based on a non-hydrolysable substituent on the silicon atom, results in a material with different structure, functionality and properties [272]. This inorganic-organic hybrid material (ORganically MOdified SILica, ORMOSIL) consists of a well-defined three-dimensional inorganic network of siloxane units that are linked by the polymer fragments or organic groups at the molecular level. The hybrid material is formed from a wide variety of organosilane compounds of the type $R'Si(OR)_3$ or related metal alkoxide derivatives. R' indicates an alkyl or aryl group and undergo polymerisation and cross-linking processes [274], [275]. The choice of organosilica precursor with various functional groups determines the functionalities and specific properties such as hydrophobic surface, catalytic or optical properties of the obtained silica material. The non-hydrolysable substituent in the silane precursor structure lowers the connectivity of the network, affecting the chemical composition of the pore surface

and the character of the material. Nevertheless, the material properties also depend on the arrangement of the hybrid network and intermolecular interactions between the organic moieties [272], [274].

1.6.2 Surface modification techniques

A wide range of functional organic moieties can be employed to functionalise the silica surface, adjusting its properties to the desired application. Two main methods of introducing the functional groups on the silica surface can be distinguished: co-condensation and grafting, resulting in the hybrid material formation. In the co-condensation process, the sol-gel hydrolysis and condensation of functionalised silane precursor, e.g. the organotrialkoxysilanes, occurs, yielding a hybrid organosilica [274]. However, in this method, the variable surface functionalisation and low interconnectivity of the material in bulk is obtained due to the distribution of the functionalised precursor over the entire gel [272]. The grafting, in turn, is the process of modifying the well-defined silica particle surface, where the surface silanol groups react with the functionalised precursors [272], [274]. The chemical functionalisation of the silica particles with organic moieties provide the stabilisation of the particles against further growth, avoid agglomeration in a solvent, enhance the compatibility with the surrounding matrix via changing the polarity, and enhance the affinity between the inorganic and organic phase [263], [274]. Surface modification with silane coupling agent with a formula R^1– $Si(OR^2)_xR_y^3$ (x = 1 or 3, y = 2 or 0) is one of the most effective techniques. This is due to the ability of the $Si(OR)_x$ section to react with hydroxyl groups on the particle surface via a condensation process and due to the functional group, which can interact with a polymer matrix by forming a covalent bond [274]. A wide variety of organofunctionalised alkoxysilane agents for silica surface modifications is available, e.g. commonly used vinyltriethoxysilane, methacryloxypropyltriethoxysilane, 3-glycidyloxypropyltrimethoxysilane, 3-aminopropyltriethoxysilane, 3-mercapto-propyltriethoxysilane [263]. The application of a particular alkoxysilane agent for silica particle modification determines the surface properties. Long alkyl chains change the particle surface to hydrophobic and render it dispersable in nonpolar solvents [274]. The organic solvents are generally used instead of aqueous systems to prevent the hydrolysis and condensation of the functionalised silane precursors and facilitate the formation of a monomolecular layer on the silica surface [272]. 3-aminopropyltriethoxysilane is one of the molecules which may undergo uncontrollable hydrolysis and polycondensation reactions in aqueous systems;

therefore, the grafting process needs to be conducted in the organic solvent. In the nonaqueous system, the organofunctionalised alkoxysilane connects with the silica surface in a direct condensation process. Also, the curvature and size of spherical silica nanoparticles are of importance in grafting the organofunctional groups to the surface. The effectiveness of chemical modification depends on the concentration of silanol groups per unit area of the silica surface [263].

The polarity and reactivity of the silica particle surface depend on the ability of the surface terminal groups to interact with each other and form hydrogen bonds. The pore surface can be terminated either by Si–O–Si group or Si–OH group; whereby, the latter group may be classified as geminal when both hydroxy groups are linked with the same atom of silicon; vicinal when hydroxy groups are linked with neighbouring silicon atoms and one oxygen is bridged with hydrogen; or isolated when the hydroxy group is linked to the silicon atom not connected with any silanol group. In the case of vicinal silanols, hydrogen bond formation occurs with stronger bonding rather on concave surfaces than on flat or convex. The extensive number of hydroxyl groups on the silica surface is responsible for a large amount of water absorbed in the gel, which may influence the optical properties such as transparency of the material. The modification of the surface by removing the hydroxyl groups followed by Si–O–Si linkage formation is used to improve the optical quality of the material. The hydroxyl groups elimination can be done either via the thermal dehydroxylation or chemical method. Thermal dehydroxylation is based on heating the gel to 800 °C, eliminating the physisorbed water first and the vicinal silanol groups subsequently. In the chemical method, the hydroxyl groups are removed in the reaction with chlorine and a high-temperature oxygen treatment [272].

1.6.3 Entrapment properties of silica particles

The sol-gel process enables the doping of various additives into the silica matrix such as organic dyes, metallic particles, quantum dots, biomolecules, metal ions, ceramic oxides, or inorganic compounds to add the functionality of the material. The additives can be doped as a part of the host network, encapsulated in the pores or immobilised in the interface [274]. Doping the additives can be done in several ways. The dopants can be incorporated into the silica network by mixing them with the initial solution of the precursor or with the already hydrolysed sol before gelation. Also, the porous network of silica material can be impregnated with the dopant from a solution or vapour phase. The additives trapped in the silica network form a hybrid material that exhibits a series of diverse optical, mechanical,

ionic, electrical, catalytic, and bio-sensing properties [289]. Recently, one of the potential key applications of hybrid silica particles is the encapsulation of bioactive or luminescent dopants in the silica network for drug delivery purposes [290]–[292], catalytic supports [293], biosensing and bioimaging in diagnosis [294]–[296].

1.7 Quantum dots

Quantum dots (QDs) are the fluorescent nanoparticles of semiconductor materials with a diameter of 2-8 nm [297] and quantum-confined in three dimensions [298], as well as characterised by composition-dependent bandgap energy. The physical dimensions of QDs are smaller than the exciton Bohr radius [299], which is the distance in an electron-hole pair. The electron-hole pair is formed when an electron (e^-) from a valence band absorb the minimal energy (higher than a bandgap) and is promoted to the conduction band, leaving a hole (h^+) in the valence band. The electron and the hole are bonded via Coulombus interaction, forming the electron-hole pair called an exciton. As an example, the exciton Bohr radius of cadmium telluride (CdTe) and cadmium selenide (CdSe) are approximately 7 and 5 nm; respectively, therefore the smaller particles are referred to as quantum dots [298].

Quantum dots consist of approximately 100-10000 atoms, and similarly to isolated atoms, exhibit narrow luminescent emission peaks. Compared with bulk material, significant differences in the optical absorption, exciton energies and electron-hole recombination are observed for QDs. The QDs photoluminescence strongly depends on size due to the changes in the surface-to-volume ratio with size and the quantum confinement effect (Figure 1.16).

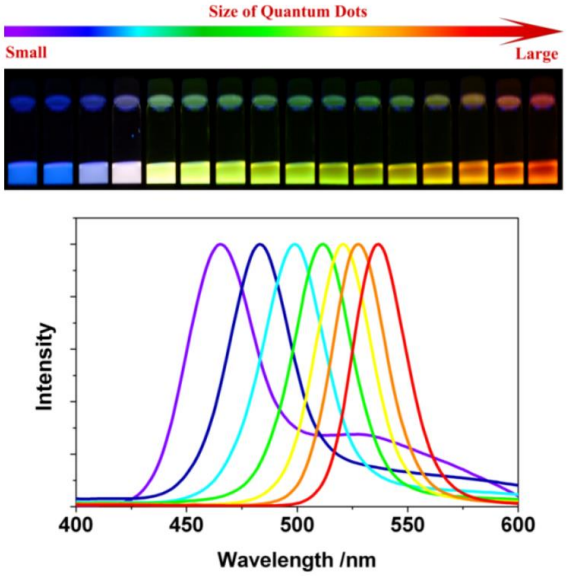

Figure 1.16 Emission colours of CdSe QDs with a size range of 1-10 nm positioned from small (blue) to large (red) excited by a NIR irradiation. The graph illustrates the photoluminescence spectra of some CdSe QDs [300]

The quantum confinement in QDs modifies the density of states near the band edges. The density of states as the energy function for various size material is pictured in Figure 1.17. With the QDs dimension decrease, the energy spectrum becomes discrete, and the energy level spacing in a nanocrystal exceeds the kT (k – Boltzmann's constant, T – temperature). The energy differences, higher than kT, limit the mobility of electrons and holes in the crystal. As a result, the bandgap starts to depend on the QDs size. With the QDs size decrease, the increase of bandgap energy and blue shift in light emission is observed [300]. QDs composed of the same material but with different sizes exhibit fluorescence emissions in different regions of light spectrum from UV to IR. However, the composition of a semiconductor also plays a role [298].

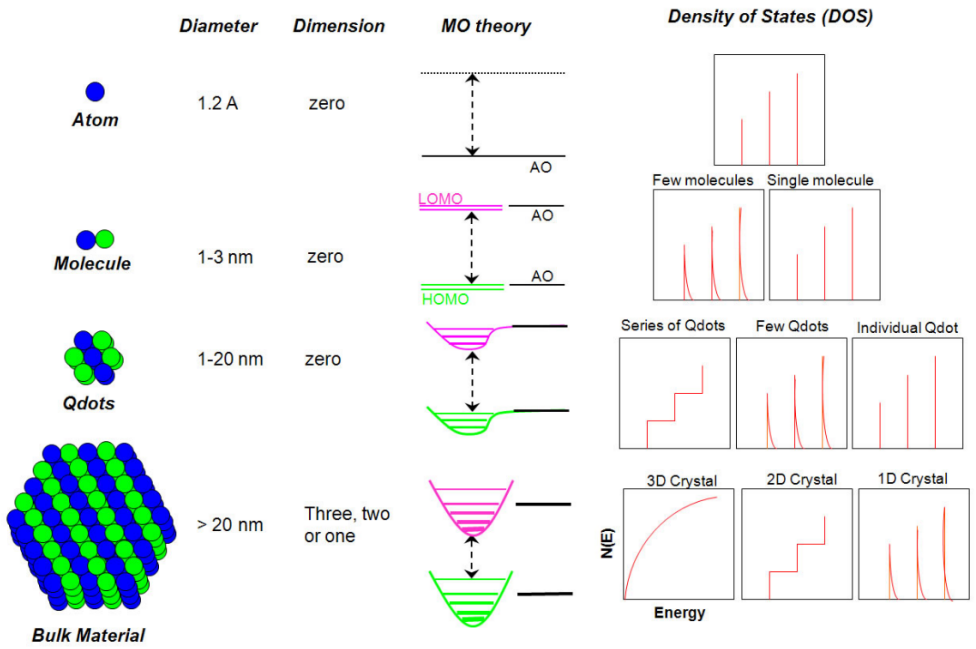

Figure 1.17 The diagrams illustrate the changes in the density of quantum states with the changes in the number of atoms in a material. MO – molecular orbital, HOMO – highest occupied MO, LUMO – lowest unoccupied MO, AO – atomic orbital [300]

Quantum dots are broadly applied in several areas like biomedical applications, including diagnostic tools, fluorescent markers, photodynamic therapies, optoelectronic applications involving light source emitters (LED), white light filters, active solar energy conversion, and analytical applications like chemical and biosensing [298]. Despite the wide range of properties and application, there are some concerns about the potential toxicity of quantum dots when used for medical and biology purposes, especially since inorganic QDs often consists of Cd, Se, Zn, Te, Hg and Pb metals [301]. However, the toxicity of each QDs type has to be characterised individually in terms of their size, concentration, charge, stability during synthesis and storage, oxidation, external coating, and functionalisation [299]. The toxicity of QDs can be related to the presence of free divalent cadmium ions, which are nephrotoxins [302], [303]. The release of cadmium ions can be facilitated by exposure to air or UV light irradiation [304]. Moreover, the toxicity depends not only on the QDs core material but also on the type of molecules that cover QDs surface. CdSe QDs coated with small thiolate ligands tend to be toxic; however, coating CdSe QDs with zinc sulfide shell render these quantum dots less prone to oxidation or degradation [302] and reduce cytotoxicity without the

influence on fluorescence stability [305]. Similarly, cadmium based QDs encapsulated in silica nanoparticles indicated low toxicity with high physicochemical stability and photostability [306]. To minimise the toxicity of the quantum dots of group II-VI, e.g. CdS, CdTe, CdSe, for which the toxicity of cadmium ions have been proven, the new, cadmium-free QDs have been proposed, including indium phosphide (InP) and indium arsenide (InAs) QDs of group III-V, copper indium sulfide ($CuInS_2$) of group I-III-VI, germanium and silicon of group IV, graphene QDs [307], silver indium sulfide ($AgInS_2$), silver sulfide (Ag_2S), and doped Zn chalcogenide [308]. The Cd-free QDs of group III-V indicate good optical stability and reduced toxicity; however, the synthesis of these QDs is difficult because of the sensitivity of the precursors and surfactants [309].

1.7.1 Optical properties

The optical and electronic properties of QDs strongly depend on the size and composition of particles as well as on other factors like shape, impurities, crystallinity or defects in the QDs structure [300]. Compared with fluorescent organic dyes or proteins, semiconductor QDs, as a new fluorophore class, exhibit several advantages. Size-tunable fluorescence emission is advantageous because changing only the particle diameter provides a broad range of available emission wavelength [298], [303]. QDs exhibit a broad absorption spectrum; thus, an electronic excitation at different wavelengths is possible, including ultraviolet and the entire visible region of the light spectrum [298], [299]. Also, symmetric luminescence spectrum ranges from ultraviolet to near-infrared region, and large Stokes shift is observed for quantum dots, enabling multicolour imaging, which eliminates spectral cross-talk. In the case of bioimaging, this is a great advantage due to the fact that absorption of tissues is minimal in the infrared and near-infrared region. The Stokes shift is the difference between the peaks of excitation and emission wavelengths. The large separation of absorption and emission spectra results in improved detection sensitivity [299].

In comparison to organic fluorophores, QDs exhibit narrower emission bands [310], higher brightness due to the high quantum yield of fluorescence also after conjugation to biological affinity molecules [299], and greater photostability, which results in increased resistance to photobleaching [297], [303], [310]. The high brightness of QDs is obtained due to the minimised overlap between excitation and emission bands, which eliminate the reabsorption of emitted light by nearby QDs. Also, QDs can absorb 10 to 50 times more photons in comparison with organic

fluorophores at the same excitation photon flux. The photobleaching occurs in organic dye molecules due to the cleaving of covalent bonds or non-specific interactions between the fluorophore and surrounding molecules. Thus, QDs can be several thousand times more stable than organic fluorophores [299]. Compared to organic fluorophores, a longer luminescence lifetime allows for longer periods of luminescence detection and eliminates autofluorescence with a short lifetime [298]. Due to the more closely spaced energy levels in larger quantum dots, the electron-hole pair can be trapped for longer, resulting in a longer fluorescence lifetime [299]. Quantum dots possess an active surface for chemical modification with a variety of organic molecules, making them an inorganic-biological nanostructure with fluorescent and biochemical properties [298], [310].

1.7.2 Synthesis and surface modification

Two main approaches can be distinguished in quantum dots synthesis: top-down and bottom-up processes. The top-down approach is based on thinning the bulk semiconductor. Several top-down synthesis processes based on electron beam lithography and etching have been developed to form quantum dots with controlled size, shape and geometry [300]. Etching is a widely applied process in nanofabrication. Dry etching is the process that involves breaking down the reactive gas molecules into more reactive species by creating plasma in the etching chamber. When the high kinetic energy species hit the surface, the volatile product is formed to etch a patterned sample. In the reactive ion etching, ions are applied as the reactive species. The process of selective etching with a masking pattern and a mixture of boron trichloride and argon can be used to fabricate GaAs/AlGaAs quantum dots with a size of 40 nm [311]. Electron beam lithography followed by etching is another method of fabricating nanostructures with any shape, precise separation and periodicity. This method is used to synthesise III-V and II-VI group QDs with a size of 30 nm. Focused ion or laser beam is another top-down process of QDs manufacturing; however, the incorporation of impurities and structural imperfections may occur in the QDs structure [312].

A wide range of bottom-up synthesis is available for quantum dots fabrication. The methods can be categorised as either wet-chemical or vapour-phase methods. Wet-chemical methods are based on conventional precipitation methods, including nucleation and limited growth of nanoparticles. A required composition, size, and shape of quantum dots can be obtained by controlling the synthesis parameters such as concentration of the precursors, solvents, surfactants, stabilisers

of micelles formation, temperature or thickness of electrostatic double-layer [300]. Sol-gel process [313]–[315] and microemulsion process [316]–[318] are among the many wet-chemical methods of QDs synthesis. The sol-gel process is relatively simple, cost-effective, and efficient [313]; however, broad size distribution and high concentration of defects are the main drawbacks [300]. In the microemulsion method, in turn, narrow size distribution is possible to obtain due to the limited size of the micelle controlled by the ratio of water-to-surfactant. Nevertheless, the recovery of the nanoparticles from the microemulsion as well as low yield and presence of impurities and defects may be problematic [300], [318]. Other typical syntheses of quantum dots involve the thermal decomposition process [319], [320], hydrothermal synthesis [321], [322], and sonic waves or microwaves [323], [324]. The thermal decomposition method involves a time and temperature controlled reaction of the precursor decomposition. The size and shape of QDs, except time and temperature, depend on the type of precursor, coordination and purity of the agent and solvent. However, the high temperature of the synthesis and toxic precursors are the main drawbacks [300], [319]. In the hydrothermal synthesis, the inorganic salts crystallise from an aqueous solution in the process controlled by temperature, time and pressure [325], [326]. Sonic waves or microwaves synthesis is based on the dissociation of the precursor and water molecules due to the energy provided by the ultrasound waves. The chemical effects are generated by acoustic cavitation. The acoustic cavitation forms a localised hotspot through adiabatic compression within the gas phase inside the collapsing bubble, enabling the reaction of QDs formation [327].

As a bottom-up process, the vapour-phase methods involve the growth of the epitaxial layers in an atom-by-atom process followed by nucleation and growth of quantum dots directly on the substrate. The self-assembly of quantum dots takes place on the substrate without patterning [312]. In the molecular beam epitaxy process (MBE), the deposition and growth of elemental or compound semiconductor nanostructures occur on a heated substrate under high vacuum conditions. The MBE process is mainly applied to self-assemble III-V and II-VI groups of semiconductor QDs. In this method, the primary process involves the evaporation of the proper elements from the Knudsen effusion cell, which are heated to the sublimation temperature to form a beam of atoms or molecules. The layer growth can be processed by physical vapour deposition (PVD) due to condensation of a solid from vapour, formed by thermal evaporation or sputtering. Another way of quantum dots self-assembly in the form of a thin film is chemical vapour deposition (CVD). The precursors subjected to a particular temperature and pressure diffuse to the heated substrate and react to form a thin film. The vapour-phase self-assembling methods

effectively fabricate QDs without templates; however, some variability on QDs size may occur, influencing the optoelectronic properties [300], [328].

Quantum dots are susceptible to photobleaching and chemical quenching due to their small size and large active surface [310]. Moreover, a bare core of QDs can be highly reactive and toxic, resulting in an unstable structure [299]. To minimise these effects and to increase the quantum yields of QDs, a core-shell structure can be used, which passivate the surface nonradiative recombination sites [310]. Modifying the QDs core with a semiconductor of higher bandgap results in increased stability and quantum yield and protects the toxic core ions against exposition to a photooxidative environment like ultraviolet light or air. The typical II-IV, IV-VI, or III-V QD cores can be covered with zinc sulfide or cadmium sulfide semiconductors with a wide bandgap to stabilise the core and improve chemical and photophysical properties at room temperature [299]. Except for the core and the shell of QDs, an important role also plays a capping ligand. Quantum dots, synthesised in organic solutions, have the outermost surface passivated with organic ligands. In order to apply QDs to biological systems, it is necessary to tune the surface to make QDs hydrophilic and soluble in an aqueous environment [329]. Modification of QDs surface with various molecules facilitate aggregation prevention or nonspecific binding. The hydrophilic QDs can be further functionalised by conjugation with, e.g. biological molecules like proteins, antibodies, peptides, or oligonucleotides in the way of covalent linkage, electrostatic attractions, adsorption or mercapto exchange [299]. One of the surface passivation methods is the ligand exchange strategy, which involves the replacement of hydrophobic surfactant molecules, e.g. oleic acid [330] or trioctylphosphine oxide [331], with bifunctional molecules. These molecules on the one end have a chemical group able to bind the QDs surface and on the other end a polar head, for example, 3-mercaptopropionic acid, 1,2-ethanedithiol, benzenedithiol [332], cysteine, glutathione, mercaptoacetic acid, mercaptosuccinic acid [329] or atomic ligands in the form of halides [330].

Surface silanisation is another strategy for QDs surface passivation and rendering the QDs water-soluble and biocompatible material. Silica coating enhances the stability of colloidal QDs as well as prevent aggregation and oxidation. Introducing silica shell onto the QDs also enables further conjugation with biomolecules [333]–[335]. The other approach is a polymer coating of QDs. In this strategy, the original ligands are preserved, and amphiphilic molecules are introduced. The hydrophobic groups of these molecules interact with the original ligand, whereas the hydrophilic group provide water solubility and enable further functionalisation [336], [337] for sensing or receptor targeting purposes. Retaining

the original surface help to preserve the photophysical properties of QDs; however, it increases the final size of QDs three to four times [338].

1.8 Upconverting nanoparticles

Upconverting nanoparticles are a valuable material that exhibits photon upconversion. A photon upconversion (UC) refers to an optical process in which the sequential absorption of two or more low-energy photons yields the emission of a single high-energy photon, called anti-Stokes emission [339]. Thereby, the UC process converts the long-wavelength infrared radiation into short-wavelength emission, e.g. UV, visible or near-infrared light [340]. Most luminescent materials like organic dyes or quantum dots exhibit down conversion, following Stokes' law, where the energy of emission photon is lower than the energy of the excitation photon [341]. The upconverting materials composed of inorganic host mostly doped with rare-earth ions or transition metal ions are broadly applied in compact solid-state lasers, optical devices, e.g. temperature sensors, [340], photovoltaic devices, multi-colour displays, data storage. The broad interest in UC material is observed in the biomedical field, involving bioimaging and theranostics [341]. The range of excitation wavelength of upconverting material corresponds with the so-called "optical transparency window" (approximately 700 – 1100 nm) for body tissues, which is the spectral range of minimal absorption. Under near-infrared excitation, the biological background auto-fluorescence is negligible, improving the signal-to-noise ratio and reducing photodamage effects. Applying NIR excitation is also advantageous due to the reduced light scattering and phototoxicity. Large anti-Stokes shifts, narrow emission bandwidths, photobleaching resistance [342], tunable colour emission, long photoluminescence lifetimes [343], low toxicity, good chemical and physical stability [344] make the upconversion material suitable for bioimaging purposes.

The optical properties of the upconversion nanoparticles are strongly dependent on their surface properties. Due to a high surface-to-volume ratio of a nanoparticle, lanthanide dopants are often subjected to surface deactivations caused by surface defects, solvents or ligands which exhibit high phonon energy. Deactivation can occur when the dopants, placed on the nanocrystal surface, are neighbouring to the surface quenching centres. On the other hand, the energy contained in the dopants settled in the centre of the nanocrystal can migrate to the surface-localised dopants or directly to the surface quenching sites resulting in low upconversion efficiency [340]. To eliminate the effects of surface quenching

or prevent the energy migration to the surface, passivation of the surface with an inert shell can be applied. Surface passivation may significantly reduce the influence of solvent or ligands on quenching and inhibit the energy migration to traps [345]. Besides, the surface of upconversion nanoparticles, obtained by the various synthesis in organic solvents, is reached in hydrophobic surfactant ligands, limiting the use of UCNPs in biomedical applications. Surface modification in the way of ligand exchange, polymer coating or silica coating leads to improved upconversion efficiency and biocompatibility and solubility in a biological environment [346], [347].

1.8.1 Composition of upconverting NPs

A typical upconversion material consists of three components: a stable host, which acts as a protector, an optically active sensitiser and activator ions as dopants, and a luminescent centre. Due to the energy transfer processes among components of upconversion material, the choice of host-dopants pair is of importance. The widely studied upconverters involve upconversion material based on rare earth (RE) trivalent ions such as Pr^{3+}, Nd^{3+}, Er^{3+}, Tm^{3+}or Yb^{3+}, transition metal (TM) ions, e.g. Ni^{2+}, Ti^{2+}, Os^{4+}, Mo^{3+}, Re^{4+}, the systems of RE and TM which are the combination of trivalent RE ions and TM ions in the same host lattice, and upconversion nanoparticles [340].

Host material

The host matrix should have low phonon energies to eliminate a drop in efficiency due to nonradiative relaxations. The host must be chemically and thermally stable and possess high transparency to facilitate NIR photons free migration in the lattice [339]. The type of host with specific optical properties may impact upconversion emission properties of a compound, e.g. may change the colour of the emission light [340]. Therefore, the host lattice match to the dopant ions should be high since it determines coordination number, the distance between the dopant ions, spatial position and types of surrounding anions [340]. Fluorides are among the most used compounds for upconversion material due to the low phonon energies (between 300 and 500 cm^{-1}) and high chemical stability. In comparison, iodides, bromides and chlorides also exhibit low phonon energy (≤ 300 cm^{-1}), but they are highly hygroscopic. On the other hand, oxides are chemically stable, but their phonon energies are larger than 500 cm^{-1} [348]. Similarly, phosphates (e.g., $LuPO_4$, YPO_4) or vanadates (e.g., YVO_4, $GdVO_4$) are chemically stable but have

larger phonon energies [339]. The ideal host candidates for upconversion phosphors are inorganic materials based on trivalent lanthanide ions since all trivalent lanthanide ions have similar ion size and chemical properties. Moreover, Na^{+}, Ca^{2+}, and Y^{3+} cations have an ionic radius close to the trivalent lanthanide dopants, preventing crystal defects formation and lattice stress. The hexagonal-phase sodium yttrium fluoride (β-$NaYF_4$) is the most efficient host among the fluorides. The upconversion efficiency of hexagonal-phase fluoride doped with ytterbium and erbium ions (β-$NaYF_4$:Yb^{3+}/Er^{3+}) is about ten times higher than that of cubic-phase fluoride (α-$NaYF_4$:Yb^{3+}/Er^{3+}) and twenty times higher than that of oxide type matrices (La_2O_3:Yb^{3+},Er^{3+}) [349].

Sensitiser

A sensitiser in the UC material is responsible for sensitising the activator. The efficient sensitiser should have a wide absorption cross-section at the required excitation wavelength. Also, the resonant energy levels of the sensitiser should match those of the activator to allow for efficient resonant energy transfer between these two ions [339]. The most commonly used sensitiser for europium or thulium activators is the ytterbium ion (Yb^{3+}). Yb^{3+} ion has a simple energy level scheme with one excited state, which matches well with the f-f transitions of some rare earth activators. The energy separation between the ground state of Yb^{3+} ion ($^2F_{7/2}$) and its excited state ($^2F_{5/2}$) closely match the transition energy between the $^4I_{11/2}$ and $^4I_{15/2}$ and the $^4F_{7/2}$ and $^4I_{11/2}$ states of Er^{3+} (Figure 1.18). A similar efficient energy transfer exists between the Yb^{3+} ion and other activators like thulium (Tm^{3+}) or holmium (Ho^{3+}) ions [349]. The concentration of ytterbium ions doped into the host lattice ranges between 18 and 20 $\%_{mol}$ [340], [350].

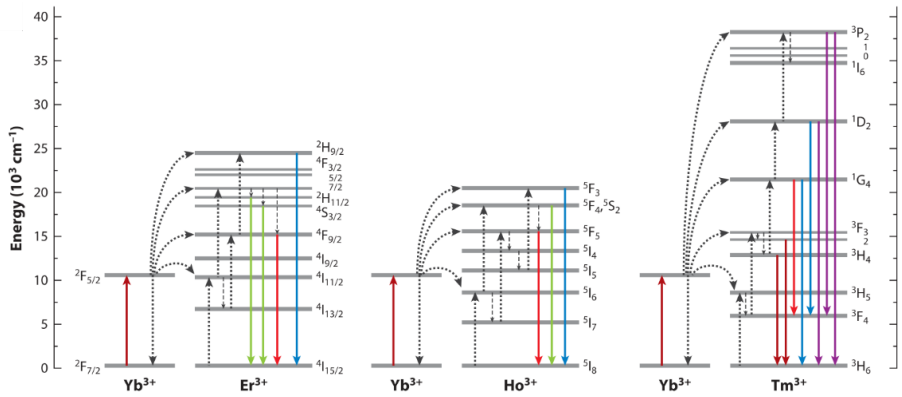

Figure 1.18 Diagrams of energy levels and upconversion energy transfer pathways in the rare earth ions pairs: Yb^{3+}-Er^{3+},Yb^{3+}-Ho^{3+}, and Yb^{3+}-Tm^{3+} [351]

Activator

An activator is an ion that absorbs the energy emitted by a sensitiser and which emits the output photon [352]. When the electrons from the ground state are excited to the intermediate-excited state, the activator ions are likely to accept the energy from the nearby excited sensitiser ions and promote further energy transfer to higher energy levels. However, the energy levels of the activator should not be too close to avoid non-radiative relaxations [353]. The energy transfer and upconversion efficiency depend on a shape of a sample and the separating distance between the dopants. The sensitiser ions should be co-doped alongside the activator, which possesses well-matched intermediate-excited states [352], [354]. Furthermore, the upconversion emission increases with the activator concentration rise, but only until the critical value above which the quenching of the excitation energy and decrease in UC emission can occur. Thus, the concentration of the activator is kept low while the concentration of doped sensitisers is much higher. However, the low content of the activator may result in low absorption of the pump light and thereby low upconversion emission efficiency [339], [340]. The trivalent erbium, thulium and holmium ions are the most common activators (emitters) due to their energy level structures which allow minimising non-radiative relaxations. The activator concentration in upconversion material is relatively low, below 2 $\%_{mol}$ [340].

1.8.2 Upconversion mechanisms

A number of different upconversion mechanisms have been identified, among which the basic ones are: excited state absorption (ESA), energy transfer upconversion (ETU), photon avalanche (PA), cooperative energy transfer upconversion (CET), and energy migration-mediated upconversion (EMU) [339], [353].

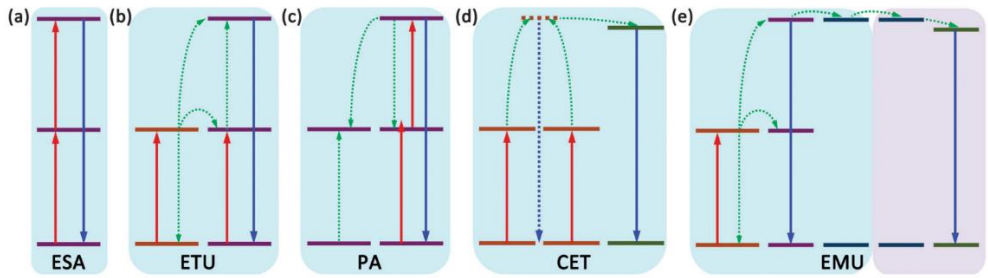

Figure 1.19 A schematic representation of basic energy transfer mechanisms of rare-earth-based upconversion emissions: (a) excited state absorption, (b) energy transfer upconversion, (c) photon avalanche, (d) cooperative energy transfer, (e) energy migration-mediated upconversion. Full red and blue arrows depict excitation and radiative emission process, respectively; green dashed arrow stands for energy transfer processes, different colours of energy levels represents different kind of luminescent centres, different background colours boundary depict a core-shell interface [353]

Excited state absorption

In the excited state absorption process, a sequential absorption of two or more pump photons by a single ground-state ion occurs. Firstly, an ion is excited from the ground state to the excited state. Subsequently, a second pump photon promotes the ion to the higher-lying excited state resulting in upconversion emission of high-energy photons (Figure 1.19 a). For an efficient ESA process, the excited ions should possess a capable absorption cross-section to absorb the second pump photon [351]. Also, multiple energy level ions are required. Some lanthanide ions like Er^{3+}, Ho^{3+}, Tm^{3+}, and Nd^{3+} have ladder-like energy level structures, and they are the commonly applied activators among ESA upconversion phosphors [340]. Moreover, the ESA process more likely occurs at low doping concentration (below 1 %). At higher doping concentration, non-radiative cross-relaxation processes are likely to occur, degrading the upconversion emission [339], [353].

Energy transfer upconversion

ETU process, similar to ESA, utilises sequential absorption of two photons to populate the metastable level (Figure 1.19 b). The difference is that energy transfer upconversion involves two neighbouring ions. Firstly, the sensitiser ion is excited from the ground state to the metastable excited level [342]. The energy is then transferred nonradiatively to the ground state of the sensitiser and the excited state of the nearest activator ion, which is subsequently excited to its higher excited state.

Then, the upconversion emission is generated from the activator ion when electrons drop back to the ground state or lower excited state of the activator [353]. In the ETU process, the upconversion efficiency is sensitive to the spatial distance between the sensitiser-activator pair and to the concentration of dopants [351]. The lanthanide ions, which possess multiple excited states, are highly suitable for the ETU process; thus, the most frequently used sensitiser/activator pair are those composed of Yb^{3+}/Eu^{3+}, Yb^{3+}/Tm^{3+}, Yb^{3+}/Er^{3+}, and Yb^{3+}/Ho^{3+}. The ytterbium ion as the sensitiser has a large absorption cross-section and only two energy levels in its electronic structure; therefore, the wide range of Yb^{3+} concentration from 10 to 100 % do not evoke cross relaxations [348], [353].

Photon avalanche

A photon avalanche process leads to upconversion emission under excitation pump power above a certain threshold value. The PA is a looping process, which involves the ESA process for excitation light and cross-relaxation process that generates feedback and leads to upconversion emission without the resonant ground-state absorption [343]. The PA process (Figure 1.19 c) takes place in three steps. Firstly, the photon avalanche is initiated when an electron in the ground state ion is promoted to intermediate-excited state level through non-resonant ground-state absorption, which is further followed by the ESA process to promote the population of upper-excited level. Finally, the upper-excited level of an ion interacts with the ground state of the neighbouring ion, and the ions undergo cross-relaxation of energy transfer yielding in two ions with an intermediate-excited level. The repeating process leads to an exponential increase in the population of higher-excited state level [340], [355]. If the cross-relaxation energy transfer is efficient, both ions will be promoted in the intermediate-excited state level, and two ions will be then available for the ESA process from intermediate to higher-excited state. The pump photon is resonant only with the transition from the intermediate excited state to the higher excited state of upconversion-emitting ion, not with the transition from the ground state of both ions. When the UC emitting ion is excited to its intermediate state, and the pump photons are resonant with the transition from the intermediate excited state to the higher excited state, it can be then excited to its higher state via the ESA process [343], [348].

Cooperative energy transfer

A cooperative energy transfer upconversion process is comparable to the ETU process; however, the process involves two similar sensitiser ions and an activator ion [348]. In the CET process (Figure 1.19 d), two sensitising ions in the intermediate-excited state are further cooperatively excited to the virtual higher-excited state level. Then, simultaneously transfer of the accumulated energy to the neighbouring activator occurs, reaching the higher-excited state. The upconversion emission takes place when the activator ion is relaxing from the higher-excited state to the ground state. The major difference between ETU and CET processes is that the activator in the CET mechanism does not have an intermediate energy level compatible with the levels of sensitisers [346]. Besides the upconversion emission from the activator, low-efficiency upconversion from cooperative sensitisers can also be noticed [353].

Energy migration-mediated upconversion

The EMU process is based on the transfer of the energy within the core-shell structure (Figure 1.19 e). Four types of luminescent centres with well-defined concentrations and integrated into separate layers of nanoparticles are involved in the process, namely sensitiser, accumulator, migrator and activator [346]. In a typical energy migration-mediated upconversion, due to the low-energy photons excitation, the higher excited state of the accumulator is populated. Next, the absorbed energy migrates to an adjacent migrator in the same region, followed by a subsequent energy transfer through the core-shell interface to the migrator ions. Finally, the energy is trapped by an activator and emit upconversion due to the electrons' return to the ground state. The upconversion emission from the accumulator also occurs in the EMU process [353].

1.8.3 Synthesis techniques

The synthesis process of upconverting material is of importance to obtain a high efficiency of upconversion. Several synthesis methods are available to achieve good optical properties, monodispersity, or facility of surface modification [339].

Thermal decomposition

This method is one of the commonly used strategies for upconverting nanoparticles synthesis. The synthesis is based on the surfactant-assisted decomposition of a precursor in the high-boiling solvents. Trifluoroacetic or oleic acid rare earth salts and rare earth halides are the commonly applied precursors [346]. Oleic acid, octadecene, oleylamine or trioctylphosphine oxide are often used surfactants [342], [346], [356], among which octadecene, with a boiling point higher than 300 °C, is often used to provide a high-temperature environment. Whereas oleic acid and oleylamine are applied as a coordinative solvent for metallic elements and surfactant due to their long alkyl chains inhibiting aggregation of nanocrystals [356]. The precursors in the organic solvents undergo decomposition under elevated temperature, and the generated ions combine into new nuclei [339]. The quality of upconversion nanoparticles, the good crystallinity, the narrow size distribution, shape and optical properties strongly depend on the synthesis parameters such as reaction time and temperature, the solvents nature, and reagent concentrations [339], [340]. The nanoparticles obtained by the thermal decomposition synthesis have uniform size, high crystallinity and high upconversion efficiency. However, there are some drawbacks like high temperature of the reaction, oxygen-free and anhydrous conditions during the synthesis process [346], air-sensitive starting materials [341], toxic fluorinated by-products, and hydrophobic ligands involving post-surface hydrophilic modification when applied for biological systems [340]. In the thermal decomposition process, fast nucleation and growth occur, leading to more structural defects resulting in a relatively lower upconversion quantum yield [342].

Coprecipitation

A chemical coprecipitation synthesis is an easy and convenient method for rare-earth-doped upconversion nanoparticles due to the relatively mild reaction conditions, simple synthesis procedures, low costs of the equipment, absence of toxic by-products, and short reaction time [344]. This approach is based on the precipitation of the desired product out of the precursor solution [356] in the presence of surface capping ligands, e.g. ethylenediaminetetraacetic acid (EDTA), polyvinylpyrrolidone [357], or polyethyleneimine (PEI), which promote the nucleation of the nanocrystals [341]. The concentration of the capping ligands influences the size of the nanoparticle [348]. The reaction temperature does not have to be high; however, synthesis in low temperatures requires a longer

processing time. For instance, the synthesis reaction time of RE-doped $NaYF_4$ UCNPs with the α-phase structure takes 24 hours, whereas the β-phase nanocrystals need ten days of the synthesis [356]. In the coprecipitation synthesis of rare earth $NaYF_4$ phosphors, the annealing step is strongly required to increase the material's crystallinity and improve the upconversion luminescence [343]. The post-heat treatment of UCNPs capped with EDTA lead to a decrease in hydrophilicity of the material due to the carbonisation of EDTA. However, further surface silanisation may result in an improvement of the hydrophilic nature of the nanomaterial but also lead to the size increase [344], [348].

Hydrothermal synthesis

In contrast to the thermal decomposition method, an aqueous solution can be applied in a solution-based hydrothermal synthesis. The synthesis can be conducted under lower reaction temperature (160–220 °C) and in the mild reaction conditions [356], [358]. Nevertheless, it is possible to add organic solvents to control the crystal growth [357]. In the hydrothermal synthesis, a mixture of reaction precursors, surfactants and solvents is heating and processing in the sealed autoclave under high temperature and pressure [347]. The common reaction precursors are rare earth chlorides, nitrates and acetates, as well as hydrofluoric acid, ammonium fluoride, sodium fluoride, ammonium hydrogen difluoride, or sodium tetrafluoroborate [356]. The process is based on the reaction between positive and negative ions, which lead to the precipitate of a nanoscale product from the solvent [347]. The crystalline phase, morphology and size of the upconverting nanoparticles is controlled by the addition of surfactants like cetyl-trimethylammonium bromide, PEI, EDTA, oleic acid, or citric acid, which have the ability to chelate the cations. Besides the surfactant, the nanocrystals parameters can also be adjusted with the pH of the reaction, the molar ratio of rare earth precursor to fluoride precursor, the fluoride source or hydroxyl ions addition [356]. A general strategy of synthesis the monodispersed NPs via hydrothermal synthesis is the “liquid-solid-solution” approach. The reaction system consists of three phases: a solid phase, e.g. sodium linoleate, a liquid phase, e.g. ethanol or linoleic acid, and a solution phase, e.g. solution of water and ethanol holding metal ions. In the case of sodium yttrium fluoride nanocrystals, the yttrium ions in the water-ethanol solution phase undergo the ion exchange to the solid phase at the solid/solution interface and coprecipitate with fluoride ions to form a product. The product stays at the bottom of the vessel due to the weight and hydrophobic nature [342], [356]. This method has several advantages, including easy operational process, relatively

low temperature of the process in comparison to thermal decomposition method [347], possibility to produce nanomaterial with controllable size and shape and high crystallinity [342], and producing fewer toxic by-products than thermal decomposition [357]. However, this approach needs a specialised autoclave which does not allow for particles' growth observation [342].

Combustion method

In comparison with thermal decomposition or hydrothermal method, combustion synthesis is a highly energy-efficient process of synthesising luminescent material in a very short time. The reaction mixture consists of an aqueous solution of an oxidiser, e.g. metal nitrate and a reducing agent, e.g. organic fuel [346]. The combustion synthesis is a highly exothermic process with temperatures ranging from 500 to 3000 °C [343]. It includes a series of controlled explosions initiated by a heat source in the form of a self-sustaining combustion wave which propagates through the reaction components [341]. The reaction mixture is balanced to release the maximum energy during the process. The size of the obtained material can be controlled by the fuel-to-oxidiser ratio [346]. The combustion method is generally applied to oxide and oxysulfide UCNPs like Y_2O_3:Er^{3+},Yb^{3+} [359], La_2O_2S:Yb^{3+},Pr^{3+} [360], Gd_2O_3:Er^{3+} [361], or $Gd_3Ga_5O_{12}Tm^{3+}$,Yb^{3+} [362]. Furthermore, this method is relatively time-, energy- and cost-effective, scalable and efficient [339]. However, the material aggregation, difficult size control, not sufficient purity and weak luminescence properties of the product are the main drawbacks [343], [346].

Sol-gel method

The sol-gel process is a wet chemical bottom-up synthesis for upconversion nanocrystals generation. The process is based on the hydrolysis and polycondensation of metal precursors, mainly alkoxides, halides or nitrates. Post-treatment calcination or annealing is often performed in order to improve the crystallinity of the material, thereby the luminescence efficiency [339], [347], and remove the solvent from the gel [339]. The main advantages of sol-gel synthesis are low reaction temperature, easy control of dopant amounts, low cost [346], and scalability of the process. On the other hand, the reaction process is relatively long, the particles are of irregular shape, not uniform size, not soluble in water [339], [347], and aggregation of the material can occur during the high-temperature calcination process [346]. The sol-gel method is often used for synthesis of metal

oxides as a matrix material e.g. Er^{3+} doped TiO_2, $BaTiO_3$ [363], ZrO_2 [364], YVO_4 [365], as well as YVO_4:Yb^{3+},Er^{3+} [366] or $Lu_3Ga_5O_{12}$:Er^{3+} [367].

Microemulsion method

The microemulsion systems are thermodynamically stable colloidal dispersions composed of organic solvent, surfactant, co-surfactant and precursors [368]. The microemulsion method can be applied to obtain upconversion nanoparticles with controlled morphology and small size of the nanoparticles [369]. The amphiphilic surfactant form a monolayer on the oil and water interface, and the reaction undergo inside the droplets. The microemulsion synthesis is a facile and cost-effective operation, yielding monodisperse and shape-controlled nanoparticles [347], [370]. However, a small yield of the product and tough product separation renders this method challenging to apply on a larger scale [347].

1.9 Lanthanide complexes

The lanthanides are a series of elements with an electronic configuration of $[Xe]4f^n$, where n is in the range of 1 for cerium ion (Ce^{3+}) to 14 for lutetium ion (Lu^{3+}) [371]. The lanthanides are metals that emit fluorescence in an aqueous solution and display decay times of 0.5 to 3 ms. In the stable trivalent oxidation state, the lanthanides have an incompletely filled 4f shell. The filled $5s^2$ and $5p^2$ orbitals shield the 4f orbital from the interactions with surroundings. The emission is displayed due to the inner transitions in 4f orbitals of an atom, which are forbidden transitions because they do not correspond to a parity change [372], [373]. Thus, lanthanides alone are weak absorbers, with extinction coefficients approx. 0.1 $M^{-1}cm^{-1}$ and their emission rates are slow. Due to the weak absorption, the lanthanides can be indirectly excited through chelated organic ligands [373]. Some organic ligands can act as photosensitisers for lanthanide ions in the lanthanide complexes, enhancing their luminescence intensity due to the energy transfer and protecting it from the non-radiative transitions [372].

The lanthanide complexes' design, photoluminescence properties and applications are widely investigated in recent years. A number of lanthanide' ligand classes have been researched so far, including macrocyclic ligands, β-diketones, calixarenes, podands, carboxylic acid derivatives, proteins, terphenyl ligands etc. Although lanthanide ions exhibit small absorption coefficients, the complexation with organic ligands significantly improves the quantum yield. The lanthanide

complexes emit luminescence in a wide range of radiation depending on the lanthanide ion, e.g. near-infrared light (Yb^{3+}, Nd^{3+}, Er^{3+}), blue (Tm^{3+}), yellow (Dy^{3+}), and orange (Sm^{3+}) in the visible region of the light spectrum, or the near-ultraviolet (Ce^{3+}, Gd^{3+}). However, most lanthanide complexes yield red or green light emission due to widely applied Eu^{3+} and Tb^{3+} ions, respectively [374]. The luminescence of the lanthanide compounds is characterised by a line-like emission, which leads to a high colour purity of emitted light [375]. Although the lanthanide complexes perform highly efficient light emission under ultraviolet light irradiation, these materials possess some drawbacks like low thermal and photochemical stability and weak mechanical properties. Also, some lanthanide complexes are in the form of hydrates with two or three molecules in the first coordination sphere of the central ion, which lead to the emission quench by the activation of nonradiative decay paths. Moreover, lanthanide complex may undergo degradation under long UV light illumination, decreasing the emission intensity [371].

The wide interest in lanthanide complexes application is directed toward lanthanide-based organic-inorganic hybrid materials. In these materials, either the molecular lanthanide complex is embedded in an inorganic host structure, or inorganic lanthanide-doped material is incorporated in an organic polymer matrix. The luminescent lanthanide complexes in hybrid materials indicate better mechanical and optical properties and thermal stability in comparison to molecular lanthanide complexes [375]. The lanthanide dopant ions such as Eu^{3+}, Er^{3+}, Nd^{3+}, Ce^{3+}, Eu^{2+}, Tr^{3+} are of immense interest due to their optical properties [376]. The lanthanide complexes provide a broad range of photonic applications like light conversion molecular devices (LCMDs), elements of the emitter layer in OLED, tunable lasers or amplifiers for optical communications. LCMDs have found the application as luminescent labels in advanced time-resolved fluoroimmunoassay [371], fluorescent lighting, luminescent sensors for chemical species (e.g. OH^-, O_2, H^+, halide ions), or solar cells antireflection coatings [374].

1.9.1 Luminescence of lanthanide complexes

The light emission of the lanthanides is often termed luminescence than fluorescence or phosphorescence. According to the IUPAC definition of those processes, the term fluorescence concerns the emission of the light by organic molecules without changing the spin (transition from excited singlet state to ground singlet state, $S_1 \rightarrow S_0$), and phosphorescence is related to the emission of the light with a spin changing (transition from excited triplet state to ground singlet state, $T_1 \rightarrow S_0$)

[375], [377]. The lanthanides narrow-line emission of light, in turn, is resulted from the transitions inside the 4f shell, thus the intraconfigurational f-f transitions [375]. As mentioned previously, the lanthanides exhibit weak light absorption due to the shielding 4f orbitals by the filled $5p^6 6s^2$ subshells. The emission intensity among the lanthanide ions varies and depends on populating the excited state and the minimised non-radiative deactivation path [378]. For efficient absorption of the lanthanide ion, the sensitisation via the surroundings (e.g. organic "antenna" chromophore) of the ion must be applied. The mechanism of energy transfer from the sensitising ligand to the metal ion was proposed by Crosby et al. [379] (Figure 1.20). The indirect sensitisation, also called antenna effect, is proceeded in a way that first the light is absorbed by the organic ligand, which is attached to the lanthanide ion. Subsequently, due to, e.g. interactions with the solvent, fast internal conversion from a vibrational level of the first excited state S_1 to the lowest vibrational excited state occurs. The efficient excitation of the ligand in its excited singlet state may be followed by either radiative deactivation to the ground state S_0 (fluorescence process) or by non-radiative intersystem crossing to its triplet state T_1. Then the energy can be either deactivated radiatively to the singlet ground state emitting phosphorescence or subsequently transferred onto one or more excited states of the lanthanide ion from where the light is finally emitted in the characteristic line-like luminescence [380], [381].

The overall quantum yield is then given by: $Q_{Ln}^{L} = \eta_{isc}\eta_{et}Q_{Ln}^{Ln}$, where Q_{Ln}^{L} Q_{Ln}^{Ln} stands for the indirect and direct excitation, respectively, η_{iscs} is the intersystem crossing process efficiency, and η_{et} stands for the efficacy of the ππ*–Ln transfer. The quantum yield of Q_{Ln}^{Ln} depends on the energy gap between the lowest-lying excited state of the lanthanide ion and the highest sublevel of its ground state. Europium, gadolinium and terbium ions have the best Q_{Ln}^{Ln} due to the widest gaps [378]. The smaller are the gaps, the easier occurs the process of non-radiative deactivation due to the interactions between the lanthanide ions and suitable vibrational modes of the surroundings, e.g., –OH groups of the solvent. The hydroxyl groups coordinated to the metal ion provide effective non-radiative deactivation due to the vibrational coupling with the vibrational states of the –OH oscillator. Therefore, the overall luminescence intensity depends on the intensity of the ligands absorption, the ligand-to-metal energy transfer, and the efficiency of metal luminescence emission [382].

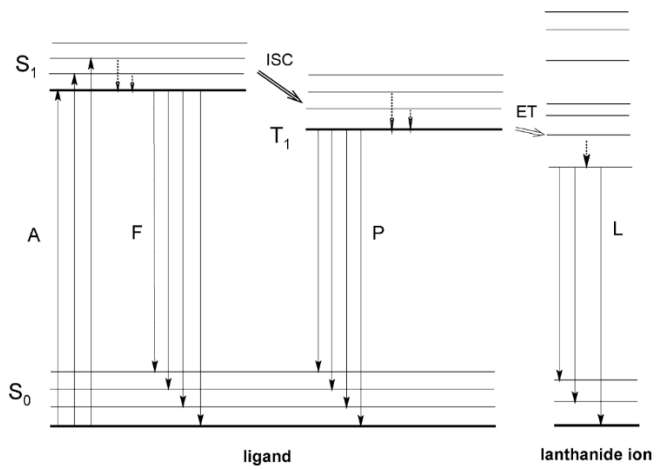

Figure 1.20 A diagram of the lanthanide (III) complexes photophysical processes – antenna effect. Abbreviations: A – absorption, F – fluorescence, P – phosphorescence, L – lanthanide-centred luminescence, S – singlet, T – triplet, ISC – intersystem crossing, ET – energy transfer. Full lines – radiative transitions, dotted lines – nonradiative transitions [381]

The advantageous coordination groups among the polydentate ligands of the lanthanide complexes are linear polydentate and multifunctional ligands, among which the rare earth β-diketonates, polyaminocarboxylates, and cyclic Schiff base derivatives are the largest classes. β-diketonates constitute the efficient coordination compounds, existing as five-unit chelate rings. The β-diketonates exhibit the bidentate nature, which frequently lead to the formation of hexa-coordinated tris-complexes. To complete the coordination sphere of the lanthanide ion, two water molecules are often coordinated, decreasing the luminescence properties of the complex. However, water molecules can be effortlessly exchanged with other organic chromophores [378]. The polyaminocarboxylates form strong complexes with metal ions, have high binding constant to lanthanides and higher than six coordination numbers [383], [384]. Cyclic Schiff base derivatives are formed in the condensation process of amine and formyl precursors, and they easily react with lanthanides to form complexes [385].

1.9.2 Properties of rare earth β-diketonates

The most widely explored rare earth coordination compounds are 1,3-diketones (β-diketonates) [386]. Due to their properties, these complexes have been broadly used in recent years as NMR shift reagents [387], extractants in solvent-solvent extraction process [388], active compounds for liquid or chelate lasers [371],

luminescent sensors in time-resolved immunoassays [389], electroluminescent matter in OLEDs and fluorescent lamps [390]. The β-diketones structure is based on two carbonyl groups separated by one α-carbon, mostly substituted with a hydrogen atom, however, the substitution with alkyl or fluorinated alkyl group, and an aromatic or heteroaromatic group is also possible. The elementary β-diketone is acetylacetone, with each carbonyl group substituted by a methyl group. Other β-diketones are formed by substituting a methyl group with other chemical species depending on the desired properties of the complex. The chemical entities such as branched alkyl chains enhance the volatility and solubility of the complex in organic solvents. Also, the aromatic groups increase the light absorption, and the perfluorinated alkyl substituents increase the Lewis acidity. Moreover, some substituents influence the position of singlet and triplet energy levels, crucial in the luminescence output [381]. The β-diketones based ligands also enhance the thermodynamic stability, volatility and luminescence properties [391].

Three main configurations of rare earth β-diketonate complexes are distinguished: tris complex, Lewis base adducts of a tris complex, and tetrakis complex. The tris complexes are neutral entities with three β-diketonate ligands coordinated to one metal ion. Due to the unsaturated coordination sphere in the six-coordinate complexes, the rare-earth ion is able to extend the coordination sphere by bridging β-diketonate ligands or by the formation of adducts with Lewis base like water, 2,2'-bipyridine, 1,10-phenanthroline [392], or tri-n-octylophosphine oxide. Tetrakis complexes are formed by the four β-diketonate ligands coordinated to the single metal ion. The electrically neutral form of these complexes can be achieved with a counter cation such as alkali metal ions like Li^+, Na^+, K^+, Rb^+, Cs^+, protonated organic bases like pyridinium, or quaternary ammonium ion like Et_4N [381], [393]. Among the myriad rare earth β-diketonate complexes, the most popular are those based on europium ion conjugated with 2-thenoyltrifluoroacetone and 1,10-phenanthroline ($[Eu(TTA)_3(Phen)]$ [394]. The most frequently used, however, are tris complexes of rare-earth ion conjugated with either 6,6,7,7,8,8,8-heptafluoro-2,2-dimethyl-3,5-octanedione (FOD) or 2,2,6,6-tetramethyl-3,5-heptanedione (THD), applied as NMR shift reagents or volatile precursors for chemical vapour deposition.

The rare earth β-diketonates are obtained in the form of crystalline powders or viscous liquids. Most of these complexes are not hygroscopic; however, the tris complexes are able to interact with up to three water molecules, forming seven, eight or nine coordinate complexes. The rare-earth complexes dissolved in a solvent undergo a fast ligand exchange due to the high kinetic lability. Among the β-diketonate ligands, those forming complexes with europium exhibit an intense visible luminescence. The β-diketonate complexes with trivalent erbium, ytterbium,

holmium, thulium, praseodymium, and neodymium ions indicate weak visible and near-infrared luminescence. Terbium ions complexes with most of the β-diketonates exhibit weak or no luminescence. Due to the high energy of 4f levels, gadolinium ion complexes indicate no metal-centred photoluminescence. Also, lanthanum and lutetium exhibit no metal-centred photoluminescence due to an empty 4f shell and a filled 4f-shell, respectively [381]. The luminescence intensity of the rare earth β-diketonates highly depends on ligand dissimilarity, ligand diversity, and centrosymmetry [395]. The amount of radiation absorbed by the ligands, the quantum yield of the complex luminescence, and the temperature are also the factors influencing the photoluminescence intensity. Whereas the quantum yield of the rare earth complex is a result of several processes such as energy transfer from the ligand to the metal ion, multiphonon relaxation, back-transfer, and cross-over to charge-transfer states [374]. In the case of europium (III) β-diketonates, the highest luminescence intensity is observed for the tetrakis complexes and a combination of aliphatic and aromatic substituents on the β-diketonates. The high luminescence intensity is due to the more efficient energy transfer from the ligand to the metal ion and the higher anisotropy around the europium ion. The slightly lower intensity indicate Lewis base adducts, with a well-known [$Eu(TTA)_3(Phen)$] complex exhibiting good luminescence intensity. The weakest luminescence was found for tris complexes. Aliphatic β-diketones coordinated to the europium ion exhibit weak luminescence due to the large energy gap between ligand triplet state and europium ion resonance levels, leading to the less efficient energy transfer [381].

The luminescence quantum yield, and thereby the luminescence quenching, depend on both ligand and metal ion. However, the luminescence decay time is related only to the extent of quenching at emitting metal ion. The luminescence decay times vary among the europium (III) β-diketonate complexes and the solvents. Ligands substituted with fluorine yield a quenching decrease and increase in the decay time at room temperature. The europium (III) β-diketonates properties are temperature-dependent; however, the tris ligand complexes exhibit larger temperature dependence and shorter luminescence lifetimes than tetrakis chelate [396].

1.10 Photoluminescence imaging of fingermarks

A photoluminescence imaging in the fingermark detection process has been developed in the seventies of the XX century. Photoluminescence is a process in

which an object absorbs the energy of light at an appropriate wavelength and subsequently reemit the light with a longer wavelength, and therefore lower energy, than was absorbed. Fluorescence and phosphorescence are the photoluminescence processes that differ in the length of time of emitted radiation. In photoluminescence imaging, the visualisation process is based on absorption/emission of light by the fingermark [397]. Fingermarks themselves show fluorescence due to the intrinsic properties of the fingermark residue components, which exhibit native fluorescence. For instance, riboflavin and pyridoxine, present in the fingermark sweat, fluoresce under UV light irradiation at 565 nm and 400 nm, respectively. Imaging the fingermark, which exhibits native fluorescence, is non-destructive and non-invasive. This enables other subsequent procedures of fingermark development in case of failure. Nevertheless, since the quantities of luminescent components in fingermark deposits are rather small, high-intensity excitation sources are needed [398]. The fingermarks may also be intentionally sensitised with a luminescent agent or contaminated with foreign substances like blood or semen, which, excited with an appropriate wavelength of light, emit luminescence. The luminescent fingermark is then visually observed through a filter that blocks the reflected excitation light and can be finally photographed through the same filter. However, numerous objects or substrates acting as a background for fingermark indicate strong fluorescence that can significantly reduce the sensitivity of the imaging object. The background interference can be suppressed either by sensitising the fingermark deposit with a luminescent agent of a different colour than the background in order to filter the background emission optically or by increasing the fingermark luminescence intensity by time-gated imaging [397].

Fluorescence imaging

Fluorescence occurs when an electron in an excited state returns to the ground state emitting the light with lower energy than the absorbed one. Electron in the excited orbital has an opposite spin orientation than the electron in the ground state orbital. Due to allowed transitions, electron return to the ground state rapidly, emitting a photon [373]. The typical fluorescence emission lifetimes vary from 10^{-9} to 10^{-6} s^{-1} [399]. A specific wavelength of excitation has to be chosen to visualise the latent fingermark in the fluorescence mode according to the nature of the luminescent developing agent. When a fluorophore is excited with the light of an appropriate wavelength, the electrons from a ground state are promoted to the excited state. Then the electrons drop to the lowest excited state due to the radiationless transitions and subsequently return to the ground state with the

emission of radiation with the lower energy than initially absorbed [60]. The fluorescence mode of imaging involves recording the fluorescence emission from developed fingermark. In fluorescence imaging, typically, a monochromatic excitation light source is applied, usually ultraviolet light (350 nm), as well as blue [400], green or yellow light of visible spectrum. The excitation of the imaged object results in the luminescence emission in the yellow, orange, red or NIR regions of the light spectrum. When the excitation radiation illuminates the examined sample bearing the fingermark, most light is scattered or reflected; only some light is absorbed. Thus, to obtain the clear fingermark image with high sensitivity, the scattered and reflected UV illumination has to be separated from the fluorescence light by applying filters between the sample and the examiner's eye or image capture device [60] [Figure 1.21]. Generally, yellow filters are used for UV to 445 nm wavelength incident light. The orange filters are applied for light sources illuminated in the range of 445 to 515 nm. The red filters are involved for 515 to 550 nm light excitation. Examining fingermarks in the fluorescence mode requires using the UV excitation protective googles by the examiner for health and safety considerations [20]. Moreover, the fluorescent mode imaging has to be conducted in the dark room, without any ambient light. Also, the exposure time needs to be minimised due to the possible quenching of fluorescent activity of the luminescent developing agent [400]. However, unlike in conventional photography, the low emission light levels often require exposure times longer than one second. To avoid overexposure of the fluorescent fingermark image, the photoluminescent object must cover 70 % of the viewing field. In photoluminescent imaging, the excited object with a fingermark emits luminescence against the background. In ideal conditions, the background would have been black; however, the objects often emit some luminescence, which is interfering with the fingermark light emission. To optimise the conditions of imaging, frequency filters can also be used. These filters increase the image quality, maximising the contrast due to the adjusted wavelength of excitation and barrier filter for background fluorescence [401].

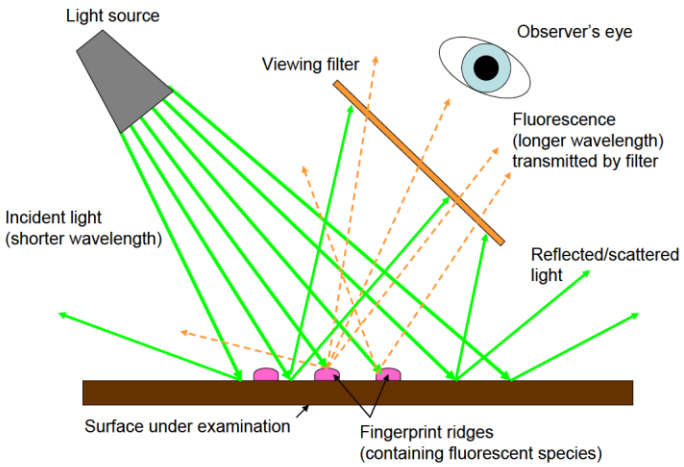

Figure 1.21 A diagram of fluorescent mode imaging of fingermark sensitised with the fluorescent species [60]

Upconversion luminescence imaging

In contrast to conventional fluorescence, upconversion luminescence is based on the conversion of two or more low-energy photons to higher-energy emission (as described in Chapter 1.8) [402]. The general principle of upconversion luminescence imaging is similar to fluorescence imaging (Figure 1.21). The differences are related to the excitation light source and applied filters. The upconversion luminescence is less efficient than conventional luminescence with the Stokes shift; therefore, a higher intensity light source is needed in the imaging process. The UCNPs can be excited by low-power lasers (1-1000 W/cm^2) [403] operating in the near-infrared light spectrum, mainly 980 nm [404]–[407]. Also, the infrared barrier filter has to be used to eliminate the detection of the reflected IR wavelengths. Applying upconverters for fingermark imaging is advantageous because this allows eliminating background interference from a variety of surfaces [217], [408]. Many consumer products exhibit luminescence when illuminated with UV or visible light. This is due to the dyes, inks, or binders present in the surface structure, which emit broadband luminescence. Much fewer surfaces fluoresce when exposed to near-infrared radiation than to UV light. Also, some dyes or inks used to secure the documents, e.g. banknotes, absorb the infrared light [404], [409].

Phosphorescence imaging

Phosphorescence occurs when the light, absorbed by the luminophore, is emitted from its triplet excited state to the singlet ground state. In this process, the electron in an excited orbital has the same spin orientation as the electron in the ground state. The transition from the excited triplet state to the ground singlet state is forbidden; therefore, the emission lifetimes, ranging from 10^3 to 10^0 s^{-1}, are much longer than in the case of fluorescence and last from milliseconds to seconds [373]. As mentioned above, the background fluorescence may be the relevant hindrance in fingermark visualisation competing with the fingermark fluorescence. Moreover, many objects, e.g. wood, emit intense and spectrally broad fluorescence, which is infeasible to filter from the fingermark fluorescence optically. However, the fluorescence lifetimes of many encountered backgrounds are typical of nanosecond orders. Thus, to address the background interference problem, time-gated imaging can be proposed. In time-gated imaging, the fingermark is sensitised with a developer, which yields a luminescence lifetime longer than the background fluorescence [103]. A great number of compounds yielding microseconds to seconds lifetimes can be applied as development agents for time-gated imaging. Menzel was the first who started to investigate lanthanides as the luminescent agents for fingermark detection with time-gated imaging. He explored europium and terbium complexes with a Ruhemann's Purple formed on the fingermark ridges within ninhydrin treatment. These complexes have a relatively long luminescence lifetime in the order of milliseconds [397], [410], [411]. A wide group of long luminescence lifetime compounds constitutes the lanthanide β-diketonates, described in Chapter 1.9, which may also be employed to fingermark detection [412], [413]. Nanophosphors with long afterglow, involving $Zn_2TiO_4:Sm^{3+}$ [414], $CaGdAlO_4:Eu^{3+}$ [415], $Ca_4(PO4)_2O:Eu^{2+}$ [416], $SrAl_2O_4$:Eu,Dy [417], or $SrGa_{12}O_{19}:Mn^{2+}$ [418] have been also investigated as a potential development agents for time-gated imaging.

Menzel developed the first system of time-gated imaging for fingermark detection in 1979. In this early device, the rotating cylinder with two slots was applied to chop the excitation light. The fingermark sample was mounted inside the cylinder. During the rotation, when one of the cylinder slots was positioned in front of the light source, both the fingermark and the background were excited. Subsequently, when the exciting light was screened (turned off), the photoluminescence started to decay. At this time, the second slot was positioned in front of the detector/photographic camera and collecting the signal using the differences in emission lifetimes of fingermark and the background. The speed of the cylinder, the position of the detector and the width of the slots determined the delay

of the detection and length of exposition time. However, due to technical limitations, this idea of fingermark imaging was postponed for several years [20]. The time-gated imaging started to be more efficient and practical since the charge-coupled device (CCD) camera was designed as well as a microchannel plate image intensifier (MCP), which increase the intensity of low luminescence light and can be switch on and off in times on the order of 10^{-8} seconds. In this imaging system, the electronic light chopper is conjugated with a gateable CCD camera, which is further controlled by the computer (Figure 1.22 A). The argon-ion laser, which is modulated by the light chopper, illuminate the fingermark. The CCD camera recording time is synchronised with the excitation laser pulses and is switched on after the background fluorescence decayed. The fingermark luminescence lifetimes, feasible to record, are of 10^{-7} seconds [397]. The photoluminescence of the phosphorescent fingermark developer decays exponentially when the excitation radiation is turned off. Due to the fact that the decay of background fluorescence is on the order of nanoseconds, when the imaging device is turned on with a delay to light source cut-off, the background fluorescence would decay, and the fingermark luminescence can be recorded. The imaging can be processed repeatedly (Figure 1.22 B) [103].

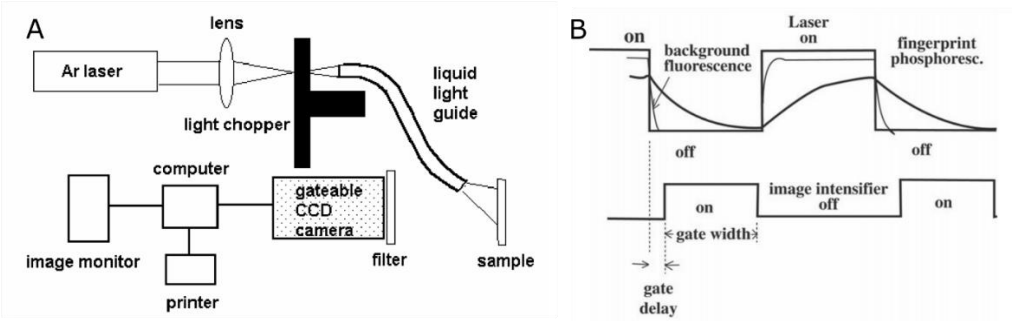

Figure 1.22 A diagram of a time-gated imaging system (A) and a scheme of gating image with an image intensifier (B) [397]

Digital imaging

The form of digital imaging in a forensic examination is closely related to the application in terms of the location of the fingermark investigation, the type and quality of objects bearing fingermarks, the form of fingermark development etc. For field-based imaging, at crime scenes, where fingermarks are developed by powdering techniques, recording the hand-held single-lens reflex (SLR) camera is frequently used due to its portability and flexibility [21], [419]. However, this imaging device can also be used in the laboratory. On the other hand, for more sensitive

processes and demanding requirements such as small field of view or low light intensity, a CCD camera can be applied. This type of imaging device offers extended exposures and multiple-averaged images, which increase the signal-to-noise ratio. Nonetheless, the image processing has to be done in the laboratory [419].

The CCD camera is a sensitive photon detector widely applied in physics, astronomy or engineering to low-light and light-sensitive applications, which require high resolution. This is a solid-state, silicon-based electrical device that converts the light input into the electronic signal. The sensor consists of an array of light-sensitive pixels which are controlled by electrodes. Photons of high enough energy, which strike the surface of the sensor, are captured due to the positive potential applied to each pixel. To minimise the number of errors in the photon detection caused by thermal processes, the CCD sensors are equipped in a cooling system [420]. The CCD camera can be of monochrome or colour type. In the colour CCD-based camera, the colour is obtained as a result of data acquisition in the three colour channels (red, green, blue, RGB), which can be done in two ways. In the first way, the CCD sensor possesses three arrays, one for each channel, and the incident light is spilt with a prism. The second way concerns a Bayer filter containing the RGB elements, which coincide with the individual photosites of a CCD chip. This enables recording the discrete RGB responses over the field of view and further interpolating raw data from the captured image to the coloured image. For fingermark imaging, the monochrome CCD camera is more suitable, especially in the case of luminescent fingermarks visualisation, where the optical filters are often used to facilitate imaging. When the optical filter, e.g., 530 nm band-pass filter, is used on the colour CCD camera, the limited response is acquired from blue- and red-filtered photosites, which is half of the collected image data [419].

Forensic Light Sources

Forensic light sources are portable, versatile devices, which offer excitation light in a range of wavelengths covering ultraviolet and the entire visible light spectrum, ideally with a narrow bandwidth from 30 to 50 nm [401]. Lasers are one of the devices applied to detect and enhance fingermarks, biological stains, fibres, footwear impressions, or paints. They produce light of high intensity and precise operating wavelength, providing a good sensitivity. Moreover, lasers can be used to enhance the fingermarks indicating weak fluorescence. However, laser properties make it an inflexible device due to the limited number of accessible wavelengths [20]. The process of laser action is based on the stimulated emission radiation (LASER is an acronym of Light Amplification by Stimulated Emission of Radiation). When an

atom in its excited state, which differs from a ground state by the energy E, is impinged by the photon of energy E, the relaxation of an atom to the ground state with the emission of the incident photon is triggered. At the same time, the atom release a photon of energy E with the same phase, polarisation and direction that the incident photon. Since the atoms are primarily in their ground state and absorption is more probable than emission, the population inversion must occur in the laser action. Thus, more atoms have to be in their excited state to activate the stimulated emission by the incident photon of a suitable wavelength. These photons trigger the subsequent stimulated emission leading to an avalanche of coherent photons [103].

The alternate to the laser is the non-laser high-powered white-light source, for instance, xenon arc lamp, equipped in a range of filters to select the desired monochromatic wavelength of excitation light. The typical non-laser light source consists of a lamp, a cold mirror to reject the infrared radiation and transmitting only UV and visible light, and the bandpass filters for selecting the monochromatic band [401]. Recently, the light-emitting diodes for fluorescence examination have also been employed in the form of hand-held torches with the output power not differing from the arc lamps, however, broader than filtered systems [60]. A light-emitting diode is a semiconductor light source consisting of three different layers in an electronic circuit. The layers are deposited on a substrate in order: a top layer which is the p-type region with electron holes as charge carrier, a middle layer which is an active region with both electrons and electron holes; and the bottom layer, which is an n-type region with electrons. The electrons in the semiconductor recombine with electron holes yielding the photons release in an electroluminescence process. The width of the semiconductor bandgap determines the colour of the emitted light [421].

1.11 Aim of the research

This research aimed to develop an efficient and user-friendly optical method of latent and natural fingermark visualisation on porous and non-porous, reflective, glossy, patterned, colourful or luminescent surfaces. Focusing on the development of the optical visualisation method, the goals to be achieved by this work were specified as follows:

1. to determine which interactions between fingermark secretion components and various organic moieties deposited on the silica surface acting as a luminophore carrier would be the most effective
2. to design a new forensic reagent that will indicate a selective affinity to the fingermark components and which at the same time will exhibit the optical properties involving long-lived luminescence or upconversion, to eliminate the background interference or staining while imaging

1.12 Bibliography

[1] J. Wang *et al.*, "Near-infrared-light-mediated imaging of latent fingerprints based on molecular recognition," *Angew. Chemie - Int. Ed.*, vol. 53, no. 6, pp. 1616–1620, 2014, doi: 10.1002/anie.201308843.

[2] A. R. W. Jackson and J. M. Jackson, *Forensic Science Third edition*, Third. Pearson Education Limited, 2011.

[3] A. A. Frick, P. Fritz, and S. W. Lewis, "Chemical methods for the detection of latent fingermarks," in *Forensic Chemistry Fundamentals and Applications*, J. Siegel, Ed. Wiley Blackwell, 2016.

[4] C. Champod, C. Lennard, P. Margot, and M. Stoilovic, *Fingerprints and other ridge skin impressions, second edition*. 2017.

[5] P. Hazarika and D. A. Russell, "Advances in fingerprint analysis," *Angew. Chemie - Int. Ed.*, vol. 51, no. 15, pp. 3524–3531, 2012, doi: 10.1002/anie.201104313.

[6] Henry C. Lee and R. E. Gaensslen, *Advances Fingerprint in Technology*, vol. 1. 2001.

[7] M. Wood, P. Maynard, X. Spindler, C. Roux, and C. Lennard, "Selective targeting of fingermarks using immunogenic techniques," *Aust. J. Forensic Sci.*, vol. 45, no. 2, pp. 211–226, 2013, doi: 10.1080/00450618.2012.744847.

[8] E. Locard, *La police et les méthodes scientifiques*. Paris: Editions Rieder, 1934.

[9] C. Lennard, "The detection and enhancement of latent fingerprints," in *13th INTERPOL Forensic Science Symposium, Lyon, France*, 2001, p. D2: 85-98.

[10] M. J. Choi, A. M. McDonagh, P. Maynard, and C. Roux, “Metal-containing nanoparticles and nano-structured particles in fingermark detection,” *Forensic Sci. Int.*, vol. 179, no. 2–3, pp. 87–97, 2008, doi: 10.1016/j.forsciint.2008.04.027.

[11] C. Lennard, “Fingermark detection and identification: current research efforts,” *Aust. J. Forensic Sci.*, vol. 52, no. 2, pp. 125–145, 2020, doi: 10.1080/00450618.2018.1474948.

[12] A. van Dam, “Visualization of fingermarks by specific labeling with antibodies,” 2010.

[13] D. Meuwly, “Fingerprint, Forensic Evidence of,” in *Encyclopedia of Biometrics*, Z. L. Stan and J. Anil, Eds. Springer US, 2009, pp. 528–535.

[14] R. A. Hicklin, “Anatomy of Friction Ridge Skin,” in *Encyclopedia of Biometrics*, S. Z. Li and A. Jain, Eds. Springer-Verlag, 2014, pp. 1–6.

[15] W. J. Tilstone, K. A. Savage, and L. A. Clark, *Forensic Science An Encyclopedia of History, Methods, and Techniques*. Santa Barbara, California,: ABC Clio, 2006.

[16] D. Meuwly, “Forensic Use of Fingerprints and Fingermarks,” in *Encyclopedia of Biometrics*, S. Li and A. Jain, Eds. Springer US, 2014, pp. 1–16.

[17] C. Champod and P. Chamberlain, “Fingerprints,” in *Handbook of Forensic Science*, J. Fraser, R. Williams, C. Champod, and P. Chamberlain, Eds. Routledge, 2009.

[18] M. R. Hawthorne, *Fingerprints Analysis and Understanding*. CRC Press, 2009.

[19] D. Clegg, “Fingerprint identification,” in *The Practice of Crime Scene Investigation*, J. Horswell, Ed. CRC Press, 2004.

[20] B. Yamashita and M. French, “Latent Print Development,” in *The Fingerprint Sourcebook*, H. J. Eric H., R. Laurie O., L. John H., B. Yamashita, and M. French, Eds. National Institute of Justice, 2011, pp. 7.1-7.67.

[21] J. Siegel and P. Saukko, *Encyclopedia of Forensic Sciences*, 2nd ed. Elsevier Ltd, 2013.

[22] R. M. Bolle, A. W. Senior, N. K. Ratha, and S. Pankanti, “Fingerprint Minutiae: A Constructive Definition,” in *Biometric Authentication*, M. Tistarelli, J. Bigun, and A. K. Jain, Eds. Springer, 2002, pp. 58–66.

[23] N. Zaeri, “Minutiae-based Fingerprint Extraction and Recognition,” in *Biometrics*, InTech, 2011.

[24] V. Drapel, A. Becue, C. Champod, and P. Margot, “Identification of promising antigenic components in latent fingermark residues,” *Forensic Sci. Int.*, vol. 184, no. 1–3, pp. 47–53, 2009, doi: 10.1016/j.forsciint.2008.11.017.

[25] D. Light and D. A. Cooley, *Cells, Tissues, and Skin*. 2004.

[26] L. B. Baker, “Physiology of sweat gland function: The roles of sweating and sweat composition in human health,” *Temperature*, vol. 6, no. 3, pp. 211–259, 2019, doi: 10.1080/23328940.2019.1632145.

[27] E. J. Baxter, *Complete Crime Scene Investigation Handbook*, vol. 1, no. 1. CRC Press, 2015.

[28] S. Cadd, M. Islam, P. Manson, and S. Bleay, “Fingerprint composition and aging: A literature review,” *Sci. Justice*, vol. 55, no. 4, pp. 219–238, 2015, doi: 10.1016/j.scijus.2015.02.004.

[29] A. Girod, R. Ramotowski, and C. Weyermann, “Composition of fingermark residue: A qualitative and quantitative review,” *Forensic Science International*, vol. 223, no. 1–3. pp. 10–24, Nov. 30, 2012, doi: 10.1016/j.forsciint.2012.05.018.

[30] M. Wood, P. Maynard, X. Spindler, C. Lennard, and C. Roux, “Visualization of latent fingermarks using an aptamer-based reagent,” *Angew. Chemie - Int. Ed.*, vol. 51, no. 49, pp. 12272–12274, 2012, doi: 10.1002/anie.201207394.

[31] A. van Dam *et al.*, “Immunolabeling and the compatibility with a variety of fingermark development techniques,” *Sci. Justice*, vol. 54, no. 5, pp. 356–362, 2014, doi: 10.1016/j.scijus.2014.06.005.

[32] A. Van Dam, M. C. G. Aalders, K. van de Braak, H. J. J. Hardy, T. G. Van Leeuwen, and S. A. G. Lambrechts, “Simultaneous labeling of multiple components in a single fingermark,” *Forensic Sci. Int.*, vol. 232, no. 1–3, pp. 173–179, 2013, doi: 10.1016/j.forsciint.2013.07.020.

[33] H. Haskell, *Dermatopathology*, 1st ed. Elsevier Inc., 2010.

[34] B. Su, “Recent progress on fingerprint visualization and analysis by imaging ridge residue components,” *Anal. Bioanal. Chem.*, vol. 408, no. 11, pp. 2781–2791, 2016, doi: 10.1007/s00216-015-9216-y.

[35] K. Wilke, A. Martin, L. Terstegen, and S. S. Biel, “A short history of sweat gland biology,” *Int. J. Cosmet. Sci.*, vol. 29, no. 3, pp. 169–179, 2007, doi: 10.1111/j.1467-2494.2007.00387.x.

[36] C. C. Zouboulis, *Pathogenesis and Treatment of Acne and Rosacea*. Springer-Verlag, 2014.

[37] A. van Dam, “Fingermarks, more than just a ridge pattern,” UvA-DARE (Digital Academic Repository), 2014.

[38] G. Honari and H. I. Maibach, “Skin Structure and Function,” in *Applied Dermatotoxicology: Clinical Aspects*, Elsevier Inc., 2014, pp. 1–10.

[39] D. R. Ifa, N. E. Manicke, A. L. Dill, and R. G. Cooks, “Latent fingerprint chemical imaging by mass spectrometry,” *Science (80-.).*, vol. 321, no. 5890, p. 805, 2008, doi: 10.1126/science.1157199.

[40] S. A. G. Lambrechts, A. van Dam, J. de Vos, A. van Weert, T. Sijen, and M. C. G. Aalders, “On the autofluorescence of fingermarks,” *Forensic Sci. Int.*, vol. 222, no. 1–3, pp. 89–93, 2012, doi: 10.1016/j.forsciint.2012.05.004.

[41] M. I. Szynkowska, K. Czerski, J. Rogowski, T. Paryjczak, and A. Parczewski, “ToF-SIMS application in the visualization and analysis of fingerprints after contact with amphetamine drugs,” *Forensic Sci. Int.*, vol. 184, no. 1–3, pp. 2008–2010, 2009, doi: 10.1016/j.forsciint.2008.11.003.

[42] C. Weyermann, C. Roux, and C. Champod, “Initial Results on the Composition of Fingerprints and its Evolution as a Function of Time by GC/MS Analysis,” *J. Forensic Sci.*, vol. 56, no. 1, pp. 102–108, 2011, doi: 10.1111/j.1556-

4029.2010.01523.x.

[43] K. T. Popov, V. G. Sears, and B. J. Jones, “Migration of latent fingermarks on non-porous surfaces: Observation technique and nanoscale variations,” *Forensic Sci. Int.*, vol. 275, pp. 44–56, 2017, doi: 10.1016/j.forsciint.2017.02.015.

[44] S. Chadwick, S. Moret, N. Jayashanka, C. Lennard, X. Spindler, and C. Roux, “Investigation of some of the factors influencing fingermark detection,” *Forensic Sci. Int.*, vol. 289, pp. 381–389, Aug. 2018, doi: 10.1016/j.forsciint.2018.06.014.

[45] C. Weyermann and O. Ribaux, “Situating forensic traces in time,” *Sci. Justice*, vol. 52, no. 2, pp. 68–75, 2012, doi: 10.1016/j.scijus.2011.09.003.

[46] A. O Hagan, “Crime scene to court: a study on finger-mark aging,” *Forensic Res. Criminol. Int. J.*, vol. 6, no. 6, pp. 491–503, 2018, doi: 10.15406/frcij.2018.06.00249.

[47] D. B. Hansen and M. M. Joullié, “The development of novel ninhydrin analogues,” *Chem. Soc. Rev.*, vol. 34, no. 5, pp. 408–417, 2005, doi: 10.1039/b315496n.

[48] H. Chen, M. Shi, R. Ma, and M. Zhang, “Advances in fingermark age determination techniques,” *Analyst*, vol. 146, no. 1, pp. 33–47, 2021, doi: 10.1039/d0an01423k.

[49] N. E. Archer, Y. Charles, J. A. Elliott, and S. Jickells, “Changes in the lipid composition of latent fingerprint residue with time after deposition on a surface,” *Forensic Sci. Int.*, vol. 154, no. 2–3, pp. 224–239, 2005, doi: 10.1016/j.forsciint.2004.09.120.

[50] R. S. Croxton, M. G. Baron, D. Butler, T. Kent, and V. G. Sears, “Variation in amino acid and lipid composition of latent fingerprints,” *Forensic Sci. Int.*, vol. 199, no. 1–3, pp. 93–102, 2010, doi: 10.1016/j.forsciint.2010.03.019.

[51] G. M. Mong, C. E. Petersen, and T. R. W. Clauss, “Advanced Fingerprint Analysis Project Final Report - Fingerprint Constituents,” 1999.

[52] V. G. Sears, S. M. Bleay, H. L. Bandey, and V. J. Bowman, “A methodology for finger mark research,” *Sci. Justice*, vol. 52, no. 3, pp. 145–160, 2012, doi: 10.1016/j.scijus.2011.10.006.

[53] J. T. Fish, L. S. Miller, M. C. Braswell, and E. W. Wallace, *Crime Scene Investigation: Third Edition*. 2013.

[54] H. L. Bandey, S. M. Bleay, V. J. Bowman, R. P. Downham, and V. G. Sears, *Fingermark Visualisation Manual*, First. Home Office Centre for Applied Science and Technology (CAST), 2014.

[55] D. J. McCaldin, “The chemistry of ninhydrin,” *Chem. Rev.*, vol. 60, no. 1, pp. 39–51, 1960, doi: 10.1021/cr60203a004.

[56] M. Friedman and L. D. Williams, “Stoichiometry of formation of Ruhemann’s purple in the ninhydrin reaction,” *Bioorg. Chem.*, vol. 3, no. 3, pp. 267–280, 1974, doi: https://doi.org/10.1016/0045-2068(74)90017-0.

[57] R. Grigg, J. F. Malone, T. Mongkolaussavaratana, and S. Thianpatanagul,

"Cycloaddition reaction relevant to the mechanism of the ninhydrin reaction. X-Ray crystal structure of protonated Ruhemann's purple, a stable 1,3-dipole," *J. Chem. Soc. Chem. Commun.*, vol. 17, no. 34, pp. 421–422, 1986, doi: 10.1002/chin.198634303.

[58] J. R. Morris and G. C. Goode, "NFN - An Improved Ninhydrin Reagent for Detection of Latent Fingerprints," *Police Res. Bull.*, vol. 24, no. 24, pp. 45–53, 1974.

[59] S. Oden, "Patent 767 341," 1957.

[60] S. M. Bleay *et al.*, *Fingerprint Source Book*. Home Office Centre for Applied Science and Technology, 2012.

[61] L. M. Amoo and R. L. Fagbenle, *Climate change in developing nations of the world*. Elsevier Ltd, 2020.

[62] I. Olszowska, P. Deacon, M. Lindsay, A. Leśniewski, J. Niedziółka-Jönsson, and K. Farrugia, "An alternative carrier solvent for fingermark enhancement reagents," *Forensic Sci. Int.*, vol. 284, pp. 53–64, 2018, doi: 10.1016/j.forsciint.2017.12.012.

[63] Y. Bin Zhao, L. X. Wang, W. J. Li, W. You, and K. Farrugia, "Effect of carrier solvent in 1,2-indanedione formulation on the development of fingermarks on porous substrates," *Forensic Sci. Int.*, vol. 318, p. 110589, 2021, doi: 10.1016/j.forsciint.2020.110589.

[64] C. Lennard, "Fingerprint Techniques," in *Encyclopedia of Analytical Science, Second edition*, Second., P. Worsfold, A. Townshend, and C. Poole, Eds. Elsevier, 2005, pp. 414–423.

[65] R. Jelly, E. L. T. Patton, C. Lennard, S. W. Lewis, and K. F. Lim, "The detection of latent fingermarks on porous surfaces using amino acid sensitive reagents: A review," *Anal. Chim. Acta*, vol. 652, no. 1–2, pp. 128–142, 2009, doi: 10.1016/j.aca.2009.06.023.

[66] C. Lennard, "Fingermark detection and identification: current research efforts," *Aust. J. Forensic Sci.*, vol. 46, no. 3, pp. 293–303, 2014, doi: 10.1080/00450618.2013.839743.

[67] R. Grigg, T. Mongkolaussavaratana, C. Anthony Pounds, and S. Sivagnanam, "1,8-diazafluorenone and related compounds. A new reagent for the detection of (α-amino acids and latent fingerprints.," *Tetrahedron Lett.*, vol. 31, no. 49, pp. 7215–7218, 1990, doi: 10.1016/S0040-4039(00)97283-6.

[68] C. Conn, G. Ramsay, C. Roux, and C. Lennard, "The effect of metal salt treatment on the photoluminescence of DFO-treated fingerprints," *Forensic Sci. Int.*, vol. 116, no. 2–3, pp. 117–123, 2001, doi: 10.1016/S0379-0738(00)00358-3.

[69] D. Wilkinson, "Study of the reaction mechanism of 1,8-diazafluoren-9-one with the amino acid, L-alanine," *Forensic Sci. Int.*, 2000, doi: 10.1016/S0379-0738(99)00219-4.

[70] V. D'Elia, S. Materazzi, G. Iuliano, and L. Niola, "Evaluation and comparison of 1,2-indanedione and 1,8-diazafluoren-9-one solutions for the enhancement

of latent fingerprints on porous surfaces," *Forensic Sci. Int.*, vol. 254, pp. 205–214, 2015, doi: 10.1016/j.forsciint.2015.07.036.

[71] R. Ramotowski, A. A. Cantu, M. M. Joullié, and O. Petrovskaia, "1,2-Indanediones: A preliminary evaluation of a new class of amino acid visualizing compound," *Fingerpr. Whorld*, vol. 23, no. 90, pp. 131–140, 1997.

[72] O. Petrovskaia, B. M. Taylor, D. B. Hauze, P. J. Carroll, and M. M. Joullié, "Investigations of the reaction mechanisms of 1,2-indanediones with amino acids," *J. Org. Chem.*, vol. 66, no. 23, pp. 7666–7675, 2001, doi: 10.1021/jo0105179.

[73] C. Wallace-Kunkel, C. Lennard, M. Stoilovic, and C. Roux, "Optimisation and evaluation of 1,2-indanedione for use as a fingermark reagent and its application to real samples," *Forensic Sci. Int.*, vol. 168, no. 1, pp. 14–26, May 2007, doi: 10.1016/j.forsciint.2006.06.006.

[74] V. Sears, R. Batham, and S. Bleay, "The effectiveness of 1,2-indandione-zinc formulations and comparison with HFE-based 1, 8-diazafluoren-9-one for fingerprint development," *J. Forensic Identif.*, vol. 59, no. 6, p. 654, 2009.

[75] R. Lam and D. Wilkinson, "Forensic Light Source and Environmental Effects on the Performance of 1,2-Indanedione–Zinc Chloride and 1,8-Diazafluoren-9-one for the Recovery of Latent Prints on Porous Substrates," *J. Forensic Identif.*, vol. 61, no. 6, pp. 607–620, 2011.

[76] M. Stoilovic, C. Lennard, C. Wallace-Kunkel, and C. Roux, "Evaluation of a 1,2-Indanedione Formulation Containing Zinc Chloride for Improved Fingermark Detection on Paper," *J. Forensic Identif.*, vol. 57, no. 1, pp. 4–18, 2007.

[77] C. Marriott *et al.*, "Evaluation of fingermark detection sequences on paper substrates," *Forensic Sci. Int.*, vol. 236, pp. 30–37, 2014, doi: 10.1016/j.forsciint.2013.12.028.

[78] S. Merrick, S. J. Gardner, V. G. Sears, and D. F. Hewlett, "An operational trial of ozone-friendly DFO and 1,2-indandione formulations for latent fingerprint detection," *J. Forensic Identif.*, vol. 52, no. 5, pp. 595–605, 2002.

[79] K. Mayse, V. G. Sears, N. Nicolasora, and S. Bleay, "An evaluation of the effect of incorporating metal salts into 1,8 diazafluoren-9-one (DFO) formulations for fingermark enhancement," *Sci. Justice*, vol. 59, no. 3, pp. 349–358, 2019, doi: 10.1016/j.scijus.2019.01.002.

[80] I. M. Alaoui, T. Troxler, and M. M. Joullié, "Fingerprint Visualization and Spectroscopic Properties of 1,2-Indanedione-alanine Followed by Zinc Chloride or Europium Chloride," *J. Forensic Identif.*, vol. 62, no. 1, pp. 1–13, 2012.

[81] X. Spindler, R. Shimmon, C. Roux, and C. Lennard, "The effect of zinc chloride, humidity and the substrate on the reaction of 1,2-indanedione-zinc with amino acids in latent fingermark secretions," *Forensic Sci. Int.*, vol. 212, no. 1–3, pp. 150–157, 2011, doi: 10.1016/j.forsciint.2011.06.005.

[82] A. Becue, S. Moret, C. Champod, and P. Margot, "Use of stains to detect fingermarks," *Biotech. Histochem.*, vol. 86, no. 3, pp. 140–160, 2011, doi:

10.3109/10520290903462838.
[83] A. Beaudoin, “New technique for revealing latent fingerprints on wet, porous surfaces: Oil Red O,” *J. Forensic Identif.*, vol. 54, no. 4, pp. 413–421, 2004.
[84] W. Escorcia, D. L. Ruter, J. Nhan, and S. P. Curran, “Quantification of lipid abundance and evaluation of lipid distribution in Caenorhabditis elegans by nile red and oil red o staining,” *J. Vis. Exp.*, vol. 2018, no. 133, pp. 1–6, 2018, doi: 10.3791/57352.
[85] R. K. Simmons, P. Deacon, and K. J. Farrugia, “Water-soaked porous evidence: A comparison of processing methods,” *J. Forensic Identif.*, vol. 64, no. 2, pp. 157–173, 2014.
[86] A. Beaudoin, “Fingerprint staining technique on dark and wetted porous surfaces: Oil Red O and rhodamine 6G,” *J. Forensic Identif.*, vol. 62, no. 4, pp. 315–329, 2012.
[87] S. D. Fowler and P. Greenspan, “Application of Nile Red, a Fluorescent Hydrophobic Probe, for the Detection of Neutral Lipid Deposits in Tissue Sections: Comparison with Oil Red O,” *J. Histochem. Cytochem.*, vol. 33, no. 8, pp. 833–836, 1985.
[88] P. Greenspan, E. P. Mayer, and S. D. Fowler, “Nile red: A selective fluorescent stain for intracellular lipid droplets,” *J. Cell Biol.*, vol. 100, no. 3, pp. 965–973, 1985, doi: 10.1083/jcb.100.3.965.
[89] T. Maes, R. Jessop, N. Wellner, K. Haupt, and A. G. Mayes, “A rapid-screening approach to detect and quantify microplastics based on fluorescent tagging with Nile Red,” *Sci. Rep.*, vol. 7, no. November 2016, pp. 1–10, 2017, doi: 10.1038/srep44501.
[90] P. Greenspan and S. D. Fowler, “Spectrofluorometric studies of the lipid probe, nile red,” *J. Lipid Res.*, vol. 26, no. 7, pp. 781–789, 1985, doi: 10.1016/s0022-2275(20)34307-8.
[91] K. Braasch *et al.*, “Nile red: Alternative to physical developer for the detection of latent fingermarks on wet porous surfaces?,” *Forensic Sci. Int.*, vol. 230, no. 1–3, pp. 74–80, 2013, doi: 10.1016/j.forsciint.2013.03.041.
[92] E. Alsolmy, W. M. Abdelwahab, V. Martinez, M. Henary, and G. Patonay, “Investigation of benzophenoxazine derivatives for the detection of latent fingerprints on porous surfaces,” *J. Photochem. Photobiol. A Chem.*, vol. 392, no. April 2019, p. 112416, 2020, doi: 10.1016/j.jphotochem.2020.112416.
[93] M. de la Hunty, X. Spindler, S. Chadwick, C. Lennard, and C. Roux, “Synthesis and application of an aqueous nile red microemulsion for the development of fingermarks on porous surfaces,” *Forensic Sci. Int.*, vol. 244, pp. e48–e55, 2014, doi: 10.1016/j.forsciint.2014.08.028.
[94] M. de la Hunty, “An investigation of latent fingermark residues and their development on porous substrates using physical developer and nile red,” University of Technology Sydney, 2017.
[95] J. D. Wilson, A. A. Cantu, G. Antonopoulos, and M. J. Surrency, “Examination of the steps leading up to the physical developer process for developing

fingerprints," *J. Forensic Sci.*, vol. 52, no. 2, pp. 320–329, 2007, doi: 10.1111/j.1556-4029.2007.00382.x.

[96] C. M. Marriott, "Evaluation of Sequences for the Detection of Latent Fingermarks on Porous Substrates," *Natl. Cent. Forensic Stud.*, vol. 2013, no. June, p. 102, 2013.

[97] S. Moret, P. L. T. Lee, M. de la Hunty, X. Spindler, C. Lennard, and C. Roux, "Single metal deposition versus physical developer: A comparison between two advanced fingermark detection techniques," *Forensic Sci. Int.*, vol. 294, pp. 103–112, Jan. 2019, doi: 10.1016/j.forsciint.2018.10.032.

[98] M. A. Wood and T. James, "ORO. The Physical Developer replacement?," *Sci. Justice*, vol. 49, no. 4, pp. 272–276, 2009, doi: 10.1016/j.scijus.2009.02.006.

[99] G. Sauzier, A. A. Frick, and S. W. Lewis, "Investigation into the performance of physical developer formulations for visualizing latent fingerprints on paper," *J. Forensic Identif.*, vol. 63, no. 1, pp. 70–89, 2013.

[100] A. Rawji and A. Beaudoin, "Oil red O versus physical developer on wet papers: A comparative study," *J. Forensic Identif.*, vol. 56, no. 1, pp. 33–54, 2006.

[101] M. de la Hunty, S. Moret, S. Chadwick, C. Lennard, X. Spindler, and C. Roux, "An effective Physical Developer (PD) method for use in Australian laboratories," *Aust. J. Forensic Sci.*, vol. 50, no. 6, pp. 666–671, 2018, doi: 10.1080/00450618.2018.1424243.

[102] H. McMorris, K. Farrugia, and D. Gentles, "An investigation into the detection of latent marks on the feathers and eggs of birds of prey," *Sci. Justice*, vol. 55, no. 2, pp. 90–96, 2015, doi: 10.1016/j.scijus.2014.12.004.

[103] E. R. Menzel, *Fingerprint detection with lasers*, 2nd ed. Dekker, 1999.

[104] G. S. Sodhi and J. Kaur, "Application of Metals and Metal Salts in Latent Fingerprint Detection : A Review," *Int. J. Forensic Sci.*, vol. 2, no. 2, pp. 71–77, 2019.

[105] O. P. Jasuja, G. D. Singh, and G. S. Sodhi, "Small particle reagents: Development of fluorescent variants," *Sci. Justice*, vol. 48, no. 3, pp. 141–145, 2008, doi: 10.1016/j.scijus.2008.04.002.

[106] H. Chen, R. liang Ma, Z. Fan, Y. Chen, Z. Wang, and L. J. Fan, "Fluorescence development of fingerprints by combining conjugated polymer nanoparticles with cyanoacrylate fuming," *J. Colloid Interface Sci.*, vol. 528, pp. 200–207, Oct. 2018, doi: 10.1016/j.jcis.2018.05.079.

[107] P. Czekanski, M. Fasola, and J. Allison, "A mechanistic model for the superglue fuming of latent fingerprints," *J. Forensic Sci.*, vol. 51, no. 6, pp. 1323–1328, 2006, doi: 10.1111/j.1556-4029.2006.00258.x.

[108] K. C. O'Neill and Y. J. Lee, "Study of the cyanoacrylate fuming mechanism by matrix-assisted laser desorption/ionization mass spectrometry," *J. Mass Spectrom.*, vol. 54, no. 3, pp. 222–226, 2019, doi: 10.1002/jms.4325.

[109] S. P. Wargacki, L. A. Lewis, and M. D. Dadmun, "Understanding the chemistry of the development of latent fingerprints by superglue fuming," *J. Forensic Sci.*, vol. 52, no. 5, pp. 1057–1062, 2007, doi: 10.1111/j.1556-

4029.2007.00527.x.
[110] G. Groeneveld, S. Kuijer, and M. De Puit, “Preparation of cyanoacrylate derivatives and comparison of dual action cyanoacrylate formulations,” *Sci. Justice*, vol. 54, no. 1, pp. 42–48, 2014, doi: 10.1016/j.scijus.2013.09.002.
[111] C. Jones, J. Fraser, P. Deacon, M. Lindsay, F. Carlysle-Davies, and K. J. Farrugia, “An assessment of a portable cyanoacrylate fuming system (LumiFume™) for the development of latent fingermarks,” *Forensic Sci. Int.*, vol. 305, Dec. 2019, doi: 10.1016/j.forsciint.2019.109966.
[112] X. Jin *et al.*, “An aggregation-induced emission luminogen combined with a cyanoacrylate fuming method for latent fingerprint analysis,” *Analyst*, vol. 145, no. 6, pp. 2311–2318, Mar. 2020, doi: 10.1039/c9an02158b.
[113] M. Tapps, L. McMullen, M. E. Gagné, and A. Beaudoin, “Revealing a decades-old fingermark with cyanoacrylate fuming and rhodamine 6G,” *Forensic Sci. Int.*, vol. 300, pp. e9–e12, 2019, doi: 10.1016/j.forsciint.2019.04.025.
[114] M. Takatsu, O. Shimoda, K. Onishi, A. Onishi, and N. Oguri, “Detection of pretreated fingerprint fluorescence using an LED-based excitation system,” *J. Forensic Sci.*, vol. 53, no. 4, pp. 823–827, 2008, doi: 10.1111/j.1556-4029.2008.00773.x.
[115] K. J. Farrugia, J. Fraser, L. Friel, D. Adams, N. Attard-Montalto, and P. Deacon, “A comparison between atmospheric/humidity and vacuum cyanoacrylate fuming of latent fingermarks,” *Forensic Sci. Int.*, vol. 257, pp. 54–70, 2015, doi: 10.1016/j.forsciint.2015.07.035.
[116] S. P. Kasper, *Latent Print Processing Guide*. Elsevier, 2016.
[117] B. K. Chesher, J. M. Stone, and W. F. Rowe, “Use of the Omniprint™ 1000 alternate light source to produce fluorescence in cyanoacrylate-developed latent fingerprints stained with biological stains and commercial fabric dyes,” *Forensic Sci. Int.*, vol. 57, no. 2, pp. 163–168, 1992, doi: 10.1016/0379-0738(92)90009-L.
[118] M. Takatsu, O. Shimoda, and H. Teranishi, “Vapor-phase Staining of Cyanoacrylate-Fumed Latent Fingerprints Using p-Dimethylaminobenzaldehyde,” *J. Forensic Sci.*, vol. 57, no. 2, pp. 515–520, 2012, doi: 10.1111/j.1556-4029.2011.01976.x.
[119] S. Chadwick, L. Xiao, P. Maynard, C. Lennard, X. Spindler, and C. Roux, “PolyCyano UV: An investigation into a one-step luminescent cyanoacrylate fuming process,” *Aust. J. Forensic Sci.*, vol. 46, no. 4, pp. 471–484, 2014, doi: 10.1080/00450618.2014.891654.
[120] K. J. Farrugia, J. Fraser, N. Calder, and P. Deacon, “Pseudo-Operational Trials of Lumicyano Solution and Lumicyano Powder for the Detection of Latent Fingermarks on Various Substrates,” *J. Forensic Identif.*, vol. 64, no. 6, pp. 556–582, 2014.
[121] V. Stewart, P. Deacon, and K. Farrugia, “A review of one-step fluorescent cyanoacrylate techniques,” *Fingerpr. Whorld*, vol. 41, no. 162, pp. 6–29, 2016.
[122] N. E. Masters and J. D. DeHaan, “Vacuum Metal Deposition and Cyanoacrylate

Detection of Older Latent Prints," *J. Forensic Identif.*, vol. 46, no. 1, pp. 32–45, 1996.

[123] S. F. Williams, D. P. Pulsifer, R. C. Shaler, R. S. Ramotowski, S. Brazelle, and A. Lakhtakia, "Comparison of the Columnar-Thin-Film and Vacuum-Metal-Deposition Techniques to Develop Sebaceous Fingermarks on Nonporous Substrates," *J. Forensic Sci.*, vol. 60, no. 2, pp. 295–302, 2015, doi: 10.1111/1556-4029.12648.

[124] J. N. Pollitt, G. Christofidis, J. Morrissey, and J. W. Birkett, "Vacuum metal deposition enhancement of friction ridge detail on ballistic materials," *Forensic Sci. Int.*, vol. 316, 2020, doi: 10.1016/j.forsciint.2020.110551.

[125] S. Knighting, J. Fraser, K. Sturrock, P. Deacon, S. Bleay, and D. H. Bremner, "Visualisation of fingermarks and grab impressions on dark fabrics using silver vacuum metal deposition," *Sci. Justice*, vol. 53, no. 3, pp. 309–314, 2013, doi: 10.1016/j.scijus.2013.01.002.

[126] J. Fraser, P. Deacon, S. Bleay, and D. H. Bremner, "A comparison of the use of vacuum metal deposition versus cyanoacrylate fuming for visualisation of fingermarks and grab impressions on fabrics," *Sci. Justice*, vol. 54, no. 2, pp. 133–140, 2014, doi: 10.1016/j.scijus.2013.11.005.

[127] L. W. L. Davis, P. F. Kelly, R. S. P. King, and S. M. Bleay, "Visualisation of latent fingermarks on polymer banknotes using copper vacuum metal deposition: A preliminary study," *Forensic Sci. Int.*, vol. 266, pp. e86–e92, 2016, doi: 10.1016/j.forsciint.2016.05.037.

[128] N. Jones, D. Mansour, M. Stoilovic, C. Lennard, and C. Roux, "The influence of polymer type, print donor and age on the quality of fingerprints developed on plastic substrates using vacuum metal deposition," *Forensic Sci. Int.*, vol. 124, no. 2–3, pp. 167–177, 2001, doi: 10.1016/S0379-0738(01)00593-X.

[129] N. Jones, M. Stoilovic, C. Lennard, and C. Roux, "Vacuum metal deposition: Factors affecting normal and reverse development of latent fingerprints on polyethylene substrates," *Forensic Sci. Int.*, vol. 115, no. 1–2, pp. 73–88, 2001, doi: 10.1016/S0379-0738(00)00310-8.

[130] B. J. Jones, R. Downham, and V. G. Sears, "Nanoscale Analysis of the Interaction Between Cyanoacrylate and Vacuum Metal Deposition in the Development of Latent Fingermarks on Low-Density Polyethylene," *J. Forensic Sci.*, vol. 57, no. 1, pp. 196–200, 2012, doi: 10.1111/j.1556-4029.2011.01952.x.

[131] R. Steiner and A. Bécue, "Effect of water immersion on multi- and mono-metallic VMD," *Forensic Sci. Int.*, vol. 283, pp. 118–127, 2018, doi: 10.1016/j.forsciint.2017.12.020.

[132] A. Becue, C. Champod, and P. Margot, "Use of gold nanoparticles as molecular intermediates for the detection of fingermarks," *Forensic Sci. Int.*, vol. 168, no. 2–3, pp. 169–176, 2007, doi: 10.1016/j.forsciint.2006.07.014.

[133] B. Schnetz and P. Margot, "Technical note: Latent fingermarks, colloidal gold and multimetal deposition (MMD) Optimisation of the method," *Forensic Sci.*

Int., vol. 118, no. 1, pp. 21–28, 2001, doi: 10.1016/S0379-0738(00)00361-3.

[134] S. Moret, A. Bécue, and C. Champod, "Nanoparticles for fingermark detection: an insight into the reaction mechanism," *Nanotechnology*, vol. 25, pp. 1–10, 2014, doi: 10.1088/0957-4484/25/42/425502.

[135] A. Becue, A. Scoundrianos, C. Champod, and P. Margot, "Fingermark detection based on the in situ growth of luminescent nanoparticles-Towards a new generation of multimetal deposition," *Forensic Sci. Int.*, vol. 179, no. 1, pp. 39–43, 2008, doi: 10.1016/j.forsciint.2008.04.008.

[136] N. Jaber, A. Lesniewski, H. Gabizon, S. Shenawi, D. Mandler, and J. Almog, "Visualization of latent fingermarks by nanotechnology: Reversed development on paper-a remedy to the variation in sweat composition," *Angew. Chemie - Int. Ed.*, vol. 51, no. 49, pp. 12224–12227, 2012, doi: 10.1002/anie.201205259.

[137] S. Shenawi, N. Jaber, J. Almog, and D. Mandler, "A novel approach to fingerprint visualization on paper using nanotechnology: Reversing the appearance by tailoring the gold nanoparticles' capping ligands," *Chem. Commun.*, vol. 49, no. 35, pp. 3688–3690, 2013, doi: 10.1039/c3cc41610k.

[138] L. Xu, C. Zhang, Y. He, and B. Su, "Advances in the development and component recognition of latent fingerprints," *Sci. China Chem.*, vol. 58, no. 7, pp. 1090–1096, 2015, doi: 10.1007/s11426-014-5294-5.

[139] D. T. Charlton, S. M. Bleay, and V. G. Sears, "Evaluation of the multimetal deposition process for fingermark enhancement in simulated operational environments," *Anal. Methods*, vol. 5, p. 5411, 2013, doi: 10.1039/c3ay40533h.

[140] R. P. Downham, E. R. Brewer, R. S. P. King, A. M. Luscombe, and V. G. Sears, "Fingermark visualisation on uncirculated £5 (Bank of England) polymer notes: Initial process comparison studies," *Forensic Sci. Int.*, vol. 275, pp. 30–43, 2017, doi: 10.1016/j.forsciint.2017.02.026.

[141] E. Stauffer, A. Becue, K. V. Singh, K. R. Thampi, C. Champod, and P. Margot, "Single-metal deposition (SMD) as a latent fingermark enhancement technique: An alternative to multimetal deposition (MMD)," *Forensic Sci. Int.*, vol. 168, no. 1, 2007, doi: 10.1016/j.forsciint.2006.12.009.

[142] P. Durussel, E. Stauffer, A. Becue, C. Champod, and P. Margot, "Single-metal deposition: Optimization of this fingermark enhancement technique," *J. Forensic Identif.*, vol. 59, no. 1, pp. 80–96, 2009.

[143] A. Becue, A. Scoundrianos, and S. Moret, "Detection of fingermarks by colloidal gold (MMD/SMD) - beyond the pH 3 limit," *Forensic Sci. Int.*, vol. 219, no. 1–3, pp. 39–49, 2012, doi: 10.1016/j.forsciint.2011.11.024.

[144] S. Moret and A. Bécue, "Single-Metal deposition for Fingermark detection - A simpler and more efficient protocol," *J. Forensic Identif.*, vol. 65, no. 2, pp. 118–137, 2015.

[145] T. G. Newland, S. Moret, A. Becue, and S. W. Lewis, "Further investigations into the single metal deposition (SMD II) technique for the detection of latent

fingermarks," *Forensic Sci. Int.*, vol. 268, pp. 62–72, 2016, doi: 10.1016/j.forsciint.2016.09.004.

[146] J. A. D'Uva, N. Brent, R. E. Boseley, D. Ford, G. Sauzier, and S. W. Lewis, "Preliminary investigations into the use of single metal deposition II (SMD II) to visualise latent fingermarks on polyethylene 'zip-lock' bags in Western Australia," *Forensic Chem.*, vol. 18, no. November 2019, p. 100229, 2020, doi: 10.1016/j.forc.2020.100229.

[147] G. Kolhatkar, C. Parisien, A. Ruediger, and C. Muehlethaler, "Latent fingermark imaging by single-metal deposition of gold nanoparticles and surface enhanced Raman spectroscopy," *Front. Chem.*, vol. 7, no. JUN, pp. 1–8, 2019, doi: 10.3389/fchem.2019.00440.

[148] A. Becue and A. A. Cantu, "Fingermark Detection Using Nanoparticles," in *Lee and Gaensslen's Advances in Fingerprint Technology - Third edition*, 3rd ed., R. S. Ramotowski, Ed. CRC Press, 2012, pp. 307–379.

[149] J. Dilag, H. J. Kobus, and A. V. Ellis, "Nanotechnology as a New Tool for Fingermark Detection: A Review," *Curr. Nanosci.*, vol. 7, no. 2, pp. 153–159, 2011, doi: 10.2174/157341311794653596.

[150] M. Naito, T. Yokoyama, K. Hosokawa, and K. Nogi, *Nanoparticle Technology Handbook*, 3rd ed. Elsevier, 2018.

[151] V. Prasad, S. Lukose, P. Agarwal, and L. Prasad, "Role of Nanomaterials for Forensic Investigation and Latent Fingerprinting—A Review," *J. Forensic Sci.*, vol. 65, no. 1, pp. 26–36, 2020, doi: 10.1111/1556-4029.14172.

[152] D. R. Ashbaugh, *Quantitative-qualitative friction ridge analysis: an introduction to basic and advanced ridgeology*. CRC Press, 1999.

[153] R. Leggett, E. E. Lee-Smith, S. M. Jickells, and D. A. Russell, "'Intelligent' fingerprinting: Simultaneous identification of drug metabolites and individuals by using antibody-functionalized nanoparticles," *Angew. Chemie - Int. Ed.*, vol. 46, no. 22, pp. 4100–4103, 2007, doi: 10.1002/anie.200700217.

[154] X. Spindler, O. Hofstetter, A. M. McDonagh, C. Roux, and C. Lennard, "Enhancement of latent fingermarks on non-porous surfaces using anti-L-amino acid antibodies conjugated to gold nanoparticles.," *Chem. Commun. (Camb).*, vol. 47, pp. 5602–5604, 2011, doi: 10.1039/c0cc05748g.

[155] M. Sametband, I. Shweky, U. Banin, D. Mandler, and J. Almog, "Application of nanoparticles for the enhancement of latent fingerprints," *Chem. Commun.*, no. 11, pp. 1142–1144, 2007, doi: 10.1039/b618966k.

[156] D. Gao, F. Li, J. Song, X. Xu, Q. Zhang, and L. Niu, "One step to detect the latent fingermarks with gold nanoparticles," *Talanta*, vol. 80, no. 2, pp. 479–483, 2009, doi: 10.1016/j.talanta.2009.07.007.

[157] I. Hussain *et al.*, "In situ growth of gold nanoparticles on latent fingerprints - From forensic applications to inkjet printed nanoparticle patterns," *Nanoscale*, vol. 2, no. 12, pp. 2575–2578, 2010, doi: 10.1039/c0nr00593b.

[158] K. Song *et al.*, "Photoacoustic and Colorimetric Visualization of Latent Fingerprints," *ACS Nano*, vol. 9, no. 12, pp. 12344–12348, 2015, doi:

10.1021/acsnano.5b05629.

[159] J. Lee and M. M. Joullié, “Novel design and approach to latent fingerprint detection on paper using a 1,2-indanedione-based bi-functional reagent,” *Tetrahedron Lett.*, vol. 56, no. 23, pp. 3378–3381, 2015, doi: 10.1016/j.tetlet.2014.12.109.

[160] J. Lee and M. M. Joullié, “Fine-tuning latent fingerprint detection on paper using 1,2-indanedione bi-functional reagents,” *Tetrahedron*, vol. 71, no. 40, pp. 7620–7629, 2015, doi: 10.1016/j.tet.2015.07.072.

[161] C. H. Su, C. C. Yu, and F. Y. Cheng, “Rapid visualization of latent fingermarks using gold seed-mediated enhancement,” *J. Nanobiotechnology*, vol. 14, no. 1, pp. 1–14, 2016, doi: 10.1186/s12951-016-0228-3.

[162] K. Li *et al.*, “Nanoplasmonic imaging of latent fingerprints and identification of cocaine,” *Angew. Chemie - Int. Ed.*, vol. 52, no. 44, pp. 11542–11545, 2013, doi: 10.1002/anie.201305980.

[163] L. Yan, Y. Yu, and Z. Xia, “Microwave-assisted in situ synthesis of fluorescent gold nanoclusters with BSA/montmorillonite and application on latent fingermark imaging,” *Sci. China Chem.*, vol. 61, no. 5, pp. 619–626, 2018, doi: 10.1007/s11426-017-9216-7.

[164] G. R. S. Andrade, C. C. Nascimento, Y. H. Santos, L. P. Costa, L. E. Almeida, and I. F. Gimenez, “Easy preparation of gold nanostructures supported on a thiolated silica-gel for catalysis and latent fingerprint detection,” *Dye. Pigment.*, vol. 155, no. November 2017, pp. 202–211, 2018, doi: 10.1016/j.dyepig.2018.03.052.

[165] V. Prasad, L. Prasad, S. Lukose, and P. Agarwal, “Latent fingerprint development by using silver nanoparticles and silver nitrate—A comparative study,” *J. Forensic Sci.*, 2021, doi: 10.1111/1556-4029.14664.

[166] W. Song *et al.*, “Detection of protein deposition within latent fingerprints by surface-enhanced Raman spectroscopy imaging,” *Nanoscale*, vol. 4, no. 7, pp. 2333–2338, 2012, doi: 10.1039/c2nr12030e.

[167] M. A. Souza, K. V. de Oliveira, F. C. C. Oliveira, L. P. Silva, and J. C. Rubim, “The adsorption of methamphetamine on Ag nanoparticles dispersed in agarose gel – Detection of methamphetamine in fingerprints by SERS,” *Vib. Spectrosc.*, vol. 98, no. April, pp. 152–157, 2018, doi: 10.1016/j.vibspec.2018.08.008.

[168] G. Qin *et al.*, “Visualizing latent fingerprints by electrodeposition of metal nanoparticles,” *J. Electroanal. Chem.*, vol. 693, pp. 122–126, 2013, doi: 10.1016/j.jelechem.2013.01.016.

[169] X. Ran, Z. Wang, Z. Zhang, F. Pu, J. Ren, and X. Qu, “Nucleic-acid-programmed Ag-nanoclusters as a generic platform for visualization of latent fingerprints and exogenous substances,” *Chem. Commun.*, vol. 52, no. 3, pp. 557–560, 2016, doi: 10.1039/c5cc08534a.

[170] Y. Yang *et al.*, “Visualization of latent fingerprints using a simple ‘silver imaging ink,’” *Anal. Methods*, vol. 8, no. 33, pp. 6293–6297, 2016, doi: 10.1039/c6ay01811d.

[171] Y. H. Cheng, Y. Zhang, S. L. Chau, S. K. M. Lai, H. W. Tang, and K. M. Ng, "Enhancement of Image Contrast, Stability, and SALDI-MS Detection Sensitivity for Latent Fingerprint Analysis by Tuning the Composition of Silver-Gold Nanoalloys," *ACS Appl. Mater. Interfaces*, vol. 8, no. 43, pp. 29668–29675, 2016, doi: 10.1021/acsami.6b09668.

[172] L. Kumar Jangir, Y. Kumari, A. Kumar, M. Kumar, and K. Awasthi, "Investigation of luminescence and structural properties of ZnO nanoparticles, synthesized with different precursors," *Mater. Chem. Front.*, vol. 1, no. 7, pp. 1413–1421, 2017, doi: 10.1039/c7qm00058h.

[173] M. Guzman, B. Flores, L. Malet, and S. Godet, "Synthesis and characterization of zinc oxide nanoparticles for application in the detection of fingerprints," *Mater. Sci. Forum*, vol. 916 MSF, no. 3, pp. 232–236, 2018, doi: 10.4028/www.scientific.net/MSF.916.232.

[174] M. J. Choi *et al.*, "An evaluation of nanostructured zinc oxide as a fluorescent powder for fingerprint detection," *J. Mater. Sci.*, vol. 43, no. 2, pp. 732–737, 2008, doi: 10.1007/s10853-007-2178-5.

[175] M. O. Amin, M. Madkour, and E. Al-Hetlani, "Metal oxide nanoparticles for latent fingerprint visualization and analysis of small drug molecules using surface-assisted laser desorption/ionization mass spectrometry," *Anal. Bioanal. Chem.*, vol. 410, no. 20, pp. 4815–4827, 2018, doi: 10.1007/s00216-018-1119-2.

[176] D. Luthra and S. Kumar, "The development of latent fingerprints by zinc oxide and tin oxide nanoparticles prepared by precipitation technique," in *2nd International Conference on Condensed Matter and Applied Physics (ICC 2017)*, 2018, vol. 1953, doi: 10.1063/1.5032584.

[177] H. N. Shivananjaiah, K. Sailaja Kumari, and M. S. Geetha, "Green mediated synthesis of lanthanum doped zinc oxide: Study of its structural, optical and latent fingerprint application," *J. Rare Earths*, vol. 38, no. 12, pp. 1281–1287, 2020, doi: 10.1016/j.jre.2020.07.012.

[178] E. Prabakaran and K. Pillay, "Synthesis and characterization of fluorescent N-CDs/ZnONPs nanocomposite for latent fingerprint detection by using powder brushing method," *Arab. J. Chem.*, vol. 13, no. 2, pp. 3817–3835, 2020, doi: 10.1016/j.arabjc.2019.01.004.

[179] A. Arshad, M. A. Farrukh, S. Ali, M. Khaleeq-ur-Rahman, and M. A. Tahir, "Development of Latent Fingermarks on Various Surfaces Using ZnO-SiO_2 Nanopowder," *J. Forensic Sci.*, vol. 60, no. 5, pp. 1182–1187, 2015, doi: 10.1111/1556-4029.12890.

[180] S. Chadwick *et al.*, "Styryl dye coated metal oxide powders for the detection of latent fingermarks on non-porous surfaces," *Forensic Sci. Int.*, vol. 219, no. 1–3, pp. 208–214, 2012, doi: 10.1016/j.forsciint.2012.01.006.

[181] J. Lee, C. W. Lee, and J. M. Kim, "A Magnetically Responsive Polydiacetylene Precursor for Latent Fingerprint Analysis," *ACS Appl. Mater. Interfaces*, vol. 8, no. 9, pp. 6245–6251, 2016, doi: 10.1021/acsami.6b00566.

[182] X. Li, Q. Li, Y. Li, L. Zhang, H. Lin, and J. Hong, "Latent Fingerprints Enhancement Using a Functional Composite of Fe_3O_4@SiO_2-Au," *Anal. Lett.*, vol. 46, no. 13, pp. 2111–2121, 2013, doi: 10.1080/00032719.2013.782553.

[183] L. Zhang, X. Zhou, and T. Chu, "Preparation and evaluation of Fe_3O_4-core@Ag-shell nanoeggs for the development of fingerprints," *Sci. China Chem.*, vol. 56, no. 5, pp. 551–556, 2013, doi: 10.1007/s11426-012-4764-x.

[184] M. J. Choi *et al.*, "Fluorescent TiO_2 powders prepared using a new perylene diimide dye: Applications in latent fingermark detection," *Forensic Sci. Int.*, vol. 173, no. 2–3, pp. 154–160, 2007, doi: 10.1016/j.forsciint.2006.09.014.

[185] D. Peng, X. Liu, M. Huang, and R. Liu, "Characterization of a Novel Co_2TiO_4 Nanopowder for the Rapid Identification of Latent and Blood Fingerprints," *Anal. Lett.*, vol. 51, no. 11, pp. 1796–1808, 2018, doi: 10.1080/00032719.2017.1391827.

[186] B. G. Fouda-Mbanga, E. Prabakaran, and K. Pillay, "Synthesis and characterization of CDs/Al_2O_3 nanofibers nanocomposite for Pb^{2+} ions adsorption and reuse for latent fingerprint detection," *Arab. J. Chem.*, vol. 13, no. 8, pp. 6762–6781, 2020, doi: 10.1016/j.arabjc.2020.06.030.

[187] B. S. Rohini, H. Nagabhushana, G. P. Darshan, R. B. Basavaraj, S. C. Sharma, and R. Sudarmani, "Fabricated CeO_2 nanopowders as a novel sensing platform for advanced forensic, electrochemical and photocatalytic applications," *Appl. Nanosci.*, vol. 7, no. 8, pp. 815–833, 2017, doi: 10.1007/s13204-017-0611-x.

[188] S. Moret, A. Bécue, and C. Champod, "Functionalised silicon oxide nanoparticles for fingermark detection," *Forensic Sci. Int.*, vol. 259, pp. 10–18, 2016, doi: 10.1016/j.forsciint.2015.11.015.

[189] P. L. T. Lee *et al.*, "Latent fingermark detection using functionalised silicon oxide nanoparticles: Method optimisation and evaluation," *Forensic Sci. Int.*, vol. 298, pp. 372–383, May 2019, doi: 10.1016/j.forsciint.2019.02.038.

[190] P. L. T. Lee *et al.*, "Latent fingermark detection using functionalised silicon oxide nanoparticles: Optimisation and comparison with cyanoacrylate fuming," *Forensic Sci. Int.*, vol. 315, 2020, doi: 10.1016/j.forsciint.2020.110442.

[191] E. Alsolmy, W. M. Abdelwahab, and G. Patonay, "A Comparative Study of Fluorescein Isothiocyanate-Encapsulated Silica Nanoparticles Prepared in Seven Different Routes for Developing Fingerprints on Non-Porous Surfaces," *J. Fluoresc.*, vol. 28, no. 5, pp. 1049–1058, 2018, doi: 10.1007/s10895-018-2268-6.

[192] W. M. Abdelwahab, E. Phillips, and G. Patonay, "Preparation of fluorescently labeled silica nanoparticles using an amino acid-catalyzed seeds regrowth technique: Application to latent fingerprints detection and hemocompatibility studies," *J. Colloid Interface Sci.*, vol. 512, pp. 801–811, 2018, doi: 10.1016/j.jcis.2017.10.062.

[193] A. Guleria *et al.*, "Glutathione-Functionalized Organosilicon Oxide

Nanoparticles for Bioimaging and Forensics," *ACS Appl. Nano Mater.*, vol. 3, no. 6, pp. 5123–5138, 2020, doi: 10.1021/acsanm.0c00420.

[194] M. Zhang *et al.*, "Systematic study of dye loaded small mesoporous silica nanoparticles for detecting latent fingerprints on various substrates," *J. Porous Mater.*, 2016, doi: 10.1007/s10934-016-0231-y.

[195] W. Wang, J. Xing, and Z. Ge, "Evaluation of Nile Red-Loaded Mesoporous Silica Nanoparticles for Developing Water-Soaked Fingerprints on Thermal Paper," *J. Forensic Sci.*, vol. 64, no. 3, pp. 717–727, 2019, doi: 10.1111/1556-4029.13959.

[196] L. Meng, Y. Ren, Z. Zhou, C. Li, C. Wang, and S. Fu, "Monodisperse silica nanoparticle suspension for developing latent blood fingermarks," *Forensic Sci. Res.*, vol. 5, no. 1, pp. 38–46, 2020, doi: 10.1080/20961790.2018.1446721.

[197] B. J. Theaker, K. E. Hudson, and F. J. Rowell, "Doped hydrophobic silica nano- and micro-particles as novel agents for developing latent fingerprints," *Forensic Sci. Int.*, vol. 174, no. 1, pp. 26–34, 2008, doi: 10.1016/j.forsciint.2007.02.030.

[198] H. Zhang *et al.*, "Non-conjugated organosilicone fluorescent nanoparticles for latent fingerprint detection," *J. Lumin.*, vol. 215, no. March, p. 116582, 2019, doi: 10.1016/j.jlumin.2019.116582.

[199] V. Divya *et al.*, "Fluorescent amphiphilic silica nanopowder for developing latent fingerprints," *Aust. J. Forensic Sci.*, vol. 52, no. 3, pp. 354–367, 2020, doi: 10.1080/00450618.2018.1533036.

[200] Y. J. Kim, H. S. Jung, J. Lim, S. J. Ryu, and J. K. Lee, "Rapid Imaging of Latent Fingerprints Using Biocompatible Fluorescent Silica Nanoparticles," *Langmuir*, vol. 32, no. 32, pp. 8077–8083, 2016, doi: 10.1021/acs.langmuir.6b01977.

[201] W. Huang, X. Li, H. Wang, X. Xu, H. Liu, and G. Wang, "Synthesis of Amphiphilic Silica Nanoparticles for Latent Fingerprint Detection," *Anal. Lett.*, vol. 48, no. 9, pp. 1524–1535, 2015, doi: 10.1080/00032719.2014.984195.

[202] L. Wang, W. Gu, Z. An, and Q. Cai, "Shape-controllable synthesis of silica coated core/shell upconversion nanomaterials and rapid imaging of latent fingerprints," *Sensors Actuators, B Chem.*, vol. 266, pp. 19–25, 2018, doi: 10.1016/j.snb.2018.03.084.

[203] Y. Yang *et al.*, "Red-emissive conjugated oligomer/silica hybrid nanoparticles with high affinity and application for latent fingerprint detection," *Colloids Surfaces A Physicochem. Eng. Asp.*, vol. 565, no. December 2018, pp. 118–130, 2019, doi: 10.1016/j.colsurfa.2019.01.009.

[204] S. N. Aisyiyah Jenie *et al.*, "Geothermal silica-based fluorescent nanoparticles for the visualization of latent fingerprints," *Mater. Express*, vol. 10, no. 2, pp. 258–266, 2020, doi: 10.1166/mex.2020.1551.

[205] F. Li, H. Li, and T. Cui, "One-step synthesis of solid state luminescent carbon-based silica nanohybrids for imaging of latent fingerprints," *Opt. Mater.*

(Amst)., vol. 73, pp. 459–465, 2017, doi: 10.1016/j.optmat.2017.09.004.

[206] D. Fernandes, M. J. Krysmann, and A. Kelarakis, "Carbogenically coated silica nanoparticles and their forensic applications," *Chem. Commun.*, vol. 52, no. 53, pp. 8294–8296, 2016, doi: 10.1039/c6cc02556k.

[207] Y.-B. Zhao *et al.*, "New luminescent nanoparticles based on carbon dots/SiO2 for the detection of latent fingermarks," *Anal. Methods*, vol. 9, no. 33, pp. 4770–4775, 2017, doi: 10.1039/c7ay01316g.

[208] H. Y. Chen and L. Liu, "Synthesis of Photoluminescent Core-Shell-Structured Carbon dots@silica Nanocomposite Fingermark Powders for Latent Fingermarks Visualization," *Nano*, vol. 14, no. 6, pp. 1–9, 2019, doi: 10.1142/S1793292019500681.

[209] M. Saif, "Synthesis of down conversion, high luminescent nano-phosphor materials based on new developed Ln^{3+}:$Y_2Zr_2O_7/SiO_2$ for latent fingerprint application," *J. Lumin.*, vol. 135, pp. 187–195, 2013, doi: 10.1016/j.jlumin.2012.10.022.

[210] M. Saif, N. Alsayed, A. Mbarek, M. El-Kemary, and M. S. A. Abdel-Mottaleb, "Preparation and characterization of new photoluminescent nano-powder based on Eu^{3+}:$La_2Ti_2O_7$ and dispersed into silica matrix for latent fingerprint detection," *J. Mol. Struct.*, vol. 1125, pp. 763–771, 2016, doi: 10.1016/j.molstruc.2016.07.075.

[211] Z. Wang, X. Jiang, W. Liu, G. Lu, and X. Huang, "A rapid and operator-safe powder approach for latent fingerprint detection using hydrophilic Fe_3O_4@SiO_2-CdTe nanoparticles," *Sci. China Chem.*, vol. 62, no. 7, pp. 889–896, 2019, doi: 10.1007/s11426-019-9460-0.

[212] S. Wei and X. Cui, "Synthesis of gold nanoparticles immobilized on fibrous nano-silica for latent fingerprints detection," *J. Porous Mater.*, 2021, doi: 10.1007/s10934-020-01030-8.

[213] F. Rowell, K. Hudson, and J. Seviour, "Detection of drugs and their metabolites in dusted latent fingermarks by mass spectrometry," *Analyst*, vol. 134, no. 4, pp. 701–707, 2009, doi: 10.1039/b813957c.

[214] A. Y. Lim and J. Seviour, "Doped silica nanoparticles for the detection of pharmaceutical terbinafine in latent fingerprints by mass spectrometry," *Anal. Methods*, vol. 4, no. 7, pp. 1983–1988, 2012, doi: 10.1039/c2ay25187f.

[215] A. Y. Lim, F. Rowell, C. G. Elumbaring-Salazar, J. Loke, and J. Ma, "Detection of drugs in latent fingermarks by mass spectrometric methods," *Anal. Methods*, vol. 5, no. 17, pp. 4378–4385, 2013, doi: 10.1039/c3ay40538a.

[216] A. Bécue, "Emerging fields in fingermark (meta)detection-a critical review," *Anal. Methods*, vol. 8, no. 45, pp. 7983–8003, 2016, doi: 10.1039/c6ay02496c.

[217] W. J. Gee, "Recent trends concerning upconversion nanoparticles and near-IR emissive lanthanide materials in the context of forensic applications," *Aust. J. Chem.*, vol. 72, no. 3, pp. 164–173, 2019, doi: 10.1071/CH18502.

[218] A. Becue, S. Moret, C. Champod, and P. Margot, "Use of quantum dots in aqueous solution to detect blood fingermarks on non-porous surfaces,"

Forensic Sci. Int., vol. 191, no. 1–3, pp. 36–41, 2009, doi: 10.1016/j.forsciint.2009.06.005.

[219] S. Moret, A. Bécue, and C. Champod, "Cadmium-free quantum dots in aqueous solution: Potential for fingermark detection, synthesis and an application to the detection of fingermarks in blood on non-porous surfaces," *Forensic Sci. Int.*, vol. 224, no. 1–3, pp. 101–110, 2013, doi: 10.1016/j.forsciint.2012.11.009.

[220] J. Liu, Z. Shi, Y. Yu, R. Yang, and S. Zuo, "Water-soluble multicolored fluorescent CdTe quantum dots: Synthesis and application for fingerprint developing," *J. Colloid Interface Sci.*, vol. 342, no. 2, pp. 278–282, 2010, doi: 10.1016/j.jcis.2009.10.061.

[221] R. Yang, Y. Wang, B. Xia, Y. Wang, and J. Liu, "Application of CdTe quantum dots to development fingerprints on adhesive surfaces," *Mater. Sci. Forum*, vol. 694, pp. 874–880, 2011, doi: 10.4028/www.scientific.net/MSF.694.874.

[222] K. Cai, R. Yang, Y. Wang, X. Yu, and J. Liu, "Super fast detection of latent fingerprints with water soluble CdTe quantum dots," *Forensic Sci. Int.*, vol. 226, no. 1–3, pp. 240–243, 2013, doi: 10.1016/j.forsciint.2013.01.035.

[223] X. Yu, J. Liu, S. Zuo, Y. Yu, K. Cai, and R. Yang, "Application of mercaptosuccinic acid capped CdTe quantum dots for latent fingermark development," *Forensic Sci. Int.*, vol. 231, no. 1–3, pp. 125–130, 2013, doi: 10.1016/j.forsciint.2013.04.027.

[224] F. Gao *et al.*, "The synthesis of newly modified CdTe quantum dots and their application for improvement of latent fingerprint detection," *Nanotechnology*, vol. 22, no. 7, 2011, doi: 10.1088/0957-4484/22/7/075705.

[225] Y. Li, C. Xu, C. Shu, X. Hou, and P. Wu, "Simultaneous extraction of level 2 and level 3 characteristics from latent fingerprints imaged with quantum dots for improved fingerprint analysis," *Chinese Chem. Lett.*, vol. 28, no. 10, pp. 1961–1964, 2017, doi: 10.1016/j.cclet.2017.04.027.

[226] C. Xu, R. Zhou, W. He, L. Wu, P. Wu, and X. Hou, "Fast imaging of eccrine latent fingerprints with nontoxic Mn-Doped ZnS QDs," *Anal. Chem.*, vol. 86, no. 7, pp. 3279–3283, 2014, doi: 10.1021/ac404244v.

[227] S. Shahbazi *et al.*, "Luminescence detection of latent fingermarks on non-porous surfaces with heavy-metal-free quantum dots," *Forensic Chem.*, vol. 18, no. January, p. 100222, 2020, doi: 10.1016/j.forc.2020.100222.

[228] J. Cui, S. Xu, C. Guo, R. Jiang, T. D. James, and L. Wang, "Highly Efficient Photothermal Semiconductor Nanocomposites for Photothermal Imaging of Latent Fingerprints," *Anal. Chem.*, vol. 87, no. 22, pp. 11592–11598, 2015, doi: 10.1021/acs.analchem.5b03652.

[229] P. Wu, C. Xu, X. Hou, J. J. Xu, and H. Y. Chen, "Dual-emitting quantum dot nanohybrid for imaging of latent fingerprints: simultaneous identification of individuals and traffic light-type visualization of TNT," *Chem. Sci.*, vol. 6, no. 8, pp. 4445–4450, 2015, doi: 10.1039/c5sc01497b.

[230] Y. F. Wang, R. Q. Yang, Y. J. Wang, Z. X. Shi, and J. J. Liu, "Application of CdSe

nanoparticle suspension for developing latent fingermarks on the sticky side of adhesives," *Forensic Sci. Int.*, vol. 185, no. 1–3, pp. 96–99, 2009, doi: 10.1016/j.forsciint.2008.12.021.

[231] T. P. Na Ayudhaya, P. Viwattana, K. Thamaphat, and K. Lomthaisong, "Room temperature synthesis of water-soluble starch-stabilized CdSe quantum dots for latent fingerprints detection," *Adv. Environ. Biol.*, vol. 8, no. 14, pp. 44–49, 2014.

[232] Y. H. Chen *et al.*, "Dual colorimetric and fluorescent imaging of latent fingerprints on both porous and nonporous surfaces with near-infrared fluorescent semiconducting polymer dots," *Anal. Chem.*, vol. 88, no. 23, pp. 11616–11623, 2016, doi: 10.1021/acs.analchem.6b03178.

[233] X. Jia *et al.*, "Facile synthesis of BCNO quantum dots with applications for ion detection, chemosensor and fingerprint identification," *Spectrochim. Acta - Part A Mol. Biomol. Spectrosc.*, vol. 203, pp. 214–221, 2018, doi: 10.1016/j.saa.2018.05.099.

[234] J. Dilag, H. Kobus, and A. V. Ellis, "CdS/polymer nanocomposites synthesized via surface initiated RAFT polymerization for the fluorescent detection of latent fingermarks," *Forensic Sci. Int.*, vol. 228, no. 1–3, pp. 105–114, 2013, doi: 10.1016/j.forsciint.2013.02.044.

[235] Y. J. Jin *et al.*, "Application of photoluminescent CdS/PAMAM nanocomposites in fingerprint detection," *Forensic Sci. Int.*, vol. 179, no. 1, pp. 34–38, 2008, doi: 10.1016/j.forsciint.2008.04.010.

[236] Y. J. Jin, Y. J. Luo, G. Z. Xu, and B. Yang, "Aged fingermarks detection with CdS/PAMAM nanocomposites," *Adv. Mater. Res.*, vol. 282–283, pp. 466–469, 2011, doi: 10.4028/www.scientific.net/AMR.282-283.466.

[237] Y. J. Jin, Y. J. Luo, G. Z. Xu, and B. Yang, "Effects of metallic ions on photoluminescence properties of CdSe/PAMAM nanocomposites and their application in fingerprint detection," *Adv. Mater. Res.*, vol. 295–297, pp. 900–906, 2011, doi: 10.4028/www.scientific.net/AMR.295-297.900.

[238] W. Dong *et al.*, "Synthesis and self-assembly of hierarchical SiO2-QDs@SiO2 nanostructures and their photoluminescence applications for fingerprint detection and cell imaging," *RSC Adv.*, vol. 4, no. 86, pp. 45939–45945, 2014, doi: 10.1039/c4ra04925j.

[239] J. Dilag, H. Kobus, and A. V. Ellis, "Cadmium sulfide quantum dot/chitosan nanocomposites for latent fingermark detection," *Forensic Sci. Int.*, vol. 187, no. 1–3, pp. 97–102, 2009, doi: 10.1016/j.forsciint.2009.03.006.

[240] M. Algarra *et al.*, "Solid luminescent CdSe-thiolated porous phosphate heterostructures. Application in fingermark detection in different surfaces," *Surf. Interface Anal.*, vol. 45, no. 2, pp. 612–618, 2013, doi: 10.1002/sia.5100.

[241] M. Algarra *et al.*, "Fingerprint detection and using intercalated CdSe nanoparticles on non-porous surfaces," *Anal. Chim. Acta*, vol. 812, pp. 228–235, 2014, doi: 10.1016/j.aca.2014.01.015.

[242] F. Gao *et al.*, "CdTe-montmorillonite nanocomposites: Control synthesis, UV

radiation-dependent photoluminescence, and enhanced latent fingerprint detection," *J. Phys. Chem. C*, vol. 115, no. 44, pp. 21574–21583, 2011, doi: 10.1021/jp205021j.

[243] F. Gao *et al.*, "Application of core-shell-structured CdTe@SiO_2 quantum dots synthesized via a facile solution method for improving latent fingerprint detection," *J. Nanoparticle Res.*, vol. 14, no. 10, 2012, doi: 10.1007/s11051-012-1191-z.

[244] P. Niu *et al.*, "CdTe@SiO_2/Ag nanocomposites as antibacterial fluorescent markers for enhanced latent fingerprint detection," *Dye. Pigment.*, vol. 119, pp. 1–11, 2015, doi: 10.1016/j.dyepig.2015.03.018.

[245] S. Singh *et al.*, "Easy, one-step synthesis of CdTe quantum dots via microwave irradiation for fingerprinting application," *Mater. Res. Bull.*, vol. 90, pp. 260–265, 2017, doi: 10.1016/j.materresbull.2017.03.003.

[246] Z. Zhao, J. Shen, and M. Wang, "Simultaneous imaging of latent fingerprint and quantification of nicotine residue by $NaYF_4$:Yb/Tm upconversion nanoparticles," *Nanotechnology*, vol. 31, no. 14, 2020, doi: 10.1088/1361-6528/ab647c.

[247] M. Wang *et al.*, "NIR-induced highly sensitive detection of latent fingermarks by $NaYF_4$:Yb,Er upconversion nanoparticles in a dry powder state," *Nano Res.*, vol. 8, no. 6, pp. 1800–1810, 2015, doi: 10.1007/s12274-014-0686-6.

[248] M. Wang, Y. Zhu, and C. Mao, "Synthesis of NIR-Responsive $NaYF_4$:Yb,Er Upconversion Fluorescent Nanoparticles Using an Optimized Solvothermal Method and Their Applications in Enhanced Development of Latent Fingerprints on Various Smooth Substrates," *Langmuir*, vol. 31, pp. 7084–7090, 2015, doi: 10.1021/acs.langmuir.5b01151.

[249] B. Y. Li *et al.*, "NIR-responsive $NaYF_4$:Yb,Er,Gd fluorescent upconversion nanorods for the highly sensitive detection of blood fingerprints," *Dye. Pigment.*, vol. 134, pp. 178–185, 2016, doi: 10.1016/j.dyepig.2016.07.014.

[250] M. Wang *et al.*, "Dual-mode fluorescent development of latent fingerprints using $NaYbF_4$:Tm upconversion nanomaterials," *Mater. Today Adv.*, vol. 8, 2020, doi: 10.1016/j.mtadv.2020.100113.

[251] J. Xu *et al.*, "Dual-Mode, Color-Tunable, Lanthanide-Doped Core-Shell Nanoarchitectures for Anti-Counterfeiting Inks and Latent Fingerprint Recognition," *ACS Appl. Mater. Interfaces*, vol. 11, no. 38, pp. 35294–35304, 2019, doi: 10.1021/acsami.9b10989.

[252] P. Du, P. Zhang, S. H. Kang, and J. S. Yu, "Hydrothermal synthesis and application of Ho^{3+}-activated $NaYbF_4$ bifunctional upconverting nanoparticles for in vitro cell imaging and latent fingerprint detection," *Sensors Actuators, B Chem.*, vol. 252, pp. 584–591, 2017, doi: 10.1016/j.snb.2017.06.032.

[253] A. Baride, G. Sigdel, W. M. Cross, J. J. Kellar, and P. S. May, "Near infrared-to-near infrared upconversion nanocrystals for latent fingerprint development," *ACS Appl. Nano Mater.*, vol. 2, no. 12, pp. 4518–4527, 2019, doi: 10.1021/acsanm.9b00890.

[254] M. K. Mahata, S. P. Tiwari, S. Mukherjee, K. Kumar, and V. K. Rai, "$YVO_4:Er^{3+}/Yb^{3+}$ phosphor for multifunctional applications," *J. Opt. Soc. Am. B*, vol. 31, no. 8, p. 1814, 2014, doi: 10.1364/josab.31.001814.

[255] X. Wang, L. Yan, S. Liu, P. Zhang, R. Huang, and B. Zhou, "Enhancing energy migration upconversion through a migratory interlayer in the core-shell-shell nanostructure towards latent fingerprinting," *Nanoscale*, vol. 12, no. 36, pp. 18807–18814, 2020, doi: 10.1039/d0nr03817b.

[256] S. K. Singh, K. Kumar, and S. B. Rai, "Multifunctional Er^{3+}-Yb^{3+} codoped Gd_2O_3 nanocrystalline phosphor synthesized through optimized combustion route," *Appl. Phys. B Lasers Opt.*, vol. 94, no. 1, pp. 165–173, 2009, doi: 10.1007/s00340-008-3261-6.

[257] D. Zhou *et al.*, "Semiconductor Plasmon Induced Up-Conversion Enhancement in mCu_2-$xS@SiO_2@Y_2O_3:Yb^{3+}/Er^{3+}$ Core-Shell Nanocomposites," *ACS Appl. Mater. Interfaces*, vol. 9, no. 40, pp. 35226–35233, 2017, doi: 10.1021/acsami.7b09850.

[258] M. Wang, "Latent fingermarks light up: Facile development of latent fingermarks using NIR-responsive upconversion fluorescent nanocrystals," *RSC Adv.*, vol. 6, no. 43, pp. 36264–36268, 2016, doi: 10.1039/c6ra04573a.

[259] C. M. Liu, L. Y. Zhang, L. Li, B. Y. Li, C. G. Wang, and T. T. Wang, "Specific detection of latent human blood fingerprints using antibody modified $NaYF_4$:Yb, Er, Gd fluorescent upconversion nanorods," *Dye. Pigment.*, vol. 149, no. September 2017, pp. 822–829, 2018, doi: 10.1016/j.dyepig.2017.11.050.

[260] J. Wang *et al.*, "Highly-luminescent Eu,Sm,Mn-doped CaS up/down conversion nano-particles: Application to ultra-sensitive latent fingerprint detection and: In vivo bioimaging," *Chem. Commun.*, vol. 54, no. 6, pp. 591–594, 2018, doi: 10.1039/c7cc07790d.

[261] J. Li, X. Zhu, M. Xue, W. Feng, R. Ma, and F. Li, "Nd^{3+}-Sensitized Upconversion Nanostructure as a Dual-Channel Emitting Optical Probe for Near Infrared-to-Near Infrared Fingerprint Imaging," *Inorg. Chem.*, vol. 55, no. 20, pp. 10278–10283, 2016, doi: 10.1021/acs.inorgchem.6b01536.

[262] A. Kumar, S. P. Tiwari, A. K. Singh, and K. Kumar, "Synthesis of $Gd_2O_3:Ho^{3+}/Yb^{3+}$ upconversion nanoparticles for latent fingermark detection on difficult surfaces," *Appl. Phys. B Lasers Opt.*, vol. 122, no. 7, pp. 1–10, 2016, doi: 10.1007/s00340-016-6468-y.

[263] I. A. Rahman and V. Padavettan, "Synthesis of Silica Nanoparticles by Sol-Gel: Size-Dependent Properties, Surface Modification, and Applications in Silica-Polymer Nanocomposites-A Review," *J. Nanomater.*, vol. 2012, p. 15, 2012, doi: 10.1155/2012/132424.

[264] H. E. Bergna and W. O. Roberts, *Colloidal silica: Fundamentals and applications*. CRC Taylor & Francis, 2006.

[265] V. Torchilin, *Handbook of Nanobiomedical Research: Fundamentals, Applications and Recent Developments*. World Scientific, 2014.

[266] R. K. Iler, *The Chemistry of Silica. Solubility, Polymerization, Colloid and Surface Properties, and Biochemistry*. John Wiley & Sons, 1979.

[267] B. E. Douglas and S.-M. Ho, *Structure and Structure and Chemistry of Crystalline Solids*. Springer, 2006.

[268] T. Koźlecki, I. Polowczyk, A. Bastrzyk, and W. Sawiński, "Improved Synthesis of Nanosized Silica in Water-in-Oil Microemulsions," *J. Nanoparticles*, vol. 2016, no. 1, pp. 1–9, 2016, doi: 10.1155/2016/8203260.

[269] L. Li *et al.*, "Classification, Synthesis, and Application of Luminescent Silica Nanoparticles: a Review," *Nanoscale Res. Lett.*, vol. 14, no. 190, pp. 1–23, 2019, doi: 10.1186/s11671-019-3006-y.

[270] I. Made Joni, Rukiah, and C. Panatarani, "Synthesis of silica particles by precipitation method of sodium silicate: Effect of temperature, pH and mixing technique," *AIP Conf. Proc.*, vol. 2219, no. 080018, 2020, doi: 10.1063/5.0003074.

[271] L. P. Singh, S. K. Agarwal, S. K. Bhattacharyya, U. Sharma, and S. Ahalawat, "Preparation of silica nanoparticles and its beneficial role in cementitious materials," *Nanomater. Nanotechnol.*, vol. 1, no. 1, pp. 44–51, 2011, doi: 10.5772/50950.

[272] J. D. Wright and N. A. J. M. Sommerdijk, *Sol-Gel Materials Chemistry and Applications*. Gordon and Breach Science Publishers, 2001.

[273] A. Fidalgo and L. M. Ilharco, "Chemical Tailoring of Porous Silica Xerogels: Local Structure by Vibrational Spectroscopy," *Chem. - A Eur. J.*, vol. 10, no. 2, pp. 392–398, 2004, doi: 10.1002/chem.200305079.

[274] D. Levy and M. Zayat, *The Sol-Gel Handbook*. Wiley-VCH, 2015.

[275] H. Maleki, L. Durães, and A. Portugal, "An overview on silica aerogels synthesis and different mechanical reinforcing strategies," *J. Non. Cryst. Solids*, vol. 385, pp. 55–74, 2014, doi: 10.1016/j.jnoncrysol.2013.10.017.

[276] W. Stober, A. Fink, and E. Bohn, "Controlled Growth of Monodisperse Silica Spheres in the Micron Size Range," *J. Colloid Interface Sci.*, vol. 26, pp. 62–69, 1968.

[277] P. A. Winsor, "Hydrotropy, Solubilisation And Related Emulsification Processes. Part I.," *Trans. Faraday Soc.*, vol. 44, pp. 376–398, 1947.

[278] A. D. Gadhave and J. T. Waghmare, "A Short Review on Microemulsion and Its Application in Extraction of Vegetable Oil," *Int. J. Res. Eng. Technol.*, vol. 03, no. 09, pp. 147–158, 2014, doi: 10.15623/ijret.2014.0309022.

[279] M. A. Malik, M. Y. Wani, and M. A. Hashim, "Microemulsion method: A novel route to synthesize organic and inorganic nanomaterials. 1st Nano Update," *Arab. J. Chem.*, vol. 5, no. 4, pp. 397–417, 2012, doi: 10.1016/j.arabjc.2010.09.027.

[280] K. S. Finnie, J. R. Bartlett, C. J. A. Barbé, and L. Kong, "Formation of silica nanoparticles in microemulsions," *Langmuir*, vol. 23, no. 6, pp. 3017–3024, 2007, doi: 10.1021/la0624283.

[281] R. Narayan, U. Y. Nayak, A. M. Raichur, and S. Garg, "Mesoporous silica

nanoparticles: A comprehensive review on synthesis and recent advances," *Pharmaceutics*, vol. 10, no. 3, pp. 1–49, 2018, doi: 10.3390/pharmaceutics10030118.

[282] Z. Li, Y. Mu, C. Peng, M. F. Lavin, H. Shao, and Z. Du, "Understanding the mechanisms of silica nanoparticles for nanomedicine," *Wiley Interdiscip. Rev. Nanomedicine Nanobiotechnology*, vol. 13, no. 1, pp. 1–23, 2021, doi: 10.1002/wnan.1658.

[283] J. Sharma and G. Polizos, "Hollow silica particles: Recent progress and future perspectives," *Nanomaterials*, vol. 10, no. 8, pp. 1–22, 2020, doi: 10.3390/nano10081599.

[284] F. Tang, L. Li, and D. Chen, "Mesoporous silica nanoparticles: Synthesis, biocompatibility and drug delivery," *Adv. Mater.*, vol. 24, no. 12, pp. 1504–1534, 2012, doi: 10.1002/adma.201104763.

[285] Z. Li, J. C. Barnes, A. Bosoy, J. F. Stoddart, and J. I. Zink, "Mesoporous silica nanoparticles in biomedical applications," *Chem. Soc. Rev.*, vol. 41, no. 7, pp. 2590–2605, 2012, doi: 10.1039/c1cs15246g.

[286] V. C. Niculescu, "Mesoporous Silica Nanoparticles for Bio-Applications," *Front. Mater.*, vol. 7, no. February, pp. 1–14, 2020, doi: 10.3389/fmats.2020.00036.

[287] J. L. Vivero-Escoto, I. I. Slowing, V. S. Y. Lin, and B. G. Trewyn, "Mesoporous silica nanoparticles for intracellular controlled drug delivery," *Small*, vol. 6, no. 18, pp. 1952–1967, 2010, doi: 10.1002/smll.200901789.

[288] C. Xu, C. Lei, and C. Yu, "Mesoporous silica nanoparticles for protein protection and delivery," *Front. Chem.*, vol. 7, pp. 1–12, 2019, doi: 10.3389/fchem.2019.00290.

[289] C. Sanchez, B. Julián, P. Belleville, and M. Popall, "Applications of hybrid organic-inorganic nanocomposites," *J. Mater. Chem.*, vol. 15, no. 35–36, pp. 3559–3592, 2005, doi: 10.1039/b509097k.

[290] Y. Alyassin *et al.*, "Application of mesoporous silica nanoparticles as drug delivery carriers for chemotherapeutic agents," *Drug Discov. Today*, vol. 25, no. 8, pp. 1513–1520, 2020, doi: 10.1016/j.drudis.2020.06.006.

[291] X. Qian, W. Wang, W. Kong, and Y. Chen, "Organic-inorganic hybrid hollow mesoporous organosilica nanoparticles for efficient ultrasound-based imaging and controlled drug release," *J. Nanomater.*, vol. 2014, 2014, doi: 10.1155/2014/972475.

[292] I. I. Slowing, J. L. Vivero-Escoto, C. W. Wu, and V. S. Y. Lin, "Mesoporous silica nanoparticles as controlled release drug delivery and gene transfection carriers," *Adv. Drug Deliv. Rev.*, vol. 60, no. 11, pp. 1278–1288, 2008, doi: 10.1016/j.addr.2008.03.012.

[293] R. S. Prakasham, P. R. Likhar, K. Rajyalaxmi, C. Subba Rao, and B. Sreedhar, "Octadecanoic acid/silica particles synthesis for enzyme immobilization: Characterization and evaluation of biocatalytic activity," *J. Mol. Catal. B Enzym.*, vol. 55, no. 1–2, pp. 43–48, 2008, doi:

10.1016/j.molcatb.2008.01.008.
[294] L. Wang, C. Yang, and W. Tan, “Dual-luminophore-doped silica nanoparticles for multiplexed signaling,” *Nano Lett.*, vol. 5, no. 1, pp. 37–43, 2005, doi: 10.1021/nl048417g.
[295] C. W. Lu *et al.*, “Bifunctional magnetic silica nanoparticles for highly efficient human stem cell labeling,” *Nano Lett.*, vol. 7, no. 1, pp. 149–154, 2007, doi: 10.1021/nl0624263.
[296] D. K. Yi, S. T. Selvan, S. S. Lee, G. C. Papaefthymiou, D. Kundaliya, and J. Y. Ying, “Silica-coated nanocomposites of magnetic nanoparticles and quantum dots,” *J. Am. Chem. Soc.*, vol. 127, no. 14, pp. 4990–4991, 2005, doi: 10.1021/ja0428863.
[297] M. Sharma, P. Easha, G. Tapasvi, and R. Reetika, *Nanomaterials in biomedical diagnosis*. INC, 2020.
[298] M. G. C. Pereira, E. S. Leite, G. A. L. Pereira, A. Fontes, and B. S. Santos, *Quantum Dots*. Elsevier Inc., 2016.
[299] S. Brkić, “Applicability of Quantum Dots in Biomedical Science,” *Ioniz. Radiat. Eff. Appl.*, 2018, doi: 10.5772/intechopen.71428.
[300] D. Bera, L. Qian, T. K. Tseng, and P. H. Holloway, “Quantum dots and their multimodal applications: A review,” *Materials (Basel).*, vol. 3, no. 4, pp. 2260–2345, 2010, doi: 10.3390/ma3042260.
[301] I. L. Medintz, H. T. Uyeda, E. R. Goldman, and H. Mattoussi, “Quantum dot bioconjugates for imaging, labelling and sensing,” *Nat. Mater.*, vol. 4, no. 6, pp. 435–446, 2005, doi: 10.1038/nmat1390.
[302] A. M. Smith, H. Duan, A. M. Mohs, and S. Nie, “Bioconjugated quantum dots for in vivo molecular and cellular imaging,” *Adv. Drug Deliv. Rev.*, vol. 60, no. 11, pp. 1226–1240, 2008, doi: 10.1016/j.addr.2008.03.015.
[303] J. Cancino-Bernardi, I. M. M. Paino, J. P. Souza, V. S. Marangoni, P. F. M. Nogueira, and V. Zucolotto, *Current Challenges in the Commercialization of Nanocolloids: Toxicology and Environmental Issues*. Elsevier Inc., 2016.
[304] A. M. Derfus, W. C. W. Chan, and S. N. Bhatia, “Probing the Cytotoxicity of Semiconductor Quantum Dots,” *Nano Lett.*, vol. 4, no. 1, pp. 11–18, 2004, doi: 10.1021/nl0347334.
[305] W. H. Chan, N. H. Shiao, and P. Z. Lu, “CdSe quantum dots induce apoptosis in human neuroblastoma cells via mitochondrial-dependent pathways and inhibition of survival signals,” *Toxicol. Lett.*, vol. 167, no. 3, pp. 191–200, 2006, doi: 10.1016/j.toxlet.2006.09.007.
[306] T. Aubert *et al.*, “Bright and stable CdSe/CdS@SiO_2 nanoparticles suitable for long-term cell labeling,” *ACS Appl. Mater. Interfaces*, vol. 6, no. 14, pp. 11714–11723, 2014, doi: 10.1021/am502367b.
[307] Z. Ranjbar-Navazi, Y. Omidi, M. Eskandani, and S. Davaran, “Cadmium-free quantum dot-based theranostics,” *TrAC - Trends Anal. Chem.*, vol. 118, pp. 386–400, 2019, doi: 10.1016/j.trac.2019.05.041.
[308] B. Zhang, Y. Wang, R. Hu, I. Roy, and K. Yong, “Cadmium-Free Quantum Dots

for Biophotonic Imaging and Sensing," in *Handbook of Photonics for Biomedical Engineering*, A. P. Ho, D. Kim, and M. Somekh, Eds. Springer, 2017, pp. 841–870.

[309] K. T. Yong *et al.*, "Imaging pancreatic cancer using bioconjugated InP quantum dots," *ACS Nano*, vol. 3, no. 3, pp. 502–510, 2009, doi: 10.1021/nn8008933.

[310] S. Plappert and F. Liebner, *Cellulose-Based Photoluminescent Nanocomposites*. INC, 2020.

[311] H. Puliyalil and U. Cvelbar, "Selective plasma etching of polymeric substrates for advanced applications," *Nanomaterials*, vol. 6, no. 6, 2016, doi: 10.3390/nano6060108.

[312] A. Valizadeh *et al.*, "Quantum dots: Synthesis, bioapplications, and toxicity," *Nanoscale Res. Lett.*, vol. 7, pp. 19–21, 2012, doi: 10.1186/1556-276X-7-480.

[313] Z. Chen, X. X. Li, G. Du, N. Chen, and A. Y. M. Suen, "A sol-gel method for preparing ZnO quantum dots with strong blue emission," *J. Lumin.*, vol. 131, no. 10, pp. 2072–2077, 2011, doi: 10.1016/j.jlumin.2011.05.009.

[314] S. Javed, M. Islam, and M. Mujahid, "Synthesis and characterization of TiO_2 quantum dots by sol gel reflux condensation method," *Ceram. Int.*, vol. 45, no. 2, pp. 2676–2679, 2019, doi: 10.1016/j.ceramint.2018.10.163.

[315] D. Bera, L. Qian, S. Sabui, S. Santra, and P. H. Holloway, "Photoluminescence of ZnO quantum dots produced by a sol-gel process," *Opt. Mater. (Amst).*, vol. 30, no. 8, pp. 1233–1239, 2008, doi: 10.1016/j.optmat.2007.06.001.

[316] C. Petit, T. K. Jain, F. Billoudet, and M. P. Pileni, "Oil in Water Micellar Solution Used to Synthesize CdS Particles: Structural Study and Photoelectron Transfer Reaction," *Langmuir*, vol. 10, no. 12, pp. 4446–4450, 1994, doi: 10.1021/la00024a012.

[317] R. D. Tilley and K. Yamamoto, "The microemulsion synthesis of hydrophobic and hydrophilic silicon nanocrystals," *Adv. Mater.*, vol. 18, no. 15, pp. 2053–2056, 2006, doi: 10.1002/adma.200600118.

[318] K. Lemke and J. Koetz, "Polycation-capped CdS quantum dots synthesized in reverse microemulsions," *J. Nanomater.*, vol. 2012, 2012, doi: 10.1155/2012/478153.

[319] S. Chen, M. Ahmadiantehrani, N. G. Publicover, K. W. Hunter, and X. Zhu, "Thermal decomposition based synthesis of Ag-In-S/ZnS quantum dots and their chlorotoxin-modified micelles for brain tumor cell targeting," *RSC Adv.*, vol. 5, no. 74, pp. 60612–60620, 2015, doi: 10.1039/c5ra11250h.

[320] F. Limosani, R. Carcione, and F. Antolini, "Formation of CdSe quantum dots from single source precursor obtained by thermal and laser treatment," *J. Vac. Sci. Technol. B*, vol. 38, no. 1, p. 012802, 2020, doi: 10.1116/1.5129661.

[321] B. Karimi, M. Shafiee Afarani, and A. M. Arabi, "Hydrothermal synthesis of cadmium selenide quantum dots: effect of reducing agent," *Appl. Phys. A Mater. Sci. Process.*, vol. 126, no. 9, pp. 1–9, 2020, doi: 10.1007/s00339-020-03903-w.

[322] X. Shao, W. Xin, and X. Yin, "Hydrothermal synthesis of ZnO quantum

dot/KNb3O8 nanosheet photocatalysts for reducing carbon dioxide to methanol," *Beilstein J. Nanotechnol.*, vol. 8, no. 1, pp. 2264–2270, 2017, doi: 10.3762/bjnano.8.226.

[323] S. Arora and S. Sundar Manoharan, "Size-dependent photoluminescent properties of uncapped CdS particles prepared by acoustic wave and microwave method," *J. Phys. Chem. Solids*, vol. 68, no. 10, pp. 1897–1901, 2007, doi: 10.1016/j.jpcs.2007.05.018.

[324] Y. Bao *et al.*, "Preparation of water soluble CdSe and CdSe/CdS quantum dots and their uses in imaging of cell and blood capillary," *Opt. Mater. (Amst).*, vol. 34, no. 9, pp. 1588–1592, 2012, doi: 10.1016/j.optmat.2012.03.033.

[325] L. Wang, L. Chen, T. Luo, and Y. Qian, "A hydrothermal method to prepare the spherical ZnS and flower-like CdS microcrystallites," *Mater. Lett.*, vol. 60, no. 29–30, pp. 3627–3630, 2006, doi: 10.1016/j.matlet.2006.03.072.

[326] H. Yang, W. Yin, H. Zhao, R. Yang, and Y. Song, "A complexant-assisted hydrothermal procedure for growing well-dispersed InP nanocrystals," *J. Phys. Chem. Solids*, vol. 69, no. 4, pp. 1017–1022, 2008, doi: 10.1016/j.jpcs.2007.11.017.

[327] J. Zhu, Y. Koltypin, and A. Gedanken, "General sonochemical method for the preparation of nanophasic selenides: Synthesis of ZnSe nanoparticles," *Chem. Mater.*, vol. 12, no. 1, pp. 73–78, 2000, doi: 10.1021/cm990380r.

[328] R. W. Kelsall, I. W. Hamley, and M. Geoghegan, *Nanoscale Science and Technology*. 2005.

[329] P. Malik, J. Singh, and R. Kakkar, "A review on CdSe quantum dots in sensing," *Adv. Mater. Lett.*, vol. 5, no. 11, pp. 612–628, 2014, doi: 10.5185/amlett.2014.4562.

[330] X. Zhang *et al.*, "Probing and Controlling Surface Passivation of PbS Quantum Dot Solid for Improved Performance of Infrared Absorbing Solar Cells," *Chem. Mater.*, vol. 31, no. 11, pp. 4081–4091, 2019, doi: 10.1021/acs.chemmater.9b00742.

[331] X. S. Wang, T. E. Dykstra, M. R. Salvador, I. Manners, G. D. Scholes, and M. A. Winnik, "Surface passivation of luminescent colloidal quantum dots with poly(dimethylaminoethly methacrylate) through a ligand exchange process," *J. Am. Chem. Soc.*, vol. 126, no. 25, pp. 7784–7785, 2004, doi: 10.1021/ja0489339.

[332] Y. Cao, A. Stavrinadis, T. Lasanta, D. So, and G. Konstantatos, "The role of surface passivation for efficient and photostable PbS quantum dot solar cells," *Nat. Energy*, vol. 1, no. 4, pp. 1–6, 2016, doi: 10.1038/NENERGY.2016.35.

[333] J. K. Oh, "Surface modification of colloidal CdX-based quantum dots for biomedical applications," *J. Mater. Chem.*, vol. 20, no. 39, pp. 8433–8445, 2010, doi: 10.1039/c0jm01084g.

[334] V. V. Goftman, A. V. Markin, S. De Saeger, and I. Y. Goryacheva, "Multicolored silica coated CdSe core/shell quantum dots," *Saratov Fall Meet. 2015 Third*

Int. Symp. Opt. Biophotonics Seventh Finnish-Russian Photonics Laser Symp., vol. 9917, p. 991716, 2016, doi: 10.1117/12.2225212.

[335] Y. Ma, Y. Li, S. Ma, and X. Zhong, "Highly bright water-soluble silica coated quantum dots with excellent stability," *J. Mater. Chem. B*, vol. 2, no. 31, pp. 5043–5051, 2014, doi: 10.1039/c4tb00458b.

[336] N. Tomczak, R. Liu, and J. G. Vancso, "Polymer-coated quantum dots," *Nanoscale*, vol. 5, no. 24, pp. 12018–12032, 2013, doi: 10.1039/c3nr03949h.

[337] D. Jańczewski, N. Tomczak, M. Y. Han, and G. J. Vancso, "Synthesis of functionalized amphiphilic polymers for coating quantum dots," *Nat. Protoc.*, vol. 6, no. 10, pp. 1546–1553, 2011, doi: 10.1038/nprot.2011.381.

[338] A. F. E. Hezinger, J. Teßmar, and A. Göpferich, "Polymer coating of quantum dots - A powerful tool toward diagnostics and sensorics," *Eur. J. Pharm. Biopharm.*, vol. 68, no. 1, pp. 138–152, 2008, doi: 10.1016/j.ejpb.2007.05.013.

[339] M. K. Mahata, H. C. Hofsäss, and U. Vetter, "Photon-Upconverting Materials: Advances and Prospects for Various Emerging Applications," in *Luminescence - An Outlook on the Phenomena and their Applications*, J. Thirumalai, Ed. Intech, 2016.

[340] F. Zhang, *Photon Upconversion Nanomaterials*. Springer, 2015.

[341] C. Altavilla, *Upconverting Nanomaterials Perspectives, Synthesis, and Applications*. CRC Press, 2017.

[342] G. Chen, H. Qiu, P. N. Prasad, and X. Chen, "Upconversion nanoparticles: Design, nanochemistry, and applications in Theranostics," *Chem. Rev.*, vol. 114, no. 10, pp. 5161–5214, 2014, doi: 10.1021/cr400425h.

[343] Q. C. Sun, Y. C. Ding, D. M. Sagar, and P. Nagpal, "Photon upconversion towards applications in energy conversion and bioimaging," *Progress in Surface Science*, vol. 92. Elsevier Ltd, pp. 281–316, Dec. 01, 2017, doi: 10.1016/j.progsurf.2017.09.003.

[344] M. Wang, G. Abbineni, A. Clevenger, C. Mao, and S. Xu, "Upconversion nanoparticles: Synthesis, surface modification and biological applications," *Nanomedicine Nanotechnology, Biol. Med.*, vol. 7, no. 6, pp. 710–729, 2011, doi: 10.1016/j.nano.2011.02.013.

[345] G. Tessitore, G. A. Mandl, M. G. Brik, W. Park, and J. A. Capobianco, "Recent insights into upconverting nanoparticles: Spectroscopy, modeling, and routes to improved luminescence," *Nanoscale*, vol. 11, pp. 12015–12029, 2019, doi: 10.1039/c9nr02291k.

[346] F. Jia, G. Li, B. Yang, B. Yu, Y. Shen, and H. Cong, "Investigation of rare earth upconversion fluorescent nanoparticles in biomedical field," *Nanotechnol. Rev.*, vol. 8, no. 1, pp. 1–17, 2019, doi: 10.1515/ntrev-2019-0001.

[347] H. Chang *et al.*, "Rare earth ion-doped upconversion nanocrystals: Synthesis and surface modification," *Nanomaterials*, vol. 5, no. 1, pp. 1–25, 2014, doi: 10.3390/nano5010001.

[348] S. P. Tiwari *et al.*, "Future prospects of fluoride based upconversion

nanoparticles for emerging applications in biomedical and energy harvesting," *J. Vac. Sci. Technol. B*, vol. 36, no. 6, p. 060801, 2018, doi: 10.1116/1.5044596.

[349] M. Haase and H. Schäfer, "Upconverting nanoparticles," *Angew. Chemie - Int. Ed.*, vol. 50, no. 26, pp. 5808–5829, 2011, doi: 10.1002/anie.201005159.

[350] S. Wang, J. Feng, S. Song, and H. Zhang, "Rare earth fluorides upconversion nanophosphors: From synthesis to applications in bioimaging," *CrystEngComm*, vol. 15, no. 36, pp. 7142–7151, 2013, doi: 10.1039/c3ce40679b.

[351] L.-D. Sun, H. Dong, P.-Z. Zhang, and C.-H. Yan, "Upconversion of Rare Earth Nanomaterials," *Annu. Rev. Phys. Chem.*, vol. 66, pp. 619–642, 2015, doi: 10.1146/annurev-physchem-040214-121344.

[352] F. Auzel, "Upconversion and Anti-Stokes Processes with f and d Ions in Solids," *Chem. Rev.*, vol. 104, pp. 139–173, 2004, doi: 10.1021/cr020357g.

[353] H. Dong, L.-D. Sun, and C.-H. Yan, "Energy transfer in lanthanide upconversion studies for extended optical applications," *Chem. Soc. Rev.*, vol. 44, pp. 1608–1634, 2015, doi: 10.1039/c4cs00188e.

[354] S. Wen, J. Zhou, K. Zheng, A. Bednarkiewicz, X. Liu, and D. Jin, "Advances in highly doped upconversion nanoparticles," *Nat. Commun.*, vol. 9, p. 2415, 2018, doi: 10.1038/s41467-018-04813-5.

[355] G. Liang *et al.*, "Recent progress in the development of upconversion nanomaterials in bioimaging and disease treatment," *J. Nanobiotechnology*, vol. 18, no. 1, pp. 1–22, 2020, doi: 10.1186/s12951-020-00713-3.

[356] X. Zhu, J. Zhang, J. Liu, and Y. Zhang, "Recent Progress of Rare-Earth Doped Upconversion Nanoparticles: Synthesis, Optimization, and Applications," *Adv. Sci.*, vol. 6, no. 22, 2019, doi: 10.1002/advs.201901358.

[357] C. F. Gainer and M. Romanowski, "A review of synthetic methods for the production of upconverting lanthanide nanoparticles," *J. Innov. Opt. Health Sci.*, vol. 7, no. 2, 2014, doi: 10.1142/S1793545813300073.

[358] J. Chen and J. X. Zhao, "Upconversion nanomaterials: Synthesis, mechanism, and applications in sensing," *Sensors*, vol. 12, no. 3, pp. 2414–2435, 2012, doi: 10.3390/s120302414.

[359] F. Vetrone, J. C. Boyer, J. A. Capobianco, A. Speghini, and M. Bettinelli, "Significance of Yb3+ concentration on the upconversion mechanisms in codoped Y_2O_3:Er^{3+},Yb^{3+} nanocrystals," *J. Appl. Phys.*, vol. 96, no. 1, pp. 661–667, 2004, doi: 10.1063/1.1739523.

[360] X. xian Luo and W. he Cao, "Ethanol-assistant solution combustion method to prepare La_2O_2S:Yb,Pr nanometer phosphor," *J. Alloys Compd.*, vol. 460, no. 1–2, pp. 529–534, 2008, doi: 10.1016/j.jallcom.2007.06.011.

[361] L. Xu *et al.*, "Synthesis and upconversion properties of monoclinic Gd_2O_3:Er^{3+} nanocrystals," *Opt. Mater. (Amst).*, vol. 30, no. 8, pp. 1284–1288, 2008, doi: 10.1016/j.optmat.2007.06.007.

[362] F. Pandozzi *et al.*, "A spectroscopic analysis of blue and ultraviolet

upconverted emissions from $Gd_3Ga_5O_{12}$:Tm^{3+}, Yb^{3+} nanocrystals," *J. Phys. Chem. B*, vol. 109, no. 37, pp. 17400–17405, 2005, doi: 10.1021/jp052192w.

[363] A. Patra, C. S. Friend, R. Kapoor, and P. N. Prasad, "Fluorescence upconversion properties of Er^{3+}-doped TiO_2 and $BaTiO_3$ nanocrystallites," *Chem. Mater.*, vol. 15, no. 19, pp. 3650–3655, 2003, doi: 10.1021/cm020897u.

[364] A. Patra, C. S. Friend, R. Kapoor, and P. N. Prasad, "Upconversion in Er^{3+}:ZrO_2 Nanocrystals," *J. Phys. Chem. B*, vol. 106, no. 8, pp. 1909–1912, 2002.

[365] Z. Cheng, R. Xing, Z. Hou, S. Huang, and J. Lin, "Patterning of light-emitting YVO_4:Eu^{3+} thin films via inkjet printing," *J. Phys. Chem. C*, vol. 114, no. 21, pp. 9883–9888, 2010, doi: 10.1021/jp101941y.

[366] K. Yang, F. Zheng, R. Wu, H. Li, and X. Zhang, "Upconversion luminescent properties of YVO_4:Yb^{3+}, Er^{3+} nano-powder by sol-gel method," *J. Rare Earths*, vol. 24, no. 1 SUPPL. 2, pp. 162–166, 2006, doi: 10.1016/S1002-0721(07)60350-0.

[367] V. Venkatramu, D. Falcomer, A. Speghini, M. Bettinelli, and C. K. Jayasankar, "Synthesis and luminescence properties of Er^{3+}-doped $Lu_3Ga_5O_{12}$ nanocrystals," *J. Lumin.*, vol. 128, no. 5–6, pp. 811–813, 2008, doi: 10.1016/j.jlumin.2007.11.015.

[368] T. Wang, Y. H. Wang, S. K. Shi, B. Li, and J. Zhou, "Synthesis and Characteristics of Infrared-to-Visible Upconversion Nanoparticles through a Microemulsion System," *Key Eng. Mater.*, vol. 336–338, pp. 101–104, 2007, doi: 10.4028/www.scientific.net/kem.336-338.101.

[369] M. Gunaseelan, S. Yamini, G. A. Kumar, D. K. Sardar, and J. Senthilselvan, "Reverse microemulsion synthesis of mixed α and β phase $NaYF_4$:Yb,Er nanoparticles: calcination induced phase formation, morphology, and upconversion emission," *J. Sol-Gel Sci. Technol.*, vol. 96, no. 3, pp. 550–563, 2020, doi: 10.1007/s10971-020-05340-w.

[370] S. Shan, X. Wang, and N. Jia, "Nanoparticles in Normal Microemulsions," *Nanoscale Res. Lett.*, vol. 6, no. 539, pp. 3–7, 2011.

[371] L. A. D. Carlos, R. A. Sa Ferreira, and V. de Zea Bermudez, "Hybrid Materials for Optical Applications," in *Hybrid Materials. Synthesis, Characterization and Application*, G. Kickelbick, Ed. Wiley-VCH, 2007, p. 337.

[372] Y. Hasegawa, Y. Wada, and S. Yanagida, "Strategies for the design of luminescent lanthanide(III) complexes and their photonic applications," *J. Photochem. Photobiol. C Photochem. Rev.*, vol. 5, no. 3, pp. 183–202, 2004, doi: 10.1016/j.jphotochemrev.2004.10.003.

[373] J. R. Lakowicz, *Principles of Fluorescence Spectroscopy*, 3rd ed. Springer, 2006.

[374] G. F. de Sa *et al.*, "Spectroscopic properties and design of highly luminescent lanthanide coordination complexes," *Coord. Chem. Rev.*, vol. 196, no. 2000, pp. 165–195, 2000, doi: 10.1007/978-1-4939-0808-0_2.

[375] K. Binnemans, "Lanthanide-based luminescent hybrid materials," *Chem. Rev.*, vol. 109, no. 9, pp. 4283–4374, 2009, doi: 10.1021/cr8003983.

[376] C. Sanchez, B. Lebeau, F. Chaput, and J.-P. Boilot, "Optical Properties of

Functional Hybrid Organic-Inorganic Nanocomposites," in *Functional Hybrid Materials*, P. Gomez-Romero and C. Sanchez, Eds. Wiley-VCH, 2004, p. 122.

[377] W. H. Melhuish, "Nomenclature, Symbols, Units and their Usage in Spectrochemical Analysis—VI: Molecular Luminescence Spectroscopy," *Pure Appl. Chem.*, vol. 56, no. 2, pp. 231–245, 1984, doi: 10.1351/pac198153101953.

[378] J.-C. G. Bu and C. Piguet, "Taking advantage of luminescent lanthanide ions," *Chem. Soc. Rev.*, vol. 34, pp. 1048–1077, 2005, doi: 10.1039/b406082m.

[379] G. A. Crosby, R. E. Whan, and R. M. Alire, "Intramolecular energy transfer in rare earth chelates. Role of the triplet state," *J. Chem. Phys.*, vol. 34, no. 3, pp. 743–748, 1961, doi: 10.1063/1.1731670.

[380] M. H. V. Werts, J. W. Verhoeven, and J. W. Hofstraat, "Efficient visible light sensitisation of water-soluble near-infrared luminescent lanthanide complexes," *J. Chem. Soc. Perkin Trans. 2*, vol. 2, no. 3, pp. 433–439, 2000, doi: 10.1039/a909662k.

[381] K. Binnemans, "Rare-earth beta-diketonates," in *Handbook on the Physics and Chemistry of Rare Earths*, vol. 35, no. 05, 2005, pp. 107–272.

[382] N. Sabbatini and M. Guardigli, "Luminescent lanthanide complexes supramolecular devices," *Coord. Chem. Rev.*, vol. 123, pp. 201–228, 1968.

[383] M. Enel *et al.*, "New polyaminocarboxylate macrocycles containing phenolate binding units: synthesis, luminescent and relaxometric properties of their lanthanide complexes," *Dalt. Trans.*, vol. 46, no. 14, pp. 4654–4668, 2017, doi: 10.1039/c7dt00291b.

[384] M. Li and P. R. Selvin, "Luminescent Polyaminocarboxylate Chelates of Terbium and Europium: The Effect of Chelate Structure," *J. Am. Chem. Soc.*, vol. 117, no. 31, pp. 8132–8138, 1995, doi: 10.1021/ja00136a010.

[385] M. T. Kaczmarek, M. Zabiszak, M. Nowak, and R. Jastrzab, "Lanthanides: Schiff base complexes, applications in cancer diagnosis, therapy, and antibacterial activity," *Coord. Chem. Rev.*, vol. 370, pp. 42–54, 2018, doi: 10.1016/j.ccr.2018.05.012.

[386] J. Kai, D. Fernandes Parra, and H. Felinto Brito, "Polymer matrix sensitizing effect on photoluminescence properties of Eu^{3+}-β-diketonate complex doped into poly-β-hydroxybutyrate (PHB) in film form," *J. Mater. Chem.*, vol. 18, pp. 4549–4554, 2008, doi: 10.1039/b808080a.

[387] M. H. V. Werts, M. A. Duin, J. W. Hofstraat, and J. W. Verhoeven, "Bathochromicity of Michler's ketone upon coordination with lanthanide(III) β-diketonates enables efficient sensitisation of Eu^{3+} for luminescence under visible light excitation," *Chem. Commun.*, no. 9, pp. 799–800, 1999, doi: 10.1039/a902035g.

[388] A. M. Wilson, P. J. Bailey, P. A. Tasker, J. R. Turkington, R. A. Grant, and J. B. Love, "Solvent extraction: The coordination chemistry behind extractive metallurgy," *Chem. Soc. Rev.*, vol. 43, no. 1, pp. 123–134, 2014, doi: 10.1039/c3cs60275c.

[389] J. C. G. Bünzli, “Lanthanide luminescence for biomedical analyses and imaging,” *Chem. Rev.*, vol. 110, no. 5, pp. 2729–2755, 2010, doi: 10.1021/cr900362e.

[390] A. P. Duarte, M. Gressier, M. J. Menu, J. Dexpert-Ghys, J. M. A. Caiut, and S. J. L. Ribeiro, “Structural and luminescence properties of silica-based hybrids containing new silylated-diketonato europium(III) complex,” *J. Phys. Chem. C*, vol. 116, no. 1, pp. 505–515, 2012, doi: 10.1021/jp210338t.

[391] K. Singh, R. Boddula, and S. Vaidyanathan, “Versatile Luminescent Europium(III)-β-Diketonate-imidazo-bipyridyl Complexes Intended for White LEDs: A Detailed Photophysical and Theoretical Study,” *Inorg. Chem.*, vol. 56, no. 15, pp. 9376–9390, 2017, doi: 10.1021/acs.inorgchem.7b01565.

[392] C. Xu, “Photophysical properties of a new ternary europium complex with 2-thenoyltrifluoroacetone and 5-nitro-1,10-phenanthroline,” *J. Rare Earths*, vol. 28, no. 6, pp. 854–857, 2010, doi: 10.1016/S1002-0721(09)60229-5.

[393] Y. K. Jeong, Y. Sohn, and J. G. Kang, “Synthesis and characterization of Eu(III)-incorporated silica nanoparticles for application to UV-LED,” *J. Colloid Interface Sci.*, vol. 423, pp. 41–47, 2014, doi: 10.1016/j.jcis.2014.02.012.

[394] K. Binnemans, P. Lenaerts, K. Driesen, and C. Go, “A luminescent tris(2-thenoyltrifluoroacetonato) europium (III) complex covalently linked to a 1,10-phenanthroline- functionalised sol–gel glass,” *J. Mater. Chem.*, vol. 14, pp. 191–195, 2004.

[395] A. I. S. Silva, N. B. D. Lima, A. M. Simas, and S. M. C. Gonçalves, “Europium complexes: Luminescence boost by a single efficient antenna ligand,” *ACS Omega*, vol. 2, no. 10, pp. 6786–6794, 2017, doi: 10.1021/acsomega.7b00647.

[396] G. E. Khalil *et al.*, “Europium beta-diketonate temperature sensors: Effects of ligands, matrix, and concentration,” *Rev. Sci. Instrum.*, vol. 75, no. 1, pp. 192–206, 2004, doi: 10.1063/1.1632997.

[397] E. R. Menzel, “Recent advances in photoluminescence detection of fingerprints,” *Scientific World Journal.*, vol. 1, pp. 498–509, 2001, doi: 10.1100/tsw.2001.76.

[398] B. E. Dalrymple, J. M. Duff, and E. R. Menzel, “Inherent fingerprint luminescence - detection by laser,” *J. Forensic Sci.*, vol. 22, no. 1, pp. 118–124, 1977.

[399] U. Noomnarm and R. M. Clegg, “Fluorescence lifetimes: Fundamentals and interpretations,” *Photosynth. Res.*, vol. 101, no. 2–3, pp. 181–194, 2009, doi: 10.1007/s11120-009-9457-8.

[400] G. Porter, “Specialised photography and imaging,” in *The Practice of Crime Scene Investigation*, J. Horswell, Ed. CRC Press, 2004.

[401] C. Lennard and M. Stoilovic, “Application of forensic light sources at the crime scene,” in *The Practice of Crime Scene Investigation*, J. Horswell, Ed. CRC Press, 2004.

[402] D. K. Chatterjee, A. J. Rufaihah, and Y. Zhang, “Upconversion fluorescence

imaging of cells and small animals using lanthanide doped nanocrystals," *Biomaterials*, vol. 29, no. 7, pp. 937–943, 2008, doi: 10.1016/j.biomaterials.2007.10.051.

[403] J. Yao, C. Huang, C. Liu, and M. Yang, "Upconversion luminescence nanomaterials: A versatile platform for imaging, sensing, and therapy," *Talanta*, vol. 208, no. April 2019, p. 120157, 2020, doi: 10.1016/j.talanta.2019.120157.

[404] R. Ma *et al.*, "Fingermark detection on non-porous and semi-porous surfaces using $NaYF_4$:Er,Yb up-converter particles," *Forensic Sci. Int.*, vol. 207, pp. 145–149, 2011, doi: 10.1016/j.forsciint.2010.09.020.

[405] X. Chen *et al.*, "Large Upconversion Enhancement in the 'islands' Au-Ag Alloy/$NaYF_4$:Yb^{3+}, Tm^{3+}/Er^{3+} Composite Films, and Fingerprint Identification," *Adv. Funct. Mater.*, vol. 25, no. 34, pp. 5462–5471, 2015, doi: 10.1002/adfm.201502419.

[406] K. Lingeshwar Reddy *et al.*, "Core-Shell Structures of Upconversion Nanocrystals Coated with Silica for Near Infrared Light Enabled Optical Imaging of Cancer Cells," *Micromachines*, vol. 9, no. 8, p. 400, 2018, doi: 10.3390/mi9080400.

[407] C. Duan, L. Liang, L. Li, R. Zhang, and Z. P. Xu, "Recent progress in upconversion luminescence nanomaterials for biomedical applications," *J. Mater. Chem. B*, vol. 6, no. 2, pp. 192–209, 2018, doi: 10.1039/c7tb02527k.

[408] H. H. Xie *et al.*, "Synthesis of bright upconversion submicrocrystals for high-contrast imaging of latent-fingerprints with cyanoacrylate fuming," *RSC Adv.*, vol. 5, no. 97, pp. 79525–79531, 2015, doi: 10.1039/c5ra15255k.

[409] R. S. P. King, P. M. Hallett, and D. Foster, "Seeing into the infrared: A novel IR fluorescent fingerprint powder," *Forensic Sci. Int.*, vol. 249, pp. e21–e26, 2015, doi: 10.1016/j.forsciint.2015.01.020.

[410] I. M. Alaoui and E. R. Menzel, "Substituent effects on luminescence enhancement in europium and terbium Ruhemann's purple complexes," *Forensic Sci. Int.*, vol. 77, no. 1–2, pp. 3–11, 1996, doi: 10.1016/0379-0738(95)01829-8.

[411] C. E. Allred and R. E. Menzel, "A novel europium-bioconjugate method for latent fingerprint detection," *Forensic Sci. Int.*, vol. 85, no. 2, pp. 83–94, 1997, doi: 10.1016/S0379-0738(96)02080-4.

[412] D. Wilkinson, "A one-step fluorescent detection method for lipid fingerprints; $Eu(TTA)_3$·2TOPO," *Forensic Sci. Int.*, vol. 99, no. 1, pp. 5–23, Jan. 1999, doi: 10.1016/S0379-0738(98)00176-5.

[413] D. A. Wilkinson and J. E. Watkin, "Europium aryl-β-diketone complexes as fluorescent dyes for the detection of cyanoacrylate developed fingerprints on human skin," *Forensic Sci. Int.*, vol. 60, no. 1–2, pp. 67–79, 1993, doi: 10.1016/0379-0738(93)90094-Q.

[414] K. M. Girish, S. C. Prashantha, R. Naik, and H. Nagabhushana, "Zn_2TiO_4: A novel host lattice for Sm^{3+} doped reddish orange light emitting

photoluminescent material for thermal and fingerprint sensor," *Opt. Mater. (Amst).*, vol. 73, pp. 197–205, 2017, doi: 10.1016/j.optmat.2017.08.009.

[415] J. Y. Park, J. W. Chung, S. J. Park, and H. K. Yang, "Versatile fluorescent $CaGdAlO_4:Eu^{3+}$ red phosphor for latent fingerprints detection," *J. Alloys Compd.*, vol. 824, 2020, doi: 10.1016/j.jallcom.2020.153994.

[416] W. T. Hong, J. Y. Park, J. Y. Je, and H. K. Yang, "Sintering temperature effect of divalent europium ion doped tetra-calcium phosphate phosphors for latent fingerprint detection," *Opt. Mater. (Amst).*, vol. 81, pp. 37–44, 2018, doi: 10.1016/j.optmat.2018.05.017.

[417] D. Chavez, C. R. Garcia, I. Ruiz-Martinez, J. Oliva, E. Rivera-Rosales, and L. A. Diaz-Torres, "Fingerprint detection on low contrast surfaces using phosphorescent nanomaterials," *AIP Conf. Proc.*, vol. 2083, no. 020001, 2019, doi: 10.1063/1.5094304.

[418] J. Lai *et al.*, "Novel organic-inorganic hybrid powder $SrGa_{12}O_{19}:Mn^{2+}$-ethyl cellulose for efficient latent fingerprint recognition: Via time-gated fluorescence," *RSC Adv.*, vol. 10, no. 14, pp. 8233–8243, 2020, doi: 10.1039/d0ra00138d.

[419] B. Comber, G. Payne, and C. Lennard, "Digital imaging," in *Lee and Gaensslen's Advances in Fingerprint Technology - Third edition*, R. S. Ramotowski, Ed. CRC Press, 2012, pp. 467–501.

[420] L. V. Upham and D. F. Englert, "Radionuclide imaging," in *Handbook of Radioactivity Analysis*, Second Edi., M. F. L'Annunziata, Ed. Elsevier Inc., 2003, pp. 1063–1127.

[421] G. B. Nair and S. J. Dhoble, *The Fundamentals and Applications of Light-Emitting Diodes. The revolution in the lighting industry*. Elsevier, 2020.

Chapter 2 Interactions between silica particles and fingermark residue

2.1 Equipment and instrumentation

Scanning Electron Microscopy

Scanning electron microscopy (SEM) images of obtained materials and developed fingermarks were taken on FEI Nova Nano-SEM 450 scanning electron microscope. The examined materials were deposited on an indium tin oxide (ITO) coated glass slide mounted on an aluminium stub using carbon adhesive tape. Each sample was connected from the top surface of the sample to the aluminium stub with a conductive copper tape.

2.2 Introduction

The numerous methods of fingermark detection based on photoluminescence have been developed for the last decades. Due to the fact that efficient fingermark development is influenced by a number of factors such as the composition of fingermark secretion, the rate of ageing, environmental factors like temperature, humidity, and also the structure of the substrate (porous, non-porous), these methods are continually being developed, optimised, evaluated as well as new solutions and developing agents are being searched for [1]. As described in Chapter 1.3 and 1.4, several conventional methods for the development of fingermarks deposited on luminescent, patterned, multi-coloured or reflective surfaces have been proposed so far, such as luminescent powders [2]–[4], cyanoacrylate fuming followed by luminescent dye staining [5] or amino acid-sensitive reagents [6]. However, the new enhancing reagents and methods based on optical techniques are still needed to efficiently eliminate strong background interference providing at the same time high sensitivity and selectivity of the developing agent toward fingermark deposits.

The goal of this dissertation was to design the material for fingermark enhancement, which on the one hand would exhibit selective affinity to the fingermark but not to the background and, on the other hand, would have optical properties such as long-lived luminescence or upconversion, which lead to

eliminating some drawbacks like background staining or surface interference. An additional feature of the material should be the ability to be applied in the form of suspension rather than a brushing powder to avoid damaging the fingermark pattern and minimise the potential risk of inhalation of the airborne particles. A potential solution that combines all these desirable features of the developing agent is the use of silica particles. This material has a number of properties that can lead to effective fingermark development. Silica is a porous matrix with an outer layer consisted of silanol groups which make it accessible for reaction with other functionalised precursors or covalent attachment with organic species [7], [8]. Silica particles can be synthesised through several procedures, among which the Stöber synthesis and reverse microemulsion are the most common [9]. Also, silica can be synthesised in the form of small particles with large surface area and high surface absorbability [10], large loading capacity for doping chemicals - important in terms of luminophore immobilisation [11], and with low toxicity [12], [13]. Additionally, the silica surface modification with various functional moieties for use in fingermark development allows interacting with the fingermark residual in a variety of ways. Several dactyloscopy applications of silica particles loaded with dyes [11], [14]–[16], and modified with organic moieties such as carboxyl groups [17], methyl groups [18], or phenyl groups [19], [20] have already been researched; however, none of them was dedicated to incorporate the luminophore for time-gated imaging. In this chapter, the three possible interactions between modified silica particles and fingermark residue components will be discussed.

Thiol-gold was the first investigated interaction. A formation of a gold-sulphur bond is the driving force of interaction between thiols and gold [21]. The formation of thiol-gold bonds depends on a variety of parameters like surface properties of gold, pH of a solution, type of a solvent, or the reaction time [22]. The environmental pH may influence the thiol-gold bond formation; the low pH inhibits the dissociation of the S-H bond, and the basic conditions favour the dissociation. When the sulfhydryl group is deprotonated at higher pH, it creates a thiyl radical, and a covalent bond is forming [22], on the contrary, at lower pH, the protonated sulfhydryl group can interact with gold forming a coordination-type bond through the sulphur lone pair electrons [22], [23]. The concept of investigating the thiol-gold interactions was to deposit gold nanoparticles preferentially on the fingermark ridges and then to deposit thiol-modified silica particles on the gold nanoparticles surface (Figure 2.1).

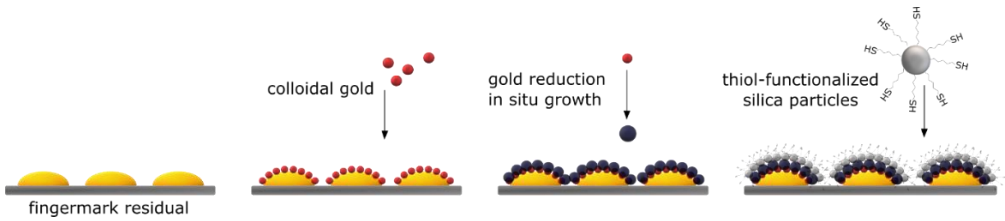

Figure 2.1 The scheme of fingermark development with SMD technique followed by thiol-functionalised silica particles deposition

To enhance the fingermark ridges with the gold nanoparticles, the Single Metal Deposition method was applied [5]. This is a two-phase development process. The first step involves treating the fingermark sample with negatively charged colloidal gold, stabilised with citrate ions at pH 2.65. In the low pH, gold nanoparticles bind preferentially via electrostatic attraction to the protonated amino acids, peptides and proteins present in fingermark constituents and serve as the nucleation sites. In the second step, the reduction of gold ions from a gold salt solution takes place, and further growth of gold on the nucleation sites is observed [24]–[26]. The fingermark enhancement using the SMD method strongly depends on the pH environment of the colloidal gold. In the range of pH 2.5–6.5, the colloidal gold nanoparticles, capped with sodium citrate, are negatively charged. At the neutral pH, all three carboxylic acid terminal groups are deprotonated. As the pH of the solution is becoming more acidic, the successive protonation of the carboxyl groups takes place, and gold nanoparticles are becoming less negatively charged. On the other hand, amino acids, fatty acids and proteins present in the fingermark residual carry a positive charge in acidic conditions, which decreases as the pH is increased. The optimal pH, at which the fingermark components are positively charged, and the negative charge of gold nanoparticles is still sufficient to facilitate electrostatic interactions is in the range of 2.5 – 2.8 [27], [28].

The second analysed interactions were lipophilic interactions between surface-functionalised silica particles and a sebaceous fraction of fingermark residual. According to the IUPAC definition, “lipophilicity” is related to the affinity of a molecule or a moiety for a lipophilic environment, and “lipophilic” is applied to molecular entities which tend to dissolve in fat-like solvents [29]. Lipophilic interactions are present in biological systems and are of importance in medicinal chemistry. This kind of attraction is often studied for structure-based drug design, drug transport and its interactions with target proteins [30], [31]. The approach to investigating the influence of this type of interaction on fingermark enhancement was based on the modification of the silica particles with either long hydrocarbon

chains or phenyl groups and deposited these materials onto the fingermark ridges in the form of a suspension in either organic solvent or water with the addition of ethanol (Figure 2.2). Such functionalised silica particles can interact well with the fingermark fatty fraction since it consists of, among others, free fatty acids, wax esters, mono- di- triglycerides, squalene, and cholesterol [32].

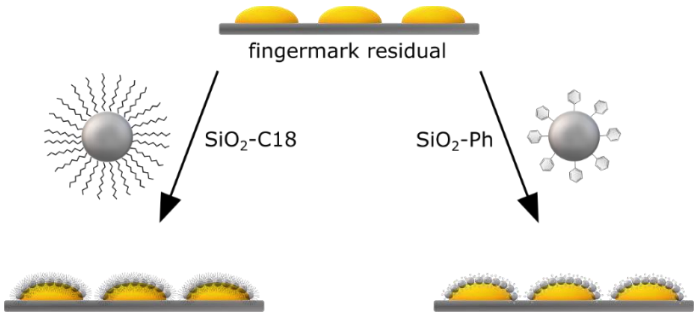

Figure 2.2 The scheme of fingermark development with silica particles surface-modified with either long hydrocarbon chains or phenyl groups

The last investigated form of interaction was amide bond formation (N–C(O)). The strategy of peptide bond formation is based on condensations between carboxylic acids and amines. In some cases, activation of the carboxylic group can be applied using acyl chlorides, reactive anhydrides or esters, or coupling reagents [33], [34]. The popular coupling agent promoting the formation of an amide bond is EDC (N-ethyl-N'-(3-dimethylaminopropyl) carbodiimide hydrochloride combined with NHS (N-hydroxysuccinimide) [35]. The concept of this approach was to investigate whether silica particles functionalised with carboxyl groups would interact selectively with fingermark residue consisting of an array of proteins, polypeptides and amino acids [32] (Figure 2.3).

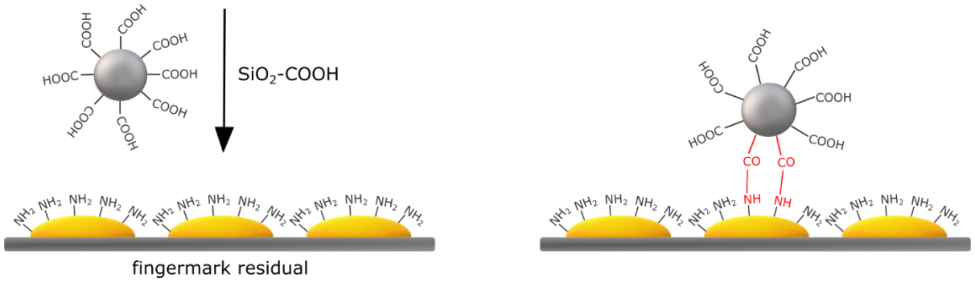

Figure 2.3 The scheme of fingermark development with silica particles functionalised with carboxyl groups

The development process was based on the carboxyl-modified silica particles water suspension, with changing parameters such as pH, immersion time, the addition of EDC/NHS, and the addition of NaCl to modify the ionic strength.

2.3 Fingermark collection

Latent fingermarks have been collected from a single donor (male) to maintain the consistency of the results. To investigate the interactions between the modified silica particles and fingermark secretion, groomed fingermarks were selected. However, for the further systematic studies of the fingermark enhancement with methods and developers described in the following chapters, the naturals fingermarks have been used according to the International Fingerprint Research Group guidelines for Phase 1 [36]. Fingermarks have been deposited on indium tin oxide (ITO) coated glass substrates. Due to the conductivity of ITO [37], fingermarks deposited on this substrate may be observed under the scanning electron microscope. The donor has been requested not to wash his hands for at least half an hour. Then, prior to the fingermark deposition on ITO substrate, the donor was asked to gently rub his forehead and touch the substrate with the thumb, index, middle, and ring finger for 2-3 seconds with moderate pressure, comparable to the force he usually uses for holding items. The samples with deposited fingermarks were aged in the Petri dishes for at least 24 hours at room temperature (ca. 21 °C) before further processing.

2.4 Thiol–gold interactions

2.4.1 Experimental

2.4.1.1 Chemicals

The following reagents were used to synthesise thiol-functionalised silica particles. 3-mercaptopropyltrimethoxysilane (95 %, MPTMS), tetrachloroauric (III) acid trihydrate (≥ 99.9 %, $AuHCl_4 \cdot 3H_2O$), hydroxylamine hydrochloride (99.999 %), tannic acid, and Tween 20 were purchased from Sigma Aldrich. Ammonium hydroxide (25%, NH_4OH) was obtained from Chempur, citric acid monohydrate

(≥ 99.0 %) was purchased from Stanlab, and sodium citrate tribasic dihydrate (≥ 99 %) from Merc Millipore. All reagents were used as received. RO/DI water was used for all the experiments.

2.4.1.2 Single Metal Deposition process

Colloidal gold solution preparation

To formulate a colloidal gold solution [38] first, three working solutions have been prepared.

- Solution I: 10 % (w/v) solution of $AuHCl_4 \cdot 3H_2O$ was obtained by dissolving 0.10 g of tetrachloroauric (III) acid trihydrate in 1 ml of H_2O.
- Solution II: 1 % (w/v) of sodium citrate solution was prepared by dissolving 0.10 g of sodium citrate tribasic dihydrate in 10 ml of water.
- Solution III: 1% (w/v) of the tannic acid solution was obtained by dissolving 0.01 g of tannic acid in 1 ml of H_2O.

Afterwards, in one flask (1), 200 ml of water was mixed with 250 µl of solution I, and in the second flask (2), 37.5 ml of water was mixed with 10 ml of solution II and 50 µl of solution III. Both flasks were heated to 60 °C while stirring. Once the temperature was reached, the content of flask 2 was rapidly poured into flask 1 under vigorous stirring. The solution was then brought to the boiling and heated as long as the colour became ruby red. After cooling down to room temperature, the flask was completed with water to the volume of 250 ml.

Fingermark enhancement with Single Metal Deposition method

The SMD development procedure was based on Becue et al. formulations [28]. First, the colloidal gold working solution was prepared. Next, 60 µl of Tween 20 was added to 60 ml of colloidal gold solution, and the solution was stirred for ten minutes. Next, the pH of the solution was brought to 2.65 with 0.1 M citric acid solution. Once the colloidal gold working solution was ready, 30 ml of the solution was poured into the Petri dish. The samples with fingermarks deposited on ITO glass slides were first rinsed in a water bath for 5 minutes and then immersed into the colloidal gold working solution for 15 minutes under low horizontal shaking. Then, the samples were rinsed in the water bath again for 5 minutes under gentle shaking. In the meantime, 30 ml of water was poured into the separate Petri dish, and 30 µl of solution I (10 % $AuHCl_4 \cdot 3H_2O$) was added, followed by the addition of 88.5 µl of

hydroxylamine hydrochloride solution (69.5 mg in 10 ml of water). The samples were immersed in this solution for 20 minutes under medium horizontal shaking (70 rpm). Finally, the samples were again rinsed in the water bath for 5 minutes and then left to dry in the air.

2.4.1.3 Synthesis of thiol-functionalised silica particles

The thiol-functionalised silica particles were synthesised with a one-step method by using an organosilane containing thiol groups as a precursor [39]. 1 g of MPTMS was added to 10 ml of acidic water (pH adjusted to 4 with 0.1 M hydrochloric acid) and stirred for 1.5 hours until the oil droplets of MPTMS disappeared. After this time, 10 µl of ammonium hydroxide was added to the reaction mixture, and the solution was stirred for 12 hours at room temperature. Subsequently, the particles were centrifuged at 10 000 rpm for 15 minutes and washed with water three times. The obtained material (SiO_2-SH) was stored in an aqueous solution.

2.4.1.4 Fingermark development

The thiol-functionalised particles dispersed in water were investigated to develop latent fingermarks on ITO glass substrates enhanced previously with the SMD method. The series of 50 mg mL^{-1}, 10 mg mL^{-1}, and 5 mg mL^{-1} concentration were tested. Each batch of SiO_2-SH particles was dispersed in water using an ultrasonication bath for 10 minutes. Each ITO glass substrate with fingermark was placed on an even surface, and a drop of 200 µl of the SiO_2-SH particle suspension was deposited on the sample surface for 15 minutes. Afterwards, the sample was gently rinsed with water and dried in a stream of argon.

2.4.2 Results and discussion

The morphology of colloidal gold nanoparticles was investigated with a scanning electron microscope (Figure 2.4). The synthesis produced monodisperse gold nanoparticles with an average diameter of ca. 14 nm (determined by analysis of SEM images in ImageJ application) [40].

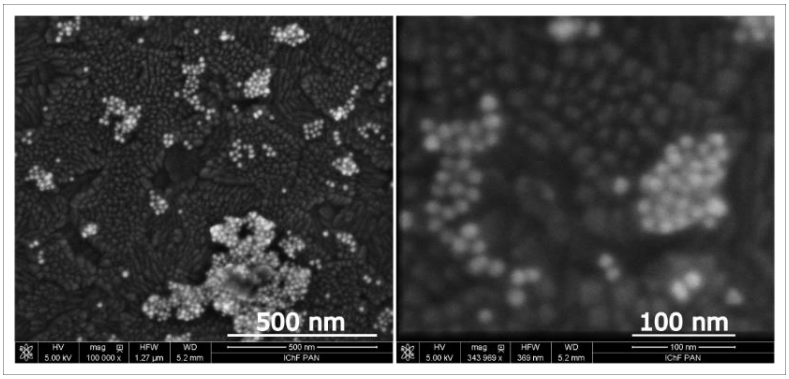

Figure 2.4 SEM images of synthesised colloidal gold nanoparticles

The 6-days-old sebaceous fingermarks deposited on the ITO glass slide were enhanced with gold nanoparticles by applying the SMD technique. The developed samples observed under white light indicated grey-blue well-defined fingermark ridges (Figure 2.5 A). The SEM and optical microscope images of the developed fingermark demonstrated that the gold nanoparticles were deposited in a fair amount on the fingermark ridges (Figure 2.6), although some deposits could have also been noticed between the ridges, visible as brighter area (Figure 2.5 B, C).

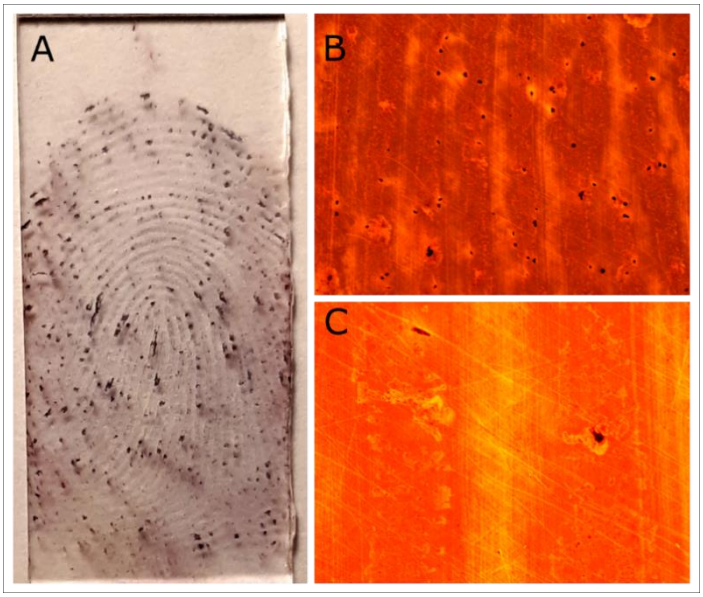

Figure 2.5 The 6-days-old sebaceous fingermark deposited on ITO glass slide enhanced with SMD technique (A) imaged under white light, (B) and (C) imaged with the optical microscope

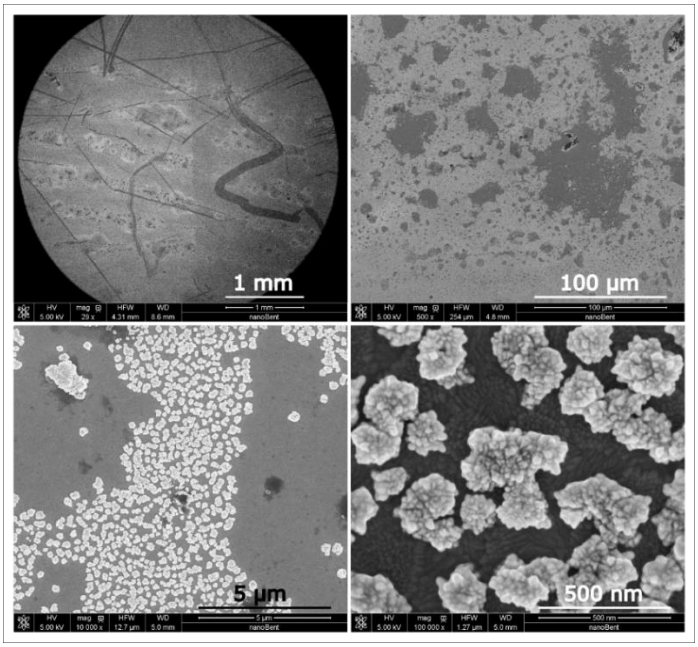

Figure 2.6 SEM images of 6-days-old sebaceous fingermark deposited on ITO glass slide imaged with SMD technique

Once the fingermarks were enhanced with the gold nanoparticles via the SMD technique, the thiol-functionalised silica particles have been applied to the samples. The thiol-modified silica was synthesised in the form of spherical particles with an average diameter of ca. 1.37 ± 0.12 µm (Figure 2.7).

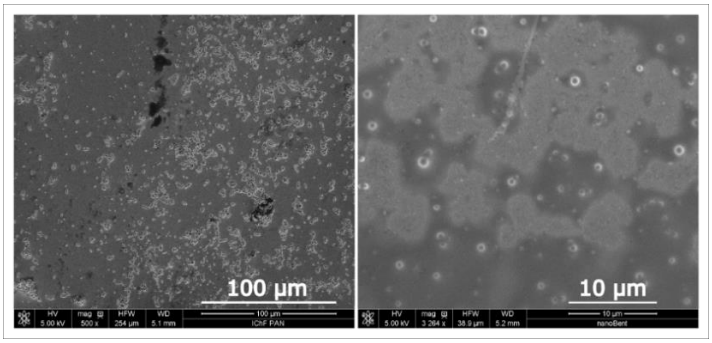

Figure 2.7 SEM images of synthesised thiol-functionalised silica particles (SiO_2-SH)

The fingermarks with gold nanoparticles deposited on its surface were further developed with the suspension of thiol-modified silica particles in various concentrations. Figure 2.8 showed SEM images of 6-days-old sebaceous fingermarks developed with SMD technique followed by the deposition of SiO_2-SH particles in the

concentration of 5 mg mL^{-1}. Very few silica particles were observed on the fingermark ridge under the highest magnification.

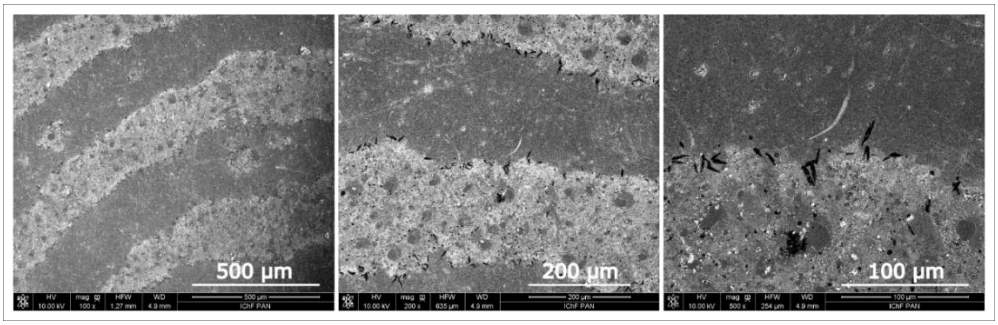

Figure 2.8 SEM images of 6-days-old sebaceous fingermark deposited on ITO glass slide enhanced with SMD technique followed by SiO_2-SH particles deposition at the concentration of 5 mg mL^{-1}

Further increase of the SiO_2-SH water suspension concentration to 10 mg mL^{-1} resulted in a greater number of silica particles deposited on fingermark ridge; however, this was still not enough to cover the most area of the ridge (Figure 2.9).

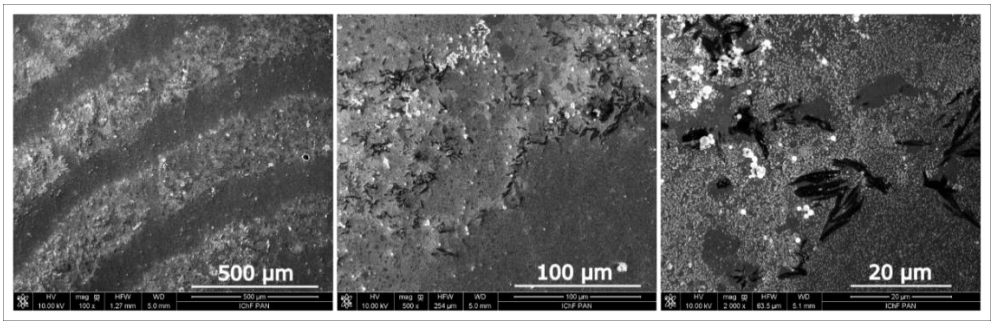

Figure 2.9 SEM images of 6-days-old sebaceous fingermark deposited on ITO glass slide enhanced with SMD technique followed by SiO_2-SH particles deposition at the concentration of 10 mg mL^{-1}

The efficacy of silica particles deposition on the fingermarks covered with gold nanoparticles was also investigated with the 50 mg mL^{-1} suspension concentration (Figure 2.10). Slightly better results were obtained than for lower concentrations; however, still, the thiol-modified silica particles were deposited on the fingermark ridges in a moderate amount. Also, some silica particles were noticed on the background surface due to the fact that gold nanoparticles in a certain quantity were present on the substrate between the ridges of the fingermark.

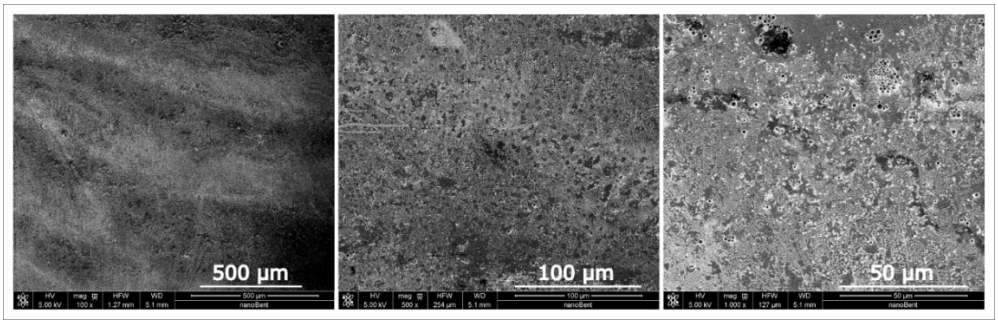

Figure 2.10 SEM images of 6-days-old sebaceous fingermark deposited on ITO glass slide enhanced with SMD technique followed by SiO_2-SH nanoparticles deposition at the concentration of 50 mg mL^{-1}

2.5 Lipophilic interactions

2.5.1 Experimental

2.5.1.1 Chemicals

The following reagents were used to synthesise silica nanoparticles and to modify the silica surface. Tetraethyl orthosilicate (98 %, TEOS) and triethoxy-phenylsilane (98 %, PTEOS) were purchased from Sigma-Aldrich. Octadecyl-trimethoxysilane (ODTMS) was purchased from Fluorochem. Ethanol (99.8 %, anhydrous) was obtained from POCH. Ammonium hydroxide (25 %, NH_4OH) was purchased from Chempur, and toluene (99.8 %, anhydrous) was obtained from Alfa Aesar. All reagents were used as received. RO/DI water was used for the experiments.

2.5.1.2 Synthesis of silica nanoparticles functionalised with 18-carbon alkyl chains

Functionalised silica nanoparticles were obtained in a two-step process. In the first step, silica nanoparticles were synthesised by hydrolysis and condensation of TEOS in alcohol solvent in the presence of ammonium hydroxide [41], [42]. First, 1.5 ml of TEOS was dissolved in 25 ml of ethanol and stirred for 10 minutes. Next, 1 ml of H_2O was added to the reaction mixture and stirred for another 10 minutes. After this time, the mixture of 25 ml of ethanol and 1.7 ml of NH_4OH was added

dropwise to the reaction, and the mixture was stirred at 40 °C for 3 hours. Subsequently, 1 ml of TEOS was added, and the reaction mixture was stirred for another 3 hours under the same conditions. Afterwards, the particles were separated by centrifugation at 9 500 rpm for 15 minutes, purified with ethanol and water three times and finally, dried in an oven at 65 °C for 5 hours. In the second step, silica nanoparticles have been modified with eighteen carbon alkyl chains by grafting functionalised organosilane (ODTMS) on the surface [42]. For this purpose, 25 mg of silica nanoparticles were dispersed in 30 ml of dry toluene in a three-necked round-bottom flask using a sonication bath. Next, the mixture was stirred for 30 minutes at 80 °C under reflux and in an argon atmosphere. Afterwards, 1 $\%_{w/w}$ of ODTMS (304.4 µl in 1 ml of toluene) was added dropwise to the reaction, and the mixture was stirred for 24 hours in the same conditions. Finally, the solution was cooled down to room temperature. The particles were then separated by centrifugation at 9 500 rpm for 15 minutes, washed with toluene and ethanol three times to remove the unreacted organosilane, and dried in the oven at 65 °C for 5 hours. The obtained material (SiO_2-C18) has a form of white powder.

2.5.1.3 Synthesis of silica particles functionalised with phenyl groups

The silica particles with hydrophobic coating were obtained in one-pot synthesis [20]. First, 24 ml of ethanol was mixed with 4 ml of water, 2 ml of TEOS, and 2 ml of PTEOS in a flask. Then, 1.6 ml of NH_4OH was added dropwise, and the reaction mixture was stirred for 12 hours. After this time, the particles were centrifuged at 3 000 rpm for 3 minutes, purified with a solution of ethanol and water (10:90, v/v) and dried in the oven at 65 °C for 12 hours. The obtained material (SiO_2-Ph) was also in the form of white powder.

2.5.1.4 Fingermark development

The silica nanoparticles functionalised with long hydrocarbon chains (SiO_2-C18) dispersed in petroleum ether were examined to enhance the latent fingermarks deposited on ITO glass slides. The series of 0.04 % (w/v) [43], 0.02 %, and 0.008 % concentration have been investigated. Each batch of SiO_2-C18 nanoparticles was dispersed in petroleum ether using an ultrasonication bath for 20 minutes. Fingermark sample was immersed in the SiO_2-C18 nanoparticles suspension for 5 minutes, followed by gentle rinsing with water and drying in the

stream of argon. Besides, shorter immersion times such as 30 seconds, 1 minute, and 3 minutes have been investigated for 0.04 % suspension.

Fingermarks deposited on ITO glass slides were also developed with phenyl-functionalised particles dispersion (SiO_2-Ph) in both petroleum ether and water suspension [20]. Fingermarks were enhanced in several ways, by immersing the samples in the suspension of SiO_2-Ph particles in water/ethanol solution, by drop cast the water/ethanol suspension of particles directly onto the fingermark sample, or by immersing the samples in the petroleum ether suspension. In the first way, the ITO glass slide with fingermark was immersed into the particle suspension for 10 minutes, then rinsed with water and dried in the stream of argon. In a second method, a drop of ca. 300 µl of particle suspension was applied on the ITO glass slide sample for 3 minutes, and then the sample was rinsed with water and dried in the stream of argon. In both cases, a 100 mg mL^{-1} concentration of particles in the water/ethanol solution (97:3 v/v) was applied. In a third way, the ITO glass slide samples were immersed in the 0.04 $\%_{w/v}$ suspension of particles in petroleum ether for 30 and 45 seconds, then rinsed with water and dried in the stream of argon.

2.5.2 Results and discussion

Silica nanoparticles functionalised with long hydrocarbon chains (SiO_2-C18)

The SEM images of silica nanoparticles morphology with the modified and unmodified surface are shown in Figure 2.11. Nanoparticles obtained in the Stöber synthesis were spherical with an average diameter of 65.78 ± 4.50 nm (Figure 2.11 A), calculated in the ImageJ application [40]. The silica nanoparticles' surface was further modified with eighteen carbon alkyl chains. The SEM image of SiO_2-C18 (Figure 2.11 B) showed the spherical nanoparticles with an average diameter of 69.28 ± 5.35 nm. It was noticed that the size of the nanoparticles has slightly increased, which may be the result of the surface modification.

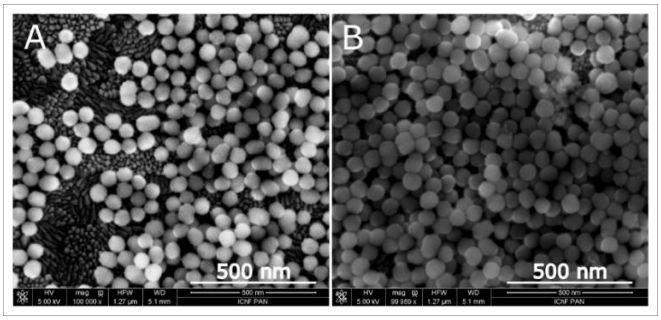

Figure 2.11 SEM images of (A) silica nanoparticles, (B) silica nanoparticles modified with 18 carbon alkyl chains (SiO_2-C18)

The 30-days-old sebaceous fingermarks deposited on the ITO glass slide were enhanced with SiO_2-C18 nanoparticles dispersed in petroleum ether at the 0.04 % concentration in the series of immersion times: 30 seconds, 1 minute, 3 minutes, and 5 minutes. Not a large number of particles were deposited on the fingermarks immersed in the suspension for 30 seconds (Figure 2.12) and 1 minute (Figure 2.13). Although the particles were dispersed in the solvent using an ultrasonic bath, quite large agglomerates were observed on the fingermark. Though most of the nanoparticles were settled on the surface of the fingermark, the total amount was too small to cover the entire ridge

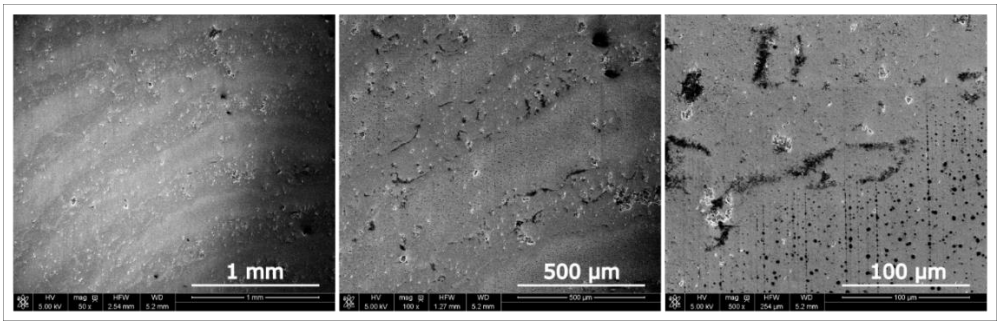

Figure 2.12 SEM images of 30-days-old sebaceous fingermark deposited on ITO glass slide enhanced with 0.04 % petroleum ether suspension of SiO_2-C18 nanoparticles by immersion for 30 seconds

Figure 2.13 SEM images of 30-days-old sebaceous fingermark deposited on ITO glass slide enhanced with 0.04 % petroleum ether suspension of SiO_2-C18 nanoparticles by immersion for 1 minute

Increasing the immersion time of the fingermark sample in SiO_2-C18 nanoparticles petroleum ether suspension to 3 minutes (Figure 2.14) resulted in a slightly higher quantity of the nanoparticles on the fingermark, but also the formation of agglomerates was noticeable. Most of the nanoparticles were deposited on the fingermark ridges but still in the amount insufficient for effective imaging.

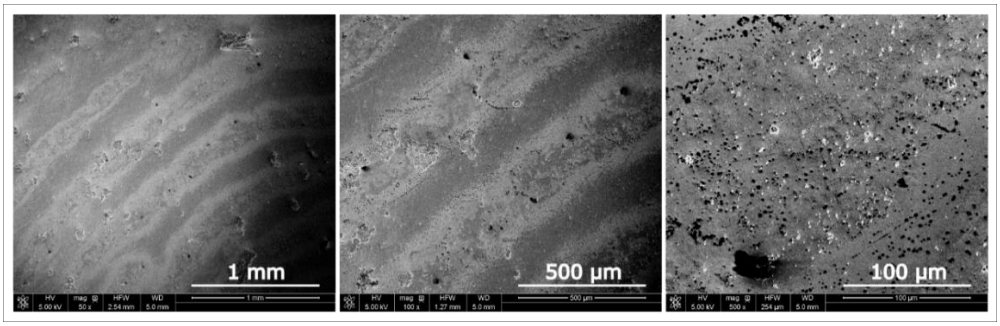

Figure 2.14 SEM images of 30-days-old sebaceous fingermark deposited on ITO glass slide enhanced with 0.04 % petroleum ether suspension of SiO_2-C18 nanoparticles by immersion for 3 minutes

A subsequent increase in the immersion time of the fingermark sample to 5 minutes (Figure 2.15) resulted in a larger amount of particles being deposited on the fingermark ridges. Noticeable fewer particles between the ridges have been observed. Nevertheless, still, the quantity of the particles scattered along the ridge was insufficient to cover its entire surface. Also, further increasing the immersion time in petroleum ether could have a destructive effect on the fingermark pattern due to the dissolving properties of the applied solvent.

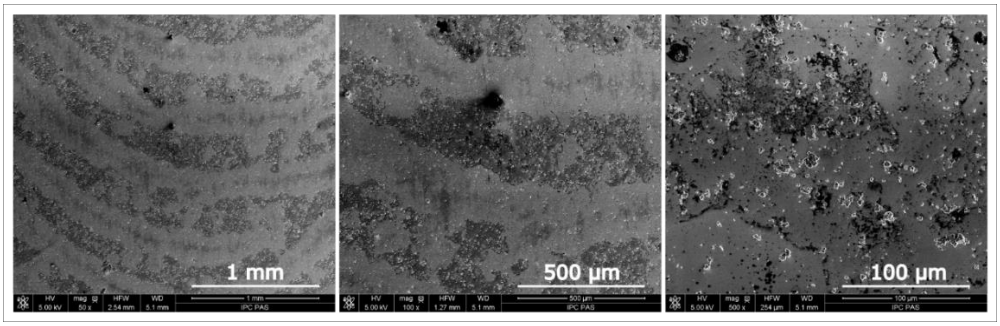

Figure 2.15 SEM images of 29-days-old sebaceous fingermark deposited on ITO glass slide enhanced with 0.04 % petroleum ether suspension of SiO_2-C18 nanoparticles by immersion for 5 minutes

The efficiency of the SiO_2-C18 particles for fingermark development was also investigated at lower concentrations of suspension in petroleum ether. When the fingermark samples were immersed for 5 minutes in a suspension of nanoparticles with a two times lower concentration (0.02 %), no improvement in deposition efficiency was achieved (Figure 2.16). The nanoparticles' agglomerates were deposited more on the fingermark ridge than on the background; however, the quantity of the particles was still not satisfactory.

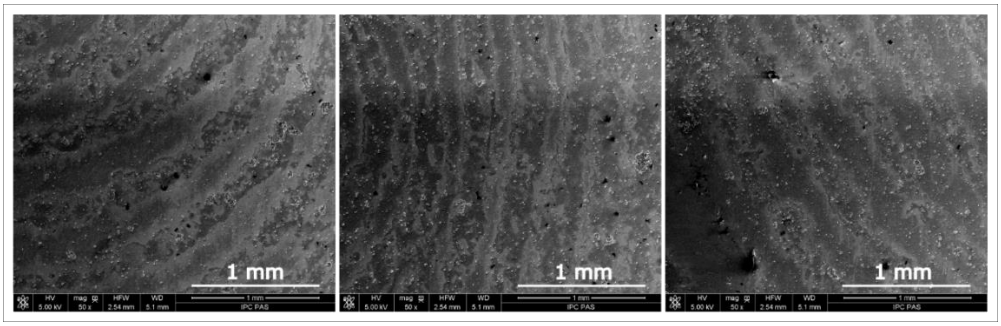

Figure 2.16 SEM images of 29-days-old sebaceous fingermark deposited on ITO glass slide enhanced with 0.02 % petroleum ether suspension of SiO_2-C18 nanoparticles by immersion for 5 minutes

In the case of a fivefold reduction in concentration (0.008 %), also no increase in the efficiency of SiO_2-C18 nanoparticle deposition was noticed (Figure 2.17). On the contrary, the quantity of the particles observed on the fingermark ridges decreased significantly.

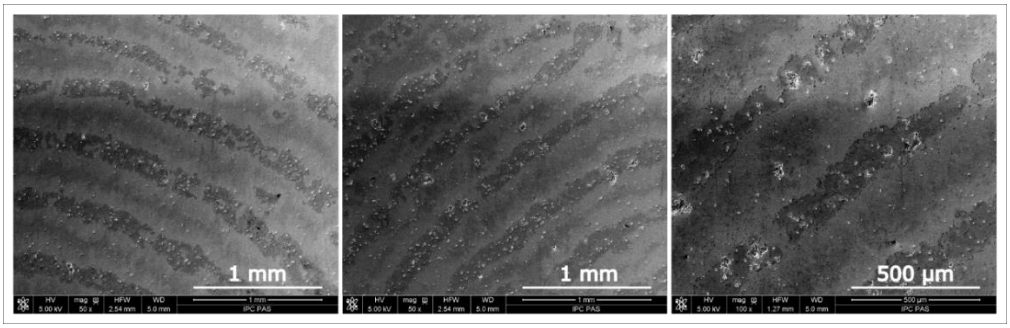

Figure 2.17 SEM images of 29-days-old sebaceous fingermark deposited on ITO glass slide enhanced with 0.008 % petroleum ether suspension of SiO_2-C18 nanoparticles by immersion for 5 minutes

Silica particles functionalised with phenyl groups (SiO_2-Ph)

Phenyl-modified silica particles were the second lipophilic material applied to enhance fingermarks. The SEM investigation exhibited that obtained silica particles were monodisperse with an average diameter of ca. 297 ± 8 nm (Figure 2.18).

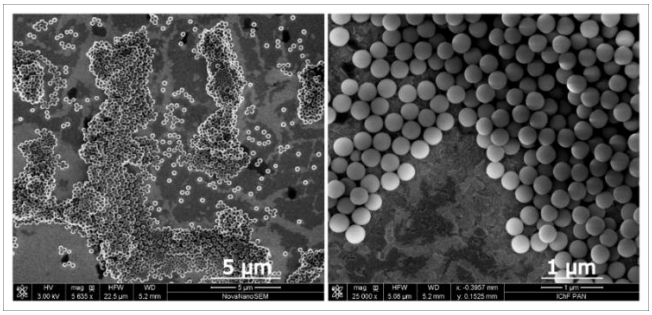

Figure 2.18 SEM images of silica particles modified with phenyl groups (SiO_2-Ph)

The 3 $\%_{vol}$ aqueous ethanol solution as well as petroleum ether were the solvents used for the working suspension of the phenyl-functionalised silica particles in the concentration of 100 mg mL^{-1} and 0.04 % (w/v), respectively. Figure 2.19 showed the 8-day-old fingermark deposited on ITO glass slides, immersed in water/ethanol suspension of particles for 10 minutes. The particles are deposited on the fingermark ridges in a fairly large amount, but unfortunately, they are also settled between the ridges, not giving the desired selectivity. Additionally, some larger agglomerates were observed on the sample's surface.

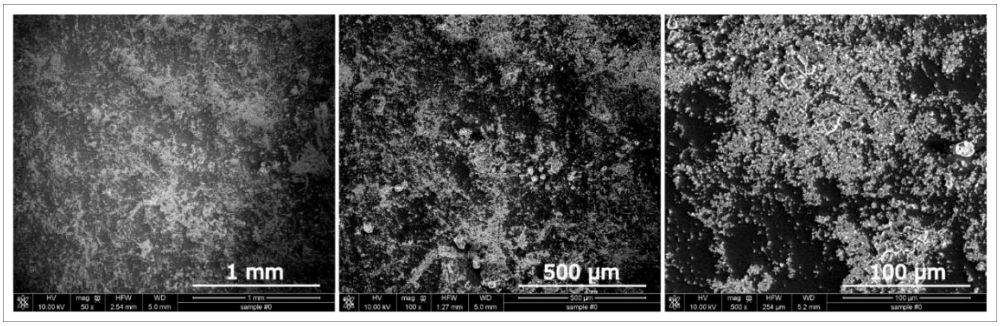

Figure 2.19 SEM images of 8-days-old sebaceous fingermark deposited on ITO glass slide enhanced with 100 mg mL^{-1} water/ethanol (97:3, v/v) suspension of SiO_2-Ph particles by immersion for 10 minutes

A similar result was obtained for the 38-days-old fingermark, which was developed by drop-casting the 300 µl of SiO_2-Ph particle water/ethanol suspension for 3 minutes (Figure 2.20). The particles abundantly deposited on the fingermark ridges, but at the same time, a number of particles were noticed on the background.

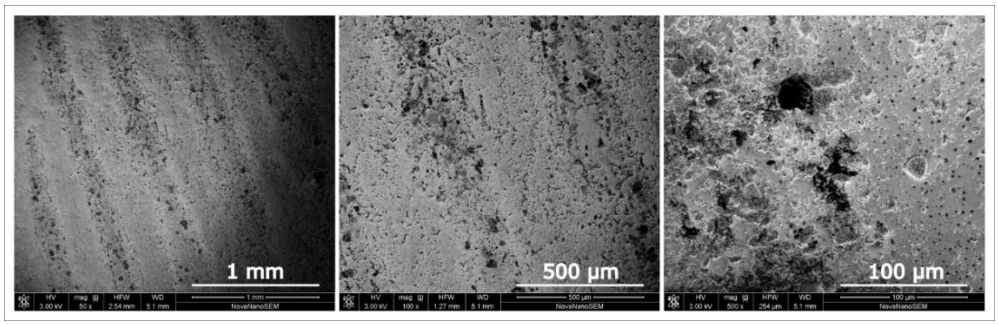

Figure 2.20 SEM images of 38-days-old sebaceous fingermark deposited on ITO glass slide enhanced with 100 mg mL^{-1} water/ethanol (97:3, v/v) suspension of SiO_2-Ph particles drop cast for 3 minutes

The effectiveness of the interaction between SiO_2-Ph particles and fingermark constituents was also investigated in the petroleum ether suspension. For this purpose, the sample with fingermark was immersed in the suspension for a short time. A very good result of 11-days-old fingermark enhancement was achieved for the sample immersed for 30 seconds (Figure 2.21). The particles settled mainly along the ridges of the fingermark, formed a thick layer. The number of particles between the ridges was incomparably smaller, allowing a satisfactory selectivity to be obtained.

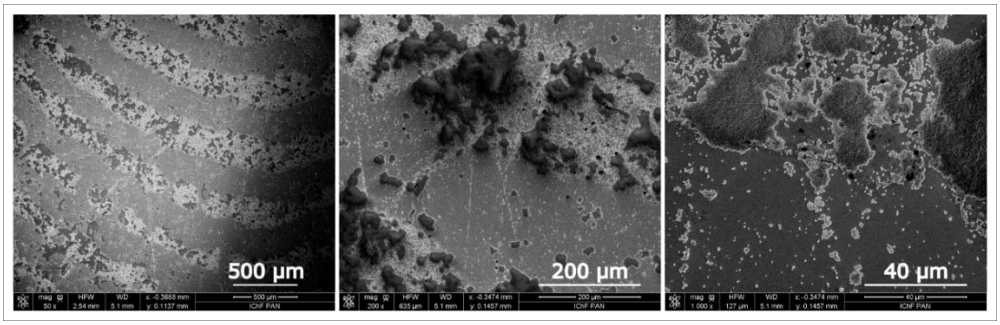

Figure 2.21 SEM images of 11-days-old sebaceous fingermark deposited on ITO glass slide enhanced with 0.04 % petroleum ether suspension of SiO_2-Ph particles by immersion for 30 seconds

Similar effectiveness of fingermark enhancement was achieved for the immersion time of 45 seconds (Figure 2.22). The particles deposited predominantly on the fingermark. Since the petroleum ether tends to dissolve the sebaceous fraction of the fingermark, a long immersion time is not favourable to not destroy the fingermark pattern. The 30 seconds of immersion time seemed to be optimal.

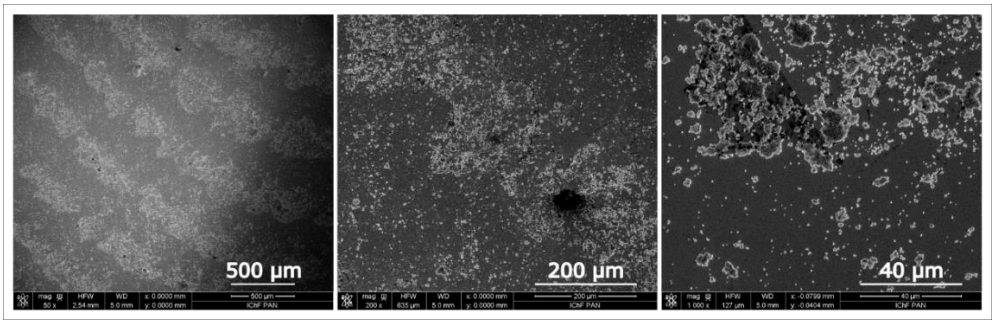

Figure 2.22 SEM images of 11-days-old sebaceous fingermark deposited on ITO glass slide enhanced with 0.04 % petroleum ether suspension of SiO_2-Ph nanoparticles by immersion for 45 seconds

2.6 Amide bond formation

2.6.1 Experimental

2.6.1.1 Chemicals

The following reagents were used to synthesise carboxyl-functionalised silica particles. 3-aminopropyltriethoxysilane (98 %, APTES), tetraethyl orthosilicate (98 %, TEOS), Triton X-100, N,N-dimethylformamide (DMF), N-(3-dimethyl-aminopropyl)-N'-ethylcarbodiimide hydrochloride (EDC) were purchased from Sigma-Aldrich. 3-(triethoxysilyl)propylsuccinic anhydride (94 %, TES PSA), carboxy-ethylsilanetriol sodium salt (CES) and n-hexanol were obtained from ABCR. N-hydroxysuccinimide (NHS) was purchased from Thermo Scientific. Ethanol (98 %, anhydrous) was purchased from POCH. Ammonium hydroxide (25 %, NH_4OH), acetone (pure p.a.), sodium chloride (pure p.a, NaCl), and hydrochloric acid (pure, HCl) were obtained from Chempur and cyclohexane from Fluorochem. All reagents were used as received. RO/DI water was used for the experiments.

2.6.1.2 Synthesis of carboxyl-functionalised silica particles

Silica particles were synthesised in two ways. The first synthesis comprised of two steps based on a modified Stöber method [44]. In the first step, the amino-functionalised silica particles have been synthesised. 47 ml of ethanol was mixed with 3.3 ml of ammonium hydroxide with stirring, followed by the addition of 4 ml of TEOS. The reaction mixture was stirred for 24 hours. After this time, 300 µl of APTES was added dropwise with vigorously stirring, and the reaction was continued for another 12 hours. Then, the amino-functionalised silica particles (SiO_2-NH_2) were centrifuged at 10 000 rpm for 20 minutes and washed with ethanol three times. In the second step, the SiO_2-NH_2 particles were dispersed in 20 ml of DMF using a sonication bath and the mixture was added dropwise to the 0.1 M solution of TES PSA in DMF (20 ml). The reaction was continued with stirring for 24 hours. Afterwards, the obtained particles (SiO_2-COOH-1) were centrifuged at 10 000 rpm for 20 minutes and purified with DMF three times.

In the second synthesis, particles were synthesised in the reversed microemulsion method [17]. 3.54 ml of Triton X-100, 15 ml of cyclohexane, 3.6 ml of n-hexanol, and 1 ml of water were mixed and stirred until the clear solution was

obtained. Then, 200 µl of TEOS followed by 120 µl of ammonium hydroxide were added to initiate the formation of the nanoparticles. The reaction mixture was stirred for 24 hours. After this time, 50 µl of TEOS and 170 µmol of CES were added dropwise, and the mixture was kept under stirring for another 24 hours. Afterwards, the system was destabilised with a large excess of ethanol. The precipitated nanoparticles (SiO_2-COOH-2) were collected by centrifugation at 5 600 rpm for 10 minutes and subsequently washed with ethanol twice and dispersed in water.

2.6.1.3 Fingermark development

Particles synthesised in two different ways have been applied to enhance the fingermarks deposited on ITO glass slides. The working solution has consisted of either SiO_2-COOH-1 particles or SiO_2-COOH-2 nanoparticles dispersed in water as a carrier solvent. In each batch, the working solution was poured into the glass dish in the amount sufficient to cover the entire sample. The samples were immersed into the working suspensions for an appropriate time, then rinsed with water to remove the loosely bound particles and finally dried in the stream of argon. Several key parameters, such as pH, the addition of NaCl, EDC and NHS, were also investigated to observe the results of particle-fingermark interaction [17].

Carboxyl-terminated silica particles synthesised by Stöber method (SiO_2-COOH-1)

The carboxyl-functionalised silica particles SiO_2-COOH-1 were first dispersed in water using an ultrasonic bath. The ITO glass slide samples bearing the fingermark were immersed in the particle suspension for 10, 20 or 30 minutes. Several modifications of the SiO_2-COOH-1 particle water suspension were implemented. First, the addition of 4 mM EDC and NHS was performed to activate the carboxyl groups and favour forming an amide bond between carboxyl-modified silica particles and amine groups present in the fingermark secretions. Also, the influence of pH on the interactions between carboxyl-functionalised particles and amine constituents of fingermark was investigated. For that purpose, the fingermark samples were immersed for 30 minutes into the SiO_2-COOH-1 water suspension with a pH set at 3 or 6 adjusted with 0.1 M HCl. Another modification of the initial particle dispersion was the addition of 0.5 M NaCl to the system to modify the ionic strength of the solution.

Carboxyl-terminated silica particles synthesised in reverse microemulsion (SiO_2-COOH-2)

Fingermarks were also enhanced with carboxyl-modified silica nanoparticles obtained in the reverse microemulsion synthesis. In order to prepare the initial working suspension, the nanoparticles obtained in the synthesis (0.1 g) were dispersed in 20 ml of water using an ultrasonic bath. In the first application mode, the working solution was diluted by two (final concentration 5 mg mL^{-1}) and then acidified with 0.1 M HCl to pH 3. The fingermarks were immersed in the SiO_2-COOH-2 water suspension for 60 minutes. The next application mode was based on diluting the initial working suspension by four and then adding 4 mM EDC and NHS. The fingermark samples were immersed for 30 minutes. In the last examined application mode, the pH of the twice-diluted working suspension was adjusted to 6, and then 0.5 M NaCl was added. The immersion time of the fingermark sample was 60 minutes.

2.6.2 Results and discussion

Carboxyl-terminated silica particles synthesised in two-step Stöber method (SiO_2-COOH-1)

The SEM images of carboxyl-functionalised silica particles morphology are shown in Figure 2.23. The synthesis led to the formation of spherical particles with an average diameter of 181 ± 8 nm, determined by analysis of SEM images in ImageJ application [40].

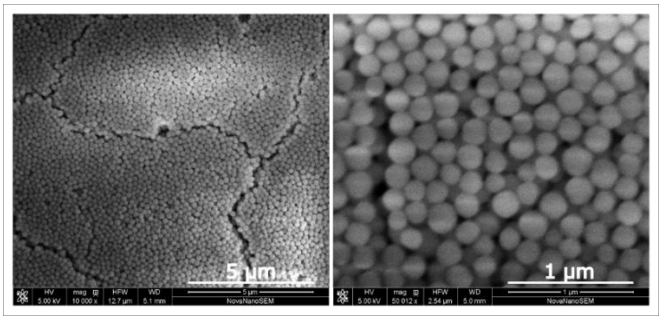

Figure 2.23 SEM images of silica particles modified with TES PSA (SiO_2-COOH-1)

The fingermarks deposited on the ITO glass slide were developed with SiO_2-COOH-1 particles dispersed in water at the concentration of 5 mg mL^{-1} for the series of immersion times 10, 20, and 30 minutes. The initial particles suspension indicated alkaline properties with the measured pH equal to 8. The reason for this may be due to the presence of ammonium hydroxide, which was not completely removed during the washing process. Quite a large number of particles have been deposited on the 6-days-old fingermark ridges when the sample was immersed for 10 minutes (Figure 2.24). However, there were plenty of particles also settled in the background. Much better results were obtained for the 20 minutes immersion time (Figure 2.25), where particles cover mainly all the fingermark ridges surface, showing good selectivity.

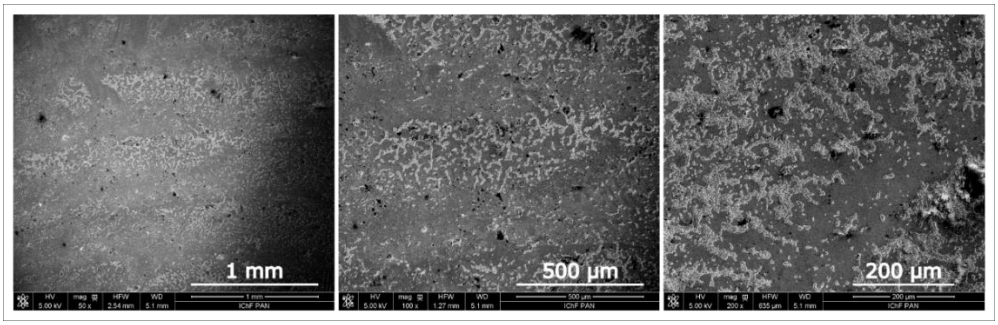

Figure 2.24 SEM images of 6-days-old sebaceous fingermark deposited on ITO glass slide enhanced with 5 mg mL^{-1} water suspension of SiO_2-COOH-1 particles by immersion for 10 minutes

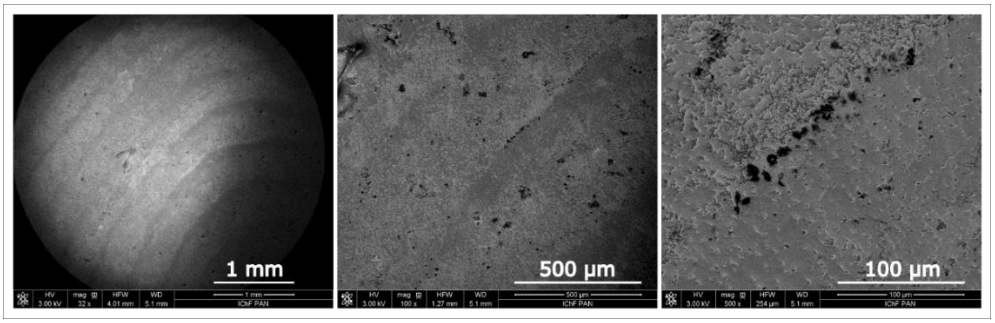

Figure 2.25 SEM images of 15-days-old sebaceous fingermark deposited on ITO glass slide enhanced with 5 mg mL^{-1} water suspension of SiO_2-COOH-1 particles by immersion for 20 minutes

Increasing the immersion time to 30 minutes resulted in a better selectivity of the particles towards the fingermark secretion than the background (Figure 2.26).

The particles cover the ridges of the fingermark in large amount, however, not homogeneously.

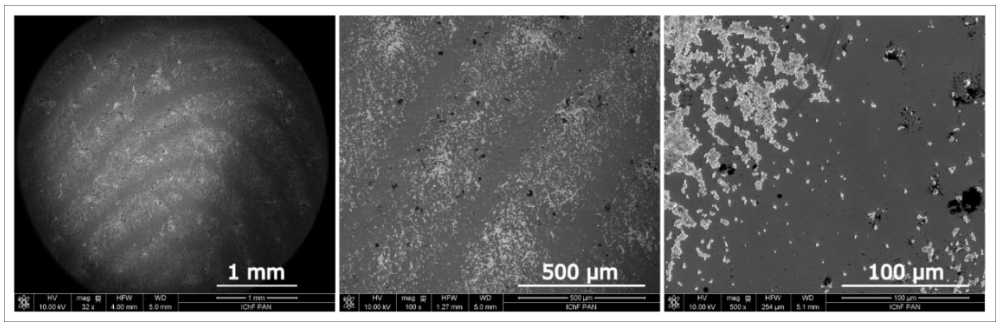

Figure 2.26 SEM images of 15-days-old sebaceous fingermark deposited on ITO glass slide enhanced with 5 mg mL^{-1} water suspension of SiO_2-COOH-1 particles by immersion for 30 minutes

To enhance the interaction between the carboxyl-functionalised silica particles and fingermark deposits containing amine-terminated compounds, the EDC and NHS have been added to the working solution. Figure 2.27 exhibits the SEM images of a developed 15-days-old fingermark. The images indicated that SiO_2-COOH-1 particles adhered to the surface of fingermark residual; however, while the particles covered the fingermark area preferably, the number of the particles was still not sufficient to overlay the ridge homogeneously.

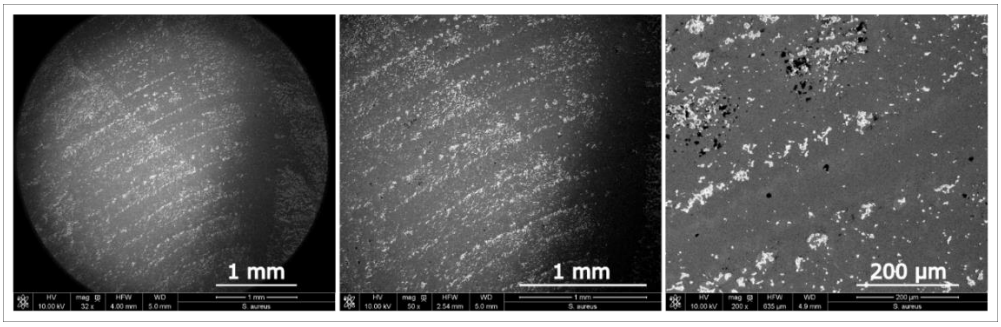

Figure 2.27 SEM images of 15-days-old sebaceous fingermark deposited on ITO glass slide enhanced with 5 mg mL^{-1} water suspension of SiO_2-COOH-1 particles with 4 mM EDC/NHS addition by immersion for 30 minutes

The initial pH of the SiO_2-COOH-1 water suspension was equal to 8. Since the activation of carboxyl groups in the presence of EDC and HNS is most efficient in the pH range between 4 and 7.2 [45], the interactions between the particles and the

fingermark were examined by immersing the sample for 30 minutes in the suspension of SiO_2-COOH-1 with the EDC and NHS addition at pH 6 (Figure 2.28). The preferential adherence to the fingermark deposit was noticed, and the fingermark ridges were homogeneously covered with the particles; however, a certain amount of the material was also deposited on the surroundings of the fingermark residual, leading to widening of the fingermark ridge.

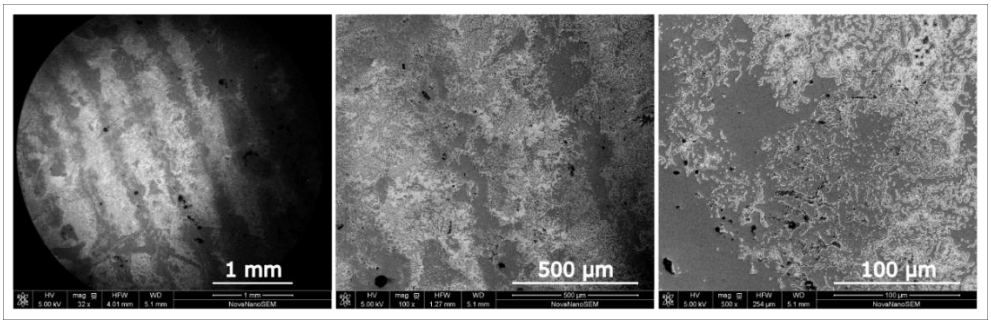

Figure 2.28 SEM images of 11-days-old sebaceous fingermark deposited on ITO glass slide enhanced with 5 mg mL^{-1} water suspension of SiO_2-COOH-1 particles with 4 mM EDC/NHS addition at pH 6 by immersion for 30 minutes

The effectiveness of the interaction between SiO_2-COOH-1 particles and the fingermark deposit in an acidic environment has also been investigated. For this purpose, the aqueous suspension of particles was acidified with 0.1 M HCl to a pH 3. The fingermark samples were immersed in the suspension for 30 minutes. The attempt to enhance the fingermark at low pH was unsuccessful. As shown in Figure 2.29, the particles were deposited almost over the entire surface of the sample. The area of the fingermark ridge can be barely distinguished from the area of the background. This may be influenced by low pH conditions. In the neutral and basic environment, the carboxylic groups on the silica surface are deprotonated and exist as negatively charged carboxyl moieties providing proper stability of silica particle suspension [46]. At low pH, however, the carboxylic groups are no longer negatively charged. The complete neutralisation of the moieties occurs, leading to lowering the absolute value of zeta potential and break the dispersion [17].

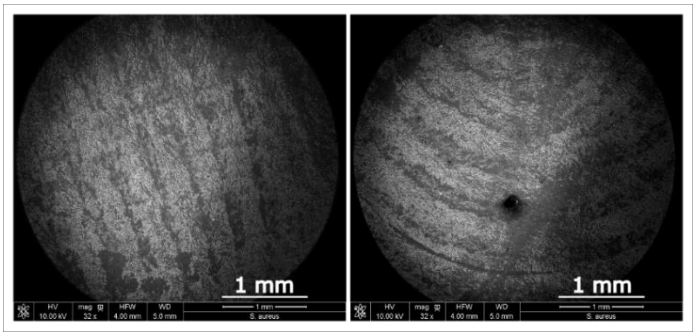

Figure 2.29 SEM images of 20-days-old sebaceous fingermark deposited on ITO glass slide enhanced with 5 mg mL^{-1} water suspension of SiO_2-COOH-1 particles at pH 3 by immersion for 30 minutes

Fingermarks were also enhanced with the SiO_2-COOH-1 water suspension at pH 6 with the addition of 0.5 M sodium chloride to lower the zeta potential of the colloid and favour the interaction between the particles and fingermark secretions. Figure 2.30 shows that the particles adhere to the papillary-ridge area forming island-shaped deposits. The particles are mostly embedded on the fingermark ridge, but a certain discontinuity in the coverage of the fingermark can be noticed, which in the case of the entire fingermark imaging may result in imprecise fingermark pattern mapping.

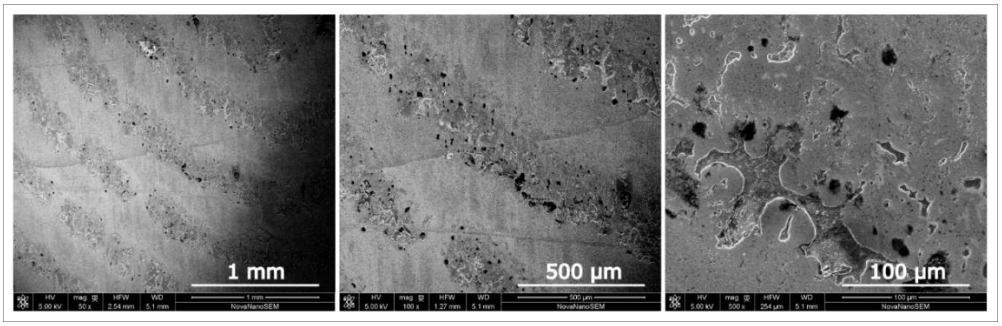

Figure 2.30 SEM images of 20-days-old sebaceous fingermark deposited on ITO glass slide enhanced with 5 mg mL^{-1} water suspension of SiO_2-COOH-1 particles with the addition of 0.5 M NaCl at pH 6 by immersion for 30 minutes

Carboxyl-terminated silica particles synthesised in reverse microemulsion (SiO_2-COOH-2)

The SEM images of carboxyl-functionalised silica obtained in the reversed microemulsion synthesis showed the monodispersed spherical nanoparticles with an average diameter of 57 ± 5 nm (Figure 2.31). The diameter of these nanoparticles is three times smaller than the diameter of particles of the previous synthesis.

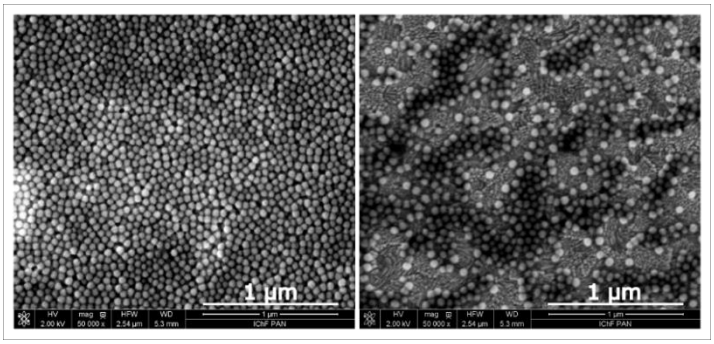

Figure 2.31 SEM images of silica nanoparticles with carboxyl-modified surface

To investigate the selective affinity towards fingermark deposits, the fingermark was enhanced with the water suspension of SiO_2-COOH-2 nanoparticles. Also, a few modifications to the initial suspension was made, as previously. First, the 21-days-old fingermark deposited on the ITO glass slide was developed with the SiO_2-COOH-2 nanoparticle water suspension at the concentration of 5 mg mL^{-1} by immersion for 30 minutes (Figure 2.32).

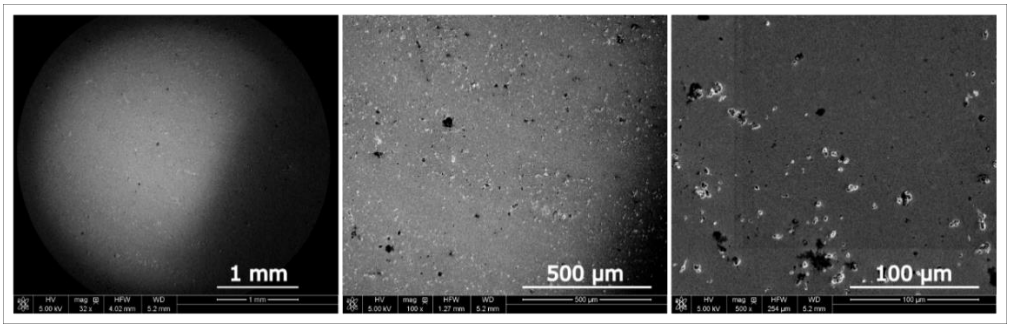

Figure 2.32 SEM images of 21-days-old sebaceous fingermark deposited on ITO glass slide enhanced with 5 mg mL^{-1} water suspension of SiO_2-COOH-2 nanoparticles by immersion for 30 minutes

The initial pH of the suspension was equal to 8.7. The particles were deposited mainly on the fingermark ridges; however, some agglomerates have been formed, and the number of the particles was not sufficient to cover the entire papillary-ridge area.

Trials were then performed on the SiO_2-COOH-2 nanoparticle suspension diluted by two (2.5 mg mL^{-1}) and acidified with 0.1 M HCl to pH 3. The ITO sample bearing the 21-days-old fingermark was immersed into the suspension for 60 minutes. The fingermark treatment resulted in no adherence of the nanoparticles to the fingermark deposit (Figure 2.33). There were merely a few agglomerates of nanoparticles randomly deposited on the sample surface.

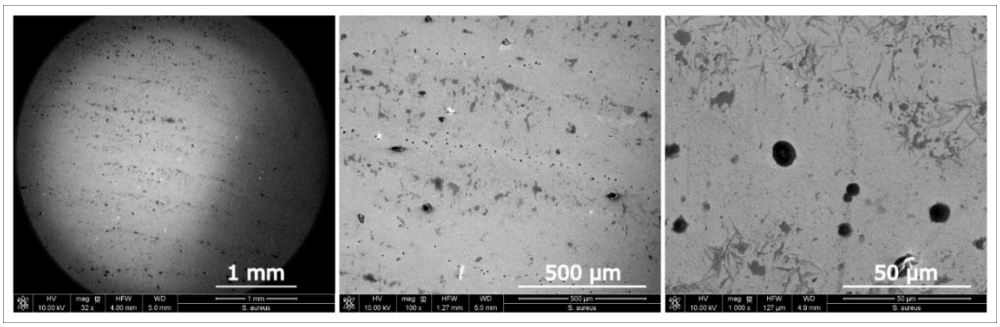

Figure 2.33 SEM images of 21-days-old sebaceous fingermark deposited on ITO glass slide enhanced with 2.5 mg mL^{-1} water suspension of SiO_2-COOH-2 particles at pH 3 by immersion for 60 minutes

Then, the addition of EDC and NHS to the 4 times diluted SiO_2-COOH-2 nanoparticles suspension (1.25 mg mL^{-1}) at pH 6 has been investigated to examine the interactions between the particles and the fingermark. The sample with an 18-days-old fingermark was immersed in the suspension for 30 minutes. No effect of fingermark development was observed (Figure 2.34). Only some residual substances can be noticed, probably organic solvents from the synthesis, which were not completely removed during the washing process.

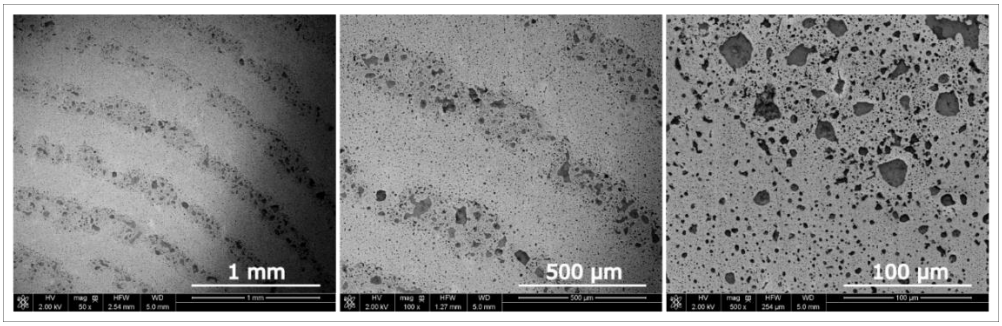

Figure 2.34 SEM images of 18-days-old sebaceous fingermark deposited on ITO glass slide enhanced with 1.25 mg mL^{-1} water suspension of SiO_2-COOH-2 nanoparticles with the EDC and NHS addition at pH 6 by immersion for 30 minutes

The last trial of fingermark development with SiO_2-COOH-2 material was performed in the nanoparticle suspension with the addition of 0.5 M NaCl at pH 6. The sample was immersed in the working suspension for 60 minutes. Unfortunately, also in these conditions, the result of fingermark enhancement was poor (Figure 2.35). Very few nanoparticles can be observed on the fingermark ridge area, as well as some crystallised sodium chloride. Such quantity of the material deposited on the papillary ridges disqualifies this material from further research.

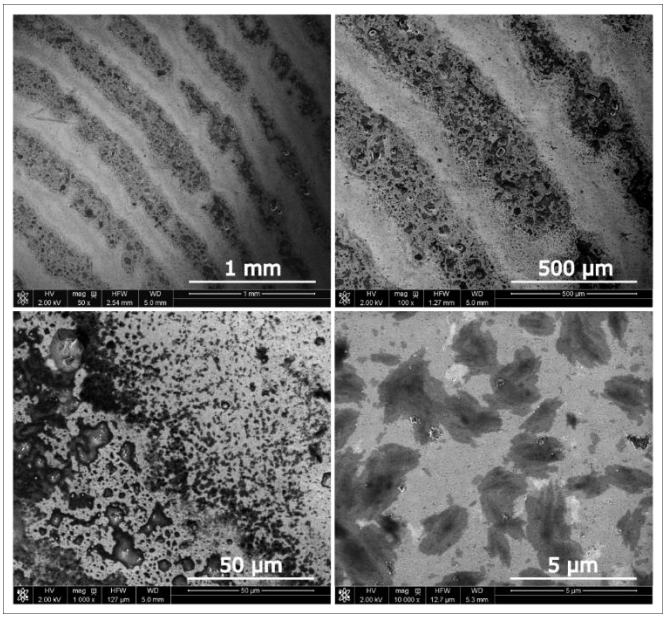

Figure 2.35 SEM images of 18-days-old sebaceous fingermark deposited on ITO glass slide enhanced with 2.5 mg mL^{-1} water suspension of SiO_2-COOH-2 nanoparticles with 0.5 M NaCl addition at pH 6 by immersion for 60 minutes

2.7 Conclusions

An analysis of the potential application of surface-functionalised silica particles for fingermark development has been done. The surface of the silica particles was modified with various functional moieties to enhance the interaction between the developing agent and the fingermark secretion. Several possible interaction types have been investigated, such as thiol-gold or lipophilic interaction and amide bond formation.

In the analysis of thiol-gold interaction, the fingermark was first modified with a thin layer of gold using the SMD method. Then, on the gold-modified fingermark area, the silica particles functionalised with thiol groups were deposited. The results of the particle deposition obtained by this method were not satisfactory. The thiol-functionalised silica particles were selectively settled on the area of gold deposits along the fingermark ridges, but the number of the particles was insufficient to cover the entire ridge of the mark continuously. Applying this method for further studies on fingermark enhancement would have resulted in poor fingermark development, discontinuity in silica particles deposition and finally, inaccurate ridge mapping of fingermark pattern.

Another type of analysed interactions was lipophilic interaction. Due to the fact that fingermark residue consists of a whole range of sebaceous components such as free fatty acids, squalene, waxes etc., silica particles modified with lipophilic functional groups could have been applied to enhance the fingermark. The results of this research showed that this type of interaction had been successfully noticed. Eighteen carbon alkyl chains (C18) and phenyl groups have been chosen as functional moieties of surface-modified silica particles to interact with fingermark deposits. Fingermark developed with C18-silica nanoparticles using petroleum ether as the particle carrier exhibited poor results. The particles formed agglomerates on the fingermark ridges, and their number deposited on the mark was minor. In comparison, fingermark enhanced with larger phenyl-modified silica particles yielded a much better outcome. The silica particles containing phenyl groups were dispersed in two different solvents: water with the addition of ethanol and petroleum ether. In the case of fingermark enhancement in water suspension, the silica particles were deposited both on the fingermark ridges and between them. However, the number of particles was greater on the fingermark. On the other hand, good development of fingermark was obtained with particles dispersed in the petroleum ether. It was observed that phenyl-functionalised silica particles have selectively interacted with fingermark deposits. The entire ridge area was covered

with a thick layer of the particles, providing sufficient projection of the ridge pattern. Nevertheless, the use of petroleum ether as a carrier solvent is more hazardous to 3 % aqueous ethanol solution. Petroleum ether is highly volatile and inflammable in the liquid and vapour phase. This solvent contains substances which are toxic to aquatic life with long-lasting effect [47]. Also, inhalation of petroleum ether may cause central nervous, respiratory and digestive systems toxicity [48]. On the other hand, a 10 % water and ethanol solution, although it is also flammable, does not contain compounds considered to be toxic or bioaccumulating [49][49]. Hence, the choice of the aqueous ethanol solution as a carrier solvent for further studies seems to be a less hazardous option.

The last investigated interaction was the formation of amide bonds between the carboxyl-modified silica particles and amine groups present in the compounds of fingermark residue. The carboxyl-functionalised silica particles synthesised in a two-step process (via amine-groups) showed high selective affinity to the fingermark. Water was used as a carrier solvent, and various modifications of the particle suspension were made to increase the effectiveness of the interaction between the particle and the fingermark, such as changing the pH, adding EDC and NHS or NaCl. The other synthesis of silica nanoparticles modified with carboxyl moieties was also performed. Nanoparticles were produced in reverse microemulsion. The obtained material was three times smaller in diameter than the particles obtained in the previous synthesis. Unfortunately, the interactions between these nanoparticles and fingermark residuals were hardly observable. Very few nanoparticles were present on the fingermark ridges. Compared to the SiO_2-COOH-1 material, the SiO_2-COOH-2 nanoparticles synthesised with the microemulsion method were also not favourable due to the difficulty in washing off all the organic solvents, which may have influenced the unsuccessful development trial. The poor results have disqualified this material for further processing.

To sum up, among the investigated interactions between modified silica particles and fingermark residual, the particles functionalised with carboxyl groups (SiO_2-COOH-1) and phenyl moieties (SiO_2-Ph) show the highest potential for fingermark development. Both the carboxyl-modified and phenyl-modified silica particles had a size greater than 100 nm (ca. 297 nm and 181 nm, respectively). In comparison, the application of nanoparticles modified with long hydrocarbon chains or carboxyl groups with a diameter of ca. 69 nm and 57 nm, respectively, resulted in poor fingermark enhancement. The use of carboxyl-modified particles is burdened with the control of additional parameters such as pH or EDC, NHS or NaCl addition; therefore, for further research on the luminescent material for fingermark detection on multi-coloured, luminescent surfaces, the lipophilic silica particles have

been employed. The silica particles or silica-coated particles with the modified surface in this way allowed to achieve the required selectivity of the particle deposition on the fingermark ridges.

2.8 References

[1] M. J. Choi, A. M. McDonagh, P. Maynard, and C. Roux, "Metal-containing nanoparticles and nano-structured particles in fingermark detection," *Forensic Sci. Int.*, vol. 179, no. 2–3, pp. 87–97, 2008, doi: 10.1016/j.forsciint.2008.04.027.

[2] G. S. Sodhi and J. Kaur, "Powder method for detecting latent fingerprints: A review," *Forensic Sci. Int.*, vol. 120, pp. 172–176, Sep. 2001, doi: 10.1016/S0379-0738(00)00465-5.

[3] A. Becue, S. Moret, C. Champod, and P. Margot, "Use of stains to detect fingermarks," *Biotech. Histochem.*, vol. 86, no. 3, pp. 140–160, 2011, doi: 10.3109/10520290903462838.

[4] Henry C. Lee and R. E. Gaensslen, *Advances Fingerprint in Technology*, vol. 1. CRC Press, 2001.

[5] C. Champod, C. Lennard, P. Margot, and M. Stoilovic, *Fingerprints and other ridge skin impressions, second edition*. CRC Press, 2017.

[6] R. Jelly, E. L. T. Patton, C. Lennard, S. W. Lewis, and K. F. Lim, "The detection of latent fingermarks on porous surfaces using amino acid sensitive reagents: A review," *Anal. Chim. Acta*, vol. 652, no. 1–2, pp. 128–142, 2009, doi: 10.1016/j.aca.2009.06.023.

[7] J. D. Wright and N. A. J. M. Sommerdijk, *Sol-Gel Materials Chemistry and Applications*. Gordon and Breach Science Publishers, 2001.

[8] M. A. Agotegaray and V. L. Lassalle, *Silica-Coated Magnetic Nano-Particles. An Insight into Targeted Drug Delivery and Toxicology*. Springer, 2016.

[9] I. A. Rahman and V. Padavettan, "Synthesis of Silica Nanoparticles by Sol-Gel: Size-Dependent Properties, Surface Modification, and Applications in Silica-Polymer Nanocomposites-A Review," *J. Nanomater.*, vol. 2012, p. 15, 2012, doi: 10.1155/2012/132424.

[10] L. Meng, Y. Ren, Z. Zhou, C. Li, C. Wang, and S. Fu, "Monodisperse silica nanoparticle suspension for developing latent blood fingermarks," *Forensic Sci. Res.*, vol. 5, no. 1, pp. 38–46, 2020, doi: 10.1080/20961790.2018.1446721.

[11] L. Liu, S. K. Gill, Y. Gao, L. J. Hope-Weeks, and K. H. Cheng, "Exploration of the use of novel SiO_2 nanocomposites doped with fluorescent Eu^{3+}/sensitizer complex for latent fingerprint detection," *Forensic Sci. Int.*, vol. 176, no. 2–3, pp. 163–172, 2008, doi: 10.1016/j.forsciint.2007.08.006.

[12] Y. Liu, C. Lou, H. Yang, M. Shi, and H. Miyoshi, “Silica Nanoparticles as Promising Drug/Gene Delivery Carriers and Fluorescent Nano-Probes: Recent Advances,” *Curr. Cancer Drug Targets*, vol. 11, no. 2, pp. 156–163, 2011, doi: 10.2174/156800911794328411.

[13] Y. Wu *et al.*, “Plant-derived fluorescent silicon nanoparticles featuring excitation wavelength-dependent fluorescence spectra for anti-counterfeiting applications,” *Chem. Commun.*, vol. 52, no. 43, pp. 7047–7050, 2016, doi: 10.1039/c6cc02872a.

[14] S. Moret, A. Bécue, and C. Champod, “Functionalised silicon oxide nanoparticles for fingermark detection,” *Forensic Sci. Int.*, vol. 259, pp. 10–18, 2016, doi: 10.1016/j.forsciint.2015.11.015.

[15] P. Niu *et al.*, “CdTe@SiO_2/Ag nanocomposites as antibacterial fluorescent markers for enhanced latent fingerprint detection,” *Dye. Pigment.*, vol. 119, pp. 1–11, 2015, doi: 10.1016/j.dyepig.2015.03.018.

[16] Y. J. Kim, H. S. Jung, J. Lim, S. J. Ryu, and J. K. Lee, “Rapid Imaging of Latent Fingerprints Using Biocompatible Fluorescent Silica Nanoparticles,” *Langmuir*, vol. 32, no. 32, pp. 8077–8083, 2016, doi: 10.1021/acs.langmuir.6b01977.

[17] S. Moret, A. Bécue, and C. Champod, “Nanoparticles for fingermark detection: an insight into the reaction mechanism,” *Nanotechnology*, vol. 25, pp. 1–10, 2014, doi: 10.1088/0957-4484/25/42/425502.

[18] M. Zhang *et al.*, “Systematic study of dye loaded small mesoporous silica nanoparticles for detecting latent fingerprints on various substrates,” *J. Porous Mater.*, 2016, doi: 10.1007/s10934-016-0231-y.

[19] W. Huang, X. Li, H. Wang, X. Xu, H. Liu, and G. Wang, “Synthesis of Amphiphilic Silica Nanoparticles for Latent Fingerprint Detection,” *Anal. Lett.*, vol. 48, no. 9, pp. 1524–1535, 2015, doi: 10.1080/00032719.2014.984195.

[20] B. J. Theaker, K. E. Hudson, and F. J. Rowell, “Doped hydrophobic silica nano- and micro-particles as novel agents for developing latent fingerprints,” *Forensic Sci. Int.*, vol. 174, no. 1, pp. 26–34, 2008, doi: 10.1016/j.forsciint.2007.02.030.

[21] T. Bürgi, “Properties of the gold-sulphur interface: from self-assembled monolayers to clusters,” *Nanoscale*, vol. 7, no. 38, pp. 15553–15567, 2015, doi: 10.1039/c5nr03497c.

[22] Y. Xue, X. Li, H. Li, and W. Zhang, “Quantifying thiol-gold interactions towards the efficient strength control,” *Nat. Commun.*, vol. 5, 2014, doi: 10.1038/ncomms5348.

[23] H. Häkkinen, “The gold-sulfur interface at the nanoscale,” *Nat. Chem.*, vol. 4, no. 6, pp. 443–455, 2012, doi: 10.1038/nchem.1352.

[24] A. A. Frick, P. Fritz, and S. W. Lewis, “Chemical methods for the detection of latent fingermarks,” in *Forensic Chemistry Fundamentals and Applications*, J. Siegel, Ed. Wiley Blackwell, 2016.

[25] H. L. Bandey, S. M. Bleay, V. J. Bowman, R. P. Downham, and V. G. Sears,

Fingermark Visualisation Manual, First. Home Office Centre for Applied Science and Technology (CAST), 2014.

[26] E. Stauffer, A. Becue, K. V. Singh, K. R. Thampi, C. Champod, and P. Margot, "Single-metal deposition (SMD) as a latent fingermark enhancement technique: An alternative to multimetal deposition (MMD)," *Forensic Sci. Int.*, vol. 168, no. 1, 2007, doi: 10.1016/j.forsciint.2006.12.009.

[27] S. M. Bleay *et al.*, *Fingerprint Source Book*. Home Office Centre for Applied Science and Technology, 2012.

[28] A. Becue, A. Scoundrianos, and S. Moret, "Detection of fingermarks by colloidal gold (MMD/SMD) - beyond the pH 3 limit," *Forensic Sci. Int.*, vol. 219, no. 1–3, pp. 39–49, 2012, doi: 10.1016/j.forsciint.2011.11.024.

[29] A. D. McNaught and A. Wilkinson, *Compendium of Chemical Terminology, IUPAC Recommendations, 2nd ed.* 1988.

[30] C. Bissantz, B. Kuhn, and M. Stahl, "A medicinal chemist's guide to molecular interactions," *J. Med. Chem.*, vol. 53, no. 14, pp. 5061–5084, 2010, doi: 10.1021/jm100112j.

[31] E. Rutkowska, K. Pająk, and K. Jóźwiak, "Lipophilicity - Methods of determination and its role in medicinal chemistry," *Acta Pol. Pharm. - Drug Res.*, vol. 70, no. 1, pp. 3–18, 2013.

[32] A. Girod, R. Ramotowski, and C. Weyermann, "Composition of fingermark residue: A qualitative and quantitative review," *Forensic Science International*, vol. 223, no. 1–3. pp. 10–24, Nov. 30, 2012, doi: 10.1016/j.forsciint.2012.05.018.

[33] E. Massolo, M. Pirola, and M. Benaglia, "Amide Bond Formation Strategies: Latest Advances on a Dateless Transformation," *European J. Org. Chem.*, vol. 2020, no. 30, pp. 4641–4651, 2020, doi: 10.1002/ejoc.202000080.

[34] A. Rimola, M. Fabbiani, M. Sodupe, P. Ugliengo, and G. Martra, "How Does Silica Catalyze the Amide Bond Formation under Dry Conditions? Role of Specific Surface Silanol Pairs," *ACS Catal.*, vol. 8, no. 5, pp. 4558–4568, 2018, doi: 10.1021/acscatal.7b03961.

[35] S. Sam *et al.*, "Semiquantitative study of the EDC/NHS activation of acid terminal groups at modified porous silicon surfaces," *Langmuir*, vol. 26, no. 2, pp. 809–814, 2010, doi: 10.1021/la902220a.

[36] J. Almog, A. A. Cantu, C. Champod, T. Kent, and C. Lennard, "Guidelines for the Assessment of Fingermark Detection Techniques," *J. Forensic Identif.*, vol. 64, no. 2, pp. 174–197, 2014.

[37] M. R. Akanda, A. M. Osman, M. K. Nazal, and M. A. Aziz, "Review—Recent Advancements in the Utilization of Indium Tin Oxide (ITO) in Electroanalysis without Surface Modification," *J. Electrochem. Soc.*, vol. 167, no. 3, p. 037534, 2020, doi: 10.1149/1945-7111/ab64bd.

[38] B. Schnetz and P. Margot, "Technical note: Latent fingermarks, colloidal gold and multimetal deposition (MMD) Optimisation of the method," *Forensic Sci. Int.*, vol. 118, no. 1, pp. 21–28, 2001, doi: 10.1016/S0379-0738(00)00361-3.

[39] J. H. Park, Y. G. Lee, and S. G. Oh, "Easy synthesis of highly monodispersed silica@M (M = Ag, Au, Pd, Pt) particles using thiol compounds as a connecting agent," *J. Ceram. Process. Res.*, vol. 12, no. 4, pp. 456–461, 2011.

[40] W. S. Rasband, "ImageJ, U. S. National Institutes of Health, Bethesda, Maryland, USA," *https://imagej.nih.gov/ij/ 1997-2018*. .

[41] W. Stober, A. Fink, and E. Bohn, "Controlled Growth of Monodisperse Silica Spheres in the Micron Size Range," *J. Colloid Interface Sci.*, vol. 26, pp. 62–69, 1968.

[42] S. A. Kulkarni, S. B. Ogale, and K. P. Vijayamohanan, "Tuning the hydrophobic properties of silica particles by surface silanization using mixed self-assembled monolayers," *J. Colloid Interface Sci.*, vol. 318, no. 2, pp. 372–379, Feb. 2008, doi: 10.1016/j.jcis.2007.11.012.

[43] M. Sametband, I. Shweky, U. Banin, D. Mandler, and J. Almog, "Application of nanoparticles for the enhancement of latent fingerprints," *Chem. Commun.*, no. 11, pp. 1142–1144, 2007, doi: 10.1039/b618966k.

[44] Y. An, M. Chen, Q. Xue, and W. Liu, "Preparation and self-assembly of carboxylic acid-functionalized silica," *J. Colloid Interface Sci.*, vol. 311, no. 2, pp. 507–513, 2007, doi: 10.1016/j.jcis.2007.02.084.

[45] ThermoFisher Scientific, "User Guide: NHS and Sulfo-NHS," *https://www.thermofisher.com/order/catalog/product/24510#/24510*.

[46] A. Feinle, F. Leichtfried, S. Straßer, and N. Hüsing, "Carboxylic acid-functionalized porous silica particles by a co-condensation approach," *J. Sol-Gel Sci. Technol.*, vol. 81, no. 1, pp. 138–146, 2017, doi: 10.1007/s10971-016-4090-4.

[47] "Petroleum Ether," *SDS No. FSUP1440 [Online]*. ThermoFisher Scientific, pp. 1–12, 2009, [Online]. Available: https://www.fishersci.co.uk/store/msds?partNumber=12616757&productDescription=1LT+Petroleum+ether+40-60°C%2C+extra+pure%2C+SLR&countryCode=GB&language=en.

[48] S. Parasuraman *et al.*, "Evaluation of sub-chronic toxic effects of petroleum ether, a laboratory solvent in Sprague-Dawley rats," *J. Basic Clin. Pharm.*, vol. 5, no. 4, p. 89, 2014, doi: 10.4103/0976-0105.141943.

[49] "Ethanol standards 10% (v/v)," in *SDS No. E2385 [Online]*, 2019, pp. 1–8, [Online]. Available: https://www.sigmaaldrich.com/MSDS/MSDS/DisplayMSDSPage.do?country=PL&language=EN-generic&productNumber=E2385&brand=SIGMA&PageToGoToURL=https%3A%2F%2Fwww.sigmaaldrich.com%2Fcatalog%2Fproduct%2Fsigma%2Fe2385%3Flang%3Dpl.

Chapter 3 Luminophore encapsulation in silica particles

3.1 Equipment and instrumentation

Fluorescence Spectroscopy

The absorption spectra of the samples have been recorded using a Shimadzu UV 2700 spectrophotometer. The emission spectra, photoluminescence decay curves in the micro- and millisecond time range, and time-gated emission spectra, corrected for the spectral sensitivity of the instrument, were collected using Horiba Jobin Yvon FL3-22 Fluorolog-3 spectrofluorometer. The build-in FL-1040 system with a UV xenon flash tube and approx. 3 μs response time was used in the time-gated measurements. The photoluminescence lifetime measurements in the nanosecond time regime were recorded using a home-built TC-SPC setup consisting of a Picoquant LDH pulsed laser with an excitation wavelength of 379 nm, 100 ps pulse, and 10 MHz repetition rate, a Spectral Products Digikröm CM110 monochromator, Becker&Hickl PMC 100-4 photomultiplier, and a PicoQuantTimeHarp 100 PC card. Also, 403 nm and 507 nm interference bandpass filters were applied to remove the scattered excitation on the emission side. The photoluminescence decay measurements in the ms time range for the whole visible spectrum of light have been performed using a home-built time-gated imaging system with a CCD camera (HARDsoft Microprocessor Systems, Poland).

Infrared Spectroscopy

The infrared spectra of the investigated powder material have been collected with a Nicolet iS50 FTIR spectrometer with a built-in all reflective, mid- and far-IR diamond attenuated total reflectance (ATR) module. Spectra were recorded throughout the entirety of experiments in absorbance units with 100 scans and 0.482 cm^{-1} data spacing being averaged into a range.

Scanning Electron Microscopy

Scanning electron microscopy (SEM) images of the obtained material and developed fingermarks were taken with FEI Nova Nano-SEM 450 scanning electron

microscope. The examined material was deposited on the ITO slide mounted on a carbon adhesive tape on an aluminium stub.

Energy-dispersive X-ray Spectroscopy (EDX)

The material was characterised by electron dispersive X-ray analysis performed with the FEI Nova Nano-SEM 450 using Sapphir X-ray detector conjugated with EDAX TSL system. EDX spectra were generated at an accelerating voltage of 20 kV.

3.2 Zinc oxide quantum dots embedded in silica particles

3.2.1 Introduction

Photoluminescent techniques for fingermark detection and imaging are a vital tool in the field of forensic science [1]. These techniques involve sensitising fingermarks with a luminescent agent, illuminating a sample with the light of an appropriate wavelength, and observing the emitted light using bandpass filters to separate the luminescence of the background from the emission of fingermark sensitiser. Due to its sensitivity, photoluminescence enhancement can be applied to fingermarks deposited on a variety of surfaces, including paper items, resulting in a fingermark contrast increase [2], [3]. However, some substrates may present reflectivity, light scattering, or strong background fluorescence producing a hindrance to fluorescence examination [4]. It may happen when the excitation band partially overlaps with the emission band of the sensitiser. In this case, the excitation radiation reflected from the background is not feasible to filter out what leads to a significant decrease in contrast. Fingermarks become hardly visible also when the luminescence of the background is stronger than of the sensitiser or when background luminescence overlaps the luminescence of a sensitised fingermark. Plenty of frequently used objects, which may be potentially the fingermark background, contain dyes that emit spectrally broad luminescence or possess colourful printed patterns that may interfere with the fingermark. Moreover, some items, e.g. banknotes or ID cards, have highly fluorescent protection marks.

A remedy to these problems has been proposed by Menzel [5], who described a time-gated strategy of fingermark imaging, described in Chapter 1.10. As mentioned before, this strategy involves fingermark treatment with

a photoluminescent sensitiser with a lifetime on the order of microseconds. In contrast, the fluorescence decay time of typical backgrounds is on the order of nanoseconds. When the examined object is excited with light, both the fingermark and the background emit luminescence. When the light source is turned off, the photoluminescence of the fingermark and the background starts to decay exponentially, but the background fluorescence decays in nanoseconds. Due to the longer luminescence lifetime of the fingermark sensitiser, one can separate its luminescence from the background by collecting the signal after a particular time of excitation light source cut-off. This imaging strategy was further developed, but in most cases, the sensitising agent has been introduced onto the LFM by powder dusting [6]–[9]. As this is an invasive application, impossible to use on adhesive or porous surfaces, and which cause the background staining, an ideal luminescent material possessing long-lived luminescence and interacting selectively with the fingermark residue is still in demand.

This section will discuss the synthesis and application of hybrid (organic-inorganic) material based on silica particles that possess long-lived luminescence to detect fingermarks on the colourful, reflective, and fluorescent porous and non-porous surfaces with the use of a particle suspension. The material consists of zinc oxide quantum dots embedded into the silica matrix with a modified surface to acquire lipophilic properties. These properties facilitate the interactions between the fatty constituents of the mark and the luminescent sensitiser, resulting in material selectivity. Employing water-based solvent allows avoiding fingermark pattern damage and background staining what is of importance in the case of adhesive surfaces. ZnO quantum dots encapsulated within the silica matrix (-SiO_2) exhibit long-lived luminescence on the order of seconds [10]. A scheme of the fingermark development process and visualisation with the time-gated imaging system is depicted in Figure 3.1. The material will be examined, including material characteristics such as morphology, composition, luminescence properties, an affinity to fingermark deposits, efficiency of fingermark imaging on several surfaces, and an advantage over conventional methods.

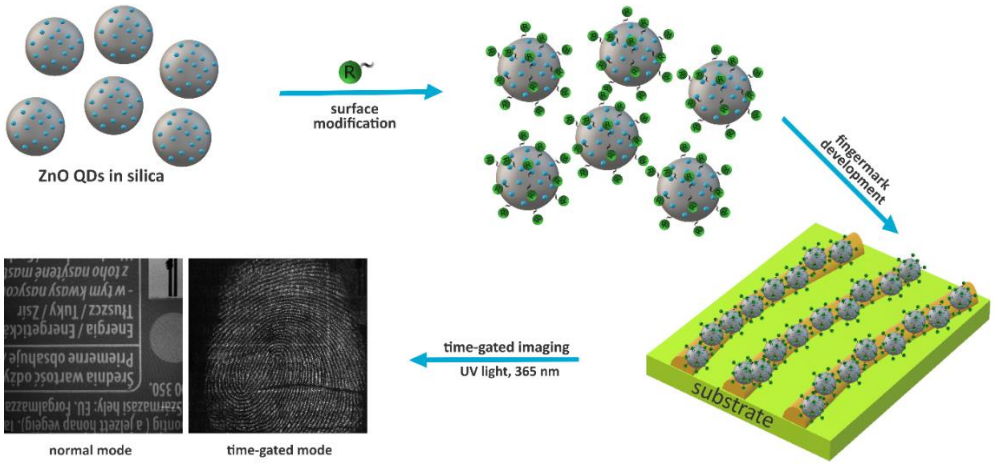

Figure 3.1 The scheme of the surface-functionalised luminescent silica particles (ZnO-SiO_2) synthesis and selective deposition on fingermark ridges for imaging in the time-gated mode

3.2.2 Experimental

3.2.2.1 Chemicals

The following reagents were used for the synthesis of ZnO-SiO_2 particles, surface modification, and benchmark development procedures. N-[3-(Trimethoxysilyl)propyl] ethylenediamine (97 %, AEAPTMS), zinc chloride (99.99 %), triethoxyphenylsilane (98 %), tetraethoxysilane (≥ 99.0 %, TEOS), (3-Aminopropyl)triethoxysilane (APTES), succinic anhydride (> 99.0 %), Triton X-100, and molybdenum (IV) sulfide (powder, < 2 µm, 99 %) were purchased from Sigma-Aldrich. Methanol (analytical grade), ethanol (anhydrous, 99.8 %), and acetone (analytical grade) were obtained from POCH. n-Octanol (extra pure) was acquired from Merck, cyclohexane (99 %), and octadecyltriethoxysilane (95 %) from Fluorochem, aqueous ammonia (25 %) from Chempur, toluene (anhydrous, 99.8 %) was purchased from Alfa Aesar and N,N-Dimethylformamide (≥ 98.0 %, DMF) from Fluka. Dioctyl sulfosuccinate sodium salt (96 %, DOSS), Basic Violet 3 (pure, BV3) were obtained from Acros Organic and Green Charge™ Fluorescent Magnetic powder was purchased from Transfarm. All reagents were used as received. RO/DI water was used for all the experiments.

3.2.2.2 Synthesis of ZnO QDs in silica matrix

The composite of zinc oxide quantum dots dispersed in the silica matrix was synthesised using a reverse microemulsion [10]. In this method, water droplets, dispersed in a continuous oil phase, form a kind of microreactors in which nucleation and growth of nanoparticles occur. First, 30 ml of cyclohexane, 6 ml of n-octanol, 6 ml of Triton X-100, and 1 ml of water were mixed and stirred 30 minutes to form a clear solution. Next, 61.33 mg (0.45 mmol Zn^{2+}) of zinc chloride was dissolved in 1 ml of ethanol, and subsequently, 32.44 µl (0.15 mmol) of AEAPTMS was added to the mixture to form an amine complex with zinc cation. The resulting mixture was added dropwise to the microemulsion and stirred for 30 minutes. Then, 0.6 ml of ammonium hydroxide was added dropwise to catalyse the silane polycondensation reaction, and the mixture was stirred for 24 hours at room temperature. Afterwards, 0.6 ml of TEOS was added dropwise to the microemulsion to cover the particles with a thin layer of silica, and the mixture was stirred for another 24 hours. After this time, the particles were precipitated by the addition of 60 ml of acetone to the mixture. The material was then centrifuged at 9 500 rpm for 15 minutes, purified with ethanol three times to remove unreacted reagents, and dried in an oven at 70 °C for 24 hours. The dried powder was calcined in a tube furnace in the air at 550 °C for 4 hours with a heating rate of 20 °C/hour to form ZnO clusters inside the silica particles. Finally, the fine white powder (ZnO-SiO_2) was washed with ethanol once, centrifuged at 9 500 rpm for 15 minutes, and dried in the oven at 70° C for 24 hours.

3.2.2.3 Surface functionalisation with organic moieties

Silica particles doped with zinc oxide quantum dots were modified in the process of grafting with reactive organic moieties such as 18 hydrocarbon chains and phenyl groups, which are able to react with fingermark components. The choice of particles modified with lipophilic moieties is the result of an analysis of the interactions between fingermark components and functionalised silica particles, described in Chapter 2.

Modification with phenyl groups

Zinc oxide silica particles were modified with phenyl groups. The modification was prepared according to a literature procedure [11]. For this purpose, 25 mg of ZnO-SiO_2 particles were dispersed in 30 ml of dry toluene in a three-necked round-bottom flask by sonication. The mixture was stirred at 80 °C for 30 minutes

under reflux and in an argon atmosphere. Then, a solution of 270 µl (1 %, w/w) of phenyltriethoxysilane in 1 ml of toluene was added dropwise, and the reaction mixture was stirred for 24 hours. Afterwards, the system was cooled down to room temperature, the solvent was evaporated in a rotary evaporator, and methanol was added to precipitate particles. The obtained material was separated by centrifugation at 9 500 rpm for 15 minutes, purified with ethanol three times, and dried in an oven for 12 hours at 65 °C.

Modification with long hydrocarbon chains

Surface modification with eighteen hydrocarbon chains was conducted in a similar way as for the phenyl group functionalisation. Instead of phenyl-triethoxysilane, a solution of 341 µl of octadecyltriethoxysilane in 1 ml of dry toluene was added dropwise. All the other reagents' quantities and synthesis steps have not been changed. The obtained material (ZnO-SiO_2-C18) also has the form of white powder.

3.2.2.4 Fingermark collection

Latent fingermark collection, substrates, and donor selection were implemented according to the International Fingerprint Research Group guidelines for Phase 1 [12]. Six donors (four females: F1, F2, F3, F4, and two males: M1, M2) have been chosen to deposit fingermarks on several common non-porous and porous substrates: aluminium foil, beverage can, glass, glossy magazine cover paper, sticky side of the adhesive tape, and copy paper. Donors have been requested not to wash their hands for at least half an hour before the fingermark deposition. Otherwise, they were advised to behave as usual to provide natural fingermarks similar to a real-case one. Before fingermark deposition, donors were instructed to rub their hands together to homogenise the fingermark secretion across the fingertips and then to touch the substrate with the thumb, index, middle, and ring finger for 2-3 seconds with moderate pressure, comparable to the force they usually use for holding items. Collected fingermarks were aged for at least 24 hours in ambient conditions before further processing.

Additionally, one of the donors (M1) was asked to leave three types of fingermark on selected substrates to establish what components of fingermark (sweaty or oily) are most likely to interact with the tested material. To deposit a sweat mark (eccrine), the donor kept his hand wrapped in a plastic bag for

30 minutes next to the heater, then left a mark on the substrate as described above. The fatty fingermark (sebaceous) was formed when the donor rubbed his fingers against the forehead and neck and then left the accumulated substance on the substrate.

3.2.2.5 Fingermark development

A suspension of 1 mg mL^{-1} ZnO-SiO_2-Ph or ZnO-SiO_2-C18 particles in a water-ethanol solution (97:3, v/v) was investigated to develop latent fingermarks on non-porous and porous surfaces. The water as a carrier of developing agents has been chosen because of its user- and environment-friendly properties. Ethanol has been added to improve the dispersion of relatively hydrophobic particles in water. A given amount of particles was dispersed in the water-ethanol solution using an ultrasonication bath for 5 minutes. Samples containing fingermarks were submerged in the developer suspension for 5 minutes, then gently rinsed with distilled water to remove the excess of particles, dried in a stream of argon, and left in the air to evaporate the rest of the solvent. In the case of fingermarks deposited on adhesive tape, the immersion of the sample in the suspension caused the tape to roll, which due to the adhesive properties, did not allow for further processing. Instead of submerging the sample, a drop of ca. 1 ml of suspension was applied on the entire tape surface, followed by gentle rinsing with distilled water after 5 minutes and then drying in the stream of argon.

3.2.2.6 Time-gated imaging of samples

In the imaging process, the fingermarks deposited on colourful, luminescent, or reflecting surfaces developed with the luminescent agent possessing long-lived luminescence were observed using a time-gated imaging system (Figure 3.2). The setup consists of an ultraviolet radiation source (365 nm LED), a CCD camera, and a computer controller. All the equipment was placed in a box with black walls inside to minimise the amount of ambient light emitted from outside the UV light source.

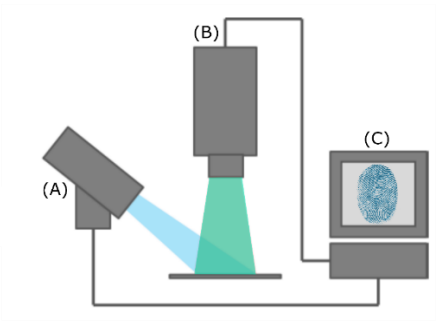

Figure 3.2 A scheme of time-gated imaging system: (A) excitation light source, (B) CCD camera, (C) computer

The object of interest may be imaged in two modes: in a normal mode, and a pulse mode also called time-gated (Figure 3.3). In the normal mode of imaging, the UV light illuminates the fingermark sample continuously. The computer-controlled CCD camera is turning on for a given period to collect the signal from the sample. The optimal length of sample exposition depends on the substrate and luminescent developer type and may vary depending on the desired contrast of fingermark to be obtained. In the time-gated mode, the examined sample is excited with short pulses of UV light radiation. During the excitation pulse, the photoluminescence intensity of both the developed fingermark and the background is increasing. The CCD sensor is switching on after a particular time from the end of the excitation pulse. The long-lived luminescence fingermark signal can be separated from the short-lived background luminescence by the precise control of the time that passes between the end of the illumination pulse and the time the CCD sensor starts to collect the signal. When the fingermark signal is weak, this illumination-collection sequence may be repeated multiple times, and the signal is summed up to increase the contrast of the fingermark.

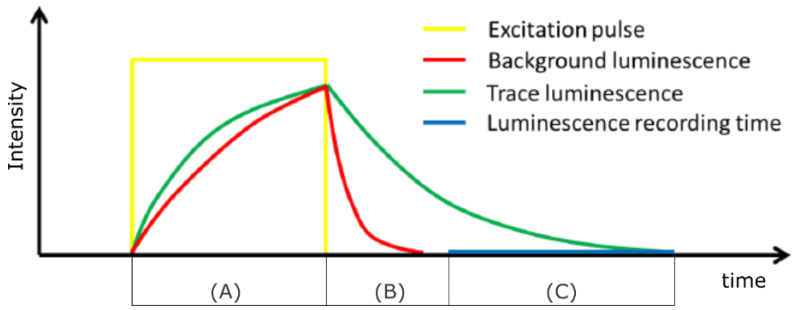

Figure 3.3 A schematic diagram of the imaging system working in the time-gated mode: (A) excitation pulse duration, (B) CCD sensor delay time, (C) luminescence recording time

To obtain the highest contrast between the fingermark ridges and the background, the duration of the individual imaging parameters A, B, and C has been optimised. For the investigated new ZnO-SiO_2 material, the best contrast had been obtained when the sample was illuminated with the UV light for 50 ms, the delay between the end of excitation and the beginning of luminescence signal collection was 0.8 ms, and the duration of recording the luminescence was 250 ms. The number of cycles for the illumination-collection sequence was set to 60 for an individual sample. With these parameters, it was possible to achieve optimal contrast and quality of the developed fingermark.

3.2.2.7 Comparison with benchmark enhancement methods

The comparative trials were conducted to verify the relative effectiveness of the new and conventional methods of latent fingermarks development deposited on colourful, reflecting, or luminescent substrates. Each trial compared the productivity of luminescent silica-based particles to one of the standard methods of latent fingermark development, such as Basic Violet 3, Small Particle Reagent, and luminescent powder dusting [13].

The study included aluminium foil, beverage can, magazine cover paper, and adhesive tape as substrate types. Each fingermark sample was cut in half after a print was deposited, as shown in Figure 3.4. One half was developed by immersing in 1% ZnO-SiO_2-Ph water-ethanol (97/3, v/v) suspension, and the other half was developed with one of the comparative methods.

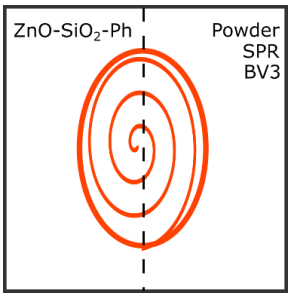

Figure 3.4 A diagram showing fingermark deposited on an individual substrate prepared to compare the fingermark development with ZnO-SiO_2-Ph particles and with other methods: powder dusting, SPR, and BV3

Basic Violet 3

Basic Violet 3 is a triphenylmethane dye that reacts with fats and lipids present in sebaceous constituents of sweat as well as with skin cells and other greasy components of the fingermark. This chemical process of fingermark staining results in the purple colour of ridges. It is mostly applied for non-porous and also adhesive surfaces. The procedure for fingermark enhancement recommended by CAST was applied [13]. First, the working solution of dioctyl sulfosuccinate was prepared. 1 g of DOSS was dissolved in 100 ml of demineralised water. Then, to prepare Basic Violet 3 dye concentrate, 0.5 g of BV3 was dissolved in 5 ml of ethanol. The BV3 working solution was made by mixing 4 ml of BV3 concentrate and 100 ml of DOSS working solution. Natural fingermarks deposited on the substrates mentioned above were developed by immersing the sample in a BV3 working solution for 10 seconds, then rinsed with tap water to remove the dye excess and dried in the gentle stream of argon.

Small Particle Reagent

SPR is a method of latent fingermark visualisation based on the interaction between hydrophobic tails of the surfactant surrounding molybdenum disulfide particles and the sebaceous components present in the fingermark residue. Metal salt deposited on fingermark results in dark grey visible ridges. SPR is usually applied to non-porous surfaces. The formulation was prepared according to CAST [13]. To prepare the final SPR working solution, first, the DOSS working solution of dioctyl sulfosuccinate was made. In a flask, 0.1 g of dioctyl sulfosuccinate was dissolved in 10 ml demineralised water. SPR concentrate was then prepared by dissolving 5 g of molybdenum disulfide in a solution of 42.5 ml water followed by the addition of 7.5 ml DOSS working solution. In the end, 50 ml of SPR concentrate was mixed with 450 ml of water. The natural fingermark samples were immersed in the SPR working solution for 30 seconds, then washed under tap water and dried in the gentle stream of argon.

Luminescent powder dusting

Powder dusting, which is still one of the most widely used fingermark enhancement processes, was applied as the last comparative development method of fingermark visualisation. It is based on the physical process where small particles of dry powder preferentially adhere to the oily components of fingermark secretion.

Fingermarks deposited on the substrates, as mentioned earlier, except adhesive tape, were developed with a luminescent magnetic powder. For effective powder deposition, the applicator with the powder stuck to it, forming a kind of cap, was passing over the examined sample as long as the clear fingermark ridges appeared. The gentle contact was only between the powder-cap surface and the analysed sample.

3.2.3 Results and discussion

This section will discuss the characteristic of the synthesised material, analysis of the interaction efficacy between fingermark and the luminescent particles, comparative analysis of fingermark development between the new material and benchmark methods.

Characterisation of the luminescent silica-based particles

The obtained luminescent silica particles unmodified and modified with long hydrocarbon chains and phenyl groups were characterised by scanning electron microscopy, fluorescence spectrometry, and FTIR.

The SEM images of ZnO-SiO_2, ZnO-SiO_2-C18, ZnO-SiO_2-Ph material (Figure 3.5) have shown the morphology of the synthesised particles. For unmodified and modified material, particles appeared spherical with comparable morphology. The particles were quite heterogeneous; however, their average size was in the range of 100 to 200 nm in diameter (determined by analysis of SEM images in ImageJ application).

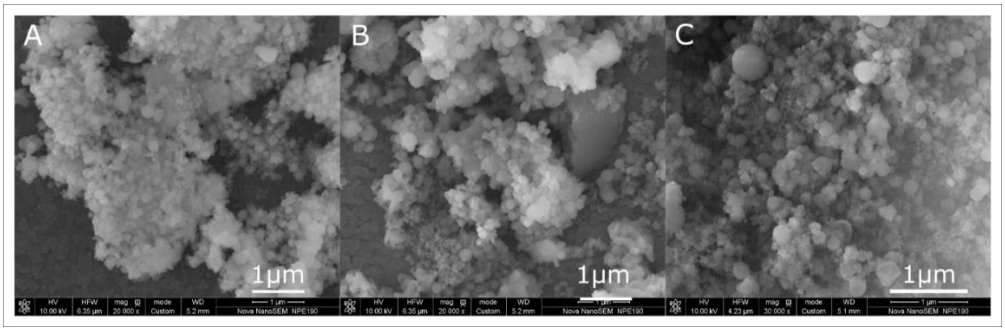

Figure 3.5 SEM images of synthesised ZnO-SiO_2 (A), ZnO-SiO_2-C18 (B), ZnO-SiO_2-Ph (C) particles

Due to the high polydispersity and fluorescent properties of the product, the results obtained in dynamic light scattering measurements were not reliable.

The white ZnO-SiO_2 powder can be freely dispersed in ethanol (Figure 3.6 A). Its photoluminescence properties are visually long-lived. Material excited with 365 nm ultraviolet light emits blue-white luminescence (Figure 3.6 B). After switching off the radiation source, a blue-green afterglow is still visible for a few seconds (Figure 3.6 C).

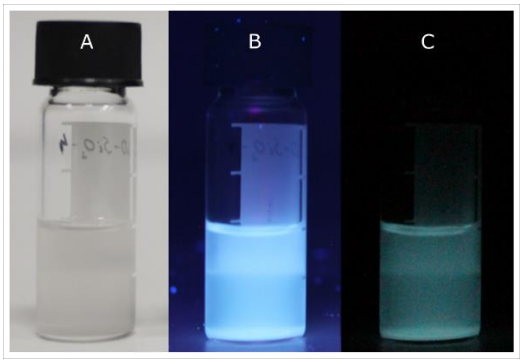

Figure 3.6 The 1 mg mL^{-1} ZnO-SiO_2 suspension in ethanol illuminated with white light (A), 365 nm UV light (B). Picture C shows the afterglow as the image was taken immediately after switching off the UV light lamp

Figure 3.7 shows the luminescence emission spectra of the ZnO-SiO_2, ZnO-SiO_2-C18, ZnO-SiO_2-Ph particles. The emission spectrum measured at 365 nm ultraviolet light excitation shows a broad emission band with a maximum at 415 nm (Figure 3.7 A). When the emission spectrum was measured 0.8 ms after the excitation decay, the maximum luminescence emission was shifted towards longer wavelengths with a peak at 510 nm (Figure 3.7 B). It is accordant with the observation of particles' luminescence after switching off the UV light (Figure 3.6 C). The shoulder observed at approx. 400 nm is related to the short-lived component. It is worth noting that organic moieties grafted on the particles' surface do not significantly influence the luminescent properties of the ZnO-SiO_2 particles.

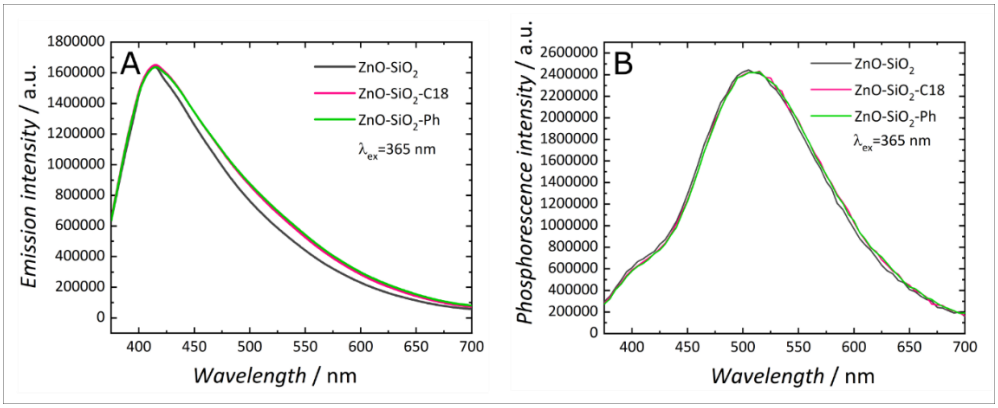

Figure 3.7 Emission spectra of ZnO-SiO_2, ZnO-SiO_2-C18 and ZnO-SiO_2-Ph particles registered under 365 nm UV light excitation: (A) stationary spectrum (B) time-gated spectrum measured 0.8 ms after excitation

According to the literature data, zinc oxide nanoparticles show UV emission centred at ca. 380 nm and a broad emission in the visible region at ca. 510-530 nm [14], [15]. The UV emission band is attributed to the radiative annihilation of the excitons [14], [16] and the broad visible emission is related to the electron-hole recombination generated by surface defects caused during the synthesis, zinc interstitials, and oxygen vacancies [10], [15]–[18]. The emission spectra of ZnO in the silica matrix, both modified and unmodified, showed the absence of a UV emission band and the presence of a broad visible emission band with the maximum at 415 nm. The blue emission may be associated with zinc oxide interstitial and surface defects.

Figure 3.8 shows the absorption spectra of ZnO-SiO_2, ZnO-SiO_2-C18, ZnO-SiO_2-Ph particles normalised at 500 nm. Mostly the scattering effect for all types of material is visible, and no absorption band from zinc oxide quantum dots was registered. The scattering light covers this relatively low signal. Also, no contribution from the organic groups has been recorded due to their small quantity in comparison with silica and zinc oxide quantum dots. It was also confirmed with the weak IR spectra of organic moieties.

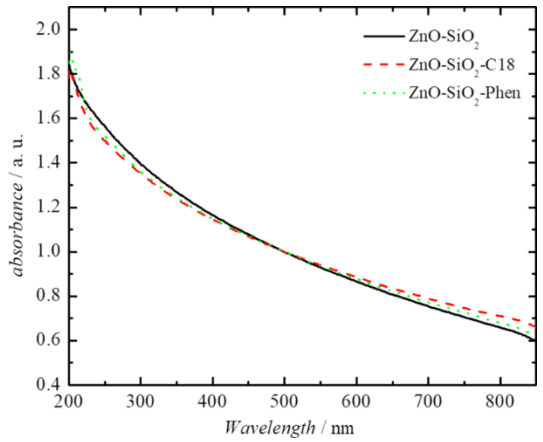

Figure 3.8 Absorption spectra for ZnO-SiO_2, ZnO-SiO_2-C18, and ZnO-SiO_2-Ph particle suspension in ethanol normalised at 500 nm.

The long-lived luminescence decay times have been examined at nanosecond and millisecond time range. The following model has been used for fitting the theoretical decay functions to the experimental data:

$$I(t) = I_{bg} + \sum_{i=1}^{n} \alpha_i \, exp\left(\frac{-t}{\tau_i}\right)$$

I_{bg} – contribution of the long decay process
α_i – percentage contribution of the individual process
τ_i – decay time of the particular process

The luminescence decays in the nanosecond range have been measured for unmodified (ZnO-SiO_2) and modified (ZnO-SiO_2-C18, ZnO-SiO_2-Ph) particles at 403 nm and 507 nm. The chosen wavelengths corresponded to the fluorescence and phosphorescence, respectively, and were dictated by the instrumentation.

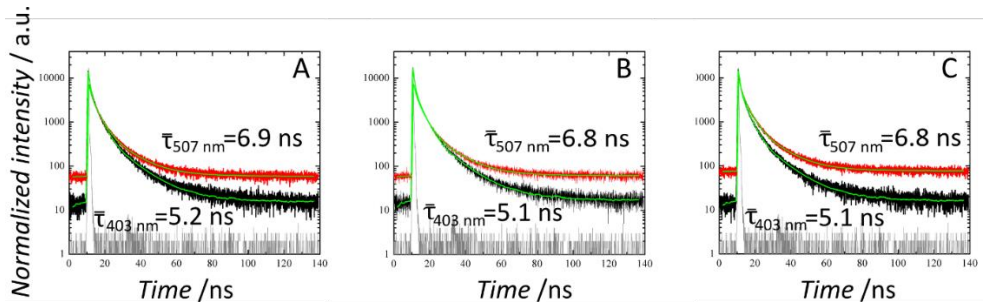

Figure 3.9 Fluorescence decay curves, normalised at maximum for (A) ZnO-SiO_2, (B) ZnO-SiO_2-C18, and (C) ZnO-SiO_2-Ph particles measured at 403 nm (–) and 507 nm (–) in the nanosecond range. The green line constitutes the fitted functions, and the grey line shows the instrument response function (IRF). The excitation wavelength is 379 nm

The conducted measurements showed that the decay times registered at 507 nm are significantly longer than those recorded at 403 nm (Figure 3.9 A, B, C). The background intensity I_{bg} fitted to the data collected at 507 nm is an order of magnitude higher than for the data collected at 403 nm (Table 3.1). Due to the complexity of the system, it is difficult to assign the fitted decay time to specific physical processes. Hence, the comparison of luminescent silica particles measured at various wavelengths was based on the average decay time ($\bar{\tau}$). This parameter have been calculated based on the fitted parameters according to the following formula

$$\bar{\tau} = \frac{\sum_{i=1}^{n} \alpha_i \tau_i^2}{\sum_{i=1}^{n} \alpha_i \tau_i}$$

The parameters of the fitted functions for all three samples have been collected in Table 3.1.

Table 3.1 Parameters of the functions fitted to the luminescence decay curves recorded for ZnO-SiO_2, ZnO-SiO_2-C18, and ZnO-SiO_2-Ph particles in the nanosecond range

	Sample	R^2	I_{bg} / a.u.	α_1 / %	τ_1 / ns	α_2 / %	τ_2 / ns	α_3 / %	τ_3 / ns	$\bar{\tau}$ / ns
403 nm	ZnO-SiO_2	0.9971	8.1	26.5	4.0	3.0	13.9	70.5	0.8	**5.2**
	ZnO-SiO_2-C18	0.9936	6.8	24.1	4.0	2.8	13.9	73.1	0.7	**5.1**
	ZnO-SiO_2-Ph	0.9922	8.2	25.7	4.0	2.8	13.9	71.5	0.8	**5.1**
507 nm	ZnO-SiO_2	0.9990	81.7	45.6	4.1	9.3	13.1	45.1	0.9	**6.9**
	ZnO-SiO_2-C18	0.9987	80.0	44.0	4.2	8.2	13.6	47.7	1.0	**6.8**
	ZnO-SiO_2-Ph	0.9989	81.0	43.3	4.2	8.8	13.2	47.9	1.0	**6.8**

No difference in decay times was observed for all three kinds of particles measured at a particular wavelength, though the decay times became longer when measured at a longer wavelength (Table 3.1). They were ca. 5 ns measured at 403 nm and ca. 7 ns measured at 507 nm.

The luminescence decays in millisecond range have been measured for ZnO-SiO_2, ZnO-SiO_2-C18, and ZnO-SiO_2-Ph particles at 400 nm and 510 nm (Figure 3.10), as the results for measurements conducted in longer timescale are of importance for time-gated imaging.

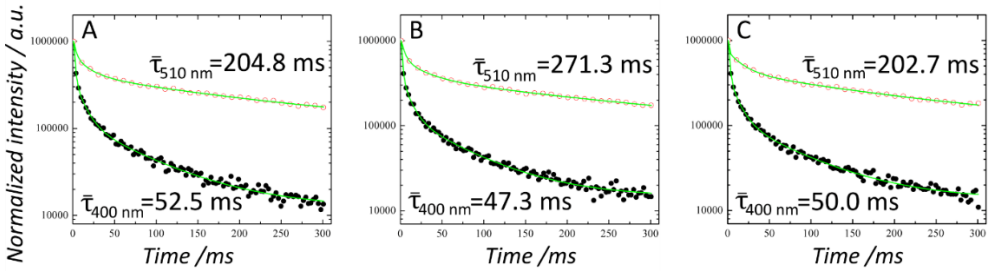

Figure 3.10 Fluorescence decay curves normalised to 1000000 for (A) ZnO-SiO_2, (B) ZnO-SiO_2-C18, and (C) ZnO-SiO_2-Phen particles measured at 400 nm (●) and 510 nm (○) in the millisecond range. The green line (—) shows the fitted functions. The excitation wavelength is 365 nm.

The theoretical decay functions have been fitted to the experimental data. As previously, for the longer wavelength (510 nm) recording, the registered decay times have been ca. 4 times longer than for measurement at 400 nm (Table 3.2). The average decay times at 400 nm were equal to 52.5 ms, 47.3 ms, and 50.0 ms for ZnO-SiO_2, ZnO-SiO_2-C18, and ZnO-SiO_2-Ph, respectively, whereas for measurement at 510 nm, the decay times were equal to 204.8 ms, 271.3 ms, and 202.7 ms, respectively. Similarly to the nanosecond measurements, among all kinds of particles, no significant differences in decay times measured at a particular wavelength have been observed. In millisecond rage analysis, the background intensity for measurements conducted at 400 nm is 4 to 7 times lower than for background intensity for the data collected at 510 nm.

Table 3.2 Parameters of the functions fitted to the luminescence decay curves recorded for $ZnO\text{-}SiO_2$, $ZnO\text{-}SiO_2$-C18, and $ZnO\text{-}SiO_2$-Ph particles in the millisecond range

	Sample	R^2	I_{bg} / a.u.	α_1 / %	τ_1 / ms	α_2 / %	τ_2 / ms	α_3 / %	τ_3 / ms	$\bar{\tau}$ / ms
400 nm	$ZnO\text{-}SiO_2$	0.9993	12371.0	71.2	1.7	20.7	11.3	8.1	77.7	**52.5**
	$ZnO\text{-}SiO_2$-C18	0.9990	14660.2	72.1	1.6	19.5	10.3	8.4	69.1	**47.3**
	$ZnO\text{-}SiO_2$-Ph	0.9993	13534.7	72.3	1.6	20.1	11.2	7.7	74.8	**50.0**
510 nm	$ZnO\text{-}SiO_2$	0.9989	93868.1	40.2	3.2	31.7	222.2	28.2	18.4	**204.8**
	$ZnO\text{-}SiO_2$-C18	0.9992	62114.8	45.6	4.8	30.1	296.7	24.4	28.4	**271.3**
	$ZnO\text{-}SiO_2$-Ph	0.9988	87846.1	52.4	0.8	24.7	218.5	22.9	18.1	**202.7**

Longer decay times obtained for measurements recorded at longer wavelengths indicated that long-lived processes are red-shifted in comparison to the short-lived ones. The average decay time for the particles measured at 510 nm is higher than 200 ms, and it can be supposed that the examined material possesses long-lived luminescence. The significant background intensity observed in all timescale measurements indicated the presence of additional long-lived processes in the system and that the overall luminescence lifetime may be longer than already measured. Above mentioned results stay in agreement with the spectra measurements, where the red-shift of the maximum peak for time-resolved spectra is observed (Figure 3.7).

The decay time measurements of the studied material have been additionally performed for the whole visible light spectrum using the time-gated imaging system (Figure 3.11).

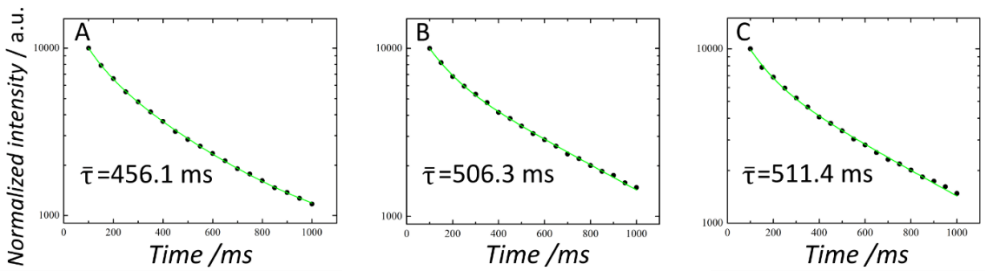

Figure 3.11 Luminescence decays normalised at the maximum for (A) $ZnO\text{-}SiO_2$, (B) $ZnO\text{-}SiO_2$-C18, and (C) $ZnO\text{-}SiO_2$-Phen. The green line (–) shows the fitted functions. The excitation wavelength is 365 nm

The theoretical functions have been fitted to the experimental data, whereby the background intensity I_{bg} has been fixed to zero (Table 3.3). The results showed biexponential decay. The average decay times for $ZnO\text{-}SiO_2$, $ZnO\text{-}SiO_2$-C18, and

ZnO-SiO_2-Ph were equal to 456.1 ms, 506.3 ms, and 511.4 ms, respectively (Figure 3.11 A, B, and C).

Table 3.3 Parameters of the functions fitted to the luminescence decay curves recorded for ZnO-SiO_2, ZnO-SiO_2-C18, and ZnO-SiO_2-Ph particles in the millisecond range for the whole visible spectrum of light

Sample	R^2	I_{bg} / a. u.	α_1 / %	τ_1 / ms	α_2 / %	τ_2 / ms	$\bar{\tau}$ / ms
ZnO-SiO_2	0.9997	0.0	60.8	119.6	39.2	566.7	**456.1**
ZnO-SiO_2-C18	0.9995	0.0	51.8	103.1	48.2	583.0	**506.3**
ZnO-SiO_2-Ph	0.9986	0.0	53.4	103.7	46.6	593.2	**511.4**

The decay times calculated for the individual types of particles do not differ significantly from each other, and these values are in agreement with the literature data [10]. It can be assumed that the surface modification of the particles with organic moieties does not affect their luminescent properties.

The composition of particles and capping moieties on the surface were identified with IR spectroscopy. The well-defined bands at 1062 cm^{-1} and 800 cm^{-1}, characteristic for asymmetric stretching vibrations and banding mode of Si-O-Si, respectively [19], were present in the spectra for all three samples ZnO-SiO_2, ZnO-SiO_2-C18, and ZnO-SiO_2-Ph. The shoulder at approx. 500 cm^{-1} can be associated with both the Zn-O bond [20] and the rocking vibration of Si-O-Si [21] (Figure 3.12 A). The additional peaks at lower frequencies 2963 cm^{-1}, 2924 $cm^{-1,}$ and 2854 cm^{-1} corresponded to the C-H stretching and were assigned to the vibrations of the methyl groups (-CH_2) in long alkyl chains [22] (Figure 3.12 B). This result confirmed that octadecyl groups were successfully grafted on the particles' surface. These bands were absent in the other spectra. The spectrum obtained for ZnO-SiO_2-Ph showed additional two characteristic peaks at 697 cm^{-1} and 1430 cm^{-1} associated with rocking vibrations of C-H and stretching vibrations of C-C bonds in the aromatic ring [23] (Figure 3.12 C, D). The presence of these peaks only in the ZnO-SiO_2-Ph spectrum confirmed the presence of the phenyl groups on the particles' surface.

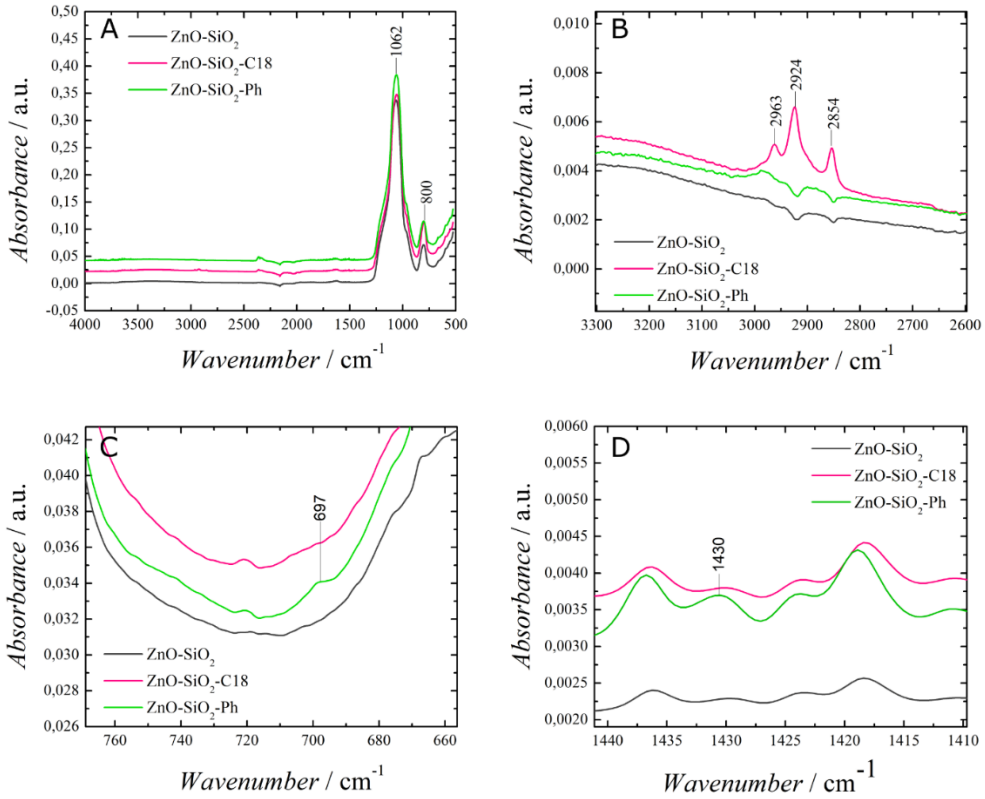

Figure 3.12 IR spectra of ZnO-SiO_2 (black), ZnO-SiO_2-C18 (pink), and ZnO-SiO_2-Ph (green). (A) Full spectra (Spectra were shifted to make the picture clear). (B, C, D) Selected fragments of spectra in high resolution

The analysis of LFM enhancement efficacy on selected substrates

The new luminescent ZnO-SiO_2 material modified with both phenyl groups or 18 hydrocarbon chains was applied to develop latent fingermarks deposited on a range of commonly encountered representative surfaces such as aluminium foil, beverage can, glass, magazine cover paper, adhesive tape, polypropylene foil (PP white and black plastic bag), and paper. The modification of particles with quantum dots allowed for visualisation developed fingermark despite the strong background luminescence. Initially, the working suspension containing 1 mg mL^{-1} of either ZnO-SiO_2-Ph or ZnO-SiO_2-C18 particles in water-ethanolic solution (97:3, v/v) was used for the enhancement process. The developed fingermarks have been imaged in the normal (fluorescence) and pulse mode. The results were collected in Figure 3.13 and Figure 3.14.

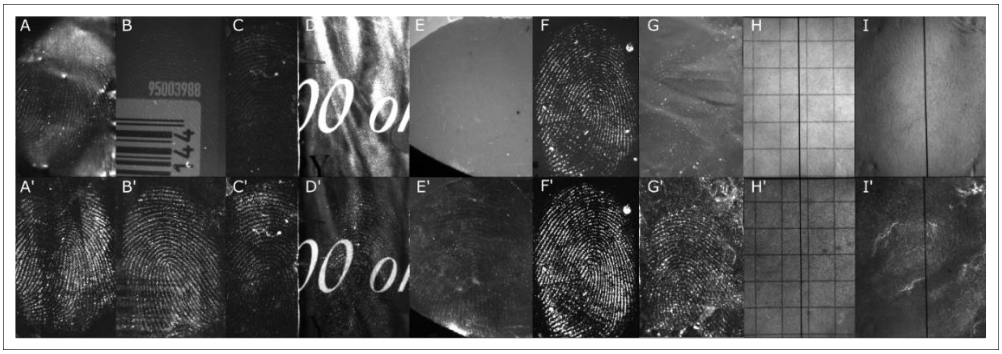

Figure 3.13 Samples of natural fingermarks developed with ZnO-SiO_2-Ph particles in water-ethanol solution (97:3, v/v) deposited on aluminium foil (A, A'), beverage can (B, B'), glass (C, C'), magazine cover paper (D, D'), sticky side of the adhesive tape (E, E'), black PP foil (F, F'), white PP foil (G, G'), notebook paper (H, H'), copy paper (I, I'). The images A-I have been recorded in the normal mode and the images A'-I' in the pulse mode

ZnO-SiO_2-Ph particles enable successive visualisation of the fingermarks on aluminium foil. The bright spots and reflections have been observed in the normal mode (Figure 3.13 A). Switching into the time-gated mode eliminated this interference and improved the contrast between the fingermark and the aluminium foil background (Figure 3.13 A'). A beverage can is a sample with a highly strong background luminescence. If observed in the normal mode, the fingermark is hardly visible (Figure 3.13 B); but switching into the pulse mode enables eliminating the interfering reflections and background fluorescence, which lead to the contrast increase between the fingermark and the substrate (Figure 3.13 B'). In the case of glass slides, fingermarks developed with ZnO-SiO_2-Ph particles enables visualisation in both normal and pulse mode (Figure 3.13 C and C'). Switching into the time-gated mode substantially increased the contrast between the fingermark ridges and the substrate. The next examined substrate was magazine cover paper. Paper is one of the most problematic surfaces to work with. Firstly, the paper usually possesses strong luminescence, which makes it problematic to image fingermarks employing conventional techniques based on fluorescent agents such as 1,2-Indanedione or 1,8-Diazafluoren-9-one (DFO). Secondly, its porous structure makes the powder dusting technique challenging to apply since the powder is likely to adsorb on both the background and the fingermark ridges. The fingermarks developed with ZnO-SiO_2-Ph particle suspension were impossible to visualise in the normal mode (Figure 3.13 D) due to the strong background luminescence, whereas switching into the pulse mode enables to image the fingermark ridges (Figure 3.13 D').

Another substrate, tough for latent fingermark development, is a sticky side of adhesive tape. It is problematic to work with for two reasons. Firstly, the sticky layer on one side of the tape excludes applying the powder dusting technique for technical reasons. Secondly, its strong luminescence may interfere with the luminescence of the developer used for fingermark enhancement. The use of ZnO-SiO_2-Ph water-ethanol suspension allowed introducing luminescent particles selectively on the fingermark. The effect of the preferential adherence of particles to the fingermark ridges can be assigned to lipophilic interactions between phenyl groups on particles' surface and fatty constituents of fingermark secretion. The strong adhesive tape luminescence hindered the fingermark imaging in the normal mode (Figure 3.13 E), while imaging in the time-gated mode yielded a good fingermark enhancement (Figure 3.13 E'). ZnO-SiO_2-Ph enables visualisation of the fingermarks on black PP foil. Fingermark imaged in the normal mode is relatively well visible (Figure 3.13 F), although using the pulse mode conduce to increase the contrast significantly (Figure 3.13F'). A quite strong luminescence effect has been observed for the fingermark deposited on white PP foil. Even though the fingermark was hardly visible in the normal mode (Figure 3.13 G), the time-gated imaging eliminated the background interference and resulted in well-visualised fingermarks (Figure 3.13 G'). The ZnO-SiO_2-Ph particles were also applied to develop fingermarks deposited on a problematic surface which is notebook and copy paper. These substrates possess high luminescence and quite porous structure. No visible fingermarks were obtained for these both items, even in the time-gated mode, where the background luminescence was eliminated (Figure 3.13 H', I'). The fingermark deposits (both oily and amino acids fraction) do not retain on the paper surface but are absorbed deep into the substrate in time [24]. The ZnO-SiO_2-Ph particles were too large to penetrate the paper structure and effectively interact with the fingermark components.

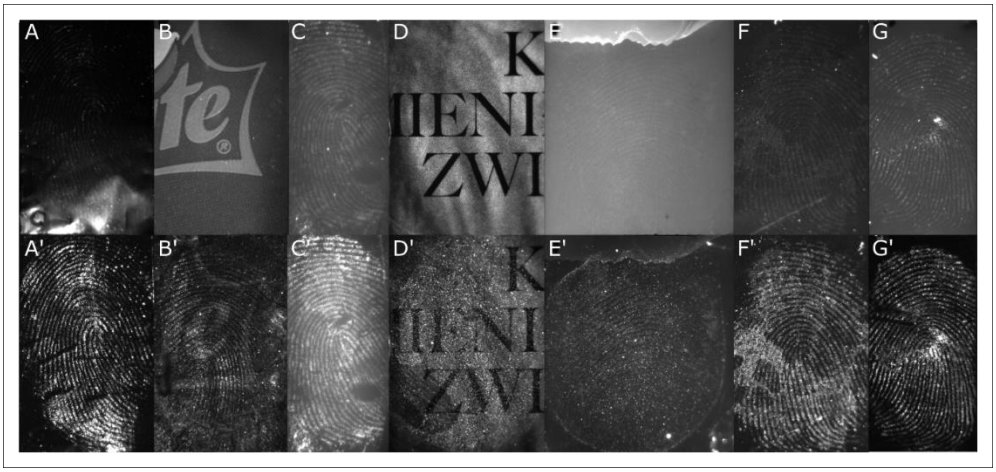

Figure 3.14 Samples of natural fingermarks developed with ZnO-SiO_2-C18 particles in water-ethanol solution (97:3, v/v) deposited on aluminium foil (A, A'), beverage can (B, B'), glass (C, C'), magazine cover paper (D, D'), sticky side of the adhesive tape (E, E'), black PP foil (F, F'), white PP foil (G, G'). The images A-G have been recorded in the normal mode and the images A'-G' in the pulse mode

ZnO-SiO_2-C18 particles effectively interact with the fingermark deposited on aluminium foil. Similar to the ZnO-SiO_2-Ph developer, in the normal mode of imaging, the fingermark is not clearly visible (Figure 3.14 A); some reflections of light have been observed that disturb the visualisation process. However, in the pulse mode, these reflections were eliminated, and a good contrast between the fingermark ridges and background was obtained (Figure 3.14 A'). The fingermarks deposited on the beverage can developed with ZnO-SiO_2-C18 suspension have been slightly visible in the normal mode (Figure 3.14 B); however, using time-gated mode lead to significant contrast enhancement (Figure 3.14 B'). The fingermarks deposited on glass substrate developed with ZnO-SiO_2-C18 particles, similarly to ZnO-SiO_2-Ph material, enabled visualisation in both normal and pulse mode (Figure 3.14 C and C'); however, applying the pulse mode lead to a significant contrast enhancement between the fingermark and glass slide. The fingermarks deposited on the magazine cover paper developed with ZnO-SiO_2-C18 particle suspension were impossible to visualise in the normal mode (Figure 3.14 D) due to the strong background luminescence. The time-gated imaging enabled increasing the contrast between the developed fingermark and paper background. (Figure 3.14 D'). However, the image showed some blurred fingermark ridges, related to the above-mentioned fact that the fingermark on the porous substrate does not retain entirely on the surface but may penetrate the depth and the interaction with the developing agent is inhibited.

For fingermarks deposited on the adhesive tape, obtained results were similar to those for ZnO-SiO_2-Ph particles. Due to the strong luminescence of the background, fingermarks were hardly visible when imaging in the normal mode (Figure 3.14 E), whereas switching into the pulse mode allowed to get rid of the luminescence of the background and increase the contrast between the fingermark and tape substrate (Figure 3.14 E'). In the case of black and white PP foil, developed fingermarks imaged in normal mode were visible, but also some interrupting reflecting spots have been recorded (Figure 3.14 F and G). This interference disappeared in pulse mode, and the contrast between fingermark and tape has been improved significantly (Figure 3.14 F' and G').

Most of the considered substrates possess strong luminescence themselves or strongly reflect the light. Therefore imaging samples developed with either ZnO-SiO_2-Ph or ZnO-SiO_2-C18 in the normal mode have weak or no effect. Applying the pulse mode for fingermark imaging increase the contrast between fingermark ridges and the substrate for both ZnO-SiO_2-Ph or ZnO-SiO_2-C18 material. However, for phenyl-modified particles, a more precise fingermark visualisation was obtained for all the samples. This observation suggests that phenyl groups can facilitate the more selective adsorption of the developer particles on the fingermark ridges than hydrocarbon modified particles. Taking into consideration the ridge quality enhancement and luminescent brightness, zinc oxide silica particles capped with phenyl moieties concluded to give the best performance. It was therefore selected for further latent fingermark enhancement analysis.

Comparison of LFM enhancement over the range of ZnO-SiO_2-Ph suspension concentration

To investigate what concentration of ZnO-SiO_2-Ph particle suspension would be optimal to obtain the best sensitivity, a series of fingermark development on various substrates at three different concentrations was performed. A scheme of a sample with fingermarks deposited for concentration comparison purposes is given in Figure 3.15. The dashed line shows the intersection of the mark before development. Results were evaluated by putting the cut sections to the original position and visualise the sample with the time-gated imaging system.

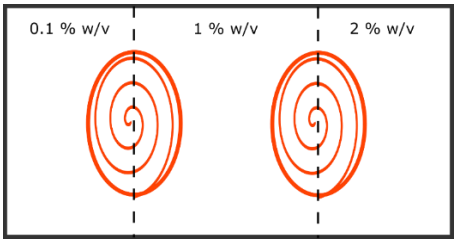

Figure 3.15 A diagram showing fingermarks deposited on an individual substrate prepared to compare the results of fingermark development at different concentrations of ZnO-SiO_2-Ph particles in water-ethanolic solution

Fingermarks deposited on aluminium foil, beverage can, coloured magazine cover paper, and adhesive tape have been developed with a ZnO-SiO_2-Ph particle water-ethanol suspension of 0.1, 1 and 2 % concentration. Each sample was cut, as mentioned above, and immersed in the suspension of proper concentration. For the adhesive tape sample, the development with a drop of the suspension was applied. Then, each sample was brought into the original position and imaged in normal and time-gated (pulse) mode. The results are presented in Figure 3.16 and Figure 3.17.

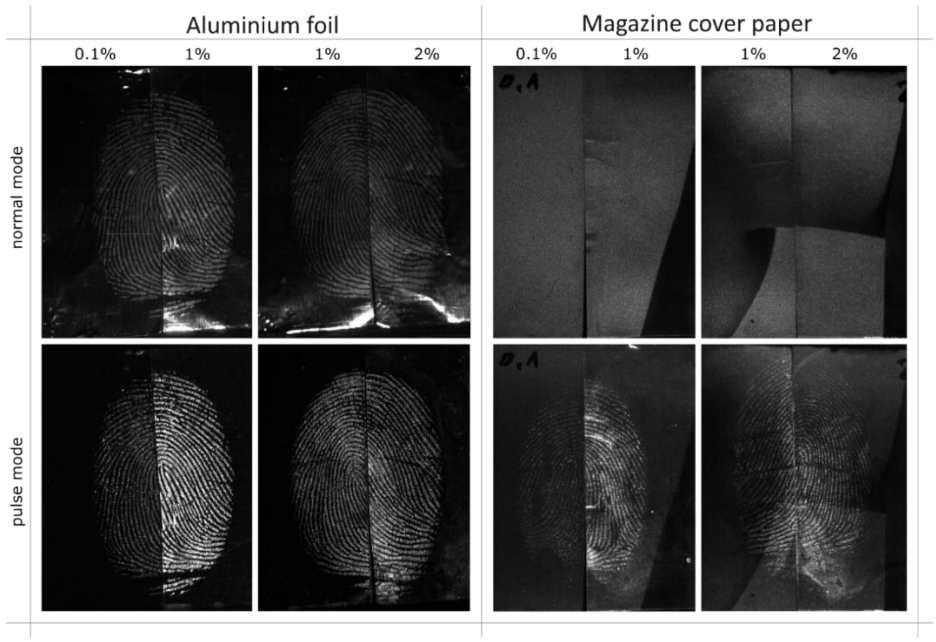

Figure 3.16 Samples of fingermarks deposited on aluminium foil and magazine cover paper developed with a suspension of ZnO-SiO_2-Ph particles under concentrations 0.1, 1, and 2 % imaged in UV light mode (upper row) and time-gated mode (lower row)

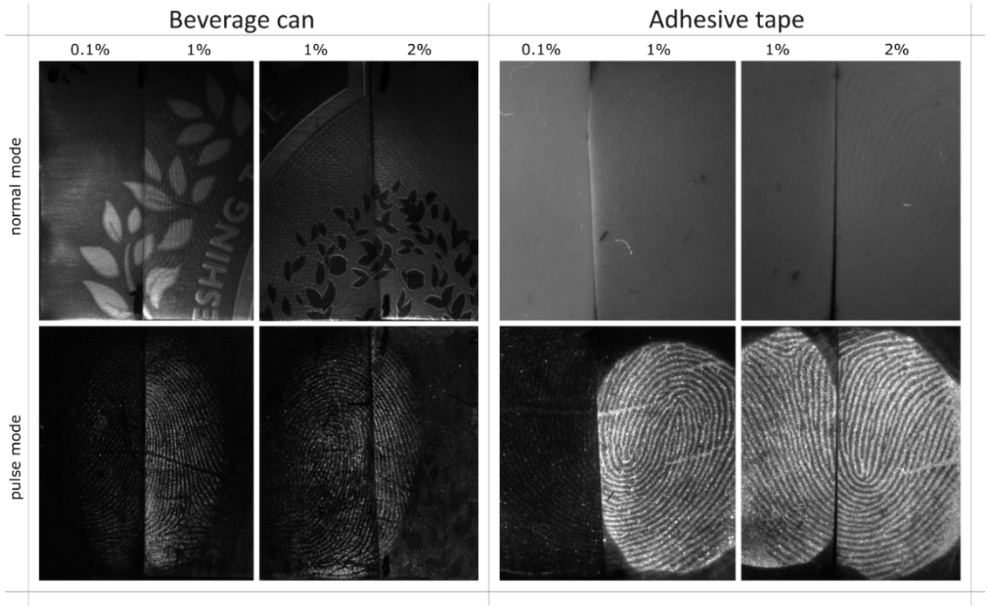

Figure 3.17 Samples of fingermarks deposited on beverage can and adhesive tape developed with a suspension of ZnO-SiO_2-Ph particles under concentrations 0.1, 1, and 2 % imaged in UV light mode (upper row) and time-gated mode (lower row)

The use of 0.1 % suspension of ZnO-SiO_2-Ph allowed for developing fingermarks on all processing substrates with satisfactory results. However, with the increase of particle concentration to 1 % or 2 %, more luminescent particles adsorbed on the fingermark ridges resulting in the efficient enhancement of fingermark development and better contrast between the mark and the background. Both 1 % and 2 % concentration provided outstanding ridge details quality. Since there is no significant difference between the fingermarks enhanced by these two concentrations, a concentration of 1 % was chosen for further processing. This formulation allowed for developing the fingermark with a high-quality second and third level of ridge details, such as ridge endings, bifurcations, pores, without background staining and background interference (Figure 3.18).

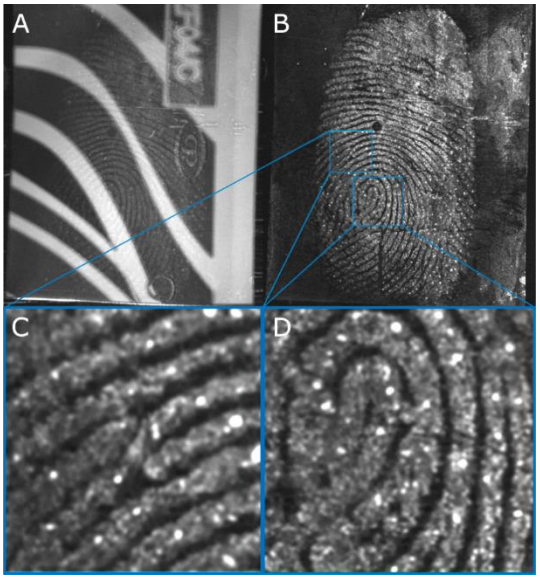

Figure 3.18 Natural fingermark deposited on a beverage can, developed with 1 % ZnO-SiO_2-Ph water-ethanol suspension, imaged in a fluorescence (A) and a time-gated (B) mode. The 2nd and 3rd level features are distinguished (C), (D).

Comparison of the interaction between ZnO-SiO_2-Ph particles and eccrine, natural and sebaceous fingermarks

The donor M1 was asked to deposit eccrine, natural, and sebaceous fingermarks on selected substrates: ITO, aluminium foil, beverage can, magazine cover, and adhesive tape to examine whether ZnO-SiO_2-Ph particles can interact sufficiently with fingermark secretion regardless of the composition of fingermark. All fingermark samples were developed with 1 % of water-ethanol (97:3, v/v) suspension. The developed eccrine, natural, and sebaceous fingermarks deposited on ITO were observed under the scanning electron microscope (Figure 3.19).

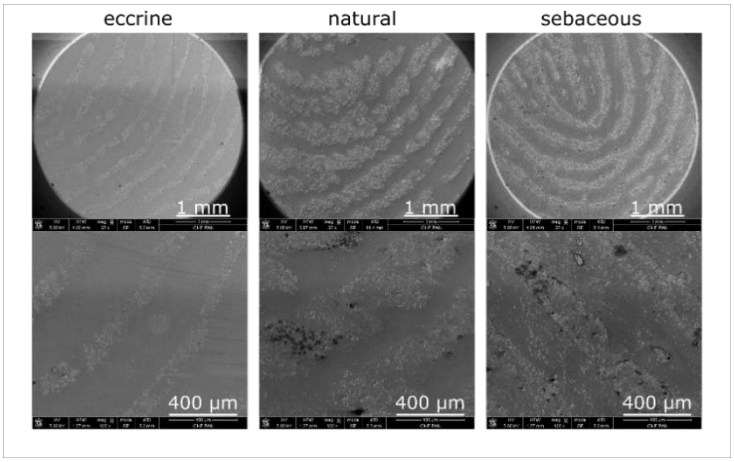

Figure 3.19 SEM images of 7 days old eccrine, natural and sebaceous fingermarks deposited on ITO and developed with 1 % ZnO-SiO_2-Ph in water-ethanolic suspension

SEM images for eccrine, natural, and sebaceous fingermark developed with ZnO-SiO_2-Ph suspension demonstrated that particles interact selectively with the fingermark residue. The particles covered the entire ridge of the mark for each type of fingermark. It is well visible in the magnified images. The hydrophobic properties of particles may play a crucial role in the fingermark development process. Hydrophobic particles interact with fatty components of the fingermark, forming a thick layer on its ridges. It is particularly visible in natural and sebaceous fingermarks. However, the eccrine mark also consists of specific oily components; hence the particles are deposited selectively on each type of mark.

A series of considered types of fingermarks were developed on surfaces such as aluminium foil, magazine cover paper, adhesive tape, and beverage can. The results are summarised below in Figure 3.20 and Figure 3.21. Images were taken in the normal and pulse mode.

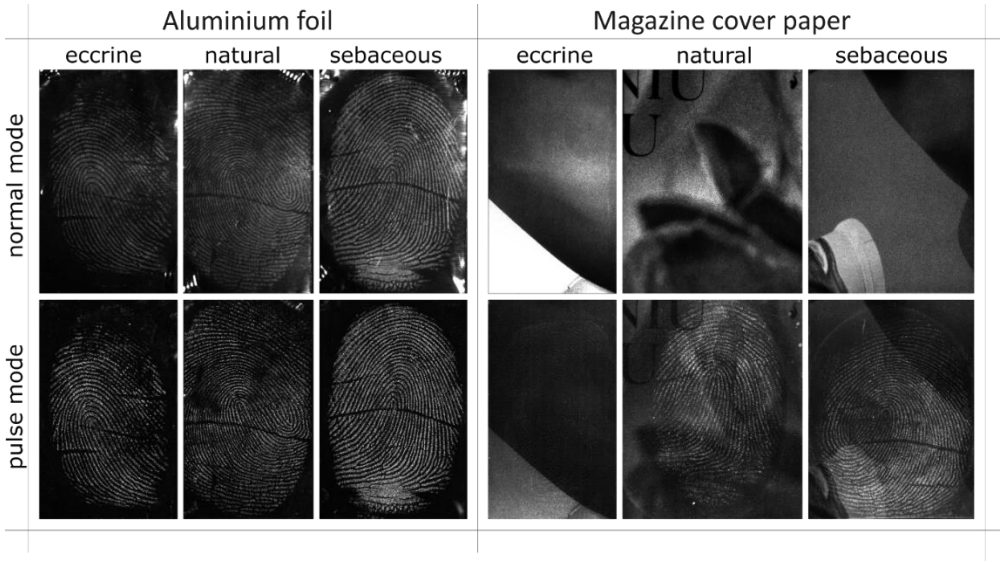

Figure 3.20 Eccrine, natural and sebaceous fingermarks on aluminium foil and magazine cover paper developed with 1 % ZnO-SiO_2-Ph in water-ethanolic solution (97:3, v/v) imaged in the normal mode (upper row) and pulse mode (lower raw)

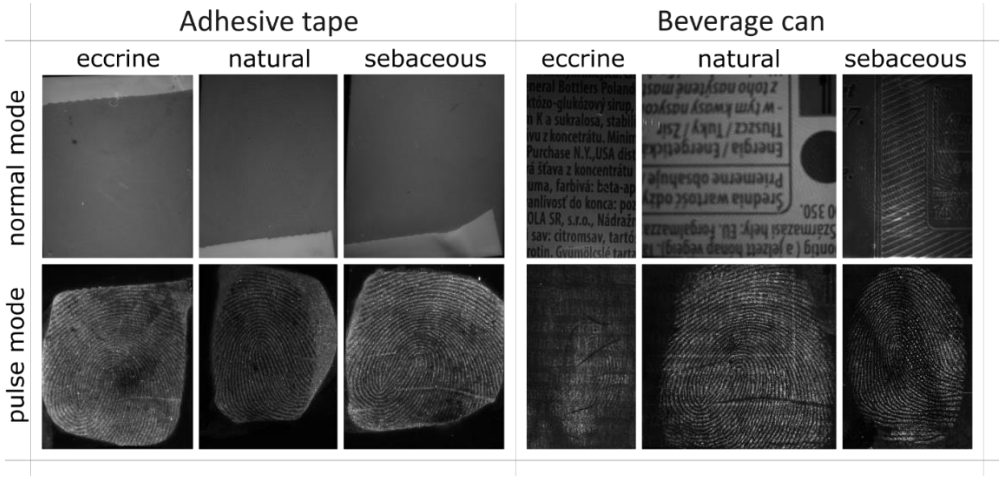

Figure 3.21 Eccrine, natural and sebaceous fingermarks adhesive tape and beverage can developed with 1 % ZnO-SiO_2-Ph in water-ethanolic solution (97:3, v/v) imaged in normal mode (upper row) and pulse mode (lower raw)

The above images showed that the new luminescent and lipophilic material could realise the development of natural and sebaceous fingermarks on each of the considered substrates with the high ridge details. As displayed in Figure 3.20, interactions between particles and typically eccrine fingermark are slightly weaker

on surfaces such as magazine cover paper. The low contrast of the image may be due to the small number of particles deposited on the mark ridges. The probable reason for this is a small number of fatty components in the eccrine residue as well as the porous structure of the substrate, which makes the fingermark residue difficult to contact with the particles. On the other hand, eccrine fingermarks deposited on adhesive tape, aluminium foil, or beverage can are of good quality. It can be concluded that the proposed luminescent lipophilic ZnO-SiO_2-Ph particles work efficiently with the entire spectrum of fingermark types on non-porous surfaces.
Time-gated imaging of developed fingermarks significantly increase the contrast between the mark and the background; therefore, well-defined ridge details were observed in these samples. Imaging fingermarks in the normal mode was ineffective due to the substantial background interference, especially for beverage can, magazine cover, and adhesive tape substrates.

Comparison of 6 donors' latent fingermarks developed on various substrates

An initial study has been completed to assess the capability and effectiveness of luminescent ZnO-SiO_2-Ph particles to enhance latent fingermarks deposited on selected substrates by various donors. For this, a series of fingermarks collected from six donors (two male, four female) on aluminium foil, beverage can, magazine cover paper, and adhesive tape was developed with 1 % ZnO-SiO_2-Ph suspension in water-ethanol solution (97:3, v/v) (Figure 3.22). The figure shows a comparison of fingermarks from 6 donors deposited on selected substrates, processed with 1 % ZnO-SiO_2-Ph water-ethanol suspension, and observed under 365 nm UV light in the time-gated mode. This mode of imaging is essential to eliminate surface interferences and improve fingermark contrast with the background, especially when the substrates are reflective or have autofluorescence. This study showed that ZnO-SiO_2-Ph particles are useful in fingermark enhancement, even on highly fluorescent or colourful surfaces. It can be observed the discernible friction ridge impressions on all considered non-porous substrates. An observable decrease in detection quality was found for the fingermarks deposited on magazine cover paper. However, even for these fingermark samples, the images still show ridge detailing. It indicates that obtained luminescent material is efficient even at a low concentration of sebaceous components of the fingermark.

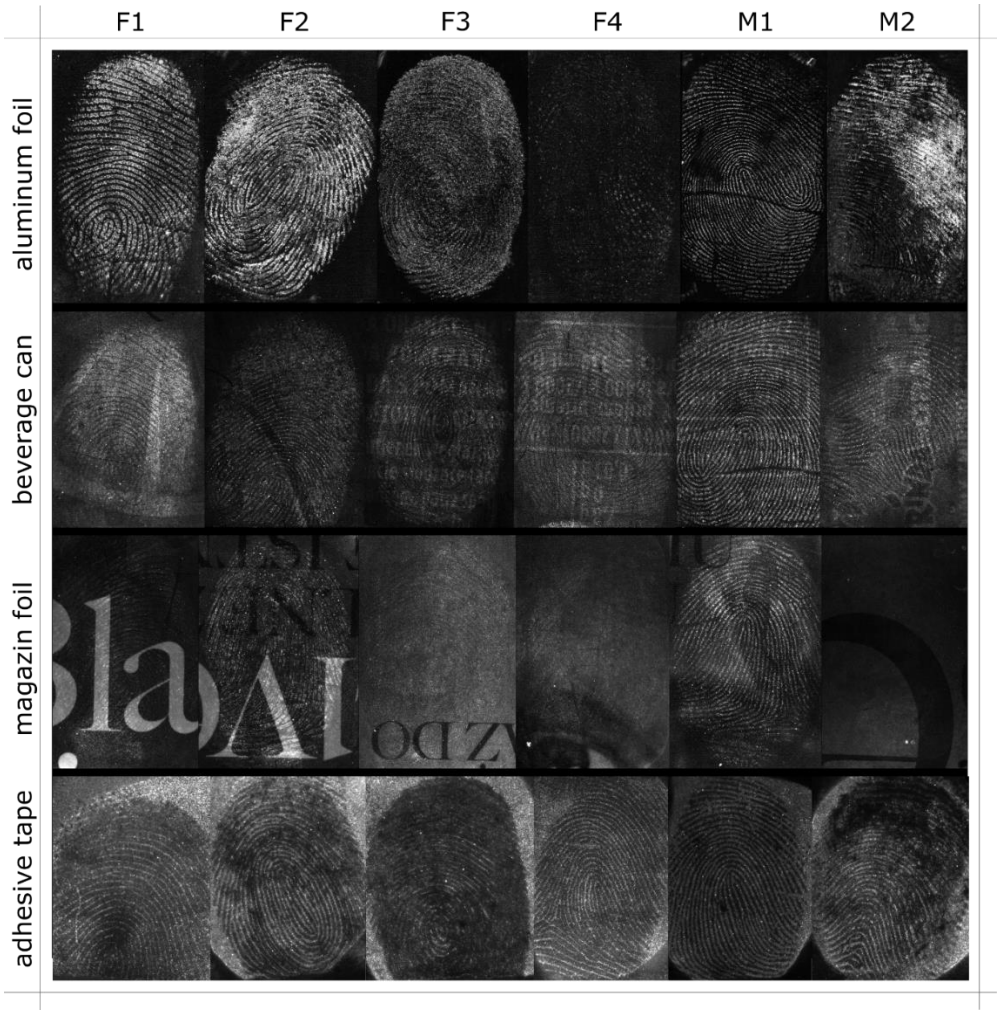

Figure 3.22 Latent fingermarks deposited by six donors (four female, two male) on aluminium foil, beverage can, magazine cover paper, and adhesive tape enhanced with a 1 % suspension of ZnO-SiO_2-Ph particles in water-ethanol solution (97:3, v/v) observed in the time-gated mode

Comparison of LFM enhancement over the depletion series

A trial of the natural fingermark depletion series was examined to assess how sensitive the ZnO-SiO_2-Ph particles are in contact with fingermark components. The depletion series was related to sequential impressions of depositing fingermarks using the same finger without recharging with secretion. The series was prepared for aluminium foil and beverage can substrates. In the series, each of the three donors (two males: M1, M2, one female: F1) was asked to deposit five fingermarks in a row

using the same finger on the appropriate substrate. Then each deposited fingermark was immersed into 1 mg mL^{-1} ZnO-SiO_2-Ph water-ethanol suspension for five minutes, then rinsed with water and dried in the stream of argon. The results were collected in Figure 3.23.

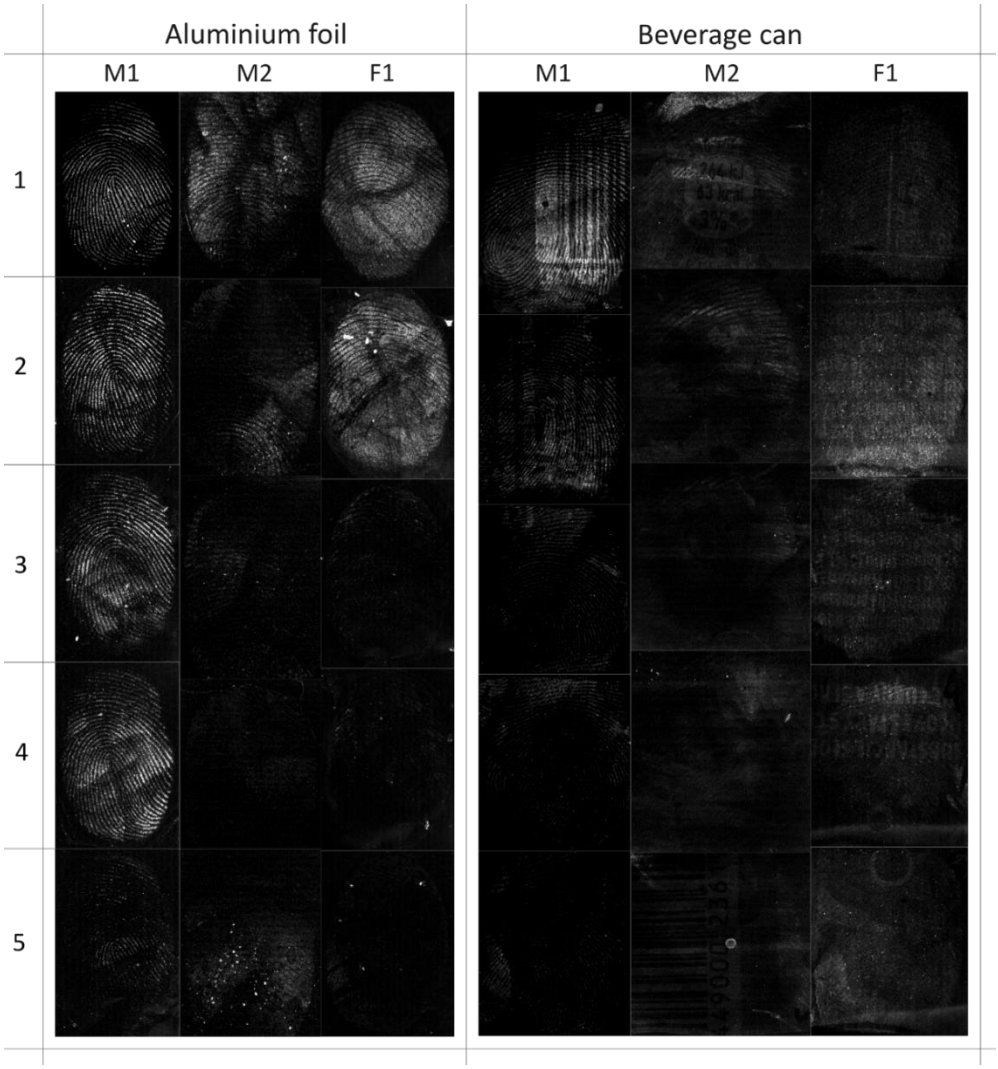

Figure 3.23 Depletion series of five fingermarks on aluminium foil and beverage can by three donors observed in the time-gated mode

Figure 3.23 shows a depletion series of fingermarks developed with ZnO-SiO_2-Ph particles. For both aluminium foil and beverage can, the ridge details were visible for all depletions of donor M1 and F1, whereas for donor M2 the assessed material provided well visible ridges only up to the third depletion. The fourth and

fifth depletion indicated less visible ridge details. It appears that the applied luminescent particles show good fingermark detection sensitivity on non-porous substrates; however, its effectiveness may depend on the donor variability.

Comparative analysis of the ZnO-SiO_2-Ph particles with conventional methods of latent fingermark visualisation

To be able to determine the efficacy of the ZnO-SiO_2-Ph particle development, a comparative study was performed between the new material and benchmark methods of fingermark detection.

Basic Violet 3

The comparison between the two methods was performed as follows. Each half of the split fingermark was developed with either ZnO-SiO_2-Ph or BV3 reagent, then halves of the samples were recombined, enabling a direct comparison of the fingermarks quality. Developed fingermarks were imaged with the CCD camera under UV light in the time-gated mode for ZnO-SiO_2-Ph particles and under white light for BV3 (Figure 3.24).

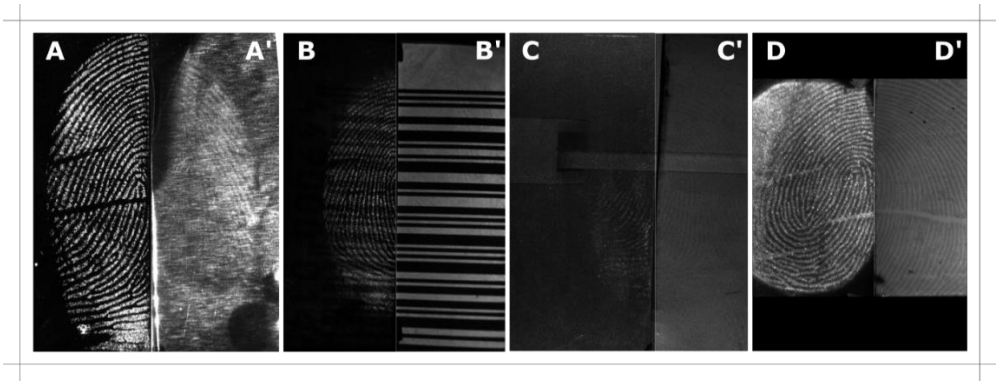

Figure 3.24 Comparison between latent fingermarks treated with 1% ZnO-SiO_2-Ph and viewed in time-gated mode (A, B, C, D) and BV3 viewed in white light (A', B', C', D') deposited on (A) aluminium foil, (B) beverage can, (C) magazine cover paper, (D) adhesive tape

Figure 3.24 displays that the better quality fingermark was obtained for ZnO-SiO_2-Ph particles on aluminium foil, beverage can, and adhesive tape in comparison to the BV3 development. The properties of these particles allow for visualisation without any interference of the substrate. In contrast, the fingermarks processed with BV3 and imaged under white light were hardly visible due to the light reflection

in the case of aluminium foil or the luminescence of the substrate in the case of colourful beverage can, which completely disrupted the registration of fingermark signal. For fingermarks deposited on magazine cover paper, development by both techniques did not give high-quality results, but ZnO-SiO_2-Ph formulation appeared to produce more visible ridge details of fingermark than BV3 agent. Fingermarks deposited on the adhesive tape showed the high quality of ridge details for both development techniques; however, the performance of luminescent particles resulted in better contrast with the background when compared to fingermarks processed with BV3.

Small particle reagent (SPR)

The split fingermark halves were developed with either ZnO-SiO_2-Ph or SPR reagent and then put back to the original position for the quality comparison assessment. Samples were examined with a CCD camera under the UV light in the delayed mode for luminescent particles and white light for SPR. The results of the fingermark enhancement on selected substrates are collected in Figure 3.25.

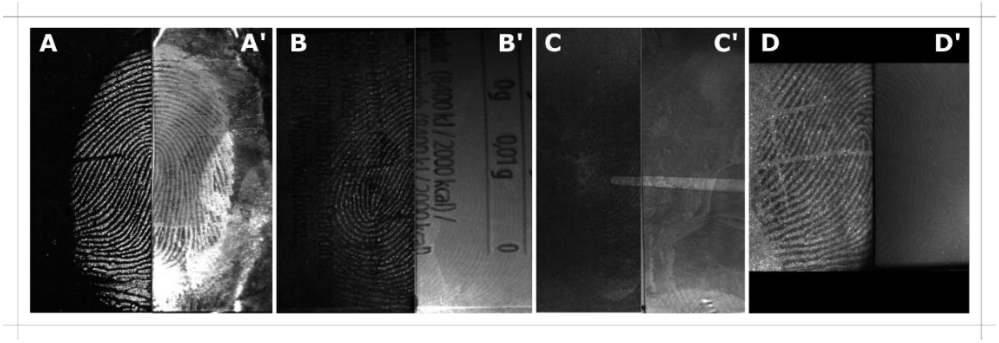

Figure 3.25 Comparison between latent fingermarks treated with 1 % ZnO-SiO_2-Ph and observed in time-gated mode (A, B, C, D) and SPR observed in white light (A', B', C', D') deposited on (A) aluminium foil, (B) beverage can, (C) magazine cover, (D) adhesive tape

There is a difference in the quality of detected ridge details when comparing zinc oxide silica particles and SPR reagent for each substrate. Luminescent particles developed considerably better quality marks than SPR on aluminium foil, beverage can, and adhesive tape. Visualising the SPR enhanced fingermark with white light disable to image the whole aluminium foil sample due to the interferences of the light reflected from the rough background. Similarly, imaging the marks deposited on colourful beverage can and adhesive tape encounters strong background luminescence. A further observation is that luminescent silica particles, as well as

SPR reagent, developed weak fingermarks on magazine cover paper. However, a bit better contrast was obtained for ZnO-SiO_2-Ph than for the SPR method.

Powder dusting

Comparison of fingermarks samples developed with luminescent powder dusting technique incorporated only aluminium foil, beverage can, and magazine cover paper substrates because this technique is not suitable for adhesive surfaces. Halves of the examined samples enhanced with either ZnO-SiO_2-Ph particles or dusted with the fluorescent powder were viewed under 365 nm UV light and recorded in time-gated mode and normal mode, respectively (Figure 3.26).

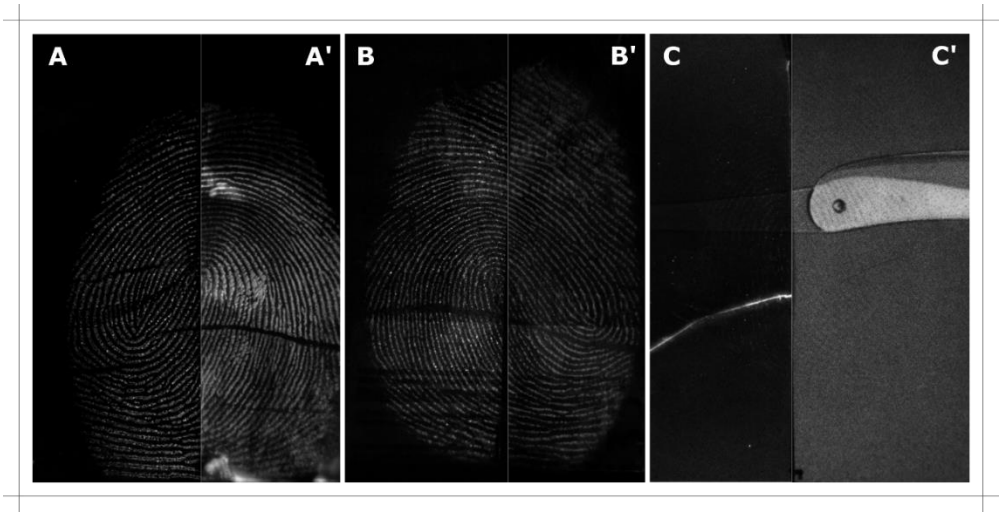

Figure 3.26 Comparison between latent fingermarks treated with 1% ZnO-SiO_2-Ph and viewed in time-gated mode (A, B, C) and luminescent powder viewed in the 365 nm UV light (A', B', C') deposited on (A) aluminium foil, (B) beverage can, (C) magazine cover

The quality of ridge details on aluminium foil and beverage can developed using ZnO-SiO_2-Ph reagent is more than or equal to that obtained using luminescent powder dusting. Both of these techniques performed well and enhanced fingermarks with very good quality. For fingermarks deposited on magazine cover paper, the comparison between ZnO-SiO_2-Ph particles and luminescent powder technique resulted in the poor quality of ridge details for both methods.

Fingermarks deposited on selected surfaces and developed with silica particles possessed long-lived luminescence resulted in a better quality of fingermark enhancement compared with other methods because surface printing and background fluorescence did not affect the visualisation process. The

development of fingermarks deposited on magazine cover paper varies significantly in quality for each method in comparison with other substrates. What affects the results is the fact that these methods do not work sufficiently for porous surfaces, where the access to the fingermark residue is slightly handicapped. Overall, ZnO-SiO_2-Ph formulation appears to develop fingermarks with the best ridge details quality for all considered substrates.

Practical application

The new ZnO-SiO_2-Ph material under optimised conditions is a valuable luminescent label for effortless fingermark development and may find a practical application in LFM visualisation on troublesome surfaces. Figure 3.27 exhibits the potential application of these particles to fingermark enhancement on a polymer ID card protected by fluorescent features. Due to the time-gated imaging, it was possible to separate the background fluorescence from the luminescence of the enhanced fingermark. Samples imaged in a white light illumination (Figure 3.27 1-4 A) exhibited no fingermark ridge details and no protective fluorescence patterns. When the illumination was changed to UV light (Figure 3.27 1-4 B), the protective features became visible; however, the signal collected by the CCD camera came mostly from the strong background fluorescence, which entirely covered the weaker luminescence of the fingermark. Switching the imaging system to the time-gated mode allowed for collecting the luminescence signal mainly from the fingermark ridges (Figure 3.27 1-4 C) since the decay time of the background luminescence is significantly shorter than the decay time of the luminescent particles deposited on fingermark ridges. Luminescent ZnO-SiO_2-Ph particles selectively adsorbed on fingermark deposits produced the clear fingermark pattern image.

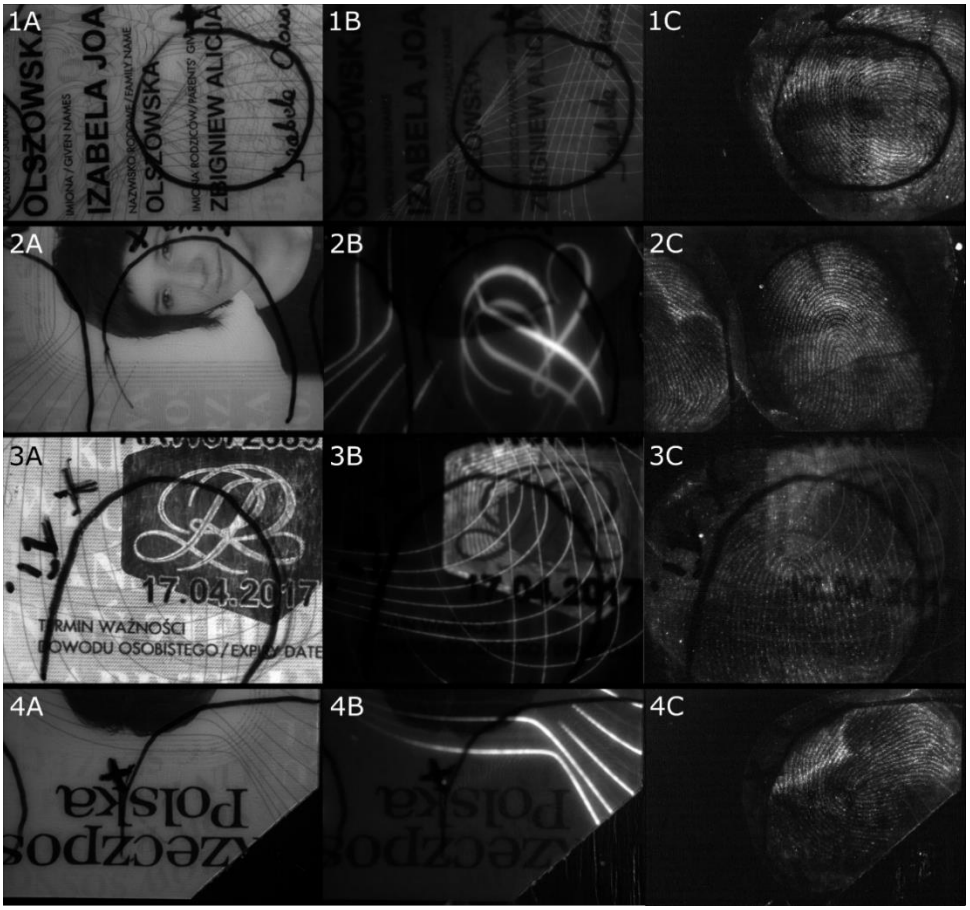

Figure 3.27 Natural fingermarks deposited on an ID card revealed with 1% ZnO-SiO_2-Ph water-ethanol suspension (97: 3, v/v). Imaging in the normal mode under white light (1-4 A), under ultraviolet light (1-4 B) and in the time-gated mode with the 800 μs delay of collecting signal (1-4 C)

3.2.4 Conclusions

A detailed study of the synthesised luminescent lipophilic particles showed the potential of the novel material for latent fingermark detection on various surfaces of forensic interest. Silica particles with immobilised zinc oxide quantum dots have been synthesised by a reverse microemulsion method and then modified by grafting phenyl groups or 18-carbon aliphatic chains. IR spectroscopy analysis confirmed the presence of both zinc oxide and silica structures, as well as organic moieties covalently attached to the silica layer. Spectrofluorimetric measurements

indicated that the material possesses luminescent properties. When excited by the light of 365 nm wavelength, particles emit visible blue light and additionally show long-lived luminescence with an average decay time of ca. 0.5 ms.

The luminescent material allowed for developing latent fingermarks deposited on non-porous substrates such as glass, aluminium foil, beverage can, polypropylene foil, magazine cover paper, and adhesive tape without background staining. However, the luminescent particles are not suitable for fingermark detection on porous surfaces such as paper due to their size and inability to penetrate into the structure of the substrate. Particles were successfully deposited on the fingermark residue via the simple wet method in which the sample was immersed in the water-ethanol suspension, making this method advantageous for two reasons. The first is that the direct interaction between the particle and fingermarks' deposit has taken place, which has no destructive effect on the fingermark pattern; in contrary to the dusting method in which the powder is deposited mechanically with the brush so that the fingermark ridges damage may occur. The second is that the non-toxic carrier solvent in the form of water with a small addition of ethanol was applied, eliminating the usage of volatile, toxic organic solvents and thus making this method user- and environmentally friendly.

The use of lipophilic silica particles with ZnO QDs makes it possible to obtain a multifunctional material. On the one hand, it can selectively interact with the fingermark constituents resulting in a clear fingermark image. On the other hand, due to the long-lived luminescence of ZnO QDs it can relevantly increase the contrast between the fingermark and the luminescent or reflective background.

In order to improve the quality of fingermark development, the concentration optimisation trial has been undertaken. The results demonstrated that 1 % ZnO-SiO_2-Ph water-ethanol suspension was adequate to obtain highly loaded fingermark ridges sufficient to visualise clear mark with essential details. The natural latent fingermarks of several donors deposited on various common surfaces have been efficiently enhanced with the ZnO-SiO_2-Ph particle suspension. A comparative evaluation of fingermarks deposited on these surfaces showed that marks developed with ZnO-SiO_2-Ph particles gave beneficial results. The particles showed selective affinity to the fingermark deposits, not to the background on each surface; however, high contrast and clear ridge details were observed on non-porous surfaces rather than on porous such as magazine cover paper or paper. It is worth noting that this material is possible to apply for the latent fingermark development on the tough substrate, which is the sticky side of the adhesive tape.

The efficiency of the new material was also evaluated in the comparative trial with commonly used reagents such as Basic Violet 3, SPR, or fluorescent powder.

This analysis showed that new luminescent particles, in most instances, developed fingermarks more successfully or comparatively to the other studied methods and that the interference from the background was overcome, unlike the BV3 or SPR reagents. The depletion series trial demonstrated the quite high sensitivity of particles, which interacted with fifth depletion fingermark deposits; however, this sensitivity was also donor-dependent. Due to the time-gated measurements enabled latent fingermark visualisation on reflective and luminescent substrates, the new material was effectively applied to develop latent fingermarks on the substrate having UV-active protected pattern.

In conclusion, the modified ZnO-SiO_2 particles have the potential to detect latent fingermarks on various tough surfaces that exhibit interfering background luminescence.

3.3 Upconverting particles with a silica shell

3.3.1 Introduction

As mentioned in Chapter 3.1, techniques of fingermark development based on photoluminescence of a sensitising agent are an essential tool in forensic sciences. Among various luminescent reagents, also upconverting nanoparticles are increasingly used in fingermark visualisation [25]–[30]. It is due to their physical and chemical properties such as relatively small size, large surface area, high fluorescence intensity, large anti-Stokes shifts, sharp emission lines, multi-coloured emissions, and photochemical stability [30]–[32]. In general, as described in Chapter 1.8, the upconversion phenomenon is based on the optical process during which the material absorbs two or more low-energy photons, followed by the single high-energy photon emission [33]. The result is the absorption of longer excitation wavelength (e.g. infrared radiation) and the emission of a shorter-wavelength photon (e.g. in visible radiation region). The widely studied upconversion materials, with the application in forensic science, are lanthanide-doped UCNPs [28], especially $NaYF_4$:Yb,Er as one of the most efficient upconverting crystals [34], [35].

One of the main advantages is that UCNPs possess large anti-Stokes shifts. Particles excited with near-infrared light emit strong visible luminescence [30], [36]. In most natural surfaces or consumer products, the upconversion is rare. Some troublesome surfaces such as multi-coloured and patterned exhibits quite often

contain dyes, inks, or security marks emitting broadband luminescence. In this case, visualising fingermarks using conventional luminescent techniques utilising ultraviolet or visible excitation radiation results in a lack of contrast between the labelling agent and the background on which the fingermark is deposited [29], [37]. Whereas, excitation of the substrate with low energy NIR radiation erases the autofluorescence of the substrate as well as the background interference and induce the visible light emission of the sensitised fingermark that leads to an increase in optical contrast and detection sensitivity [28].

The other merit of UCNPs is that a laser, as a source of IR excitation radiation, emits relatively low energy, which is less harmful to DNA in fingermark residue, human skin, or eyes, unless the focusing lens is used, compared to ultraviolet radiation [30]. However, IR lasers employed to fingermark visualisation may be destructive to some types of surfaces, such as polymer thin films, causing their shrinking or melting [37].

Also, the size and shape of UCNPs can be controlled during the synthesis, and a nanoparticle surface modification can be easily performed in the process of silica coating or organic moieties grafting, which is important from the fingermark enhancement point of view. Surface functionalisation with a layer of lipophilic groups (e.g., phenyl group or long hydrocarbon chains) may lead to an increase in the selective affinity to fingermark ridges as well as a rise of upconversion efficiency [32]. Commercial UCNPs are usually not uniform in size, ranging from 0.2 to 2 μm, and in shape. Therefore, particles could not adequately cover the fingermark deposit, causing background staining, and also some specific features like sweat pores may be undetected, leading to detection sensitivity decrease [25], [30]. Besides, UCNPs for fingermark development are mostly deposited with the powder dusting technique [25], [28]–[30], [37]. As this application may be destructive for fingermark ridges, small UCNPs with uniform size and shape, high upconversion efficiency, strong luminescence, and excellent affinity to fingermark residuals are still desirable.

This section discusses two approaches to monodispersed, hexagonal $NaYF_4$:Yb,Er crystals synthesis. The first one is based on a hydrothermal method with sodium citrate as a shape and size modifier in an aqueous solution. The second approach concerns a solid-liquid-thermal-decomposition (SLTD) method with sodium difluoride as sodium and fluoride precursors and oleic acid together with 1-octadecene as a liquid phase. UCNPs obtained from both syntheses were coated with silica and further modified with either phenyl groups or long hydrocarbon chains to give them lipophilic properties facilitating the interactions with fingermark residuals. Also, in this section, the results of the UCNPs application to latent fingermark visualisation on non-porous and porous surfaces are presented. The NIR

luminescent UCNPs excited with 980 nm infrared laser indicate strong emission in the green region of visible light. The developed fingermarks were visualised with either a CCD camera or an SLR camera with an IR filter. A scheme of the fingermark development process and imaging is shown in Figure 3.28. The results of the material examination are also discussed in this section, including UCNPs characteristics, affinity to fingermark ridges, the efficiency of fingermark imaging on various backgrounds, and comparison with conventional methods of visualisation.

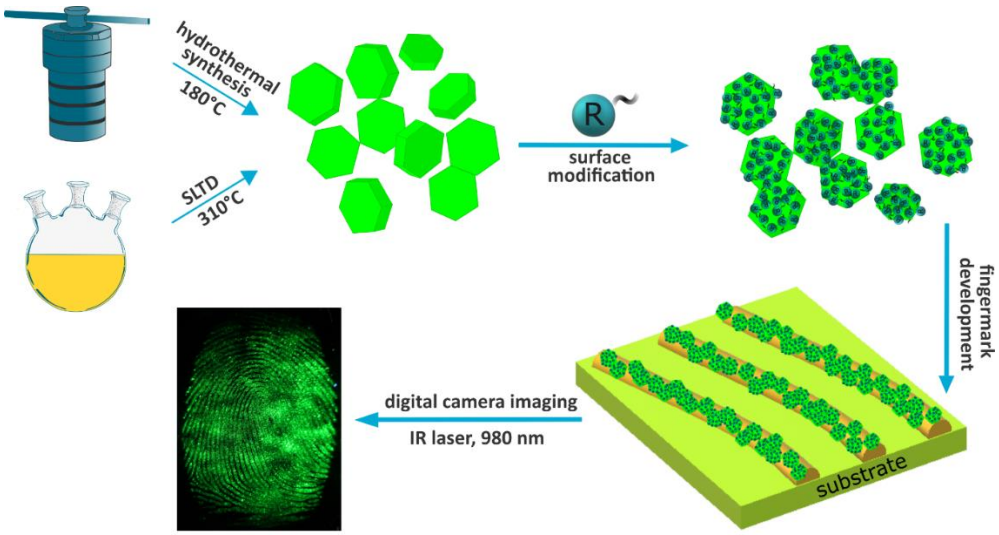

Figure 3.28 Schematic presentation of fingermark detection with surface-modified $NaYF_4$:Yb,Er UCNPs obtained in two different synthesis

3.3.2 Experimental

3.3.2.1 Chemicals

The following reagents were used for the synthesis of β-$NaYF_4$:Yb,Er upconverting crystals and surface modification: yttrium (III) chloride (anhydrous, YCl_3), ytterbium (III) chloride (anhydrous, $YbCl_3$), and erbium (III) chloride (anhydrous, $ErCl_3$) were purchased from Apollo Scientific. Yttrium oxide (99.99 %), ytterbium oxide (99.9 %), erbium oxide (99.99 %), ytterbium(III) acetate hydrate (99.95 %, $Yb(CH_3COO)_3$), yttrium (III) acetate hydrate (99.9 %, $Y(CH_3COO)_3$), erbium (III) acetate hydrate (99.9 %, $Er(CH_3COO)_3$), 1-Octadecene (for synthesis, ODE), sodium hydrogen

difluoride (98 %, $NaHF_2$), tetraethoxysilane (≥ 99.0 %), triethoxyphenylsilane (98 %), poly(vinylpyrrolidone) with average molar mass of 40 kg mol^{-1} (PVP-40), were obtained from Sigma-Aldrich. Sodium fluoride (analytical grade), trisodium citrate dihydrate (analytical grade), and ethanol (anhydrous, 99.8 %) were purchased from POCH. Methanol (analytical grade) and aqueous ammonia (28-30 %) were acquired from Merck. Octadecyltriethoxysilane (95 %) was purchased from Fluorochem, oleic acid (pure) was obtained from Chempur and toluene (anhydrous, 99.8 %) from Alfa Aesar. RO/DI water was used for all the experiments. All reagents were used as received.

3.3.2.2 Synthesis of β-$NaYF_4$:Yb,Er particles

Hydrothermal synthesis of β-$NaYF_4$:Yb,Er particles

The hexagonal β-$NaYF_4$:Yb,Er upconversion particles (UCPs) with a molar ratio of rare-earth ions (RE^{3+}, Y^{3+}:Yb^{3+}:Er^{3+}) equal to 80:17:3 were synthesised via the hydrothermal method [38]. First, yttrium, ytterbium, and erbium chlorides were prepared by reacting the appropriate rare earth metal oxides with 10 % hydrochloric acid at an elevated temperature until the acid had entirely evaporated and white powder was formed. Then, the 0.2 M rare earth chloride stock solution was prepared by dissolving 0.3280 g YCl_3, 0.9975 g $YbCl_3$ and 0.1724 g $ErCl_3$ in 10.5 ml of water. The stock solution was subsequently added into 20 ml of an aqueous solution containing 2 mmol (0.5882 g) of sodium citrate (molar ratio of citrate to RE^{3+} - 1:1). The mixture was stirred for 30 minutes at room temperature. After this time, 30 ml of an aqueous solution containing 25 mmol of NaF (1.05 g) was added into the reaction solution, and the mixture was stirred for 10 minutes. In the next step, the reaction mixture was transferred into a teflon vessel, which was then put into a stainless steel autoclave, sealed and placed in an oven. The reaction was held at 180 °C for 24 hours. After this time, the vessel was cooled down to room temperature, and the precipitate was centrifuged at 10 000 rpm for 15 minutes. The obtained material was washed with ethanol and water in sequence and dried in the air at 80 °C for 12 hours. The obtained upconversion particles were labelled as β-$NaYF_4$:Yb,Er-1. In order to obtain crystals with an appropriate size, shape, and luminescence intensity strong enough for latent fingermark development, the synthesis was repeated for the following citrate to RE^{3+} molar ratios: 2:1, 1:2, 1:4, 1:8. Also, to verify if there is any difference in the material properties, the particles were synthesised with the molar ratio 1:1 of citrates to rare-earth ions, employing

the chlorides directly from the supplier instead of chlorides prepared from corresponding oxides.

Solid-liquid-thermal-decomposition method of β-$NaYF_4$:Yb,Er particles synthesis

The β-$NaYF_4$:Yb,Er upconversion particles were synthesised via a solid-liquid-thermal-decomposition method [39]. To obtain 1 mmol of a final product, 0.8 mmol of $Y(CH_3COO)_3$ (0.2128 g), 0.18 mmol of $Yb(CH_3COO)_3$ (0.063 g), and 0.02 mmol of $Er(CH_3COO)_3$ (0.0069 g) were mixed with 8 ml of oleic acid and 12 ml of 1-octadecene in a 100 ml three-necked round-bottom flask. The mixture was first degassed with argon for 10 minutes, then heated to 180 °C under reflux in the argon atmosphere and continuously stirred for 20 minutes until the solution became optically clear. Then, the reaction mixture was cooled down to room temperature naturally, prior to the addition of 2 mmol of $NaHF_2$ (0.124 g). The flask was then resealed, heated to 250 °C under reflux and argon flow, and stirred for 30 minutes. After that, the temperature of the reaction mixture was increased to 310 °C with vigorous stirring for 60 minutes. Subsequently, the system was left to cool down to room temperature. The addition of ca. 25 ml of ethanol precipitated a product. The material was then collected by centrifugation at 9 000 rpm for 5 minutes, washed with both cyclohexane and ethanol three times, and finally dried in the air at 55 °C for 12 hours. The obtained material was labelled as β-$NaYF_4$:Yb,Er-2.

3.3.2.3 Surface modification of upconverting particles

β-$NaYF_4$:Yb,Er-1 upconverting particles were coated with silica layer and then modified in the process of grafting with reactive organic moieties such as 18 hydrocarbon chains and phenyl groups. Whereas β-$NaYF_4$:Yb,Er-2 upconverting particles were coated with a silica shell and functionalised only with phenyl groups via the grafting process. The choice of lipophilic moieties for surface modification resulted from an interaction analysis between fingermark residuals and modified particles characterised in Chapter 2.

Silica coating of β-$NaYF_4$:Yb,Er-1 and β-$NaYF_4$:Yb,Er-2 particles

The procedure of coating both the β-$NaYF_4$:Yb,Er-1 and β-$NaYF_4$:Yb,Er-2 upconverting particles with a silica shell, was carried out in two steps [40]. In the first

stage, the PVP-40, acting as a coupling agent, was adsorbed on the particle surface to stabilise the colloid in water. In the second stage, the stabilised particles were transferred into an ammonia/ethanol solution for silica layer growth by the addition of tetraethoxysilane. Firstly, 24 mg of either β-$NaYF_4$:Yb,Er-1 UCPs or β-$NaYF_4$:Yb,Er-2 UCPs were dispersed in 5 ml of water via sonication using an ultrasonic bath for 10 minutes and an ultrasonic probe sonicator for 1 minute. In a separate flask, 41 mg of PVP-40 was dissolved in 8.7 ml of water, followed by 15 minutes of sonication in an ultrasonic bath. Afterwards, the PVP-40 solution was added into the UCPs suspension and stirred for 24 hours at 600 rpm at room temperature. After this time, the PVP-stabilised UCPs were centrifuged, transferred into the 8.63 ml of ammonium hydroxide in ethanol solution (4.2 % vol) and stirred for 10 minutes. Subsequently, 872 µl of 10 $\%_{vol}$ TEOS in ethanol solution was added dropwise into the reaction system, and the mixture was stirred for 12 hours at 600 rpm. Finally, the particles were centrifuged at 9 500 rpm for 15 minutes, followed by threefold washing with ethanol and drying at 65 °C for 12 hours. The obtained products were labelled as β-$NaYF_4$:Yb,Er-1-SiO_2 and β-$NaYF_4$:Yb,Er-2-SiO_2.

β-$NaYF_4$:Yb,Er-1-SiO_2 particles modified with long hydrocarbon chains

β-$NaYF_4$:Yb,Er-1-SiO_2 particles were further modified by the eighteen hydrocarbon chains based on the same procedure, as described in Chapter 3.1. First, 25 mg of as-prepared β-$NaYF_4$:Yb,Er-1-SiO_2 particles were dispersed in 30 ml of dry toluene by sonication in a three-necked round-bottom flask. The mixture was stirred at 80 °C for 30 minutes under reflux and in an argon atmosphere. Afterwards, the solution of 341 µl (1 %, w/w) of octadecyltriethoxysilane in 1 ml of toluene was added dropwise into the reaction flask, and the mixture was stirred for 24 hours. Then, the system was cooled down to room temperature, followed by the solvent evaporation in a rotary evaporator and methanol addition to precipitate particles. Finally, the obtained β-$NaYF_4$:Yb,Er-1-SiO_2-C18 particles were separated by centrifugation at 9 500 rpm for 15 minutes, purified with ethanol three times, and dried in an oven 12 hours at 65 °C.

β-$NaYF_4$:Yb,Er-1-SiO_2 and β-$NaYF_4$:Yb,Er-2-SiO_2 particles modified with phenyl groups

The surface of β-$NaYF_4$:Yb,Er-1-SiO_2 and β-$NaYF_4$:Yb,Er-2-SiO_2 particles was also functionalised with phenyl groups. The grafting process was conducted similarly to eighteen hydrocarbon chains modification with a difference in the amount of the

precursor solution, which for the phenyltriethoxysilane was 270 µl in 1 ml of dry toluene. All the other synthesis stages and reagent amounts remained unchanged. The modified particles were labelled as β-$NaYF_4$:Yb,Er-1-SiO_2-Ph and β-$NaYF_4$:Yb,Er-2-SiO_2-Ph.

3.3.2.4 Fingermark collection

Three donors were chosen (two males and one female) to deposit natural LFM for further fingermark processing with synthesised UCPs. According to the International Fingerprint Research Group guidelines Phase 1 [12] concerning collection and storage, fingermarks were deposited on a couple of non-porous and semi-porous surfaces such as aluminium foil, glass, beverage can, black PP foil, polyethylene (PE) foil (protective sheet), magazine cover paper, and the sticky side of the adhesive tape. Also, copy paper was chosen as the representative of a porous surface. Donors have been asked not to wash their hands for at least half an hour before deposition. They were also requested to behave normally to provide natural fingermarks, similar to the real-case ones. Donors were also instructed to rub their hands together to homogenise the fingermark secretion across the fingertips and then to touch the substrate with the thumb, index, middle, and ring finger for 2-3 seconds with moderate pressure, comparable to the force they usually use for holding items. Collected fingermarks were aged in polystyrene Petri dishes for at least 24 hours in ambient conditions before further processing.

3.3.2.5 Fingermark development

Latent fingermarks were developed with a 1 mg mL^{-1} aqueous-ethanol suspension (97:3 v/v) of β-$NaYF_4$:Yb,Er-1-SiO_2-C18, β-$NaYF_4$:Yb,Er-1-SiO_2-Ph or β-$NaYF_4$:Yb,Er-2-SiO_2-Ph particles. Water, as a developing agent carrier, is user- and environment-friendly in contrast to organic solvents used in some of the conventional techniques. The addition of ethanol significantly improved the dispersion of the hydrophobic particles in the suspension. The typical LFM development process was conducted as follows. First, a given amount of appropriate particles was dispersed in the water-ethanol solution using the ultrasonication bath or the ultrasonic finger for 5 to 10 minutes. Each substrate with fingermark was immersed into the working suspension for 3 minutes, then gently rinsed with water to remove the material excess and dried in the stream of argon.

Besides, samples with LFM were also developed with the 1 mg mL^{-1} suspension of particles in organic, volatile solvents such as petroleum ether for β-$NaYF_4$:Yb,Er-1-SiO_2-C18 particles or methanol for β-$NaYF_4$:Yb,Er-1-SiO_2-Ph particles. The procedure for fingermark treatment was the same as described above.

3.3.2.6 Imaging of samples

The latent fingermarks developed with $NaYF_4$:Yb,Er-1-SiO_2-C18 and $NaYF_4$:Yb,Er-1-SiO_2-Ph upconverting particles were visualised with the imaging system, described in Chapter 3.1 (Figure 3.2). The system consists of the monochromatic, low-noise, water-cooled CCD camera, an excitation source with a 980 nm infrared laser, and the computer controller. Since the intensity of the excitation of the upconversion particles needs to be high, a powerful 5W semiconductor laser was applied. The laser was connected with the optical fibre to the system of lenses, which scatter the beam so that the whole area of the fingermark could have been illuminated. The samples were imaged in the normal mode. This means that the IR radiation illuminated the surface with deposited LFM permanently, and the shutter of the camera was opened for a specific time to collect the signal from the sample. The length of the sample exposition depended on the upconverting developer. Imaging the samples developed with particles functionalised with eighteen hydrocarbon chains involved up to 100 seconds of signal collecting, whereas the exposure time of fingermarks enhanced with the particles modified with phenyl groups oscillated between 1 to 8 seconds. The IR cut-off filter was applied to eliminate the reflected infrared radiation.

Latent fingermarks developed with $NaYF_4$:Yb,Er-2-SiO_2-Ph upconverting particles were imaged with a digital SLR camera with 24 mm lens (f/2.8) with micro rings and with IR optical filter. The samples were illuminated with the same IR laser. Compared to particles synthesised in the hydrothermal method, $NaYF_4$:Yb,Er-2-SiO_2-Ph particles indicated much stronger luminescence, which allowed applying the digital camera to visualise the fingermarks. As the luminescence intensity of the hydrothermal-synthesised material was relatively weaker, the CCD camera with high sensitivity was required for the imaging process.

Fingermark processed with cyanoacrylate (CA) fuming and stained with Rhodamine 6G (R6G) were imaged with an SLR camera with 60 mm lens (f/4.5) and illuminated with a Rofin Polilight® PL500 forensic light source (Rofin Australia Pty Ltd). The fingermark samples were illuminated with light of 530 nm wavelength and observed using a 590 nm band-pass barrier filter.

3.3.2.7 Comparison with conventional method

The effectiveness of fingermark development with β-$NaYF_4$:Yb,Er-2-SiO_2-Ph particles has been compared with a conventional method applied for non-porous and semi-porous surfaces, which is cyanoacrylate fuming followed by a Rhodamine 6G staining (CA-R6G). Upconversion particles modified with phenyl groups have been chosen for the comparison process due to their strong luminescence facilitating easier fingermark imaging, contrary to upconverting particles obtained in the hydrothermal synthesis. For the purpose of comparison, four types of surfaces have been chosen: glass, aluminium foil, PP foil, and PE foil. Split depletion series has been done for five different fingers from each of three donors. Each fingermark sample was cut in half after the print was deposited and aged 14 days. The example of the fingermark deposition and split matrix for one donor and one substrate is presented in Figure 3.29.

One half of each fingermark was processed by immersing the sample in 1 mg mL^{-1} water-ethanol suspension (97:3 v/v) of β-$NaYF_4$:Yb,Er-2-SiO_2-Ph and the other half of each fingermark was fumed with cyanoacrylates in a chamber followed by Rhodamine 6G staining.

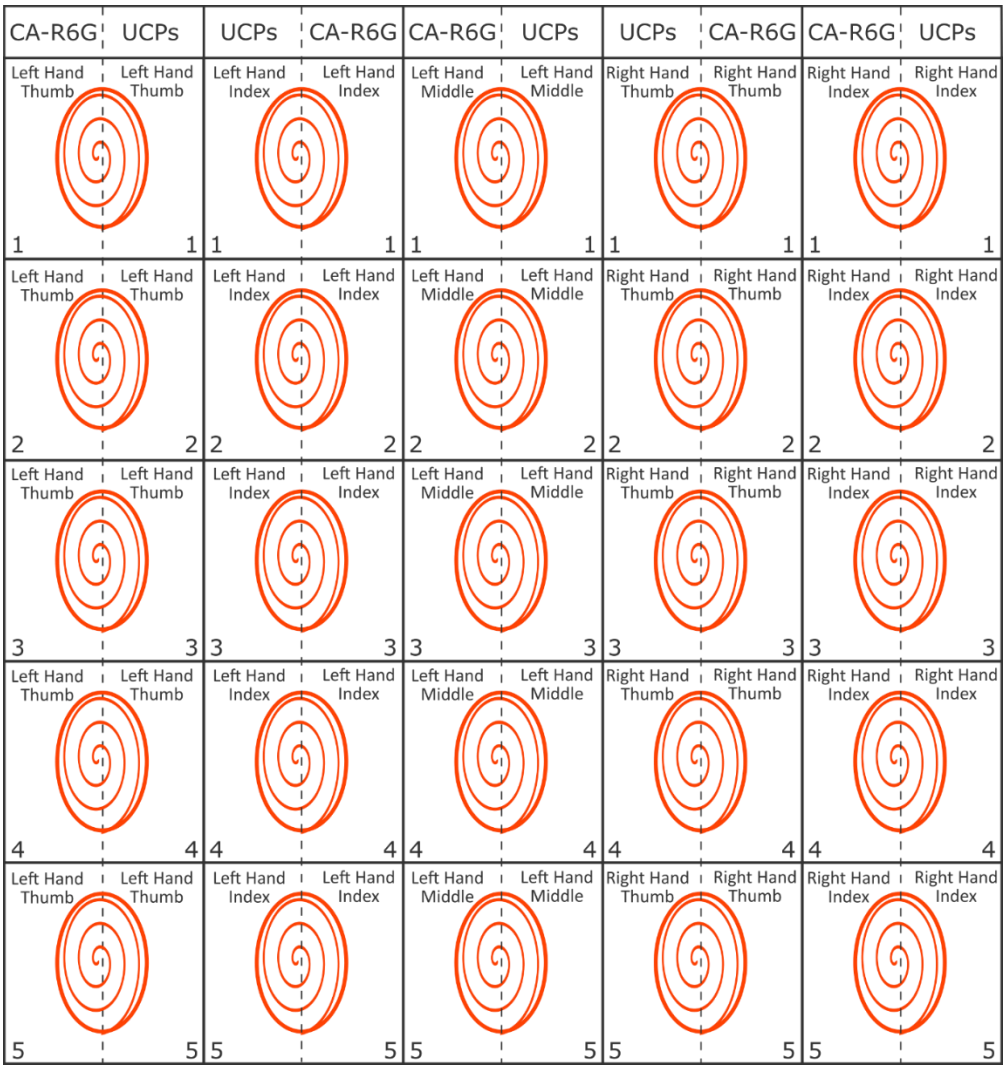

Figure 3.29 A fingermark deposition and split depletion matrix for one donor and one substrate to compare β-$NaYF_4$:Yb,Er-2-SiO_2-Ph suspension technique (UCP) with cyanoacrylate fuming (CA-R6G)

After the fingermark treatment process, the corresponding halves were digitally put back to the original position with Adobe Photoshop® software, without any digital enhancement. Three assessors graded the fingermark images using the University of Canberra comparative fingermark assessment scheme [41] (Table 3.4), generating 900 fingermark scores. The "+ 1" and "+ 2" score was related to an increase in enhancement with β-$NaYF_4$:Yb,Er-2-SiO_2-Ph particles in comparison to cyanoacrylate fuming followed by Rhodamine 6G staining. The "00" score indicated no detection of the fingermark. "0" score was used when β-NaYF4:Yb,Er-2-SiO2-Ph

particles developed the fingermark, but no enhancement was observed when compared with CA-R6G, while "- 1" and "- 2" reflected a decrease in enhancement with β-$NaYF_4$:Yb,Er-2-SiO_2-Ph particles in comparison to CA-R6G.

Table 3.4 The comparative scale used for the fingermark assessment [12], [41]

Score	Definition
+ 2	Significant increase in enhancement for the assessed technique when compared to the CA-R6G
+ 1	Slight increase in enhancement for the assessed technique when compared to CA-R6G
0	Developed fingermark but no enhancement by the assessed technique when compared to CA-R6G
– 1	Slight decrease in enhancement of the assessed technique when compared to CA-R6G
– 2	Significant decrease in enhancement of the assessed technique when compared to CA-R6G
00	No detection on either half of the fingermark

Cyanoacrylate fuming followed by dye staining

This technique of latent fingermark enhancement is based on a polymerisation reaction of cyanoacrylate monomers directly on the fingermark residue, producing a white deposit. The polymerisation is initiated by water and other fingermark components. In this chemical process, the items or surfaces with latent fingermarks are exposing to cyanoacrylate vapours in a special fuming cabinet at high humidity maintained between 75 and 90 %. The polymerised cyanoacrylates form the visible, white “noodle-like” fibres on the fingermark ridges. Rhodamine 6G is an effective dye for dyeing marks developed with cyanoacrylates, yielding high fluorescence. The dye absorbs in the green range of the visible light spectrum (495-540 nm) and emits in the yellow region (560 nm) what is convenient to visualise fingermark. Also, sequencing cyanoacrylate fuming with Rhodamine 6G staining results in an increase of the identified fingermark number [3], [13], [42], [43].

The fingermark enhancement process was conducted in the MVC® 1000 fuming cabinet (Foster + Freeman Ltd., UK) with super bonder prism Loctite - 406 (Blackwoods, Australia) as the cyanoacrylate monomer. For each run, 0.5 g of Loctite was placed on a heat source. The developing items were placed in the cabinet with sufficient room for air circulation. The heater was allowed to reach 120 °C, and the

humidity level within the cabinet was maintained at 80%. The exposition time was set to 6-8 minutes, varying by substrates. All CA fumed items were then left for three days, followed by dye staining. Each item was immersed in the Rhodamine 6G solution (0.2 g in 200 mL of 2-propanol and 300 mL of methyl ethyl ketone), rinsed to remove dye excess and left to dry in the air.

3.3.3 Results and discussion

In this section, the upconverting material, synthesised via thermal method and solid-liquid-thermal-decomposition, will be characterised. Also, the analysis of the interaction between modified particles and fingermark residuals will be performed as well as a comparative study of fingermark development with the suspension of new material versus cyanoacrylate fuming as a benchmark method.

Characterisation of the β-$NaYF_4$:Yb,Er-1, β-$NaYF_4$:Yb,Er-1-SiO_2 and β-$NaYF_4$:Yb,Er-1-SiO_2-Ph particles

The as-prepared upconverting crystals were investigated using scanning electron microscopy. As observed in the images (Figure 3.30), a variety of particles' morphology has resulted from the molar ratio of citrates to rare earth cations used in the synthesis. For the molar ratios 2:1, 1:1, 1:2, and 1:4 the particles had similar homogeneous and hexagonal morphology with the average diameter of 1.19 ± 0,10 μm, 1.50 ± 0,13 μm, 3.70 ± 0,44 μm, and 3.14 ± 028 μm, respectively, and average height of 0.30 ± 0,05 μm, 0.45 ± 0,06 μm, 1.81 ± 0,38 μm, and 1.68 ± 0,36 μm, respectively (determined by the analysis of SEM images with ImageJ application). For the molar ratio of 1:8, the synthesised particles were not regular in shape and size; the average height was ca. 4.62 ± 1.0 μm. Particles synthesised using RE^{3+} chlorides directly from the supplier were homogenous with an average diameter of 0.34 ± 0.03 μm and height of 0.07 ± 0.007 μm. The size analysis showed that the number of citrate ions determined the size of the particles. The decrease in the presence of citrates resulted in an increase in particle size and changes in morphology. For molar ratios 2:1 and 1:1, the smallest and uniform particles were obtained with smooth top, bottom, and side planes (Figure 3.30 A, B). Reducing the amount of the citrates increased the dimensions of the diameter and height but also influenced the shape of the particles – the clear concave centres formed on the bottom and top planes (Figure 3.30 C, D).

Further decrease in citrates concentration resulted in further crystals lengthwise growth. Also, shape irregularity and a coarse surface were observed (Figure 3.30 E). The sodium citrate influenced crystal nucleation and growth kinetics. It may slow down the nucleation and crystal growth of $NaYF_4$, due to the formation of stable complexes with Y^{3+} ions through coordination interaction. In high temperature and pressure during hydrothermal synthesis, the complex starts to weaken, and the slow release of Y^{3+} ions takes place [44]. The growth of the crystal depends on the growth rate of different crystal facets in the β-$NaYF_4$:Yb,Er-1 hexagonal microprism. In general, sodium citrate may inhibit longitudinal growth and enhance the growth of the sideways in the crystal. With the increase of the citrates, the smoother surfaces of all facets were observed, and the top and bottom plane concaves disappeared [38]. Besides the impact of citrate to RE^{3+} molar ratio, also, the type of precursor influenced the crystal size (Figure 3.30 F). The use of anhydrous yttrium, ytterbium, and erbium chlorides directly from the supplier resulted in a significantly smaller size of the crystals than using the chlorides prepared from the corresponding oxides in hydrochloric acid. The reason for this may be insufficiently evaporated water from the chlorides prepared from oxides or some additional by-products of the reaction that interfere with the nucleation and crystal growth [45].

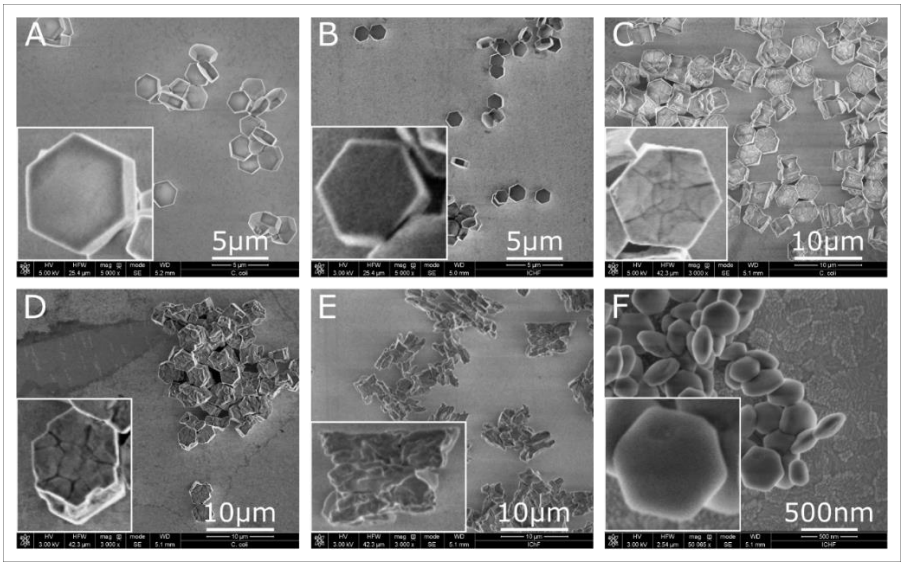

Figure 3.30 SEM images of β-$NaYF_4$:Yb,Er-1 crystals obtained for various molar ratio of sodium citrate to RE^{3+}: (A) 2:1, (B) 1:1, (C) 1:2, (D) 1:4, (E) 1:8, (F) 1:1 – RE^{3+} chlorides used in the synthesis directly from the supplier. In the insets, higher-magnification images of the corresponding crystals were introduced

The distribution of the components in the silica coating β-$NaYF_4$:Yb,Er-1 crystal, was identified by SEM/EDX element mapping. As presented in Figure 3.31, the mapping of sodium, yttrium, fluorine, and ytterbium reveals that the host lattice of $NaYF_4$ was successfully doped with ytterbium. Also, the silicon and oxygen uniform distribution in the area of the crystal suggests effective silica coating of the β-$NaYF_4$:Yb,Er-1 surface. The presence of carbon is related to the glassy-carbon SEM plate.

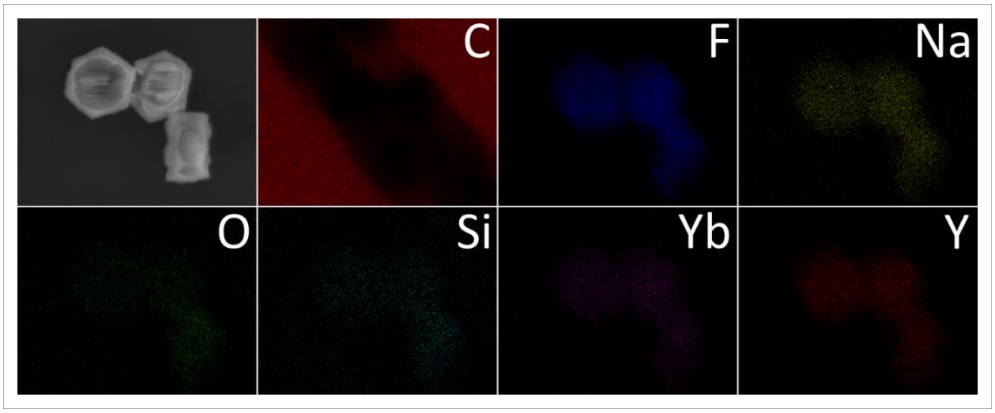

Figure 3.31 SEM/EDX mapping of β-$NaYF_4$:Yb,Er-1-SiO_2 crystal showing the distribution of sodium (Na), yttrium (Y), fluorine (F) in the host lattice doped with ytterbium (Yb), and also silicon (Si) and oxygen (O) in the silica coating. C is corresponding to carbon present in a glassy-carbon SEM plate

Figure 3.32 shows a dependence of the crystal size, and indirectly the citrate to RE^{3+} molar ratios, on a luminescence intensity of β-$NaYF_4$:Yb,Er-1 particles. The luminescence intensity was measured with the CCD sensor under laser excitation with a 980 nm wavelength. A signal from the sample was collected for 100 µs. The analysis of the luminescence intensity reveals that the smallest crystals have lower emission intensity. The highest luminescence intensity was indicated by bigger crystals, synthesised with a lesser amount of sodium citrate. A significant increase in the intensity appeared between crystals obtained with the ratio 1:4 and 1:2. The crystals synthesised with the 1:4 molar ratio had a little smaller diameter and height dimensions. The highest intensity values were observed for large heterogeneous crystals obtained with the molar ratio of 1:8. Due to the size of these crystals, which may adversely affect the LFM development process, the slightly smaller and homogeneous crystals obtained with a molar ratio of 1:2 were selected for further analysis.

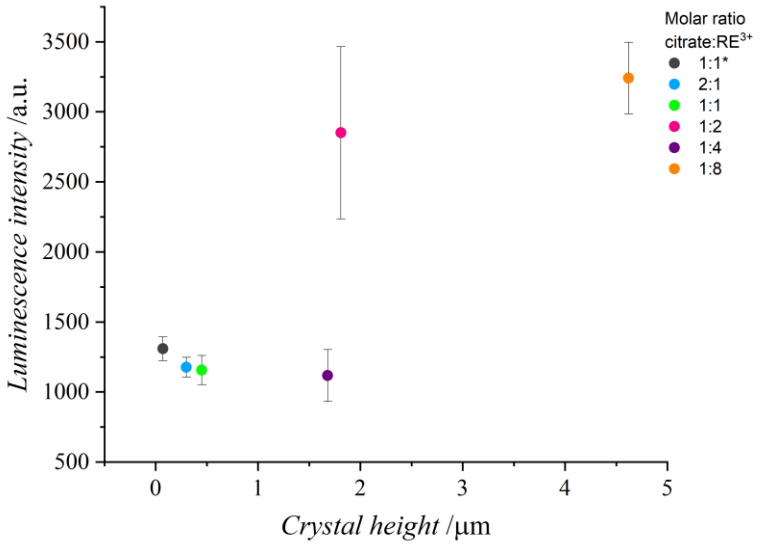

Figure 3.32 A diagram of the luminescence intensity dependence on the β-$NaYF_4$:Yb,Er-1 crystal height. The molar ratio marked as 1:1* corresponds to the synthesis applying rare earth chlorides directly from the supplier

According to the literature, upconverting luminescence efficiency in the lanthanide-doped crystals can be affected, among others, by particle size. With the particle size decrease, the surface-to-volume ratio is increasing, which boosts the number of ions on the particle's surface. These unsaturated reactive ions increase the surface energy. Therefore they are likely to react with the environment in order to reduce their free energy in a non-radiative way, leading to the quenching process. Also, decreasing the particle size leads to an increase in the number of surface defects with large vibrational modes, resulting in non-radiative relaxation. To suppress the luminescence quenching effect, a uniform core-shell structure of the particle can be formed to block energy transfer from the activators in the core to defects on the surface, ligands, or environment [36],[46]. For this purpose, the obtained β-$NaYF_4$:Yb,Er-1 crystals were coated with a silica layer. Furthermore, to change the properties of the particles into hydrophobic for effective fingermark enhancement, the surface of the material was modified with either phenyl groups or eighteen hydrocarbon chains. The analysis of the luminescence intensity of non-modified and modified crystals confirmed the above statements (Figure 3.33). The coverage of the crystals' surface with the thin silica layer yielded a significant increase of luminescence intensity. Moreover, the further surface modification did not affect the luminescence emission levels.

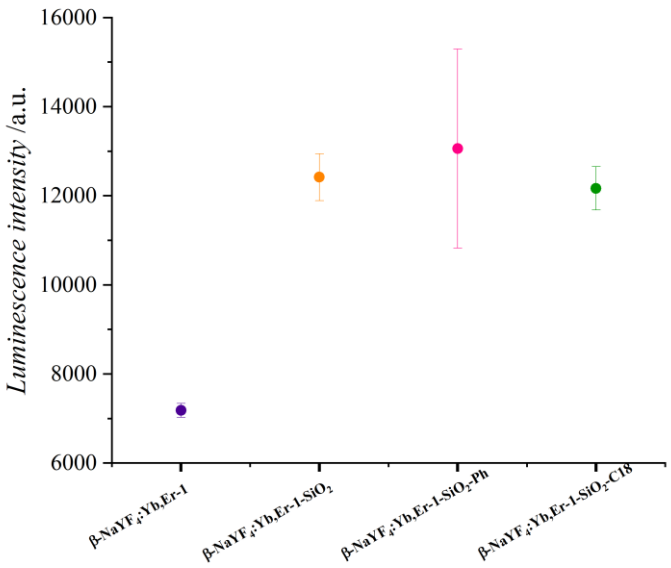

Figure 3.33 A diagram of the β-$NaYF_4$:Yb,Er-1 crystal surface modification on luminescence intensity dependence

The analysis of modified β-$NaYF_4$:Yb,Er-1-SiO_2 particles enhancement efficacy on selected substrates

The new upconverting β-$NaYF_4$:Yb,Er-1-SiO_2 particles modified with either phenyl groups or 18 hydrocarbon chains were employed to enhance latent fingermarks deposited on a range of substrates such as aluminium foil, beverage can, glass, ITO, magazine cover paper, adhesive tape and polypropylene foil (PP black plastic bag). The working suspension containing 1 mg mL^{-1} of the appropriate particles in water-ethanolic solution (97:3, v/v) or organic solvent was used for the enhancement process.

The developed natural fingermark deposited on ITO was observed under the scanning electron microscope to see whether the hydrophobic particles interact with the fingermark residuals. The results presented in Figure 3.34 show that the particles selectively attach to the fingermark ridges; however, the quantity of the deposited material may not be enough to visualise the ridge details effectively.

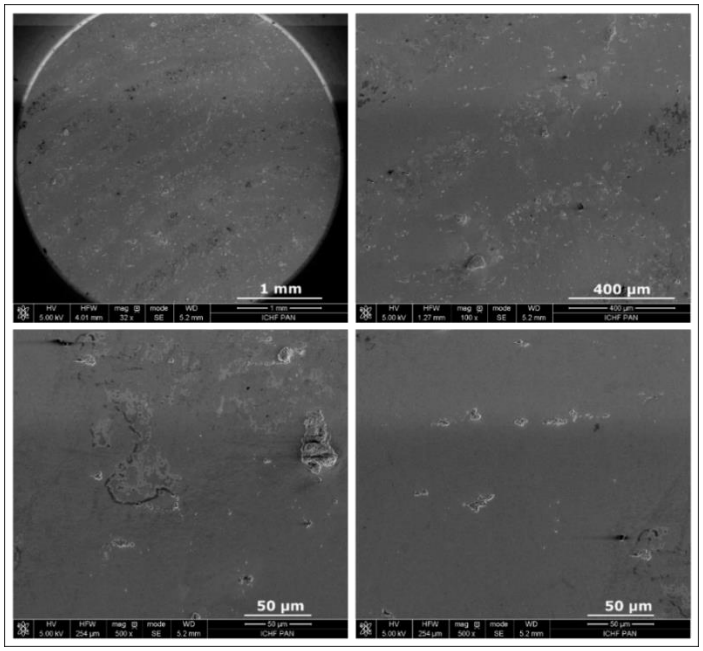

Figure 3.34 SEM images of 5-days-old natural fingermark on ITO developed with β-$NaYF_4$:Yb,Er-1-SiO_2 -Ph particles in water-ethanol solution (97:3, v/v)

The fingermarks developed with modified UCPs deposited on the other surfaces have been imaged in the normal mode of imaging setup under 980 nm laser excitation. The signal was collected with the CCD sensor with the IR filter for 100 seconds. The emission intensity of the particles was too low to collect the images with the SLR camera.

First, the fingermarks were enhanced with β-$NaYF_4$:Yb,Er-1-SiO_2-C18 particles in water-ethanol suspension. The results are collected in Figure 3.35.

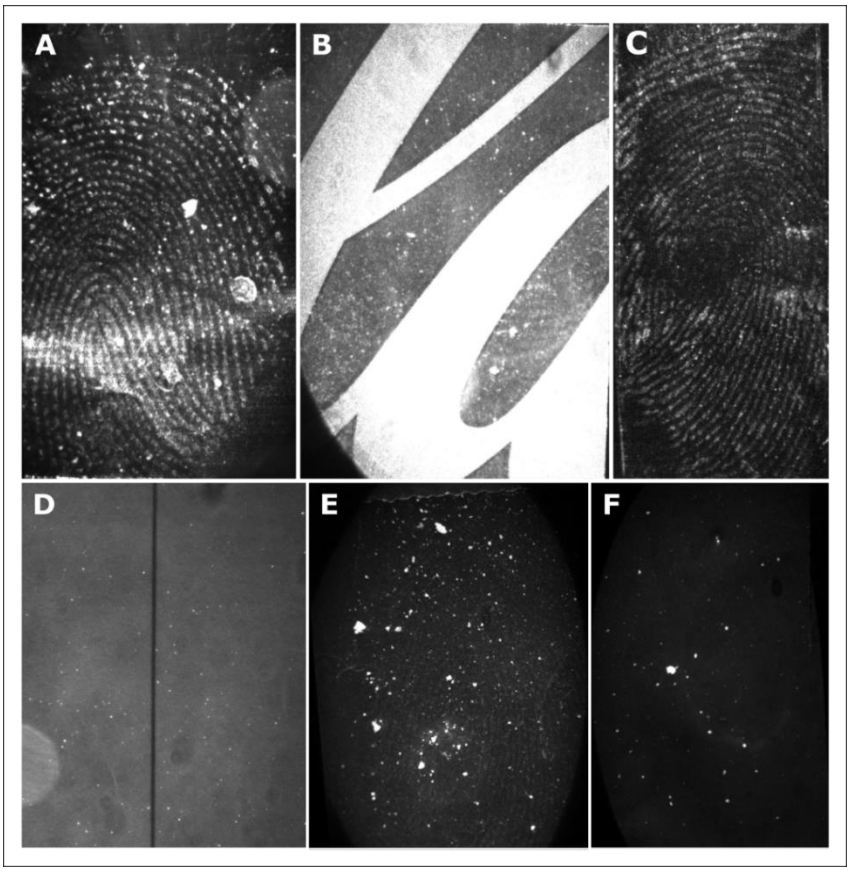

Figure 3.35 Samples of natural fingermarks developed with β-$NaYF_4$:Yb,Er-1-SiO_2-C18 particles in water-ethanol solution (97:3, v/v) deposited on aluminium foil (A), beverage can (B), glass (C), copy paper (D), sticky side of the adhesive tape (E), black PP foil (F)

β-$NaYF_4$:Yb,Er-1-SiO_2-C18 particles efficiently interacted with the fingermark residue on aluminium foil and glass substrate. The ridges are clearly visible, and good contrast was obtained on both samples. However, some reflections of IR light on aluminium foil were also recorded (Figure 3.35 A, C). The beverage can, with a white pattern, is an example of a sample showing strong background reflectance. The particles were deposited on the fingermark ridges in a small amount, which is visible in Figure 3.35 B. The fingermark visualisation was impossible due to the intense light reflection on the white impressions of beverage can surface. A latent fingermark deposited on a copy paper was not developed at all (Figure 3.35 D). Paper is a porous surface, and fingermark residuals can diffuse into its matrix, hindering the access of the micron-size β-$NaYF_4$:Yb,Er-1-SiO_2-C18 particles. The next substrate examined for fingermark detection was the sticky side of the adhesive tape (Figure 3.35 E). The use of β-$NaYF_4$:Yb,Er-1-SiO_2-C18 particles in water-ethanol suspension introduces

a relatively small amount of particles to the fingermark ridges, resulting in a poor quality fingermark with some aggregates deposited across the sample. The black PP foil proved to be the most challenging substrate to visualise due to shrinking under the heat of IR laser. The latent fingermark on the PP foil, observed using a cover glass slide, was unfortunately not visible except for some particles' aggregates present on the sample (Figure 3.35 F).

The alternative approach to fingermark development with hydrophobic β-$NaYF_4$:Yb,Er-1-SiO_2-C18 particles was changing a solvent to petroleum ether. The results are collected in Figure 3.36. Employing the organic solvent for fingermark development with β-$NaYF_4$:Yb,Er-1-SiO_2-C18 particles did not improve the visualisation effects. For both beverage can and glass substrates, the results were even worse than for water-ethanol formulation. There is no fingermark visible on the beverage can (Figure 3.36 A), and there is a poor quality fingermark on the glass slide (Figure 3.36 B). Fingermarks deposited on adhesive tape and black PP foil were slightly better enhanced (Figure 3.36 C, D) in comparison with water-ethanol suspension development. However, still, the fingermark quality is not satisfying, and the problem of shrinking foil remained. Again, no fingermark was developed on the paper sample (Figure 3.36 E).

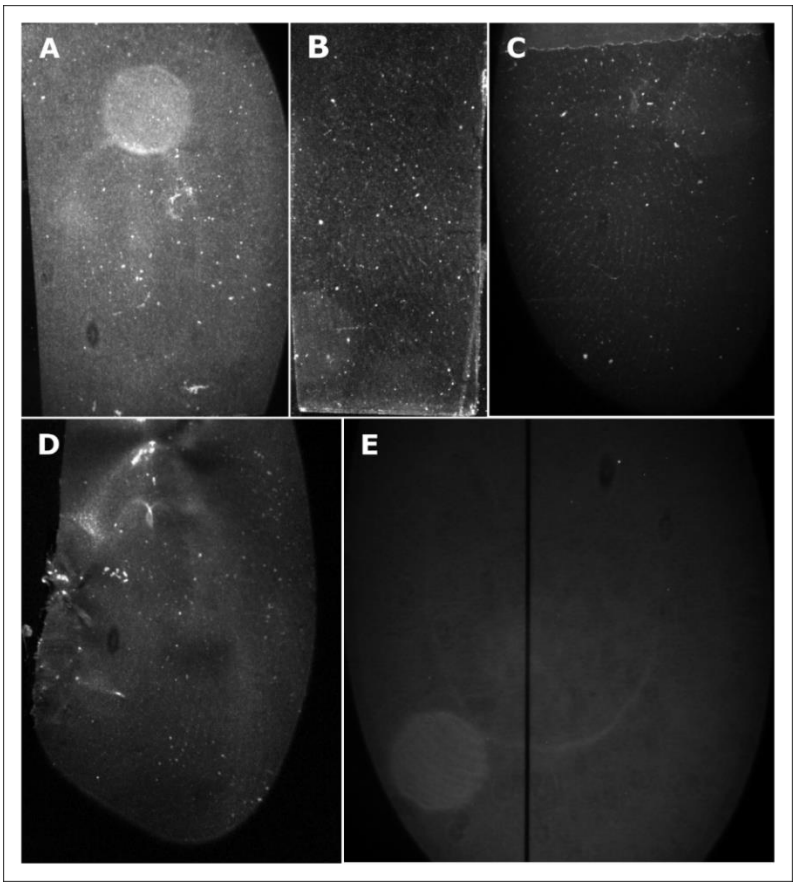

Figure 3.36 Samples of natural fingermarks developed with β-$NaYF_4$:Yb,Er-1-SiO_2-C18 particles in petroleum ether, deposited on beverage can (A), glass (B), sticky side of the adhesive tape (C), black PP foil (D), copy paper (E)

The exact development process was conducted for the suspension of β-$NaYF_4$:Yb,Er-1-SiO_2-Ph particles in water-ethanol solution, and methanol. Particles dispersed in water-ethanolic solution enable effective deposition and visualisation of the fingermarks on aluminium foil and glass (Figure 3.37 A, F). On the other hand, the fingermarks deposited on the beverage can, magazine cover paper, and copy paper was not visible after processing. The luminescent material was distributed randomly in small aggregates, and no ridge details were observed (Figure 3.37 B, D, E). The fingermarks deposited on the adhesive tape have been slightly visible what means that particles selectively interact with the residuals. However, the layer of particles covered the ridge was too thin to record luminescence from upconverting particles with relatively weak luminescence intensity (Figure 3.37 C).

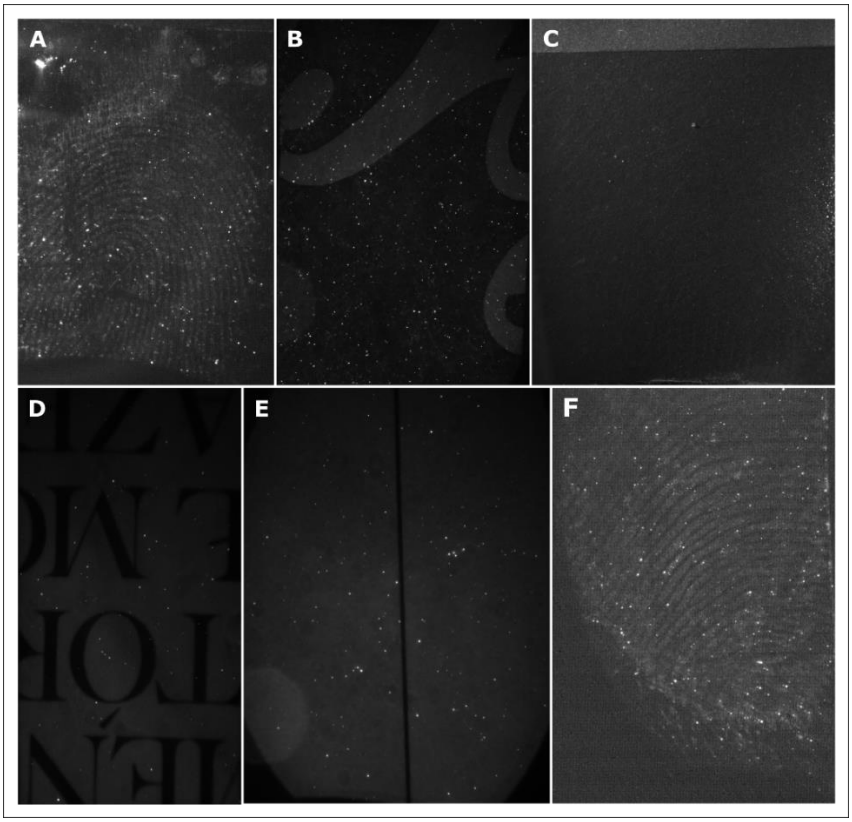

Figure 3.37 Samples of natural fingermarks developed with β-$NaYF_4$:Yb,Er-1-SiO_2 -Ph particles in water-ethanol solution (97:3, v/v) deposited on aluminium foil (A), beverage can (B), sticky side of the adhesive tape (C), magazine cover paper (D), copy paper (E), glass (F)

The fingermark development on several substrates was also examined for β-$NaYF_4$:Yb,Er-1- SiO_2-Ph particles dispersed in methanol. In this case, no enhancement results were obtained for fingermarks deposited on each substrate (Figure 3.38). The particles attached to the surface randomly forming tiny aggregates.

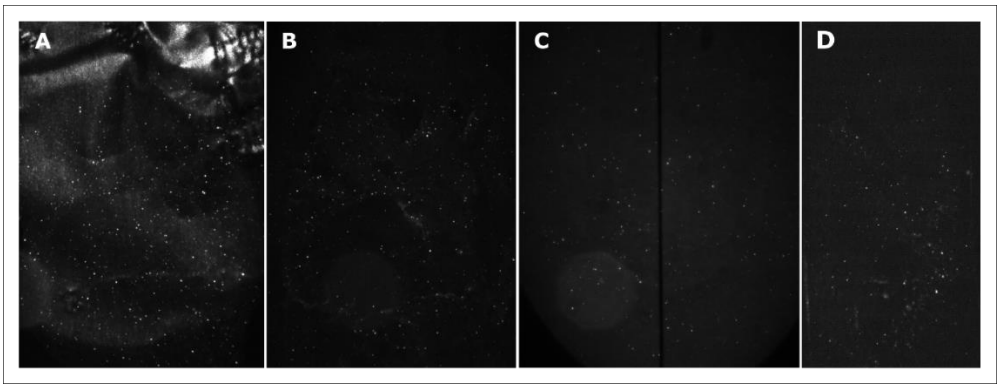

Figure 3.38 Samples of natural fingermarks developed with β-$NaYF_4$:Yb,Er-1-SiO_2-Ph particles in methanol, deposited on aluminium foil (A), beverage can (B), copy paper (C), glass (D)

Characterisation of the β-$NaYF_4$:Yb,Er-2, β-$NaYF_4$:Yb,Er-2-SiO_2 and β-$NaYF_4$:Yb,Er-2-SiO_2-Ph particles

Morphology of the particles synthesised via solid-liquid thermal decomposition was characterised by scanning electron microscopy. The analysis of SEM images has shown homogenous hexagonal-phase β-$NaYF_4$:Yb,Er-2 particles with an average diameter and height of 121 ± 5 nm and 76 ± 2 nm, respectively (Figure 3.39 A) (determined by analysis of SEM images using ImageJ software). The size of the as-prepared particles is ten times smaller than crystals obtained in the hydrothermal synthesis. Silica coated UCP (Figure 3.39 B), and UCPs further modified with phenyl groups (Figure 3.39 C) appeared with comparable morphology. An average diameter of β-$NaYF_4$:Yb,Er-2-SiO_2 and β-$NaYF_4$:Yb,Er-2-SiO_2-Ph particles is of 158 ± 8 nm and 158 ± 4 nm, respectively, and an average height of 85 ± 2 nm and 82 ± 5 nm, respectively.

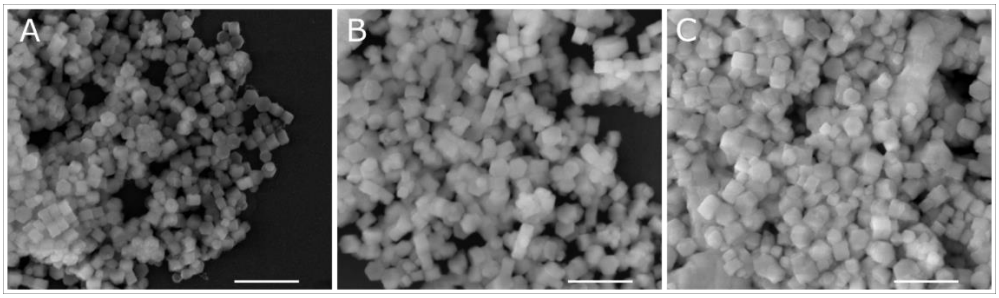

Figure 3.39 SEM images of (A) β-$NaYF_4$:Yb,Er-2, (B) β-$NaYF_4$:Yb,Er-2-SiO_2, (C) β-$NaYF_4$:Yb,Er-2-SiO_2-Ph particles synthesised via solid-liquid-thermal-decomposition. The scale length bar is 500 nm

The white powder of β-$NaYF_4$:Yb,Er-2 particles indicated hydrophobic properties. The material was not able to disperse in water. The particles dispersed in ethanol and excited with infrared radiation with 980 nm laser has shown the strong green emission (Figure 3.40).

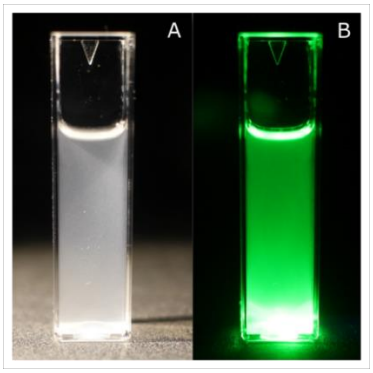

Figure 3.40 The 1 mg mL^{-1} β-$NaYF_4$:Yb,Er-2 particles suspension in ethanol illuminated with white light (A), 980 nm IR light (B)

To confirm the β-hexagonal phase of the obtained material, the X-ray diffraction (XRD) analysis of the particles has been performed. The XRD patterns showed peaks characteristic of the hexagonal shape crystal according to the standard X-ray diffraction of Joint Committee on Powder Diffraction (JCPDS file number 16-0334) (Figure 3.41).

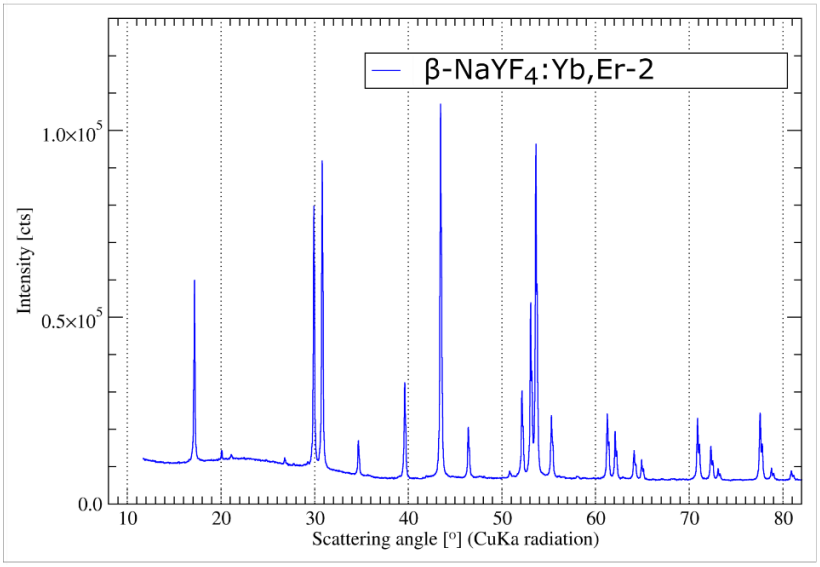

Figure 3.41 The XRD analysis of β-$NaYF_4$:Yb,Er-2 particles

Energy-dispersive X-ray analysis was performed on unmodified β-$NaYF_4$:Yb,Er particles as well as on the silica-coated and phenyl group modified UCPs to determine the composition of the materials (Figure 3.42). Sodium, fluorine and yttrium are present in the host lattice of the crystals doped with ytterbium and erbium (Figure 3.42 A). The presence of silicon and oxygen peaks in the EDX spectra of modified UCPs (Figure 3.42 B, C) confirms the effective silica coating of the particles. The peak corresponding to carbon, observed in all samples, is related to the glassy-carbon slide used as a substrate for the SEM analysis.

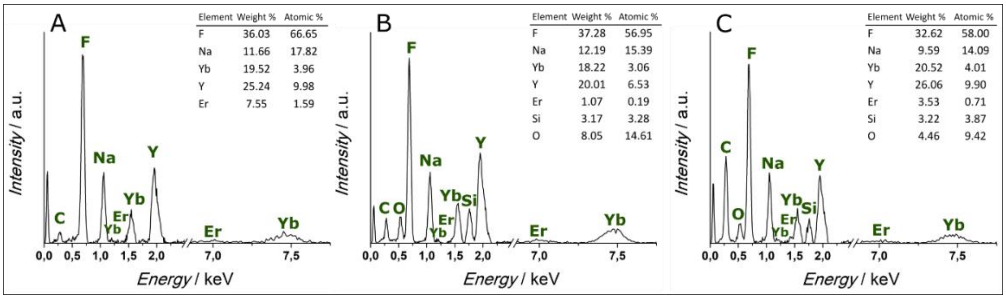

Figure 3.42 The EDX spectra of (A) β-$NaYF_4$:Yb,Er-2-Ph, (B) β-$NaYF_4$:Yb,Er-2-SiO_2, (C) β-$NaYF_4$:Yb,Er-2-SiO_2-Ph. The insets: elemental compositions of UCPs obtained from the EDX results

The Diffuse Reflectance Infrared Fourier Transform Spectroscopy (DRIFT) spectra were recorded to identify the composition of modified β-$NaYF_4$;Yb,Er-2-SiO_2 and β-$NaYF_4$;Yb,Er-2-SiO_2-Ph particles (Figure 3.43). The bands at ~1080 cm^{-1} and ~800 cm^{-1}, characteristic for asymmetric and symmetric stretching vibrations of the Si–O–Si framework [19], [47], [48], respectively, are observed for both β-$NaYF_4$;Yb,Er-2-SiO_2 and β-$NaYF_4$;Yb,Er-2-SiO_2-Ph particles (Figure 3.43B, C), while for β-$NaYF_4$;Yb,Er-2 spectrum they are not visible. A broad band at ~3360 cm^{-1} is associated with the surface hydroxyl groups [49] (Figure 3.43 B, C). Additional bands at ~1560 cm^{-1}, ~1465 cm^{-1}, ~1430 cm^{-1}, ~1227 cm^{-1}, and ~1164 cm^{-1} (Figure 3.43 C) present in the β-$NaYF_4$;Yb,Er-2-SiO_2-Ph spectrum, not observed in β-$NaYF_4$;Yb,Er-2-SiO_2, suggest the presence of phenyl groups in the material [23], [47], [48].

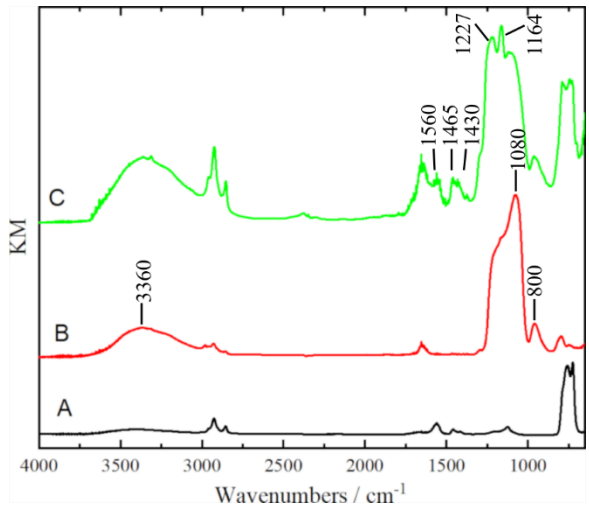

Figure 3.43 The DRIFT spectra of (A) β-$NaYF_4$:Yb,Er- 2, (B) β-$NaYF_4$:Yb,Er-2-SiO_2, (C) β-$NaYF_4$:Yb,Er-2-SiO_2-Ph

The analysis of β-$NaYF_4$:Yb,Er-2-SiO_2-Ph enhancement efficacy on selected substrates

The new β-$NaYF_4$:Yb,Er-2-SiO_2-Ph luminescent particles modified with phenyl groups, were applied to enhance latent fingermarks deposited on several commonly used non-porous and porous substrates such as glass, aluminium foil, polypropylene foil (PP), polyethylene foil (PE), polystyrene (PS), polyethylene terephthalate (PET), beverage can, magazine, copy and notebook paper. Initially, the working suspension of 1 mg mL^{-1} particles in water-ethanol solution (97:3 v/v) was prepared. To investigate the efficacy of the new material, a natural fingermark deposited on ITO developed in working suspension was observed under the scanning electron microscope (Figure 3.44). The particles covered almost the entire ridge of the fingermark, which is quite well visible in the magnified images. The hydrophobic particles interact with the fatty components of the fingermark, forming a thick layer on its ridges. The β-$NaYF_4$:Yb,Er-2-SiO_2-Ph particles were observed to indicate a slightly better affinity to fingermark than particles obtained in the hydrothermal synthesis. This superior affinity may be the result of the particle size, which is ten times lower for β-$NaYF_4$:Yb,Er-2-SiO_2-Ph particles. The small fine particles generally have a higher affinity to fingermark residuals than bigger ones [50]. However, a very thin layer of particles between the ridges in some regions was also visible under SEM.

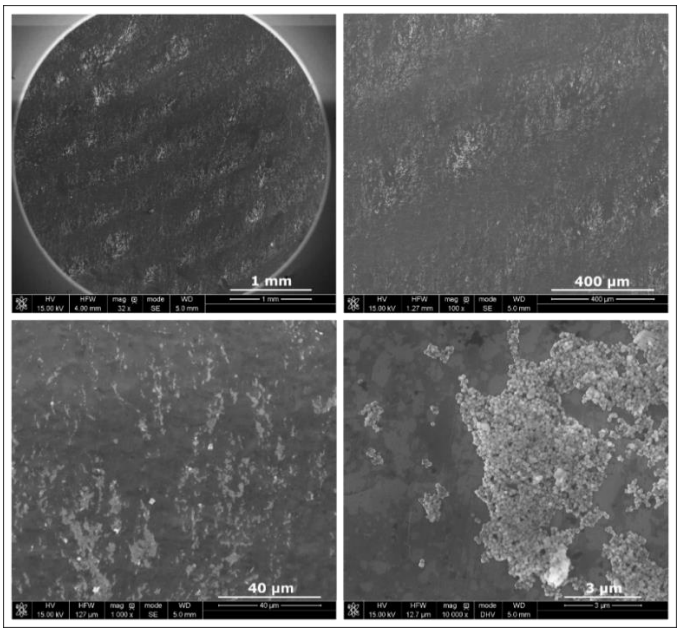

Figure 3.44 SEM images of 28-month-old natural fingermark on ITO developed with β-$NaYF_4$:Yb,Er particles in water-ethanol solution (97:3, v/v)

To investigate an optimal concentration of β-$NaYF_4$:Yb,Er-2-SiO_2-Ph particles in the water-ethanol suspension and optimal development time to obtain the best sensitivity, two natural fingermarks deposited on aluminium foil were examined. Each aluminium foil sample was cut in half. The left halves were immersed in the 0.1 mg mL^{-1} suspension for either 5 or 10 minutes (Figure 3.45 A, B), and the other halves were immersed in 1 mg mL^{-1} suspension for either 5 or 10 minutes also (Figure 3.45 A', B'). Then the halves were recombined and compared.

Fingermarks developed with 0.1 mg mL^{-1} suspension of β-$NaYF_4$:Yb,Er-2-SiO_2-Ph particles were of poor quality for both 5 minutes and 10 minutes of processing. The ridge details were not clear, and the material was spread unequally along the ridges in the form of a thin layer. Increasing the concentration to 1 mg mL^{-1} resulted in a very good fingermark quality for both longer and shorter processing time and no background staining. This formulation allows for obtaining good ridge features with 2^{nd} level minutiae details and contrast between fingermark ridges and the background (Figure 3.46).

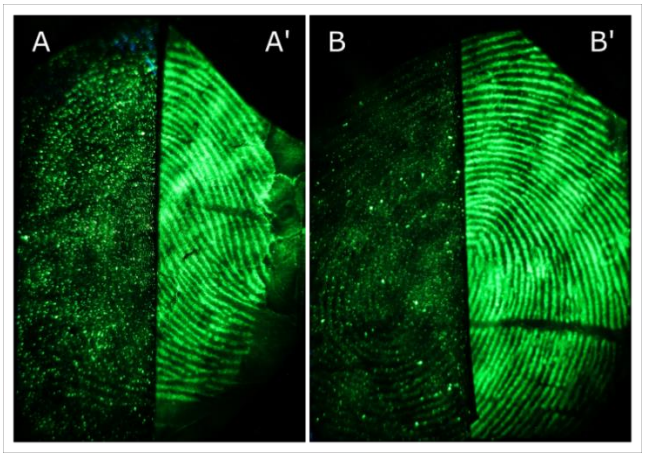

Figure 3.45 Samples of fingermarks deposited on aluminium foil developed with a water-ethanol suspension of β-$NaYF_4$:Yb,Er-2-SiO_2-Ph particles under concentrations: 0.1 mg mL^{-1} (A, B) and 1 mg mL^{-1} (A', B') with the immersion time 5 minutes (A, A') and 10 minutes (B, B')

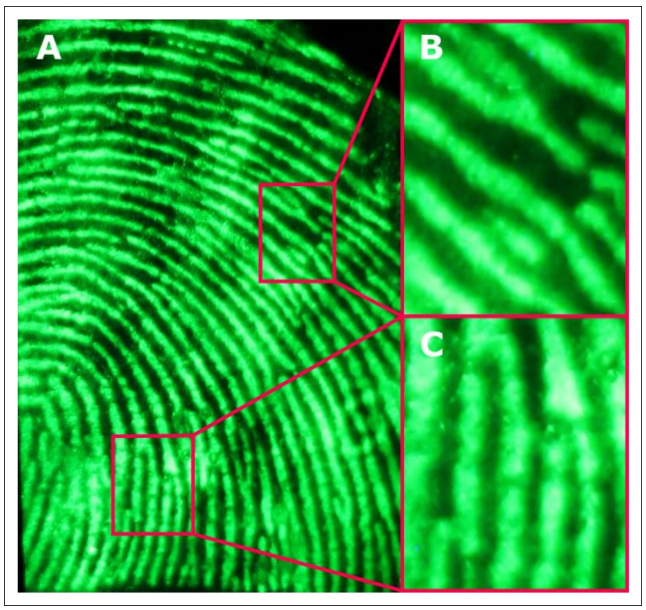

Figure 3.46 A natural fingermark deposited on aluminium foil, developed with 1 mg mL^{-1} β-$NaYF_4$:Yb,Er-2-SiO_2-Ph particles in the water-ethanol suspension, imaged with a digital camera under 980 nm laser illumination (A). The 2nd level features (minutiae) are distinguished (B), (C).

For further investigation of the β-$NaYF_4$:Yb,Er-2-SiO_2-Ph particles utility, a few latent fingermarks on several substrates such as aluminium foil, PET, PP foil, polystyrene, beverage can, magazine cover paper, notebook and copy paper, and

glass have been processed. The samples were imaged with the digital SLR camera under 980 nm laser illumination.

On aluminium foil, the luminescent particles revealed fingermark with the number of ridge details and without background staining (Figure 3.47 A). Slightly less clear fingermarks were developed on PET and glass surfaces (Figure 3.47 B, I). On both samples, the 2nd ridge details were observable; however, the background staining has occurred. On black PP foil, the β-$NaYF_4$:Yb,Er-2-SiO_2-Ph particles adhered both to the ridges and the background, yielding no contrast of the fingermark (Figure 3.47 C). Fingermarks deposited on a polystyrene substrate as well as on the beverage can were slightly enhanced with the particles but demonstrated weak ridge details and high background staining (Figure 3.47 D, E). No results were obtained for porous surfaces such as magazine cover paper, copy paper, and notebook paper (Figure 3.47 F, G, H). The particles were deposited over the entire surface of the sample, and it was virtually impossible to distinguish the fingermark ridges from the background.

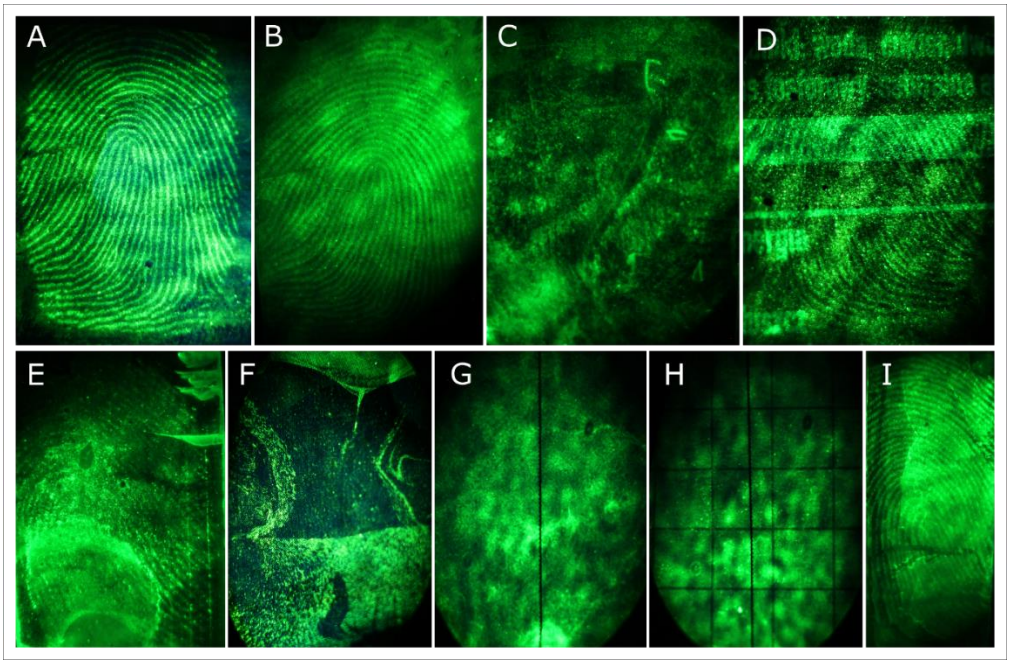

Figure 3.47 Samples of natural fingermarks developed with β-$NaYF_4$:Yb,Er-2-SiO_2-Ph particles in the water-ethanol solution (97:3, v/v) deposited on aluminium foil (A), PET (B), black PP foil (C), beverage can (D), polystyrene (E), magazine cover paper (F), copy paper (G), notebook paper (H), glass (I)

Comparative analysis of the β-$NaYF_4$:Yb,Er-2-SiO_2-Ph particles with cyanoacrylate fuming followed by Rhodamine 6G staining

A comparative study of split depletion series has been performed to assess the capability and selectivity of β-$NaYF_4$:Yb,Er-2-SiO_2-Ph particles in latent fingermark enhancement process against cyanoacrylate fuming followed by rhodamine 6G staining. In the comparison experiment, the five natural fingermark depletions were collected from 3 donors on selected substrates: PP foil, aluminium foil, glass, and PE foil prior to ageing for 14 days in the laboratory environment. Each half of the depletion series was treated with either cyanoacrylate fuming followed by Rhodamine 6G staining or β-$NaYF_4$:Yb,Er-2-SiO_2-Ph particles suspension, and then recombined. Fingermark halves treated with cyanoacrylates and Rhodamine 6G were imaged with a Canon EOS 750D camera fitted with a Canon Macro EF 60 mm lens under 530 nm excitation of Rofin Polilight® PL500 light source and viewed at 590 nm. The other halves developed with β-$NaYF_4$:Yb,Er-2-SiO_2-Ph particles were imaged with a Canon EOS 550D SLR Camera fitted with 24 mm lens and additional external IR filter. The images were captured with excitation at 980 nm resulting in green luminescence. Some of the results are shown in Figure 3.48 and Figure 3.49. Fingermarks developed with either CA-R6G or β-$NaYF_4$:Yb,Er-2-SiO_2-Ph particles were subjected to evaluation. The presence of any clear ridge details on the fingermark sample was determined as the main criterion.

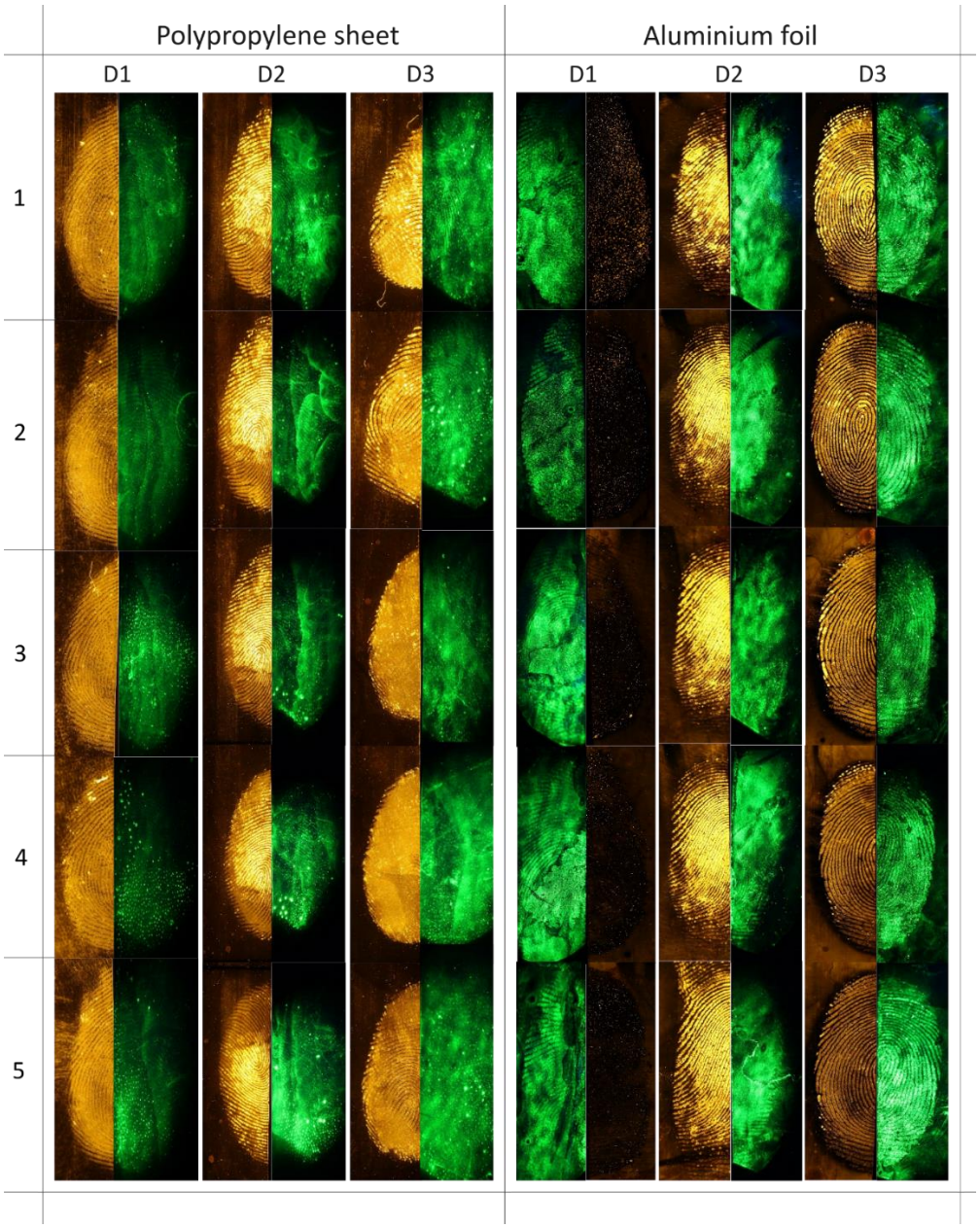

Figure 3.48 Fingermarks in the depletion series (1-5) on polypropylene protective sheet and aluminium foil by different donors (D1, D2, D3) after 14 days ageing developed with: cyanoacrylate fuming - Rhodamine 6G, viewed at 590 nm (**yellow mark**), and processed with β-$NaYF_4$:Yb,Er-2-SiO_2-Ph particles, imaged with SLR Camera under 980 nm excitation (**green mark**)

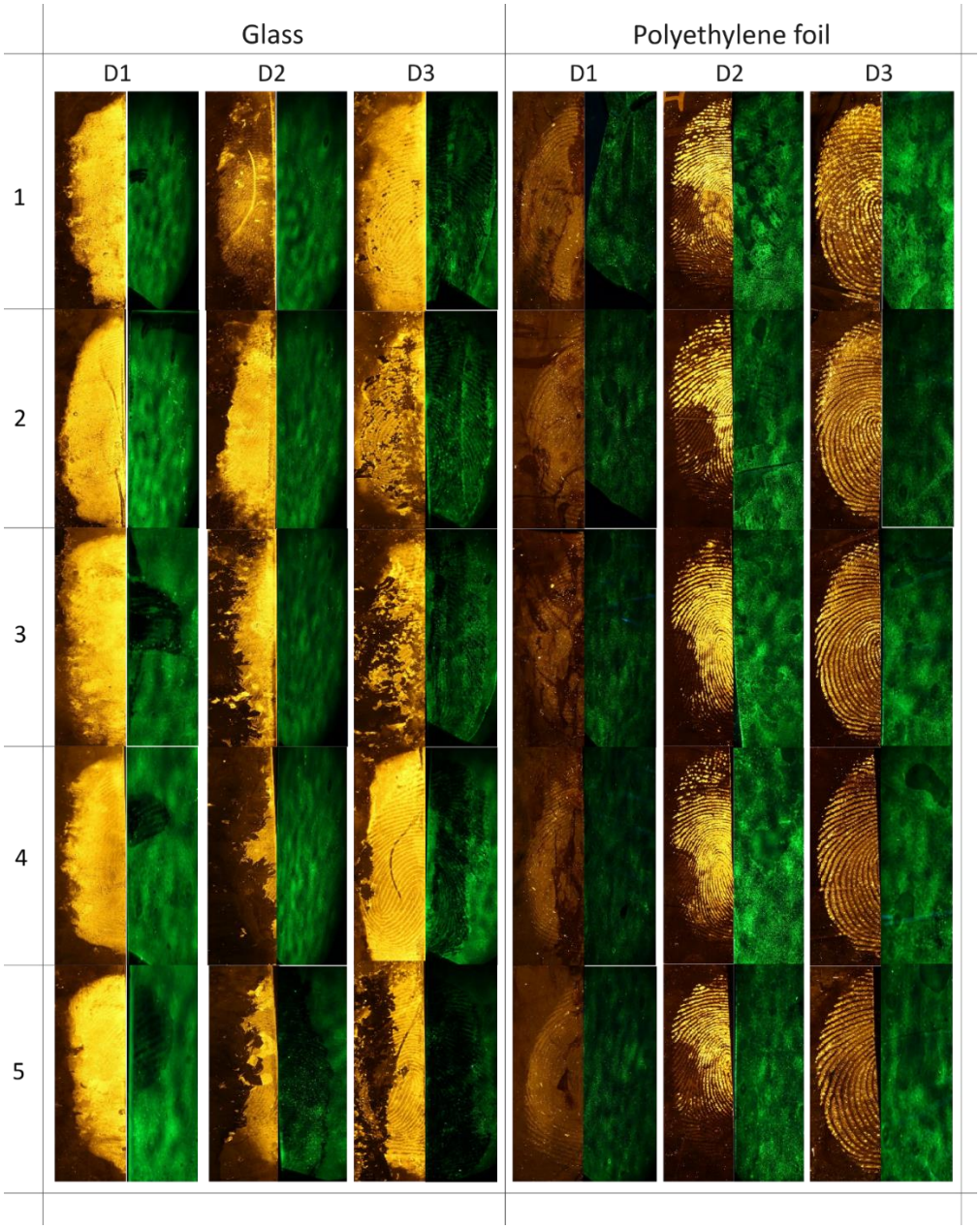

Figure 3.49 Fingermarks in the depletion series (1-5) on a glass slide and polyethylene foil (garbage bag) by different donors (D1, D2, D3) after 14 days ageing developed with: cyanoacrylate fuming-Rhodamine 6G, viewed at 590 nm (**yellow mark**), and processed with β-$NaYF_4$:Yb,Er-2-SiO_2-Ph particles, imaged with SLR Camera under 980 nm excitation (**green mark**)

As observed throughout the comparison trial, the UCPs are affected by fingermark donor variability - very few fingermarks of donor 2 were enhanced, and also by surface type – no results for polyethylene foil and poor results for polypropylene sheet were obtained. On the other hand, CA fuming with RG6 staining indicated the variability across the surface types. Almost no fingermark was detected on the glass substrate, and background staining was observed.

Considering the β-$NaYF_4$:Yb,Er-2-SiO_2-Ph particle treatment on polypropylene foil, significant background staining was observed for all three donors' split depletion halves. In the first two depletion series of each donor, one can distinguish small areas of sufficiently developed ridges, but for the remaining series, the ridge details were almost invisible. In the case of CA fuming and R6G staining, the ridge details were visible for nearly all split depletion halves. The second donor's fingermarks contained a lot of visible 2^{nd} level details. The ridges were well developed for each depletion series halves provided good contrast between the ridge and the background. The first and third donor's fingermarks were a bit overdeveloped; however, the details were quite well visible in each depletion halves of donor one and 1^{st}, 2^{nd} and 5^{th} depletion of donor 3. In the case of aluminium foil, the sensitivity was inferior under β-$NaYF_4$:Yb,Er-2-SiO_2-Ph particle treatment and was dependant on the donor. Fingermarks from the first and third donor were recovered sufficiently enough to see the 1^{st} and, in some cases, 2^{nd} level ridge details for each depletion series. Fingermarks from donor 2 were all overdeveloped; however, some visible areas were present on the 4^{th} and 5^{th} depletion series halves. The CA fuming was efficiently applied for fingermarks of donors 2 and 3. The second and even third level of ridge details were visualised, and excellent contrast between the ridge and the substrate has been obtained. On the other hand, poor fingermarks were observed for CA fuming of first donor split depletion halves.

For both CA fuming and β-$NaYF_4$:Yb,Er-2-SiO_2-Ph particles treatment of fingermarks deposited on glass, only the third donor split depletion halves were visible. The fingermarks were mostly overdeveloped, but some first and second level ridge details were noticed. The fingermarks of the first and second donor were weakly observable for all depletion series. Not a single fingermark on polyethylene foil has been developed with β-$NaYF_4$:Yb,Er-2-SiO_2-Ph particles. The material was deposited on the entire surface of the split depletion halves. A considerable difference was observed for items treated with CA fuming. The fingermarks from donors 2 and 3 were developed with good contrast and ridge details. Each split depletion halves from donor 1 were slightly overdeveloped; however, there were some areas with the first and second level of ridge details.

The systematic comparison of fingermarks developed with β-$NaYF_4$:Yb,Er-2-SiO_2-Ph particles and CA-R6G has also been made. A total of 900 fingermark scores have been collated and analysed for the general trends. The overall score distribution and score distributions for each depletion separately are shown in Figure 3.50.

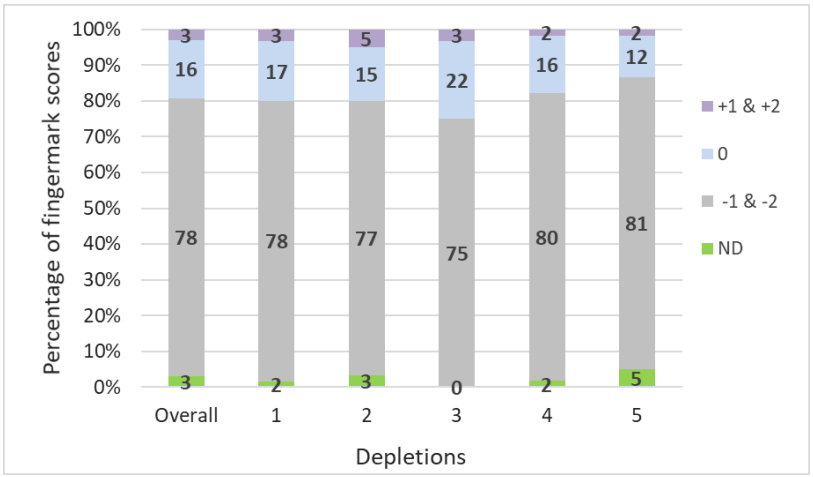

Figure 3.50 The overall distribution of fingermark scores across the five depletions

The combined "+1" and "+2" scores as well as "-1" and "-2" scores have been taken into consideration. A total of 78 % of the fingermarks have been developed with β-$NaYF_4$:Yb,Er-2-SiO_2-Ph particles with lower efficiency than fingermarks developed with CA-R6G. The increase in fingermark enhancement with the β-$NaYF_4$:Yb,Er-2-SiO_2-Ph material was noticed for only 3 % of developed fingermarks. However, 16% of fingermarks have been developed with both β-$NaYF_4$:Yb,Er-2-SiO_2-Ph particles and CA-R6G with comparable efficiency. The CA-R6G has shown a better detection method in comparison to UCPs. The number of fingermarks with increased enhancement with β-$NaYF_4$:Yb,Er-2-SiO_2-Ph particles was consistent across the depletions; however, the second depletion had a slightly higher percentage in this category. A minor increase was observed for fourth and fifth depletion in the case of combined "-1" and "-2" scores. This indicates that CA-R6G is more sensitive for weaker fingermarks than tested UCPs.

It is observed from the distribution of scores across all three donors (Figure 3.51) that CA-R6G detect fingermarks with superior efficiency compared to β-NaYF4:Yb Er-2-SiO_2-Ph particles. However, the low rate of "no detection" scores indicates that both techniques can efficiently detect fingermark.

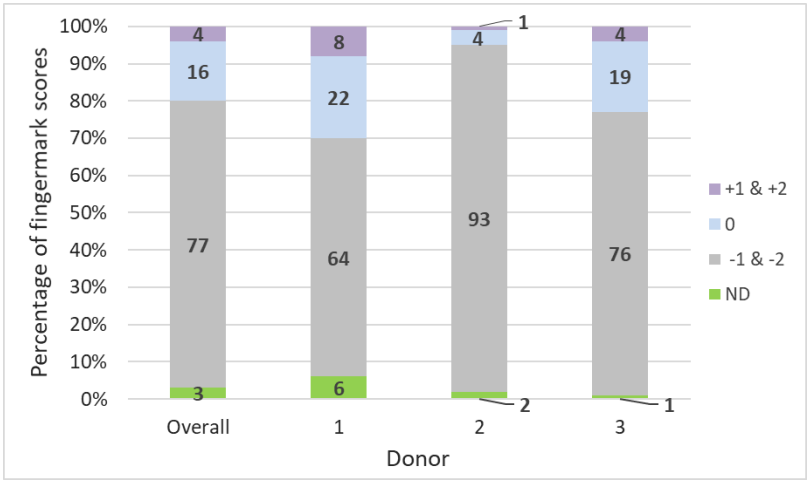

Figure 3.51 The distribution of fingermark scores across the three donors

The impact of four different substrates on the fingermark development process was also investigated (Figure 3.52). On average, CA-R6G provides a higher number of more efficiently enhanced latent fingermarks deposited on all four substrates than β-NaYF4:Yb Er-2-SiO_2-Ph particles.

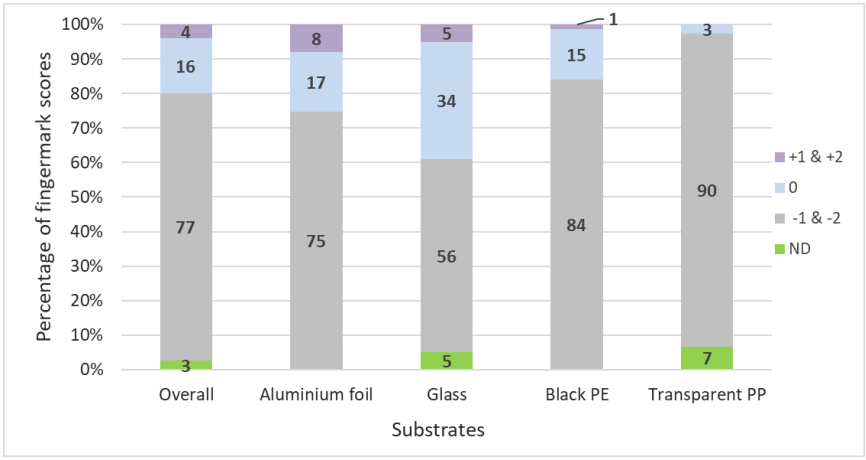

Figure 3.52 The distribution of fingermark scores across the four substrate types

Considering only the fingermarks developed with β-$NaYF_4$:Yb,Er-2-SiO_2-Ph particles, this technique performs better on aluminium foil and glass substrates, yielding a higher number of detected fingermark compared to PE and PP substrates. Also, it is worth noting that in the case of aluminium foil and polyethylene foil, all deposited fingermarks have been detected.

From the above results, the benchmark method, which was cyanoacrylate fuming followed by Rhodamine 6G staining, gave superior results compared to β-NaYF4:Yb,Er-2-SiO_2-Ph suspension method for most of the examined substrates. However, these two methods were equally less effective for fingermark enhancement on the glass surface. The results from the split depletion series showed that the β-$NaYF_4$:Yb,Er-2-SiO_2-Ph particles indicated a moderate affinity for fingermark ridges on PP film, aluminium foil, and no affinity on PE foil. On all surfaces, higher background staining occurred upon upconverting material than CA fuming. Of the three donors involved in the trial, only two provided visible fingermarks on aluminium foil, and only one provided visible fingermarks on polypropylene foil and glass after upconversion particles treatment. In summary, the split depletion study that investigated the efficiency and selectivity of β-$NaYF_4$:Yb,Er-2-SiO_2-Ph particles in comparison with the conventional technique indicated no significant increase in fingermark ridge quality across the commonly used substrates.

Comparison of the detection efficiency of β-$NaYF_4$:Yb,Er-2-SiO_2-Ph particles and CA-R6G on a highly luminescent substrate

The efficiency of β-$NaYF_4$:Yb,Er-2-SiO_2-Ph particles, as a latent fingermark development method on a multicoloured luminescent substrate, was compared with the CA-R6G method of fingermark detection. The natural fingermarks were collected on the Fanta can substrate, aged for five days and then processed with either β-$NaYF_4$:Yb,Er-2-SiO_2-Ph water-ethanol suspension or cyanoacrylate fuming followed by Rhodamine 6G staining in the same manner as previously mentioned (Figure 3.53). Both methods provided good fingermark development. Slightly more clear ridge details were observed on the fingermark developed with the CA-R6G method. However, the β-$NaYF_4$:Yb,Er-2-SiO_2-Ph particles significantly eliminate the background interference compared to the CA-R6G method.

Figure 3.53 5-day-old fingermark deposited on a Fanta can developed with either CA-R6G or β-$NaYF_4$:Yb,Er-2-SiO_2-Ph particles and imaged under 530 nm or 980 nm light excitation, respectively

3.3.4 Conclusions

A detailed analysis of hydrophobic upconverting particles for fingermark detection on porous and non-porous substrates was performed. For application purposes, the hexagonal structure (β phase) of β-$NaYF_4$:Yb,Er upconverting crystals, which exhibits higher upconversion luminescence intensity, unlike the cubic phase [51], has been chosen for synthesis. The upconverting particles were successfully synthesised in two ways: by hydrothermal synthesis and by solid-liquid-thermal-decomposition approach. The surface of the particles was then modified with either long hydrocarbon chains or phenyl groups in order to make them hydrophobic. SEM and XRD analysis confirmed the hexagonal structure of the material obtained via both syntheses. Besides, EDX mapping validated the elemental composition of the $NaYF_4$:Yb,Er crystal. The upconversion luminescence measured with CCD camera with the IR filter showed that the luminescence emission intensity of particles obtained in hydrothermal synthesis depends on the molar ratio of citrates to RE^{3+} ions and also on the surface modification. The β-$NaYF_4$:Yb,Er particles modified with organic moieties were applied to enhance fingermarks deposited on porous and non-porous surfaces such as paper, aluminium foil, beverage can, glass, sticky side of the adhesive tape, PP and PE foil. The fingermarks were developed by the wet technique in which the samples were immersed in the non-toxic water-ethanol suspension. This form of application yields non-destructive interaction between fingermark ridges and developing agent, unlike the brushing technique. Modifying the surface of β-$NaYF_4$:Yb,Er particles with silica and hydrophobic moieties was aimed at increasing

the interactions between the luminescent agent and the fingermark residuals. In that, a multifunctional material was obtained, which on the one hand had upconversion luminescence properties emitting visible light under infrared excitation, and on the other hand was hydrophobic, what increase the affinity to the fingermark residue consisting of fatty acids, waxes, triglycerides, etc.

The trial study of fingermarks enhancement with modified β-$NaYF_4$:Yb,Er-1 particles indicated that the material effectively interacted with fingermarks substance only on aluminium foil or glass substrates, while on the sticky side of adhesive tape, PP foils, colourful beverage can resulted in poor quality fingermarks. Even changing the carrier solvent to petroleum ether or methanol did not improve the fingermark development. This material also failed in fingermark development on paper; the small amount of luminescent material was randomly scattered on the surface. Also, this material possessed relatively low emission intensity, which was of three orders of magnitude lower in comparison to the emission intensity of upconverting particles obtained in SLTD synthesis. Therefore, the imaging process required collecting the signal for at least a few seconds.

The SLTD synthesis allowed to obtain the particles with significantly higher emission intensity compared to the particles synthesised via hydrothermal synthesis. Moreover, the SLTD synthesised particles were of one order of magnitude smaller than hydrothermally synthesised material. It influenced the efficiency of selective deposition on fingermark ridges, observed under SEM. Since these particles exhibited the potential for fingermark enhancement due to their strong luminescence facilitating easier fingermark imaging with an SLR camera, they were selected for further comparative study. Cyanoacrylate fuming followed by Rhodamine 5G staining was selected for this analysis as a recommended method for non-porous substrates. The study involved four substrates onto which three donors deposited depletion series of five fingermarks. The results showed that β-$NaYF_4$:Yb,Er-2-SiO_2-Ph particles did not enhance fingermarks as efficiently as cyanoacrylate fuming with Rhodamine 6G dyeing. The background staining was observed in most items, which means that the required selectivity has not been achieved. Moreover, on PE foil, the particles were deposited on the entire surface of the sample. But on the other side, high sensitivity was observed for a few fingermarks that were successfully developed (for two donors on aluminium foil and one donor on glass) because each of the five fingermarks in the depletion series was developed with a high level of detail.

The advantage of the obtained particles, such as small size, unfortunately, might have prevented their effective application to fingermark development. The

non-selective deposition on the substrates could have been caused by the shape of the particles. Particles with a relatively large flat surface and also deposited outside the ridges could interact with the surface so strongly that rinsing the sample did not weaken these interactions [42].

In conclusion, the modified β-$NaYF_4$:Yb,Er upconversion crystals do not allow for the utterly effective development of fingermarks on non-porous and porous surfaces. Nevertheless, the performed analysis showed that it is possible to develop fingermarks with good contrast with $NaYF_4$:Er,Yb material. The UCPs may also be good candidates for fingermark detection on multicoloured and highly luminescent substrates where the conventional CA-R6G method is less effective due to the background interference. Further optimisation of such parameters as suspension concentration, immersing time, rinsing technique, carrier solvent is needed. Due to the limited time of the research, this work may have been undertaken at a later date.

3.4 References

[1] E. J. Baxter, *Complete Crime Scene Investigation Handbook*, vol. 1, no. 1. CRC Press, 2015.

[2] C. Champod, C. Lennard, P. Margot, and M. Stoilovic, *Fingerprints and other ridge skin impressions, second edition*. CRC Press, 2017.

[3] B. Yamashita and M. French, "Latent Print Development," in *The Fingerprint Sourcebook*, H. J. Eric H., R. Laurie O., L. John H., B. Yamashita, and M. French, Eds. National Institute of Justice, 2011, pp. 7.1-7.67.

[4] J. Dutta, S. A. Ramakrishna, and I. Mekkaoui Alaoui, "Fingerprint visualization enhancement by deposition of columnar thin films and fluorescent dye treatment," *Forensic Sci. Int.*, vol. 228, no. 1–3, pp. 32–37, 2013, doi: 10.1016/j.forsciint.2013.02.018.

[5] E. R. Menzel, "Recent advances in photoluminescence detection of fingerprints," *ScientificWorldJournal.*, vol. 1, pp. 498–509, 2001, doi: 10.1100/tsw.2001.76.

[6] F. M. Hauser, G. Knupp, and S. Officer, "Improvement in fingerprint detection using Tb(III)-dipicolinic acid complex doped nanobeads and time resolved imaging," *Forensic Sci. Int.*, vol. 253, pp. 55–63, 2015, doi: 10.1016/j.forsciint.2015.05.010.

[7] L. Liu, Z. Zhang, L. Zhang, and Y. Zhai, "The effectiveness of strong afterglow phosphor powder in the detection of fingermarks," *Forensic Sci. Int.*, vol. 183, no. 1–3, pp. 45–49, Jan. 2009, doi: 10.1016/j.forsciint.2008.10.008.

[8] X. Xiong, X. Yuan, J. Song, and G. Yin, "Time-resolved detection of fingermarks

on non-porous and semi-porous substrates using $Sr_2MgSi_2O_7:Eu^{2+},Dy^{3+}$ phosphors," *Appl. Spectrosc.*, vol. 70, no. 6, pp. 995–1000, 2016, doi: 10.1177/0003702816641266.

[9] L. K. Seah, U. S. Dinish, S. K. Ong, Z. X. Chao, and V. M. Murukeshan, "Time-resolved imaging of latent fingerprints with nanosecond resolution," *Opt. Laser Technol.*, vol. 36, no. 5, pp. 371–376, Jul. 2004, doi: 10.1016/j.optlastec.2003.10.006.

[10] D. Sriramulu, S. P. Turaga, A. X. Yi, A. A. Bettiol, and S. Valiyaveettil, "Synthesis, characterization and application of luminescent silica nanomaterials," *J. Mater. Chem. C*, vol. 4, no. 47, pp. 11190–11197, 2016, doi: 10.1039/c6tc03677e.

[11] S. A. Kulkarni, S. B. Ogale, and K. P. Vijayamohanan, "Tuning the hydrophobic properties of silica particles by surface silanization using mixed self-assembled monolayers," *J. Colloid Interface Sci.*, vol. 318, no. 2, pp. 372–379, Feb. 2008, doi: 10.1016/j.jcis.2007.11.012.

[12] J. Almog, A. A. Cantu, C. Champod, T. Kent, and C. Lennard, "Guidelines for the Assessment of Fingermark Detection Techniques," *J. Forensic Identif.*, vol. 64, no. 2, pp. 174–197, 2014.

[13] H. L. Bandey, S. M. Bleay, V. J. Bowman, R. P. Downham, and V. G. Sears, *Fingermark Visualisation Manual*, First. Home Office Centre for Applied Science and Technology (CAST), 2014.

[14] A. B. Djurišić *et al.*, "Defect emissions in ZnO nanostructures," *Nanotechnology*, vol. 18, no. 9, pp. 1–8, 2007, doi: 10.1088/0957-4484/18/9/095702.

[15] D. Li *et al.*, "Different origins of visible luminescence in ZnO nanostructures fabricated by the chemical and evaporation methods," *Appl. Phys. Lett.*, vol. 85, no. 9, pp. 1601–1603, 2004, doi: 10.1063/1.1786375.

[16] H. K. Yadav, K. Sreenivas, V. Gupta, S. P. Singh, and R. S. Katiyar, "Effect of surface defects on the visible emission from ZnO nanoparticles," *J. Mater. Res.*, vol. 22, no. 9, pp. 2404–2409, 2007, doi: 10.1557/jmr.2007.0321.

[17] O. Arslan, L. Belkoura, and S. Mathur, "Swift synthesis, functionalization and phase-transfer studies of ultrastable, visible light emitting oleate@ZnO quantum dots," *J. Mater. Chem. C*, vol. 3, no. 45, pp. 11965–11973, Nov. 2015, doi: 10.1039/c5tc03377b.

[18] V. Prasad, C. D'Souza, D. Yadav, A. J. Shaikh, and N. Vigneshwaran, "Spectroscopic characterization of zinc oxide nanorods synthesized by solid-state reaction," *Spectrochim. Acta - Part A Mol. Biomol. Spectrosc.*, vol. 65, no. 1, pp. 173–178, Sep. 2006, doi: 10.1016/j.saa.2005.10.001.

[19] J.-D. Brassard, D. K. Sarkar, and J. Perron, "Fluorine Based Superhydrophobic

Coatings," *Appl. Sci.*, vol. 2, pp. 453–464, May 2012, doi: 10.3390/app2020453.

[20] A. B. Lavand and Y. S. Malghe, "Synthesis, characterization and visible light photocatalytic activity of nitrogen-doped zinc oxide nanospheres," *J. Asian Ceram. Soc.*, vol. 3, no. 3, pp. 305–310, Sep. 2015, doi: 10.1016/j.jascer.2015.06.002.

[21] D. K. Sarkar, D. Brassard, M. A. E. Khakani, and L. Ouellet, "Dielectric properties of sol-gel derived high-k titanium silicate thin films," *Thin Solid Films*, vol. 515, no. 11, pp. 4788–4793, Apr. 2007, doi: 10.1016/j.tsf.2006.11.155.

[22] Y. Sha, C. Deng, and B. Liu, "Development of C18-functionalized magnetic silica nanoparticles as sample preparation technique for the determination of ergosterol in cigarettes by microwave-assisted derivatization and gas chromatography/mass spectrometry," *J. Chromatogr. A*, vol. 1198–1199, no. 1–2, pp. 27–33, Jul. 2008, doi: 10.1016/j.chroma.2008.05.049.

[23] Y. S. Li, Y. Wang, and S. Ceesay, "Vibrational spectra of phenyltriethoxysilane, phenyltrimethoxysilane and their sol-gels," *Spectrochim. Acta - Part A Mol. Biomol. Spectrosc.*, vol. 71, no. 5, pp. 1819–1824, Jan. 2009, doi: 10.1016/j.saa.2008.04.027.

[24] A. A. Frick, P. Fritz, and S. W. Lewis, "Chemical methods for the detection of latent fingermarks," in *Forensic Chemistry Fundamentals and Applications*, J. Siegel, Ed. Wiley Blackwell, 2016.

[25] M. Wang *et al.*, "NIR-induced highly sensitive detection of latent fingermarks by $NaYF_4$:Yb,Er upconversion nanoparticles in a dry powder state," *Nano Res.*, vol. 8, no. 6, pp. 1800–1810, 2015, doi: 10.1007/s12274-014-0686-6.

[26] M. Wang, "Latent fingermarks light up: Facile development of latent fingermarks using NIR-responsive upconversion fluorescent nanocrystals," *RSC Adv.*, vol. 6, no. 43, pp. 36264–36268, 2016, doi: 10.1039/c6ra04573a.

[27] Z. Zhao, J. Shen, and M. Wang, "Simultaneous imaging of latent fingerprint and quantification of nicotine residue by $NaYF_4$:Yb/Tm upconversion nanoparticles," *Nanotechnology*, vol. 31, no. 14, 2020, doi: 10.1088/1361-6528/ab647c.

[28] J. Wang *et al.*, "Near-infrared-light-mediated imaging of latent fingerprints based on molecular recognition," *Angew. Chemie - Int. Ed.*, vol. 53, no. 6, pp. 1616–1620, 2014, doi: 10.1002/anie.201308843.

[29] R. Ma *et al.*, "Fingermark detection on non-porous and semi-porous surfaces using $NaYF_4$:Er,Yb up-converter particles," *Forensic Sci. Int.*, vol. 207, pp. 145–149, 2011, doi: 10.1016/j.forsciint.2010.09.020.

[30] M. Wang, Y. Zhu, and C. Mao, "Synthesis of NIR-Responsive $NaYF_4$:Yb,Er Upconversion Fluorescent Nanoparticles Using an Optimized Solvothermal

Method and Their Applications in Enhanced Development of Latent Fingerprints on Various Smooth Substrates," *Langmuir*, vol. 31, pp. 7084–7090, 2015, doi: 10.1021/acs.langmuir.5b01151.

[31] F. Auzel, "Upconversion and Anti-Stokes Processes with f and d Ions in Solids," *Chem. Rev.*, vol. 104, pp. 139–173, 2004, doi: 10.1021/cr020357g.

[32] Q. C. Sun, Y. C. Ding, D. M. Sagar, and P. Nagpal, "Photon upconversion towards applications in energy conversion and bioimaging," *Progress in Surface Science*, vol. 92. Elsevier Ltd, pp. 281–316, Dec. 01, 2017, doi: 10.1016/j.progsurf.2017.09.003.

[33] C. Ye, L. Zhou, X. Wang, and Z. Liang, "Photon upconversion: from two-photon absorption (TPA) to triplet-triplet annihilation (TTA)," *Phys. Chem. Chem. Phys.*, vol. 18, pp. 10818–10835, 2016, doi: 10.1039/c5cp07296d.

[34] J. F. Suyver *et al.*, "Novel materials doped with trivalent lanthanides and transition metal ions showing near-infrared to visible photon upconversion," *Opt. Mater. (Amst).*, vol. 27, pp. 1111–1130, Mar. 2005, doi: 10.1016/j.optmat.2004.10.021.

[35] S. Heer, K. Kömpe, H.-U. Güdel, and M. Haase, "Highly Efficient Multicolour Upconversion Emission in Transparent Colloids of Lanthanide-Doped $NaYF_4$ Nanocrystals," *Adv. Mater.*, vol. 16, no. 23–24, pp. 2102–2105, Dec. 2004, doi: 10.1002/adma.200400772.

[36] H. Dong, L.-D. Sun, and C.-H. Yan, "Energy transfer in lanthanide upconversion studies for extended optical applications," *Chem. Soc. Rev.*, vol. 44, pp. 1608–1634, 2015, doi: 10.1039/c4cs00188e.

[37] R. S. P. King and D. A. Skros, "Sunlight-activated near-infrared phosphorescence as a viable means of latent fingermark visualisation," *Forensic Sci. Int.*, vol. 276, pp. e35–e39, Jul. 2017, doi: 10.1016/j.forsciint.2017.04.012.

[38] C. Li, Z. Quan, J. Yang, P. Yang, and J. Lin, "Highly Uniform and Monodisperse-$NaYF_4$:Ln^{3+} (Ln = Eu, Tb, Yb/Er, and Yb/Tm) Hexagonal Microprism Crystals: Hydrothermal Synthesis and Luminescent Properties," *Inorg. Chem.*, vol. 46, no. 16, pp. 6329–6337, 2007, doi: 10.1021/ic070335i.

[39] W. You *et al.*, "Large-scale synthesis of uniform lanthanide-doped $NaREF_4$ upconversion/downshifting nanoprobes for bioapplications," *Nanoscale*, vol. 10, pp. 11477–11484, 2018, doi: 10.1039/c8nr03252a.

[40] C. Graf, D. L. J. Vossen, A. Imhof, and A. Van Blaaderen, "A general method to coat colloidal particles with silica," *Langmuir*, vol. 19, no. 17, pp. 6693–6700, 2003, doi: 10.1021/la0347859.

[41] P. L. T. Lee *et al.*, "Latent fingermark detection using functionalised silicon oxide nanoparticles: Optimisation and comparison with cyanoacrylate

fuming," *Forensic Sci. Int.*, vol. 315, 2020, doi: 10.1016/j.forsciint.2020.110442.

[42] S. M. Bleay *et al.*, *Fingerprint Source Book*. Home Office Centre for Applied Science and Technology, 2012.

[43] V. Stewart, P. Deacon, and K. Farrugia, "A review of one-step fluorescent cyanoacrylate techniques," *Fingerpr. Whorld*, vol. 41, no. 162, pp. 6–29, 2016.

[44] M. Ding *et al.*, "Simultaneous morphology manipulation and upconversion luminescence enhancement of β-$NaYF_4$:Yb^{3+}/Er^{3+} microcrystals by simply tuning the KF dosage," *Sci. Rep.*, vol. 5, pp. 1–14, 2015, doi: 10.1038/srep12745.

[45] M. D. Taylor, "Preparation of anhydrous lanthanon halides," *Chem. Rev.*, vol. 62, no. 6, pp. 503–511, 1962, doi: 10.1021/cr60220a001.

[46] G. Tessitore, G. A. Mandl, M. G. Brik, W. Park, and J. A. Capobianco, "Recent insights into upconverting nanoparticles: Spectroscopy, modeling, and routes to improved luminescence," *Nanoscale*, vol. 11, pp. 12015–12029, 2019, doi: 10.1039/c9nr02291k.

[47] T. Kang, I. Jang, and S. G. Oh, "Surface modification of silica nanoparticles using phenyl trimethoxy silane and their dispersion stability in N-methyl-2-pyrrolidone," *Colloids Surfaces A Physicochem. Eng. Asp.*, vol. 501, pp. 24–31, 2016, doi: 10.1016/j.colsurfa.2016.04.060.

[48] X. mei Wang, X. zhen Du, C. lan Li, and X. Cao, "Direct synthesis and characterization of phenyl-functionalized SBA-15," *Appl. Surf. Sci.*, vol. 254, no. 13, pp. 3753–3757, 2008, doi: 10.1016/j.apsusc.2007.11.031.

[49] L. S. Solaree, A. Monshi, and H. Ghayour, "A New Approach for the Fabrication of Hydrophobic Silica Coatings on Glass Using Sol-Gel Method," *Synth. React. Inorganic, Met. Nano-Metal Chem.*, vol. 45, no. 12, pp. 1769–1772, 2015, doi: 10.1080/15533174.2013.872132.

[50] G. S. Sodhi and J. Kaur, "Powder method for detecting latent fingerprints: A review," *Forensic Sci. Int.*, vol. 120, pp. 172–176, Sep. 2001, doi: 10.1016/S0379-0738(00)00465-5.

[51] R. A. Janjua *et al.*, "Na^+-Driven Nucleation of $NaYF_4$:Yb,Er Nanocrystals and Effect of Temperature on Their Structural Transformations and Luminescent Properties," *J. Phys. Chem. C*, vol. 122, no. 40, pp. 23242–23250, 2018, doi: 10.1021/acs.jpcc.8b09327.

Chapter 4 Diaquatris(thenoyltrifluoroacetonate)europium(III) complex for time-gated visualisation

4.1 Introduction

The results of the study on the visualisation of fingermarks deposited on luminescent, reflective or patterned surfaces, described in Chapter 3, have shown that applying time-gated imaging for fingermarks developed with luminescent silica particles can be an effective alternative to widely applied methods such as luminescent powder dusting or cyanoacrylate fuming followed by luminescent dye staining; however, mainly for non-porous substrates. Some porous surfaces like paper exhibit strong background luminescence, which lead to the contrast decrease or even make the fingermark invisible when imaged in the fluorescence mode. Thus, to efficiently visualise latent fingermarks deposited on paper-based porous surfaces, firstly, it is necessary to use the developing agent, which is able to interact with fingermark components highly selectively. Secondly, it is essential to apply a developing agent with a long luminescence lifetime and to use time-gated imaging to eliminate the strong background luminescence. In the case of porous surfaces, some difficulties occur during the development process. Essentially, the fingermark residuals do not retain on the porous surface but penetrate into the substrate in time, so that after one day, most components, both sebaceous and amino acids, are hidden in the porous structure [1]. The luminescent silica particles applied for time-gated visualisation were not small enough; hence, they were not able to diffuse into the paper matrix and interact with the fingermark.

Numerous luminescent developing reagents and methods employed for fingermark enhancement have been described in Chapter 1.3 and 1.4, including widely used amino acid-sensitive reagents such as ninhydrin with zinc salt posttreatment, 1,8-diazafluoren-9-one (DFO), 1,2-indanedione. Among the other luminophores, a group that may find an application for LFM detection is the lanthanide β-diketonates, with europium complexes as popular rare-earth coordination compounds, introduced in Chapter 1.9.

Until now, the lanthanide complexes, due to their strong emission and wide gaps between excitation and emission bands, have already been employed to develop latent fingermarks on porous or semi-porous surfaces. The visualisation methods were mostly based on radiation frequency filtration; nonetheless, some

limitations have also been reported, mainly concerning the interference of the background, working only on sebaceous or fresh marks, or using the organic solvents. Wilkinson et al. had examined cyanoacrylate fuming followed by several europium tris chelates to detect latent fingermarks on skin. The best results were obtained for europium tris(thenoyltrifluoroacetone); however, organic solvents had to be used to transfer the europium complex to cyanoacrylate deposited on the fingermark. The authors also pointed out that further improvements might have been obtained by using time-resolved imaging [2]. Also, europium tris(thenoyl-trifluoroacetone) with water molecules replaced with trioctylphosphine oxide was investigated as LFM developing agent; nevertheless, the sensitivity of this formulation on natural fingermarks was inferior to benchmark method such as physical developer [3]. The other europium complex that was studied to visualise LFM on porous and non-porous surfaces was tris (6,6,7,7,8,8-heptafluoro-2,2dimethyl-3,5-octanedionato)europium (III) known as [Eu(fod)$_3$] which indicated high reactivity towards functional groups present in fingermark residue [4]. The [Eu(fod)$_3$] complex treatment resulted in a good fingermark enhancement, but the benchmark visualisation method based on DFO treatment yielded better results.

To avoid the necessity of the selective modification of the fingermarks deposited on porous surfaces, eliminate the surface interference and increase the signal-to-background ratio, the strategy based on *in situ* generation of new compounds that possess long luminescence lifetimes was a subject of the study. A developing reagent, distributed over the entire sample surface, interacted only with fingermark components, locally generating compounds with desirable luminescence properties, eliminating the need for selective deposition. A scheme of the latent fingermark visualisation on paper with the time-gated imaging system using *in situ* interactions between the development agent and fingermark components is shown in Figure 4.1.

In this chapter, the synthesis and application of a diaqua-tris(thenoyltrifluoroacetonate)europium(III) complex [Eu(TTA)$_3$(H$_2$O)$_2$] to develop latent fingermarks deposited on paper-based surfaces with a simple spray-coating technique will be discussed. Due to the fact that efficient latent fingermark development is based on the selective interaction between the development agent and latent fingermark components, the understanding of interactions between chosen europium complex and representative LFM components was studied, including the influence of the interactions on the Eu(TTA)$_3$(H$_2$O)$_2$ complex luminescence lifetimes. The chosen europium complex possess several advantages. Beside the narrow emission band in the visible spectrum of light and large Stoke shift

[5], the complex also indicates the high luminescence intensity due to the thenoyltrifluoroacetone (TTA) ligand, which acts as an antenna, efficiently absorbing and transferring light to the europium cation via intramolecular energy transfer [6], [7]. Moreover, the two water molecules present in the complex structure may be relatively easily exchanged for various latent fingermark components [8] what may change the complex properties [9]. Taking these properties into account, $Eu(TTA)_3(H_2O)_2$ complex seems to be the valuable candidate to enhance latent fingermark development/visualisation on porous surfaces. Furthermore, the europium complex will be examined, including material characteristics, an affinity to fingermark deposits, efficiency of fingermark imaging on various paper-based surfaces, LFM visualisation optimisation and the comparison of development efficiency with benchmark methods, including enhancement of LFM on wetted papers.

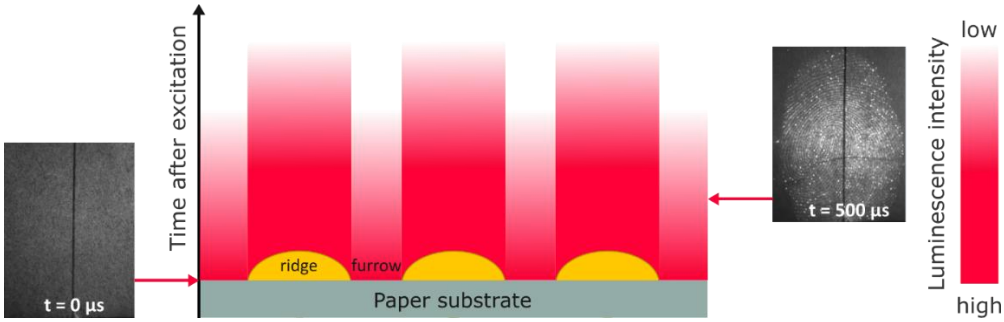

Figure 4.1 The scheme of time-gated imaging of LFM deposited on paper developed with $Eu(TTA)_3(H_2O)_2$ complex, which generates *in situ* interactions with latent fingermark components resulting in the change of the luminescence properties; t represents the delay-to-shutter time

4.2 Experimental

4.2.1 Equipment and Instrumentation

Fluorescence Spectroscopy

The excitation and emission spectra of the $Eu(TTA)_3(H_2O)_2$ complex have been measured with FS5 Spectrofluorometer (Edinburgh Instruments, UK) in a classic 1 cm quartz cuvette. Excitation spectra have been recorded for the emission

monitored at 613 nm. Emission spectra have been registered with an excitation wavelength at 387 nm. The photoluminescence decay measurements for the whole visible spectrum of light have been performed using a home-built time-gated imaging system with a CCD camera (HARDsoft Microprocessor Systems, Poland).

Diffuse Reflectance Infrared Fourier Transform Spectroscopy (DRIFT)

The IR spectra of $Eu(TTA)_3(H_2O)_2$ complex with or without latent fingermark components (oleic acid (OA), squalene, L-serine) have been collected with an FTIR Nicolet iS50 FT-IR spectrometer. Spectra were recorded in diffuse reflectance mode using a continuous flow Harrick Praying Mantis chamber, and typically 45 scans were collected at a resolution of 1 cm^{-1}.

Nuclear Magnetic Resonance (NMR)

^{1}H and ^{13}C NMR measurements of $Eu(TTA)_3(H_2O)_2$ complex were performed on the 7.05 T Bruker AVANCE II spectrometer equipped with a 5 mm BBI Bruker probe head and VT-NMR unit temperature controller. The 5 mm NMR sample tubes were purchased from WILMAD glassware. The spectra for all the samples were acquired with standard Bruker pulse programs for ^{1}H and ^{13}C NMR spectra acquisition. The acquisition parameters: the relaxation delay, number of scans, and acquisition times were the same for each sample. Samples with oleic acid, squalene, and L-serine were combined with samples contained the europium complex.

4.2.2 Chemicals

The following reagents were used for the synthesis of diaquatris(thenoyl-trifluoroacetonate)europium (III) complex $[Eu(TTA)_3(H_2O)_2]$, analysis of the complex, fingermark enhancement and comparative methods of fingermark development. Europium (III) chloride hexahydrate (99.99 %, trace metal basis), L-serine (99 %), squalene (≥ 98 %), ninhydrin (≥ 99 %) were purchased from Sigma-Aldrich. Ethanol (anhydrous, 99.8 %), methanol (pure p.a. 99.8 %), sodium hydroxide (p.a.) were obtained from POCH. 2-thenoyltrifluoroacetone (TTA) was purchased from Fluorochem, oleic acid from Chempur, and 1,2-indanedione from BVDA. RO/DI water was used for all the experiments. All chemicals were used as received. For ^{1}H NMR and ^{1}C NMR analysis, deuterated solvents were purchased from EUROISOTOP and were used without any further purification.

4.2.3 Synthesis of europium β-diketonate complex

The luminescent diaquatris(thenoyltrifluoroacetonate)europium (III) complex was synthesised according to the literature procedure [10]. First, a solution of 0.73 g (2 mmol) of europium (III) chloride hexahydrate in 10 mL of water, as well as 6 mL of 1 M NaOH, was prepared. Then, 1.33 g (6 mmol) of 2-thenoyl-trifluoroacetone was dissolved in 30 mL of ethanol. Europium chloride and sodium hydroxide solutions were successively added to the TTA solution under stirring, followed by pouring 200 mL of water. The reaction mixture was heated to 60 °C under constant stirring for several minutes. When the europium complex started to precipitate, the mixture was cooled down to room temperature. Finally, the precipitate was filtered off with a water pump, rinsed three times with 200 mL of water, and then dried in an oven at 55 °C for 12 hours. The pale yellow powder was obtained.

4.2.4 Fingermark collection

Latent fingermark collection on paper and donor selection was done according to the International Fingerprint Research Group guidelines for Phase 1 [11]. Three donors were chosen (two males, one female) to deposit fingermarks on white paper surfaces. Donors were requested not to wash their hands for at least 30 minutes, and they were advised to behave in a natural way to provide fingermarks comparable to the real-case ones. Before the fingermark deposition, donors were guided to touch paper with a thumb, index, middle and ring finger for 2-3 seconds with moderate pressure, comparable to the force they usually use for holding items. The samples with fingermarks were aged for at least 24 hours in the ambient conditions before further processing.

4.2.5 Fingermark development

To prepare the working solution of $Eu(TTA)_3(H_2O)_2$, europium complex powder was dissolved in methanol with a concentration of 50 mg mL^{-1}. The solution was stirred for several minutes to completely dissolve the powder and then poured into the glass bottle sprayer. Each paper sample was sprayed twice upon the whole area from a distance of ca. 10 centimetres and then left to dry in the air.

4.2.6 Time-gated imaging of samples

The imaging process of LFM on paper substrates and europium complex luminescence lifetime measurements were conducted using the time-gated imaging system previously described in Chapter 3.2.2.6. The apparatus consists of a pulse controller, a computer-controlled CCD camera and a 365 nm ultraviolet light excitation source.

Latent fingermarks deposited on paper substrates and developed with $Eu(TTA)_3(H_2O)_2$ complex were visualised using the time-gated mode of the CCD sensor due to the relatively long luminescence lifetime of the complex deposited on fingermark ridges. The paper sample placed in the camera field of view was first illuminated with a UV excitation pulse, then the radiation source was switched off, and after a particular time, the CCD sensor started to collect the luminescence signal. The precise control of the parameters such as excitation length, the time between the end of the excitation pulse and the opening of the shutter to collect the luminescence signal (delay-to-shutter), and signal collection (shutter time) allows for successful separation of europium complex luminescence on LFM from the luminescence of the background. The optimal contrast between the fingermark ridges and paper background was obtained for illumination time 200 μs, delay to shutter 800 μs, and luminescence signal collecting 100 μs. The illumination-collection sequence was repeated in 1000 cycles to get the optimal contrast.

The time-gated system was also involved in measuring the europium complex luminescence lifetimes. For this purpose, a decay curve was constructed for each sample. The europium complex and LFM components deposited on the glass and paper samples were placed in the camera field of view. Each sample was illuminated with 365 nm UV radiation for 200 μs, and the signal was collecting by opening the shutter for 20 μs. To prepare the decay curve, the average luminescence intensities were extracted from the selected area of the images taken for delay-to-shutter times ranging from 10 to 990 μs. For each decay curve, 50 measuring points and one thousand cycles for each point have been set. The time lag, which is the time between two separate cycles of measurement, was ranging from 900 to 10 μs to compensate the delay-to-shutter time. Finally, to calculate the luminescence lifetime, a monoexponential decay was fitted to each decay curve.

4.2.7 Comparison with conventional enhancement techniques

The selectivity and effectiveness of fingermark enhancement with $Eu(TTA)_3(H_2O)_2$ complex was compared to two benchmark methods: ninhydrin and 1,2-indanedione treatment. These two compounds are, among others, the reagents of choice for paper substrates [12]–[15]. They react with amino acids present in the fingermark residue resulting in colourful or fluorescent products.

Natural fingermarks were deposited on paper substrates. Each sample was then cut in half, as shown in Figure 4.2, and one half was treated with either ninhydrin or 1,2-indanedione working solution and the other half was sprayed with $Eu(TTA)_3(H_2O)_2$ complex. Then the halves were recombined for comparison. Also, the effectiveness of the europium complex, ninhydrin and 1,2-indanedione was investigated for the fingermarks deposited on paper samples which were subsequently wetted. In this case, the fingermark deposited on the paper substrate was immersed in a water bath for 10 minutes under gentle shaking, then dried in the air and cut in half for further processing.

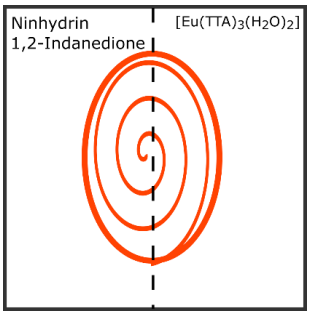

Figure 4.2 A diagram showing fingermark deposited on a paper substrate prepared to compare the fingermark development with $Eu(TTA)_3(H_2O)_2$ complex (right) and with routine developing agents: ninhydrin or 1,2-indanedione (left)

Ninhydrin treatment

This method of fingermark visualisation is based on the reaction between ninhydrin and primary and secondary amines of amino acids present in the fingermark secretion. The reaction product is a non-fluorescent purple-coloured compound, also called Ruhemann's purple, composed of two molecules of ninhydrin linked by a nitrogen atom [1], [16]. The enhancement process demands the elevated temperature to increase the reaction rate and thereby reduce the duration of fingermark development [17]. For the ninhydrin treatment, each fingermark sample

was immersed in 1.5 % of ninhydrin ethanolic working solution [18] and left to dry in the air. Afterwards, the samples were loaded into an oven at 80 °C for 4 minutes.

1,2-Indanedione treatment

1,2-indanedione applied for fingermark development acts in a similar way to ninhydrin. A product of the reaction with amino acids is a fluorescent analogue of the Ruhemann's purple and results in pale pink colouration seen under white light and strong fluorescence emission visible under blue-green light excitation [13], [17], [19]. Visualising fingermarks treated with 1,2-indanedione in the fluorescence mode results in superior sensitivity in comparison to ninhydrin [14]. For the development procedure, 4 mM of 1,2-indanedione working solution in methanol was prepared [20]. The samples were first immersed in the working solution, then left to dry in the air and next placed in the oven at 100 °C for at least 10 minutes.

4.2.8 Interactions of europium β-diketonate complex with fingermark secretion constituents of fingermark

The composition of fingermark secretion is a mixture of compounds produced in the eccrine and sebaceous glands. Eccrine secretion mainly consists of water (98 %) [21] and amino acids with a concentration of 0.3 to 2.59 mg L^{-1} [1], among which L-serine is the most abundant [22]. The main constituents of the sebaceous fraction are lipids consist of glycerides (33 %), fatty acids (30%), wax esters (22 %), squalene (10 %) and others [1]. Among all identified in the fingermark free fatty acids, oleic acid constitutes an abundant fraction (32-1675 ng in fingermark) [22].

The interactions between $Eu(TTA)_3(H_2O)_2$ complex and latent fingermark constituents have been investigated by spectroscopic methods. Three exemplary compounds found in the secretion have been chosen: oleic acid and squalene as the representatives of the sebaceous fraction and L-serine as the representative of the eccrine fraction of fingermark secretion. For excitation and emission spectra, DRIFT and decay time measurements, the $Eu(TTA)_3(H_2O)_2$ complex in a concentration of 0.59 mM was mixed with oleic acid, squalene, and L-serine in methanol, ethanol, and ethanol:water solution (2:1 v/v), respectively, in various molar ratios ($[X]:[Eu(TTA)_3(H_2O)_2]$) ranging from 0 to 4 (from 0 to 1 in 0.1 steps and from 1 to 4 in 0.5 steps), where [X] concerned the concentration of LFM components. The choice of solvents was related to the optimal solubility of the representative compounds

and europium complex. To study the influence of chosen LFM components on europium complex luminescence lifetime (τ), a series of luminescence decay times have been measured for an above-mentioned range of concentrations of LFM constituents and europium complex. Each of the mixtures was drop cast three times with either 5 µl on a microscope glass slide or 1 µl on notebook paper sample at intervals allowing the solvent to evaporate. Apart from this, it was also investigated how the europium complex luminescence lifetime changes when it reacts with the fingermark constituents deposited on a paper sample. For this purpose, the solutions of pure oleic acid, squalene or L-serine at 0.1 M concentration in methanol, ethanol and ethanol:water (2:1 v/v), respectively, was separately spotted on copy paper sample followed by subsequently spraying the $Eu(TTA)_3(H_2O)_2$ complex in methanol.

In the case of ^1H NMR and ^1C NMR measurements, the samples were prepared as follows: 5 mg of oleic acid and 5 mg of squalene was dissolved in 0.5 mL methanol-d_4 and ethanol-d_6, respectively. L-serine (5 mg) was dissolved in 0.5 mL of ethanol-d_6/water-d_2 solution (1:1 v/v). Additionally, 10 mg, 10 mg, and 5 mg of $Eu(TTA)_3(H_2O)_2$ complex was mixed in methanol-d_4, ethanol-d_6, and ethanol-d_6/water-d_2 solution (1:1 v/v), respectively.

4.3 Results and discussion

This section will discuss the characteristic of the $Eu(TTA)_3(H_2O)_2$ complex and the analysis of the interactions between the europium complex and representative fingermark secretion components. Also, the effectiveness of the latent fingermark enhancement on paper and the results of a comparative study of fingermark development with europium complex and benchmark methods will be presented.

Characterisation of the luminescent $Eu(TTA)_3(H_2O)_2$ complex

The pale yellow $Eu(TTA)_3(H_2O)_2$ powder showed hydrophobic properties. It barely dissolved in water, in contrast with ethanol. The material excited with 365 nm ultraviolet light has shown the strong orange luminescence emission (Figure 4.3).

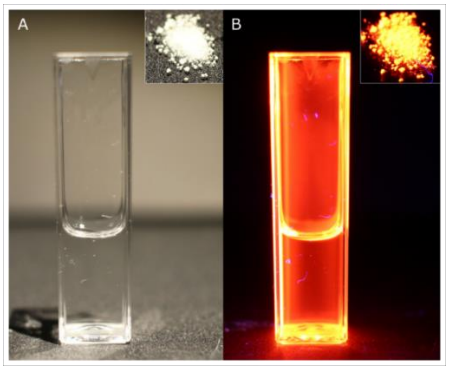

Figure 4.3 The 1 mg mL^{-1} $Eu(TTA)_3(H_2O)_2$ solution in ethanol illuminated with (A) white light, (B) 365 nm UV light. The insets: powder $Eu(TTA)_3(H_2O)_2$

Figure 4.4 A shows the excitation spectrum of $Eu(TTA)_3(H_2O)_2$ complex recorded in the range of 350 to 450 nm and monitoring the emission at 613 nm.

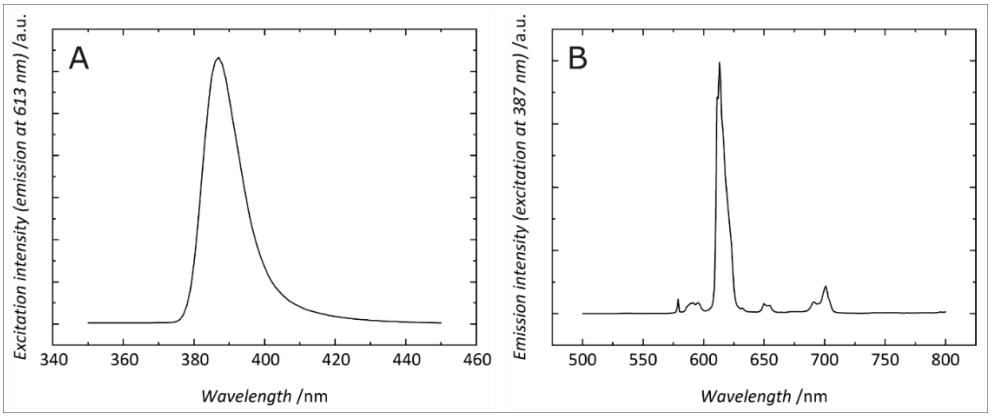

Figure 4.4 (A) Excitation spectrum (emission monitored at 613 nm) of 0.59 mM $Eu(TTA)_3(H_2O)_2$ solution in ethanol; (B) emission spectrum (excitation at 387 nm) of 0.59 mM $Eu(TTA)_3(H_2O)_2$ solution in ethanol

The excitation light was efficiently absorbed by the organic ligand, and the complex displayed a broad absorption band with the maximum peak at 387 nm, which was related to the π-π* transition of the carbonyl group in TTA ligand coordinated to europium ion [23]–[25]. The luminescence emission spectrum of $Eu(TTA)_3(H_2O)_2$ complex (Figure 4.4 B) recorded in the range of 500 – 800 nm under 387 nm excitation radiation exhibits several narrow bands, among which the most intense is a band with the maximum at 613 nm attributed to $^5D_0 \rightarrow {}^7F_2$ transition [26], [27]. According to the literature data, the lanthanide ion, when excited directly with 395 nm radiation, is characterised by weak light absorption due to the forbidden

4f-4f transitions. Only a small amount of photons is absorbed in the 4f levels, which results in low luminescence intensity [23], [28]. The low absorption of light by the lanthanide ion is boost by the intense UV absorbing of TTA chelating ligand [6], [23], [27]. The intramolecular energy transfer from the organic ligand excited state to the metal ion, resulting in the narrow emission band, is called the “antenna effect” [29], [30]. A TTA ligand in the europium complex, irradiated with the UV light in the range of 300 – 400 nm, absorbs the energy that results in excitation to the first excited singlet state ($S_0 \rightarrow S_1$). After internal conversion to the lowest vibrational level of the excited singlet state, the nonradiative intersystem crossing (ISC) from the S_1 state of the ligand to its triplet state T_1 takes place, followed by the subsequent intramolecular energy transfer (ET) from ligand triplet state to Eu^{3+} excited states (^5D_J). After the transition of electrons from higher excited states to $^5D_0$ state by internal conversion, Eu^{3+} finally emits the line-like photoluminescence during the transition to its ground state [28], [30].

The excitation and emission spectra were recorded for the mixtures of 0.59 mM $Eu(TTA)_3(H_2O)_2$ complex and oleic acid, L-serine or squalene in the range of molar ratios from 0 to 4 (Figure 4.5).

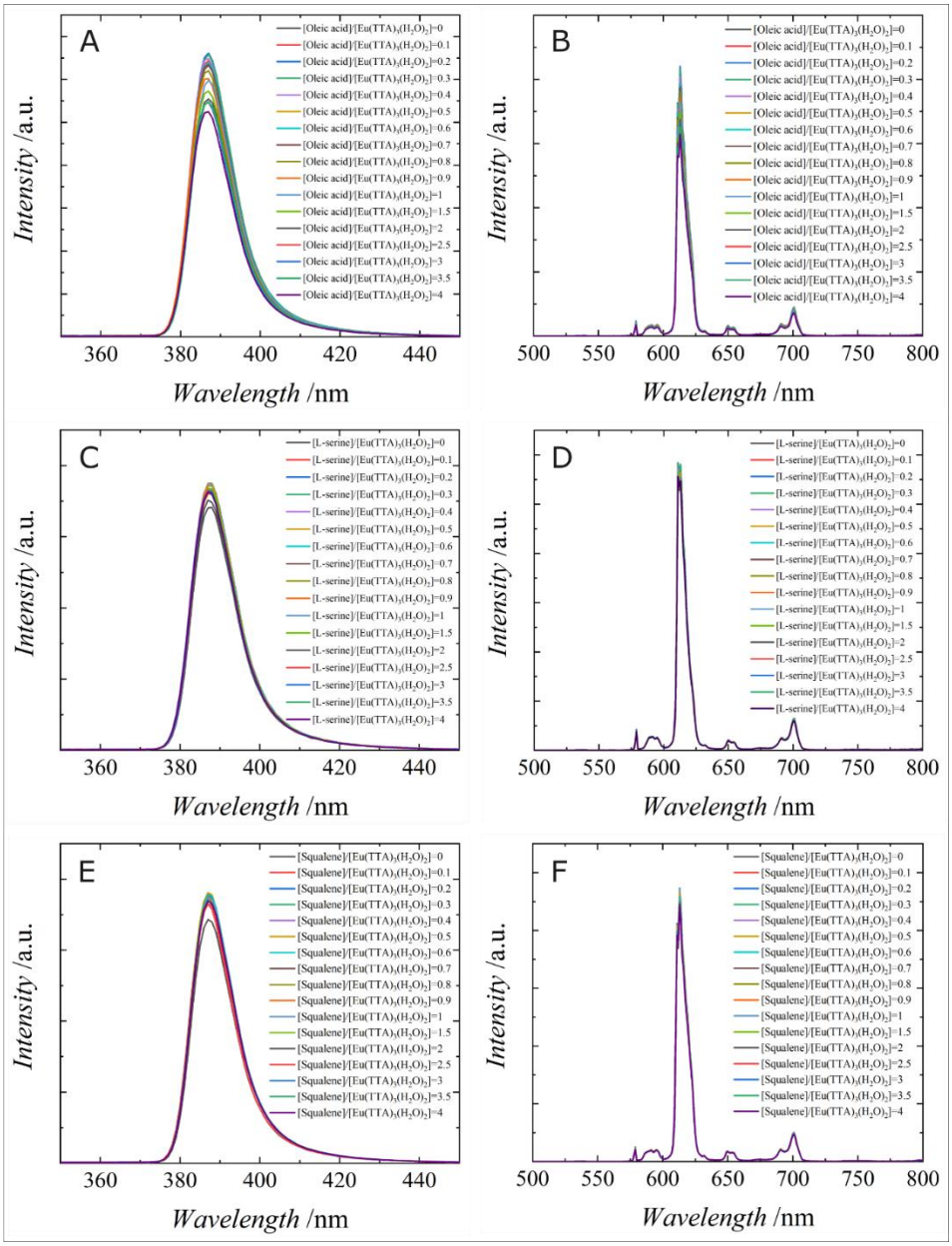

Figure 4.5 Excitation spectra (A, C, E) and emission spectra (B, D, F) of 0.59 mM $Eu(TTA)_3(H_2O)_2$ complex mixed with oleic acid (A, B), L-serine (C, D) and squalene (E, F) in the range of molar ratio 0-4

The addition of LFM components did not significantly affect the shifts of excitation maxima. This is due to the fact that oleic acid, L-serine and squalene do not absorb light in the considered spectral region. Also, no influence of LFM

components on emission maxima was noticed because the source of the luminescence emission (europium cation) remained unchanged. Nonetheless, it was noticed that the addition of the individual LFM components to the europium complex mixture had an observable effect on the maximum emission intensity (Figure 4.6).

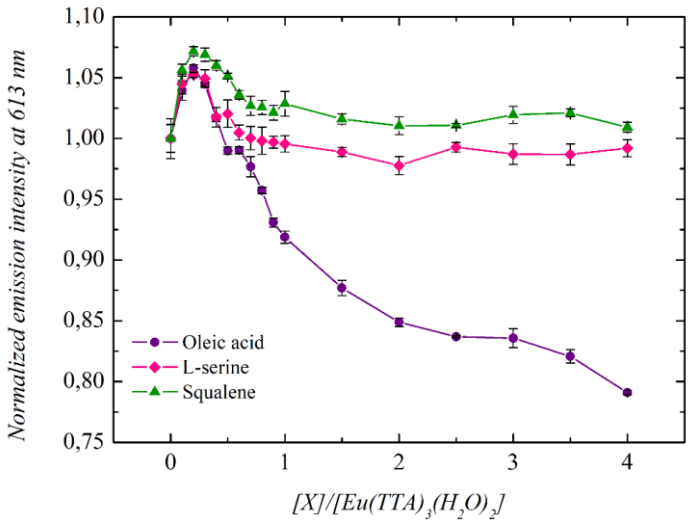

Figure 4.6 Maximum emission intensities of the $Eu(TTA)_3(H_2O)_2$ complex mixtures with LFM constituents – oleic acid (violet), L-serine (pink) and squalene (green) in the range of concentration 0-4, normalised to the maximum emission intensity for the $Eu(TTA)_3(H_2O)_2$ complex without any addition

The addition of oleic acid to the europium complex solution firstly increased the emission intensity, reaching the maximum at 1.05 of the starting value for the molar ratio [X]:[$Eu(TTA)_3(H_2O)_2$] equal to 0.2. Further addition of oleic acid led to a decrease in the emission intensity far below the starting value. A similar effect was observed for the addition of L-serine and squalene to the europium complex solution. Firstly, the emission intensity of the europium complex increased, reaching the maximum at 1.05 and 1.07 of the starting value for L-serine and squalene, respectively, for the molar ratio [X]:[$Eu(TTA)_3(H_2O)_2$] also equal to 0.2. However, further L-serine or squalene addition lowered the europium complex emission intensity and stabilised the emission around the starting value at the molar ratio of 1.5 for both compounds. The initial boost of the europium complex emission intensity is influenced by small amounts of LFM components and their roles as centrosymmetry breakers, while the TTA ligand keeps the antenna role [31]. Also, the exchange of the water molecules in the initial europium complex to the new

ligands may result in the emission intensity boost due to the elimination of the luminescence quenching produced by coupling with vibrational modes of water molecule [27], [32], [33]. On the other hand, the subsequent decrease of the emission intensity while the concentration of LFM components is increasing may be related to the complex decomposition and stripping the antenna ligand from the europium central atom [34].

The DRIFT spectra have been recorded for pure $Eu(TTA)_3(H_2O)_2$ complex, pure oleic acid, L-serine and squalene, and for the mixture of LFM components with europium complex to investigate the interactions between LFM components and the complex (Figure 4.7).

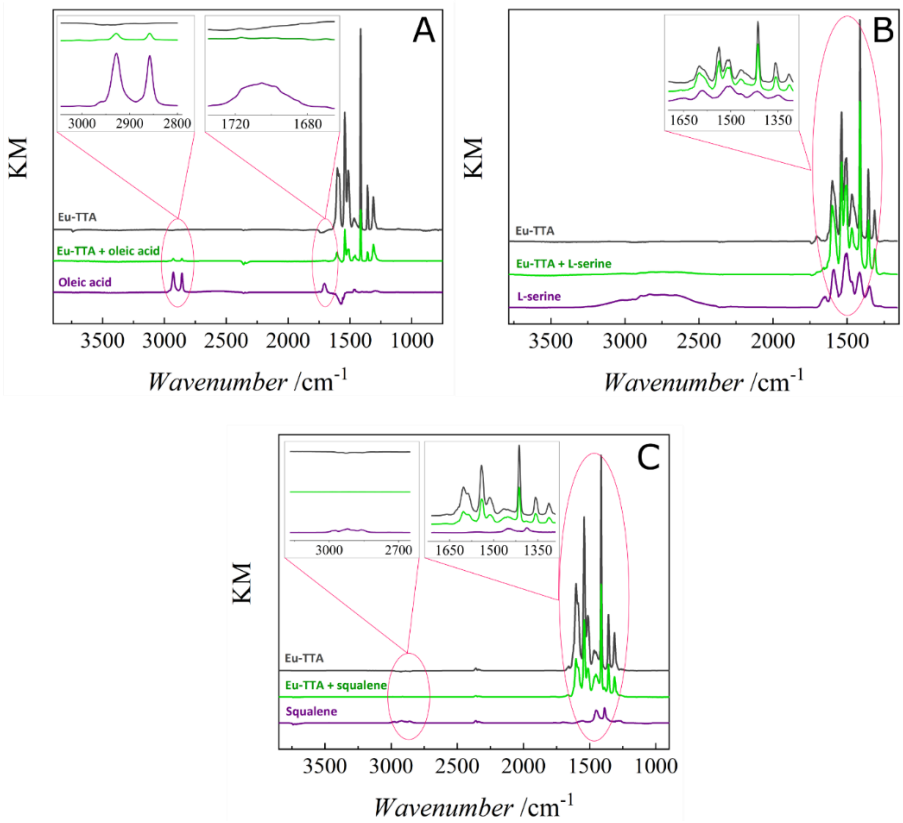

Figure 4.7 The DRIFTS spectra of (A) $Eu(TTA)_3(H_2O)_2$ complex (grey), oleic acid (violet) and the mixture of both compounds (green); (B) $Eu(TTA)_3(H_2O)_2$ complex (grey), L-serine (violet) and the mixture of both compounds (green); (C) $Eu(TTA)_3(H_2O)_2$ complex (grey), squalene (violet) and the mixture of both compounds (green)

In the spectrum of pure oleic acid (Figure 4.7 A), the peak localised at 1711 cm^{-1} assigned to the stretching vibration of a double bond in carbonyl group

(C=O) of oleic acid is absent in the spectrum of the $Eu(TTA)_3(H_2O)_2$ and OA mixture [35]. Also, the two intense peaks at 2925 cm^{-1} and 2855 cm^{-1} present in the oleic acid spectrum, related to the asymmetric and symmetric stretching modes of $–CH_2$ groups in the long chain, are also visible in the $Eu(TTA)_3(H_2O)_2$ and OA mixture spectrum. This confirmed the chelation of the europium ion in the complex [36], [37]. Furthermore, in the $Eu(TTA)_3(H_2O)_2$ and OA mixture spectrum, there are two intense peaks at ca. 1540 cm^{-1} and 1459 cm^{-1}, which are assigned to the presence of carboxylate group (COO–) and its stretching asymmetric and symmetric modes, respectively. The wavenumber separation of those two bands (Δ) define the nature of the carboxylate coordination mode; for $\Delta < 110$ cm^{-1} the coordination type can be interpreted as a bidentate. For the mixture of oleic acid and europium complex, the value of Δ is equal to 81 cm^{-1}, which indicates that two oxygen atoms in the carboxylate group of oleic acid symmetrically chelate the europium ion [35], [36]. The DRIFT spectra for both $Eu(TTA)_3(H_2O)_2$ and L-serine mixture as well as for $Eu(TTA)_3(H_2O)_2$ and squalene mixture are simply a sum of the spectra of pure reagents, so no specific interactions between LFM components and europium complex have been observed within the DRIFT spectroscopy measurements.

The interactions between LFM components and the europium complex have also been investigated with NMR spectroscopy. The ^1H NMR and ^{13}C NMR spectra have been recorded for pure europium complex, individual LFM components and the mixture of LFM compounds and $Eu(TTA)_3(H_2O)_2$ complex to compare the displacement of resonances associated with europium complex mixtures and the substrates (Figure 4.8).

In the ^1H NMR spectra for pure oleic acid and the mixture with $Eu(TTA)_3(H_2O)_2$ complex, the 0.1 ppm and 0.065 ppm shifts of signals assigned to the hydrogen atoms at carbons **1** and **2** in oleic acid, respectively, have been noticed (Figure 4.8 A). These shifts may correspond to the interaction of europium cation with the oleic acid carboxyl group [38]. Also, the resonance of the proton from the **f** position in the europium complex, which is upfield shifted for approximately 0.07 ppm, may indicate the interaction between the molecule of oleic acid and the complex. The impact of oleic acid on the europium complex was also confirmed with the ^{13}C NMR spectra (Figure 4.8 B). The shift of the resonance of the carbon from the carbonyl group of oleic acid by approximately 1.05 ppm was observed. Also, the shift of the resonance position of carbon **1** in oleic acid by 1.36 ppm was noticed [31]. This is in good agreement with DRIFT analysis, where the disappearance of the band (1711 cm^{-1}) assign to the stretching vibration of a double bond in the carbonyl group (C=O) of oleic acid was observed.

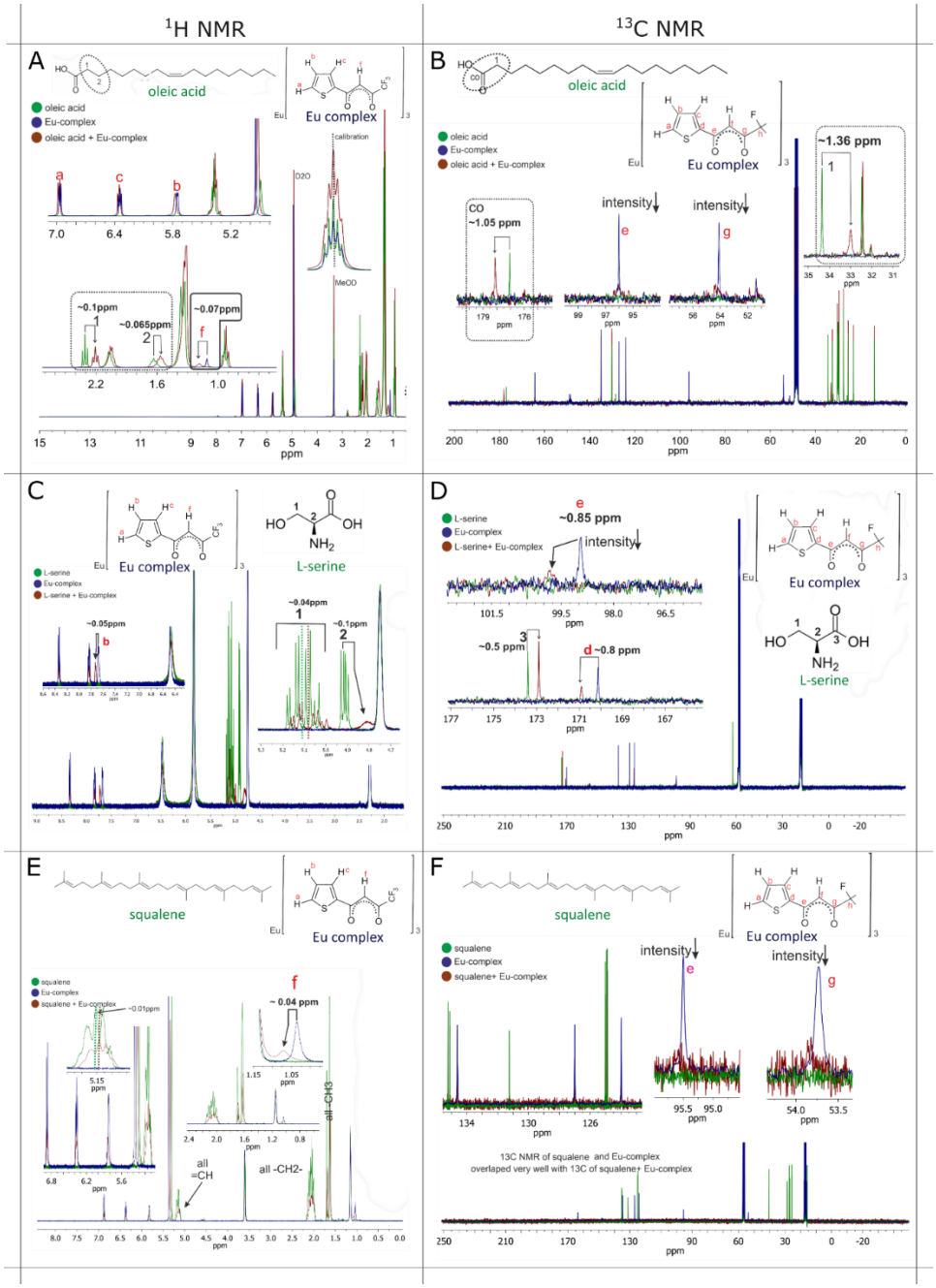

Figure 4.8 The superposition of the ^{1}H NMR (A, C, E) and ^{13}C NMR (B, D, F) of pure oleic acid (A, B), L-serine (C, D), squalene (E, F), pure $Eu(TTA)_3(H_2O)_2$, and the mixture which contains $Eu(TTA)_3(H_2O)_2$ and oleic acid (A, B) or L-serine (C, D) or squalene (E, F)

Some changes can be observed in the ^{1}H NMR spectrum and the ^{13}C NMR spectrum of the $Eu(TTA)_3(H_2O)_2$ and L-serine mixture (Figure 4.8 C, D), although the DRIFT analysis indicated that the spectrum of the mixture was simply a sum of the spectra of the individual compounds. In the ^{1}H NMR spectra of L-serine and its mixture with europium complex, the most visible changes are noticed for two hydrogens from the first position (**1**) and one hydrogen from the second position (**2**) in the L-serine molecule (Figure 4.8 C). For hydrogen **1** the group of signals was shifted approximately 0.04 ppm, and for hydrogen **2** the signal was shifted for about 0.1 ppm and broadened. The changes were also confirmed in the ^{13}C NMR spectrum of pure europium complex and its mixture with L-serine. Firstly, the resonance of the carbon from the third position (**3**) in the L-serine molecule was changed by approximately 0.5 ppm. Secondly, the changes associated with resonances of carbon in the position **d** and **g** of $Eu(TTA)_3(H_2O)_2$ complex molecule were shifted for approximately 0.8 ppm and 0.85 ppm, respectively, whereby the intensity of the signal was suppressed for both positions of carbon (Figure 4.8 D). These changes indicated some interactions between the L-serine and europium complex.

For pure squalene and the mixture with $Eu(TTA)_3(H_2O)_2$ complex, in both ^{1}H NMR and the ^{13}C NMR spectrum, the very slight shift differences are noticed (Figure 4.8 E, F). In the ^{13}C NMR spectrum for the carbons in **e** and **g** position in the europium complex, only the suppression of the signal intensity was observed (Figure 4.8 F). The spectrum of $Eu(TTA)_3(H_2O)_2$ complex mixture with squalene was only a sum of the spectra of the individual components, similarly to DRIFT spectra for this mixture. The small resonance shift for squalene in comparison to oleic acid may be related to the presence of carboxyl group in the oleic acid, which are susceptible to interaction with $Eu(TTA)_3(H_2O)_2$ complex, whereas, in the squalene molecule, these groups are not present.

The impact of oleic acid, L-serine and squalene on the europium complex luminescence lifetime (τ) was investigated by measuring the series of decay times for each mixture drop cast on the glass slide in the range of molar ratio $[X]:[Eu(TTA)_3(H_2O)_2]$ from 0 to 4 (Figure 4.9).

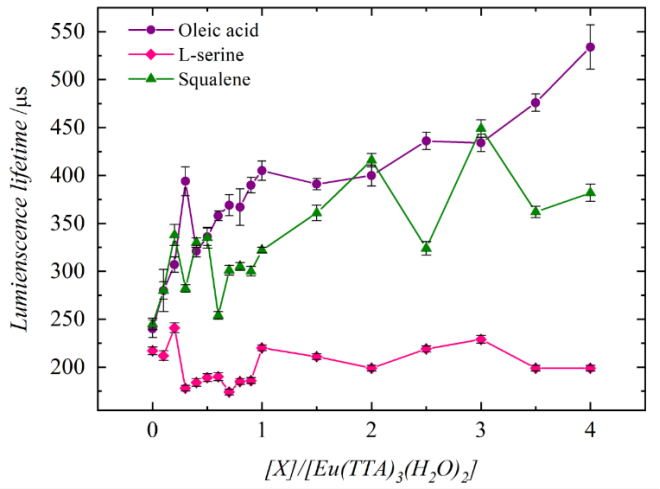

Figure 4.9 Luminescence lifetimes of the mixtures of $Eu(TTA)_3(H_2O)_2$ complex with LFM constituents – oleic acid (violet), L-serine (pink) and squalene (green) in the range of molar ratio from 0 to 4 drop-cast on the glass slides

The initial τ values, which were measured for the pure europium complex ([X]:[$Eu(TTA)_3(H_2O)_2$]=0] in each LFM component series, varied slightly due to the crystallisation from different solvents. The addition of oleic acid and squalene (sebaceous LFM components) increased substantially the luminescence lifetime of the europium complex from the initial value of ca. 250 µs to 400 µs for [X]:[$Eu(TTA)_3(H_2O)_2$] molar ratio of 2. The increase of $Eu(TTA)_3(H_2O)_2$ complex luminescence lifetime after the addition of LFM components may be related to the ligand exchange. The new ligand can break the symmetry and decrease the nonradiative decay rate [31]. Besides, the exchange of water molecules for the new ligands may reduce the luminescence quenching generated by coupling with vibrational modes of H_2O [32], [39]. Also, due to the unsaturated character of oleic acid and squalene, which led to their bent shape, the molecules may trap the europium emitter and form the hydrophobic environment around, protecting the emitter from water molecules [40]. In the case of the addition of L-serine to the europium complex mixture, there were no significant changes in the luminescence lifetime. The lifetimes for the whole range of molar ratios oscillated around the starting value of ca. 200 µs, and no maximum was observed. The polar L-serine molecule in any considered concentration did not interact with the europium emitter in a way as oleic acid or squalene did. Water molecules, which significantly reduce the luminescence lifetime, were eliminated. Therefore, it may be concluded that the stripping of the antenna ligand, while LFM component concentration

increase, had an impact only on europium complex luminescence intensity and had no influence on its lifetime.

To include the impact of the paper matrix on the luminescence lifetimes of the europium complex, another experiment concerning the influence of oleic acid, L-serine and squalene on the complex was conducted. The series of decay times were measured for each mixture deposited on paper in the range of molar ratios ([X]:[$Eu(TTA)_3(H_2O)_2$]) from 0 to 4 (Figure 4.10).

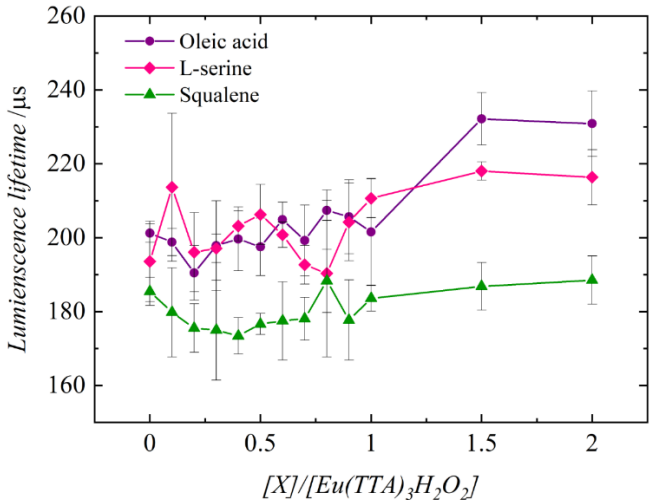

Figure 4.10 Luminescence lifetimes of the mixtures of $Eu(TTA)_3(H_2O)_2$ complex with LFM constituents – oleic acid (violet), L-serine (pink) and squalene (green) in the range of molar ratio from 0 to 4 drop cast on the notebook paper

The luminescence decay times obtained in the experiment significantly differed from the results obtained for the europium complex mixtures deposited on glass. No particular correlation between the luminescence lifetime of the europium complex and LFM components concentration has been observed. For all three LFM components, the luminescence decay times for the whole range of molar ratios slightly fluctuate around the initial luminescence lifetime of the pure europium complex. What probably caused this inconsistency in results is the chromatographic effect which occurred when the mixture of europium complex and LFM components was drop cast on paper and soaked into its matrix. The $Eu(TTA)_3(H_2O)_2$ complex is highly polar, as is the paper which consists of cellulose, so its retention factor is low, and the complex stayed at the surface of the paper. The less polar LFM components might diffuse more in-depth into the paper structure. The decay times of the

europium complex mixtures measured for the whole range of molar ratios might have been, in fact, the decay time of the pure europium complex.

Due to the fact that the luminescence lifetimes measured for drop cast europium complex mixtures on paper turned out to be unreliable, another decay time measurement experiment was performed. In this experiment, pure oleic acid, L-serine and squalene were spotted individually on a paper surface in the concentration of 0.1 M. Also, the mixture of all LFM components was drop cast on a separate paper sample. Each sample was then spray-coated with the solution of $Eu(TTA)_3(H_2O)_2$ complex in methanol, and then the series of decay time measurements were performed (Figure 4.11).

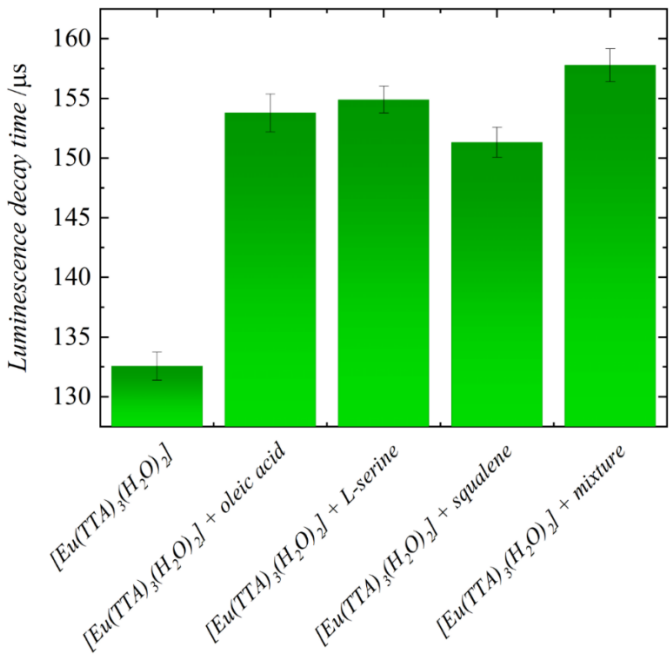

Figure 4.11 Luminescence lifetimes of the $Eu(TTA)_3(H_2O)_2$ complex spray-coated on the notebook paper without LFM constituents, with oleic acid, L-serine, squalene and the mixture of LFM components drop-cast in the 0.1 M concentration

The luminescence decay time measured for europium complex spray-coated on the pure paper surface was equal to 133 ± 1 µs, and for the oleic acid, L-serine, squalene, and the mixture of all three components was equal to 154 ± 2 µs, 155 ± 1 µs, 152 ± 1 µs, and 158± 1 µs, respectively. The presence of LFM components in the paper structure increased the luminescence lifetime of the europium complex by ca. 15 % in relation to the lifetime of the pure complex on paper.

LFM visualisation optimisation

The process of optimising the fingermark visualisation with the time-gated system was conducted in order to obtain the highest contrast between the fingermark ridges and the background. An important parameter of imaging that utilises the difference in luminescence lifetime of $Eu(TTA)_3(H_2O)_2$ complex on paper and $Eu(TTA)_3(H_2O)_2$ complex on LFM ridge was the delay-to-shutter time. In the process of optimisation, this parameter varied from 0.05 to 1900 μs, whereas the excitation time and the shutter time were fixed to 200 μs and 100 μs, respectively.

The paper sample with deposited LFM was first spray-coated with $Eu(TTA)_3(H_2O)_2$ complex in methanol and then imaged with a CCD camera. When the sample was visualised in the fluorescence mode with the constant UV illumination, no fingermark pattern could have been distinguished from the background due to the fact that the complex was evenly distributed over the paper surface resulting in uniform fluorescence emission (Figure 4.12 A). Furthermore, in the fluorescence mode, a significant contribution to luminescence emission had the paper's own fluorescence. In the time-gated mode, the contrast between fingermark ridges and the background started to improve with an increase of the delay-to-shutter parameter (Figure 4.12 B).

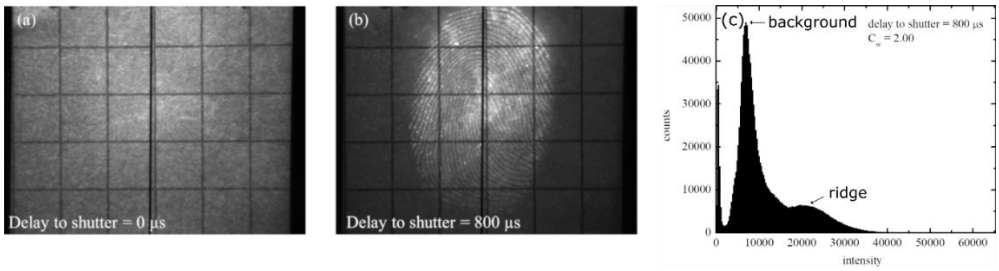

Figure 4.12 LFM on paper sample spray-coated with $Eu(TTA)_3(H_2O)_2$ complex imaged in the time-gated mode with a delay-to-shutter (A) 0 μs, (B) 800 μs. (C) A histogram extracted from an image captured with delay-to-shutter time 800 μs

Within the optimisation process, LFM on paper developed with $Eu(TTA)_3(H_2O)_2$ complex were photographed with the delay-to-shutter times ranging from 0.05 to 1900 μs, captured every 100 μs, and for each captured image, a histogram has been generated. The crucial parameter of LFM imaging, which is the contrast between fingermark ridges and the background, was defined utilising the Weber formula [41], [42]:

$$C_w = \frac{I_{ridge} - I_{background}}{I_{background}}$$

where, C_w denoted the Weber contrast, I_{ridge} – the emission intensity in the region of the fingermark ridge, and $I_{background}$ – the emission intensity of the background region. The values of Weber contrast for each image were calculated based on histograms (Figure 4.12 C). In each histogram, man can distinguish three main peaks: the first one corresponding to the black areas of the image, the second corresponding to the background intensity and the last one corresponding to the fingermark ridges emission intensity. The values associated with the background and ridge intensities were applied to calculate the value of the contrast C_w. The contrast values for individually captured images at various delay-to-shutter times are presented in Figure 4.13.

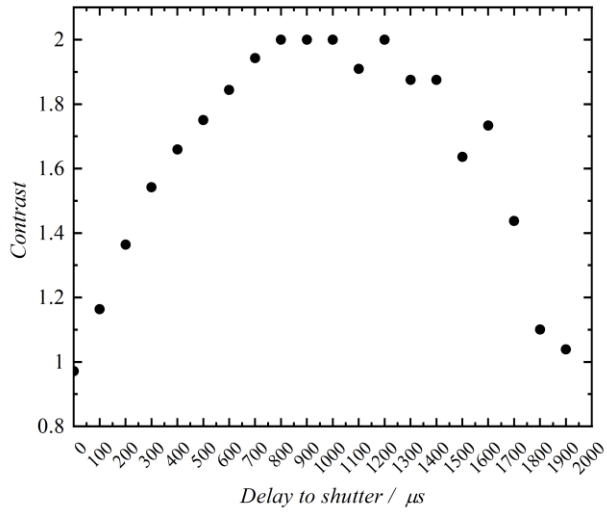

Figure 4.13 A diagram of image contrast C_w calculated for the range of delay-to-shutter times from 0.05 to 1900 μs

The contrast was increasing with the increase of the delay-to-shutter time, reaching the maximum at a value of ca. 2 for the delay-to-shutter times in the range of 800 – 1200 μs. Further increase of the delay-to-shutter parameter resulted in the decrease of the contrast down to the minimal value of 1. This is because, for the initial delay-to-shutter values, the difference between I_{ridge} and $I_{background}$ was getting higher in comparison to $I_{background}$ value. But, further exceeding the delay-to-shutter parameter resulted in the weak signal of I_{ridge} and $I_{background}$ so that the thermal noise started to play a significant role causing the contrast decrease. Taking into consideration the above observations, the delay-to-shutter of 800 μs has been chosen as the optimal value for further experiments, where the contrast C_w was equal to 2.

LFM enhancement with $Eu(TTA)_3(H_2O)_2$ complex on various paper substrates

A series of fingermarks on notebook paper has been developed with $Eu(TTA)_3(H_2O)_2$ complex methanol solution in the concentrations of 1, 10, 50 and 100 mg mL^{-1} by spray-coating to investigate what concentration would be optimal to obtain the best contrast between fingermark ridges and the background (Figure 4.14).

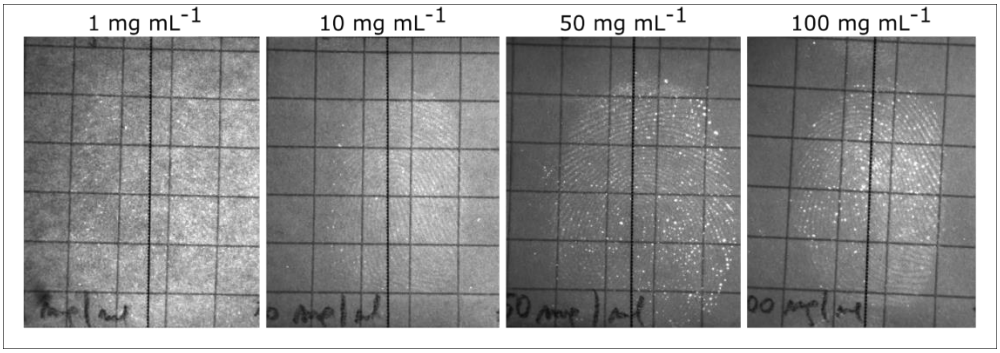

Figure 4.14 Samples of 1-day-old fingermarks deposited on paper, spray-coated by a solution of $Eu(TTA)_3(H_2O)_2$ complex in concentrations 1, 10, 50 and 100 mg mL^{-1}, imaged in the time-gated mode

Using the lowest concentration as well as the concentration of 10 mg mL^{-1} for fingermark development resulted in a very weak fingermark contrast. Increasing the concentration to 50 mg mL^{-1} and 100 mg mL^{-1} allowed for the efficient enhancement of ridge details and good contrast between fingermark ridges and the background. Due to the fact that both concentrations provided satisfactory results of fingermark enhancement, a concentration of 50 mg mL^{-1} was chosen for further processing.

Fingermarks were visualised with the imaging system in both fluorescence and time-gated mode (Figure 4.15). When the sample was visualised in the fluorescence mode, and the image was captured under constant ultraviolet excitation light, no fingermark pattern could have been distinguished from the background (Figure 4.15 A). This is due to the fact that the spray-coated europium complex is uniformly deposited over the whole sample and that the paper possesses its own fluorescence. The optimal contrast between fingermark ridges and the paper background has been obtained for excitation time 200 μs, delay-to-shutter time 800 μs, and the luminescence recording time 100 μs. This formulation and imaging

parameters allowed for getting high-quality ridge details with 2nd level features such as ridge endings or bifurcation (Figure 4.15 B, C, D).

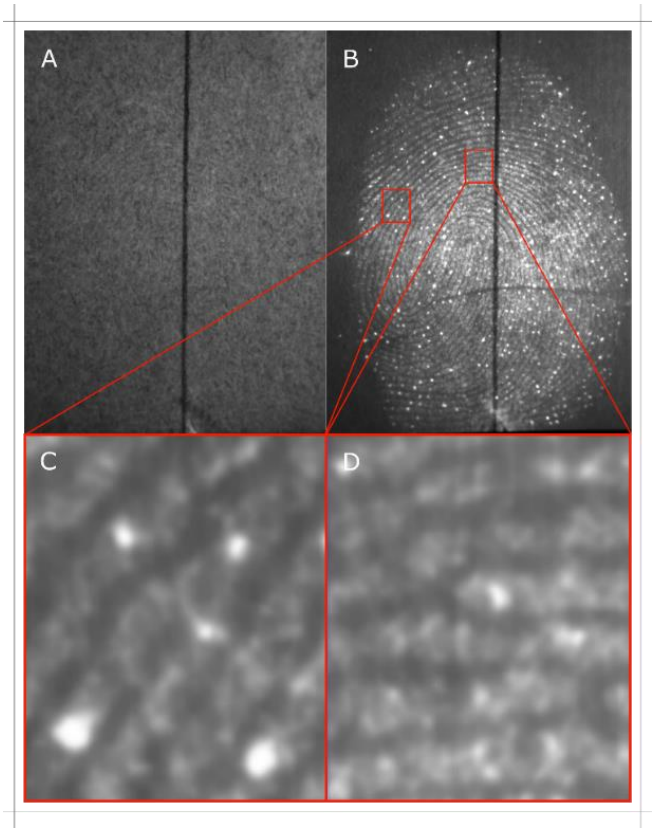

Figure 4.15 Natural fingermark deposited on a copy paper, developed with 50 mg mL^{-1} $Eu(TTA)_3(H_2O)_2$ complex methanol solution, imaged in (A) fluorescence mode, (B) time-gated mode. The 2nd level features (minutiae) are distinguished (C), (D).

For further investigation of $Eu(TTA)_3(H_2O)_2$ complex applicability, a few natural latent fingermarks deposited on several commonly used paper substrates such as magazine paper, thermal paper, copy paper, notebook paper have been processed. The samples were imaged with the time-gated mode under 365 nm UV excitation light (Figure 4.16).

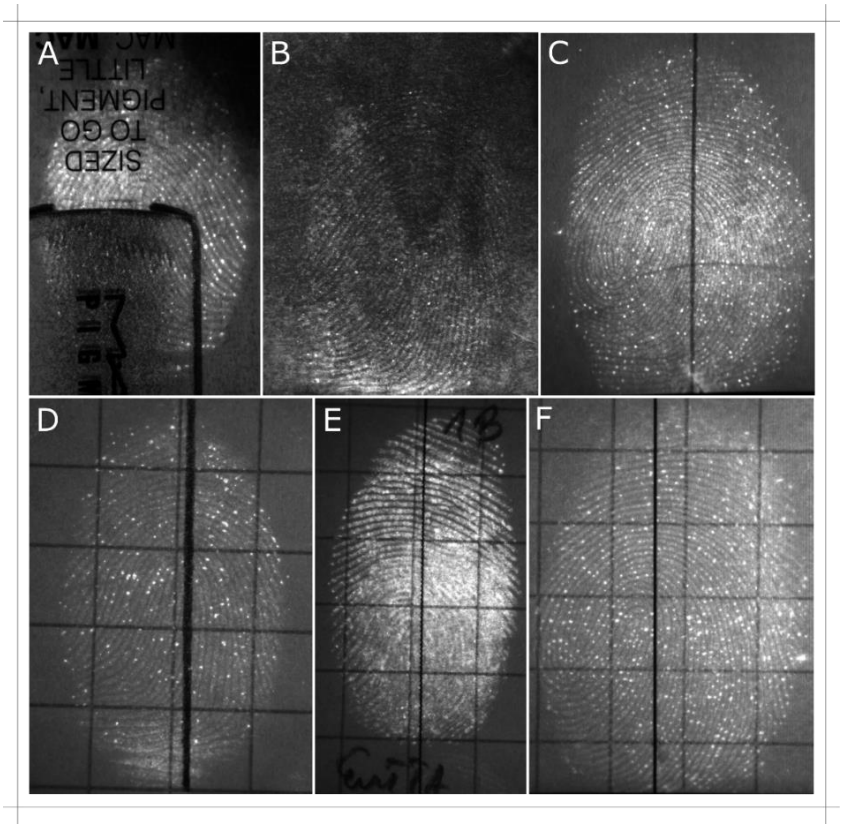

Figure 4.16 Samples of natural fingermarks deposited on porous substrates: (A) magazine paper, (B) thermal paper, (C) copy paper, (D-F) various notebooks paper, spray-coated with $Eu(TTA)_3(H_2O)_2$ complex in methanol solution, and imaged with the CCD camera in the time-gated mode

$Eu(TTA)_3(H_2O)_2$ complex efficiently interacted with the fingermark components. The ridges were clearly visible on all presented paper types, even on thermal paper. Development of the fingermarks deposited on thermal paper is troublesome due to the fact that some organic solvents used for e.g. ninhydrin or 1,2-indanedione, may cause overdevelopment like darkening of the surface leading to the contrast decrease [43], [44]. The possibility of applying time-gated imaging allowed overcoming the problem of paper darkening and eliminating the interfering paper's own fluorescence because the europium complex in contact with fingermark components is characterised by a longer luminescence decay time.

Comparison of the interaction between $Eu(TTA)_3(H_2O)_2$ complex and eccrine, natural and sebaceous fingermarks

Sebaceous and eccrine fingermarks on paper have been developed with europium complex to compare the quality of enhancement with the natural ones. For eccrine mark deposition, the donor was asked to keep his hand wrapped in a plastic bag for 30 minutes, and for the sebaceous fingermark, the donor rubbed his fingers against the forehead and neck prior to deposition on paper. All the samples were sprayed with the methanol solution of $Eu(TTA)_3(H_2O)_2$ complex. The developed eccrine, natural, and sebaceous fingermarks were imaged with time-gated mode (Figure 4.17).

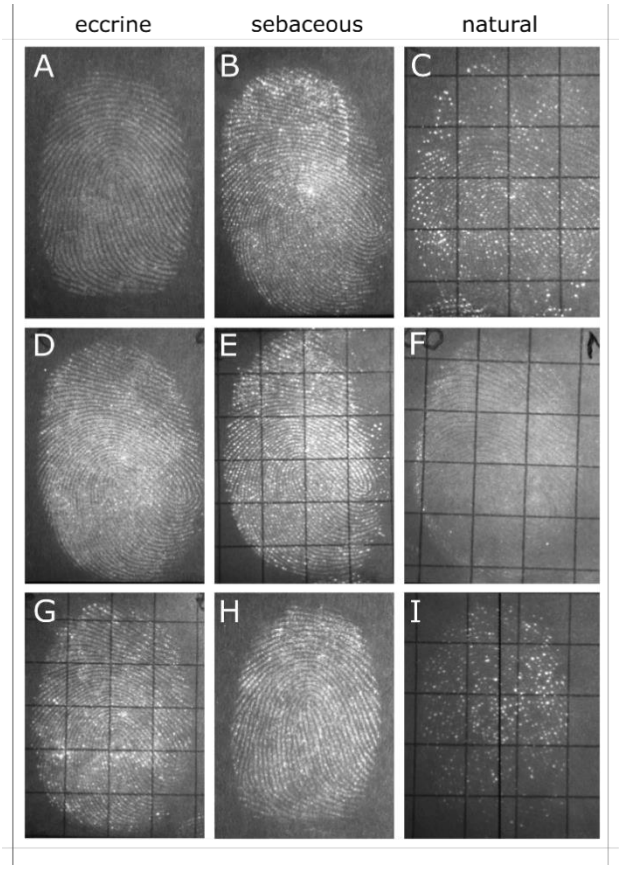

Figure 4.17 Images of 1-day- old eccrine(A, D, G), sebaceous (B, E, H) and natural (C, F, I) fingermarks on paper developed with $Eu(TTA)_3(H_2O)_2$ complex methanol solution, visualised in the time-gated mode

It was noticed that developing charged fingermarks (sebaceous or eccrine) is much more efficient since the amount of accumulated LFM material is incomparably higher in comparison with natural fingermarks. However, the fingermarks found in the real crime scenes are mostly natural, and they are not perfect. For all the rest of the experiments, the natural (ungroomed) fingermarks have been used to mimic the typical casework scenarios.

Comparative analysis of the $Eu(TTA)_3(H_2O)_2$ complex with benchmark methods of latent fingermark visualisation on paper

The efficiency of LFM enhancement with $Eu(TTA)_3(H_2O)_2$ complex has been compared with two conventional developing agents used for the development of LFM on the porous surfaces – ninhydrin and 1,2-indanedione. The main criterion for this assessment study was the contrast and the amount of clear ridge detail present on fingermark images.

Ninhydrin

The comparison between the two methods was performed as follows. The set of few paper samples with deposited natural fingermarks have been cut in half. One half was developed with the $Eu(TTA)_3(H_2O)_2$ complex, and the other half was stained with ninhydrin. The fingermark samples enhanced with the $Eu(TTA)_3(H_2O)_2$ complex were examined with the CCD camera in the time-gated mode under 365 nm UV light. Fingermarks developed with ninhydrin were photographed with a digital SLR camera under white light. In the end, halves were put back to the original position for quality comparison assessment (Figure 4.18).

After recombining the paper samples, it was found that treating fingermarks with $Eu(TTA)_3(H_2O)_2$ complex and visualising them in the time-gated mode resulted in similar or better contrast of the fingermark in comparison to ninhydrin development. Fingermarks processed with ninhydrin resulted in pale violet ridges, which in some cases were hardly visible (Figure 4.18 3, 7, 8). The further observation is that the europium complex developed LFM with a considerably better quality of the ridges. The Weber contrast (C_w) measured for sample 1 and 1’ (Figure 4.18) was equal to 0.09 and 0.86, respectively. The significantly higher contrast of fingermark developed with europium complex indicated that fingermarks details were much easier to specify.

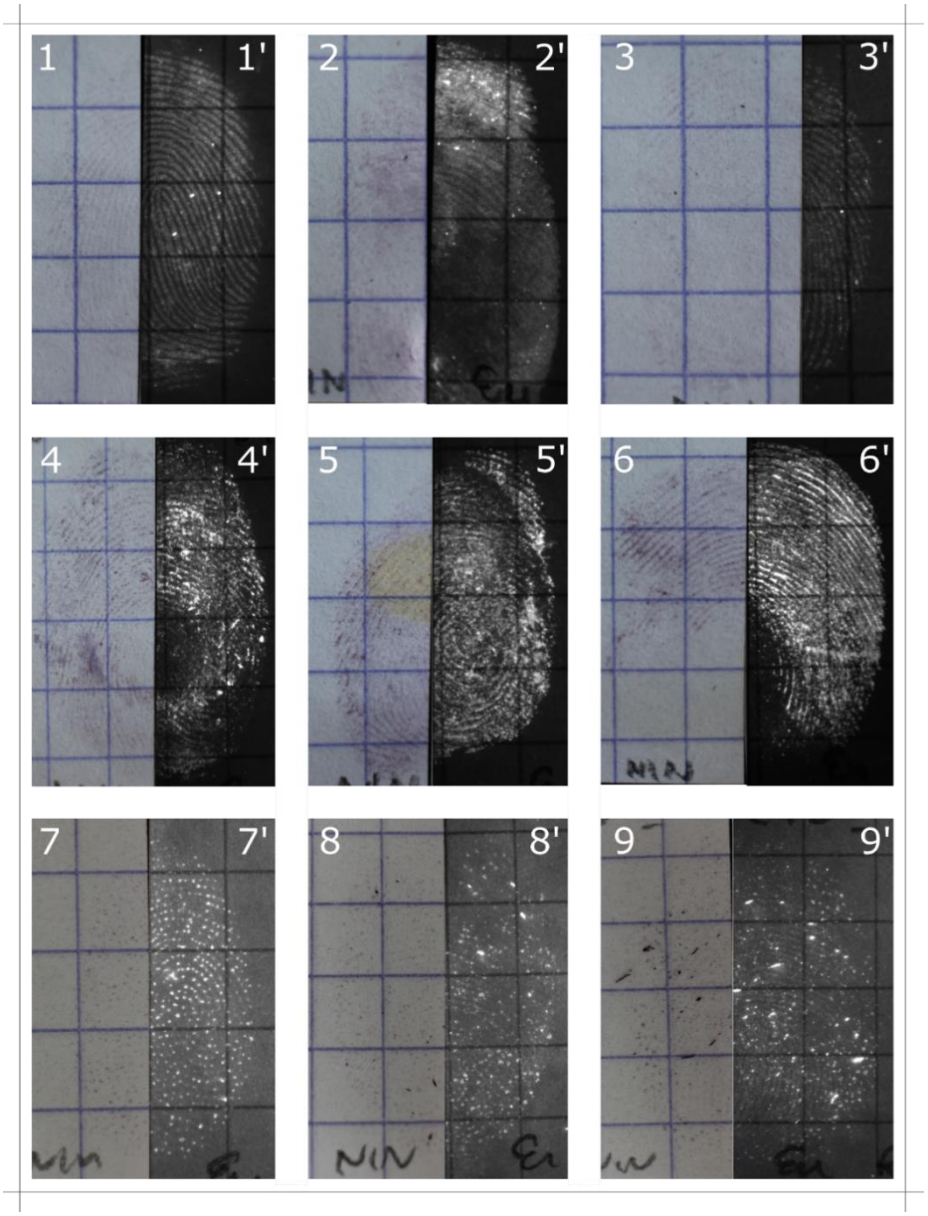

Figure 4.18 One-day-old latent fingermarks deposited on paper, developed with ninhydrin (1-9, left halves) compared to fingermarks enhanced with $Eu(TTA)_3(H_2O)_2$ complex (1'-9', right halves)

The potential of the $Eu(TTA)_3(H_2O)_2$ complex has also been demonstrated for the paper samples which were exposed to the water environment. For this purpose, the samples with deposited fingermarks were immersed in a water bath for 10 minutes under gentle shaking. After this time, the samples were dried in the air,

then cut in half and treated with either europium complex or ninhydrin. Afterwards, the appropriate halves were put back together and imaged either with the time-gated system or digital camera.

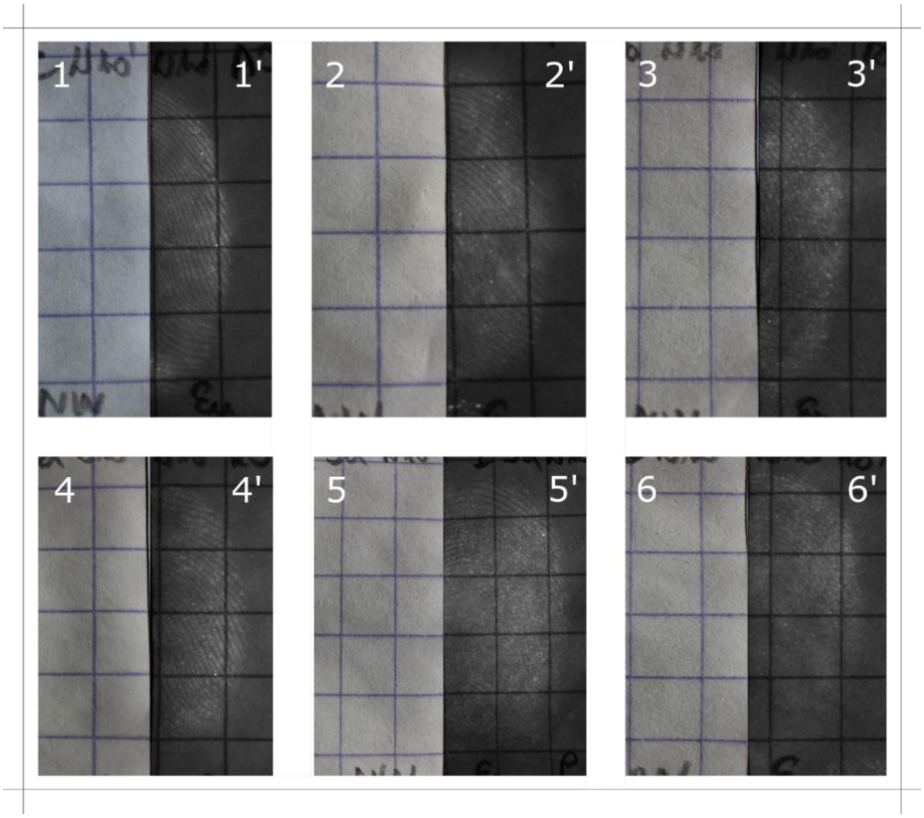

Figure 4.19 One-day-old latent fingermarks deposited on paper and washed with water 10 minutes developed with ninhydrin (1-6, left halves) compared to fingermarks enhanced with $Eu(TTA)_3(H_2O)_2$ complex (1'-6', right halves)

For comparison between $Eu(TTA)_3(H_2O)_2$ complex and ninhydrin on a porous surface, it is demonstrated that after aqueous treatment, only when the europium complex was used, decent enhancement of fingermarks was obtained (Figure 4.19). Ninhydrin stained samples did not result in fingermark enhancement due to the lack of amino acids in fingermark residuals because most of the eccrine fraction was eluted in the water bath. On the contrary, europium complex development, based on the interaction between the developing agent and sebaceous fraction of the fingermark, yielded satisfactory fingermarks. The Weber contrast (C_w) measured for sample 1' (Figure 4.19) was equal to 0.44, whereas it was impossible to calculate the contrast value for sample 1 due to the lack of visible ridges.

1,2 – indanedione

The split natural fingermark halves on paper were developed with either 1,2-indanedione working solution or $Eu(TTA)_3(H_2O)_2$ complex and then put back to the original position for quality comparison assessment. Samples enhanced with europium complex were examined with the CCD camera in the time-gated mode under 365 nm UV light, and samples stained with 1,2-indanedione were imaged with a digital SLR camera under blue light excitation and 600 nm long-pass filter in the darkroom (Figure 4.20).

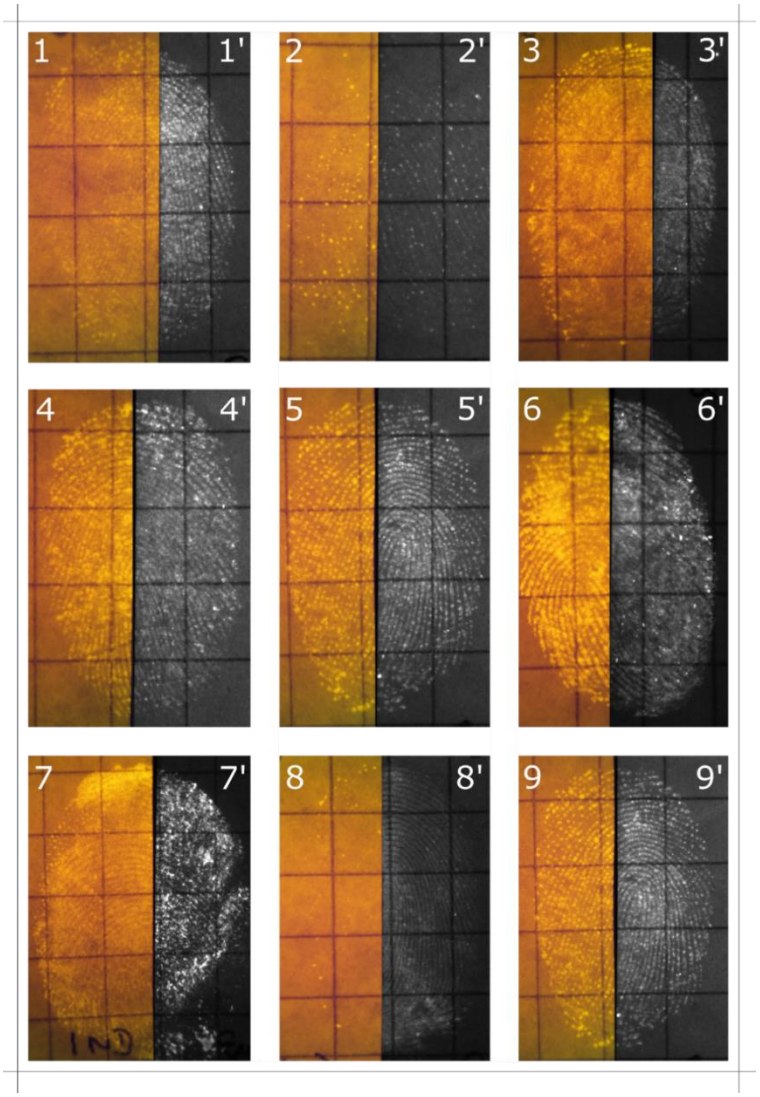

Figure 4.20 One-day-old latent fingermarks deposited on paper substrate developed with 1,2-indanedione (1-9) or $Eu(TTA)_3(H_2O)_2$ complex (1'-9')

The $Eu(TTA)_3(H_2O)_2$ complex developed latent fingermarks on paper with the same quality as 1,2-indanedione did. The luminescence of both developing agents was sufficient to yield visible fingermarks with good ridge details. The Weber contrast calculated for fingermarks enhanced with europium complex and 1,2-indanedione was equal to 0.33 and 0.39, respectively. Similar results of LFM enhancement with these two development agents allowed to set europium complex among efficient methods of background interference elimination. Moreover, the new method – *in situ* complex formation - demonstrated superior results for the development of LFM deposited on porous surfaces that have been exposed to water (Figure 4.21). For this purpose, similarly to the ninhydrin experiment, the paper samples with latent fingermarks were first immersed in the water bath for 10 minutes under gentle shaking, then dried in the air, cut in half, developed with either 1,2-indanedione or $Eu(TTA)_3(H_2O)_2$ complex and recombined for the imaging process.

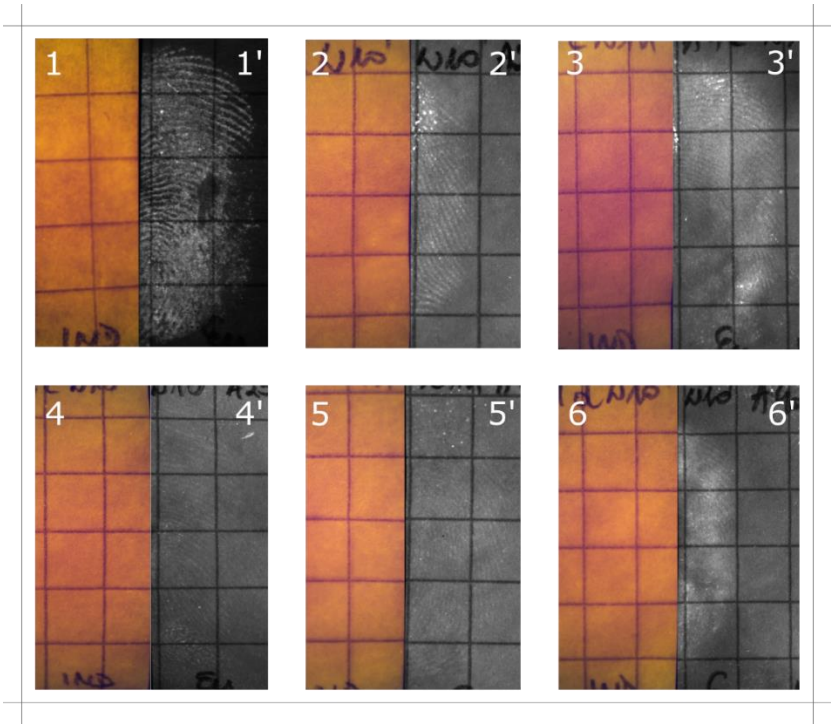

Figure 4.21 One-day-old latent fingermarks deposited on paper and washed with water 10 minutes developed with 1,2-indanedione (1-6, left halves) compared to fingermarks enhanced with $Eu(TTA)_3(H_2O)_2$ complex (1'-6', right halves)

As a result, no visible fingermarks were obtained for the samples developed with 1,2-indanedione, although, for europium complex treatment, fingermark ridges

were clearly visible, and the calculated Weber contrast was equal to 1.95. Again, the process of washing the samples leached the amino acids from the fingermark residuals; hence no possible reaction between indanedione and eccrine fraction took place, which yielded no visible fingermarks.

Comparison of LFM enhancement over the depletion series

A series of depleted fingermarks on paper have been done to examine the sensitivity of the $Eu(TTA)_3(H_2O)_2$ complex in contact with fingermark components. In the series, each of three donors (2 males, 1 female) was asked to touch the paper sample five times in a row using the same finger. Then the samples were sprayed with the europium complex in methanol, dried in the air and imaged in the time-gated mode. Figure 4.22 shows a depletion series for all donors. In the case of the first donor, the ridge details were visible for all depletions with good quality, whereas donor 2 provided only the first three depletion of good quality. The fourth and fifth depletion indicated less visible ridge details. Donor 3 provided weak all fingermarks; however, the quality of fingermark contrast is uniform for each of 5 depletion. The reason might be in not sufficient pressure used to deposit the mark on the paper or donor's individual feature.

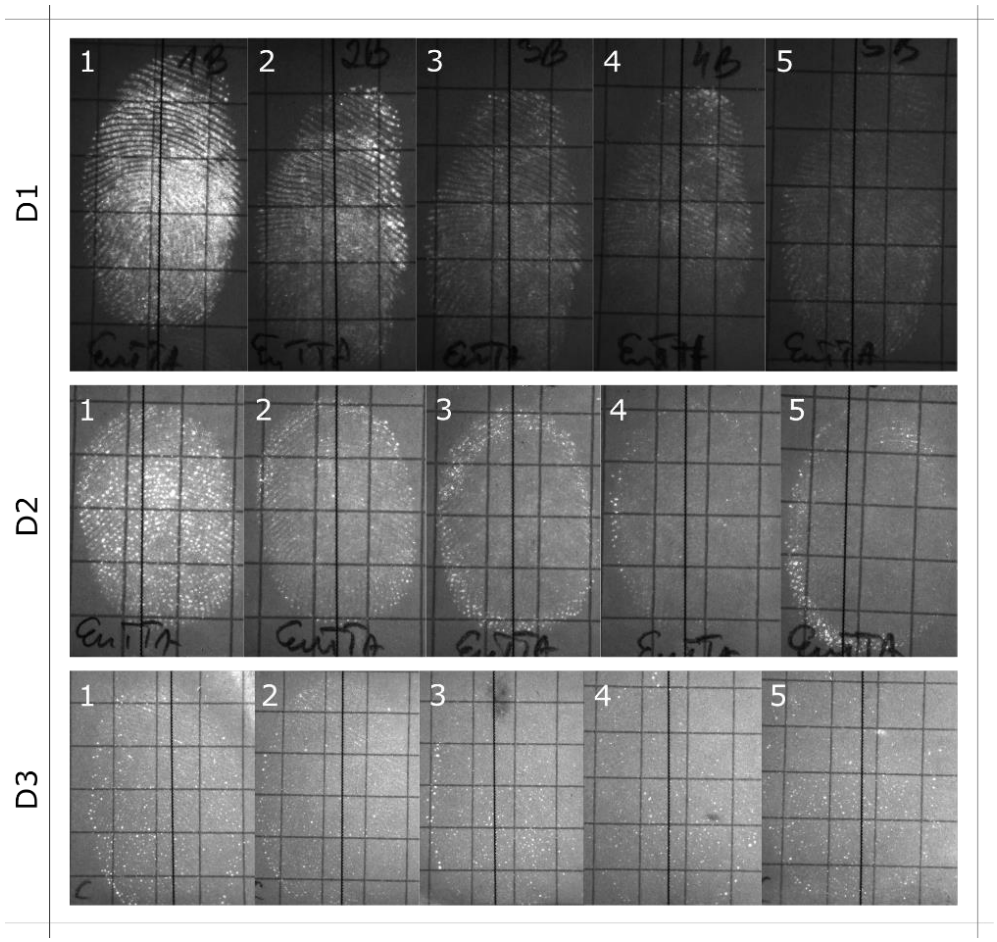

Figure 4.22 Depletion series of five fingermarks on paper deposited by three donors, developed with $Eu(TTA)_3(H_2O)_2$ complex in methanol and observed in the time-gated mode

Also, the split depletion series was done to compare the effectiveness of $Eu(TTA)_3(H_2O)_2$ complex and 1,2-indanedione on fingermark enhancement. Again, each of three donors (two male, one female) was asked to touch the paper samples five times in a row to deposit fingermarks. Then each paper sample was cut in half, treated with a different developing agent, recombined and finally imaged. Figure 4.23 compares the enhancement of the fingermarks obtained by the europium complex observed in the time-gated mode under 365 nm UV radiation and by 1,2-indanedione observed under blue light and 600 nm long-pass filter. For both developing agents, only the first three depletions of donor 1 and 3 were of good quality and contrast, and no significant difference between these agents was seen. For depletion 4 and 5, the contrast was weak; however, more visible ridges were observed for indanedione enhancement. On the other side, all five depletions of

donor 2 have been effectively enhanced by both developing agents, and more visible ridges were obtained for europium complex recovery. The split depletion trial indicated that these two developing agents give comparable results in terms of fingermark quality and sensitivity.

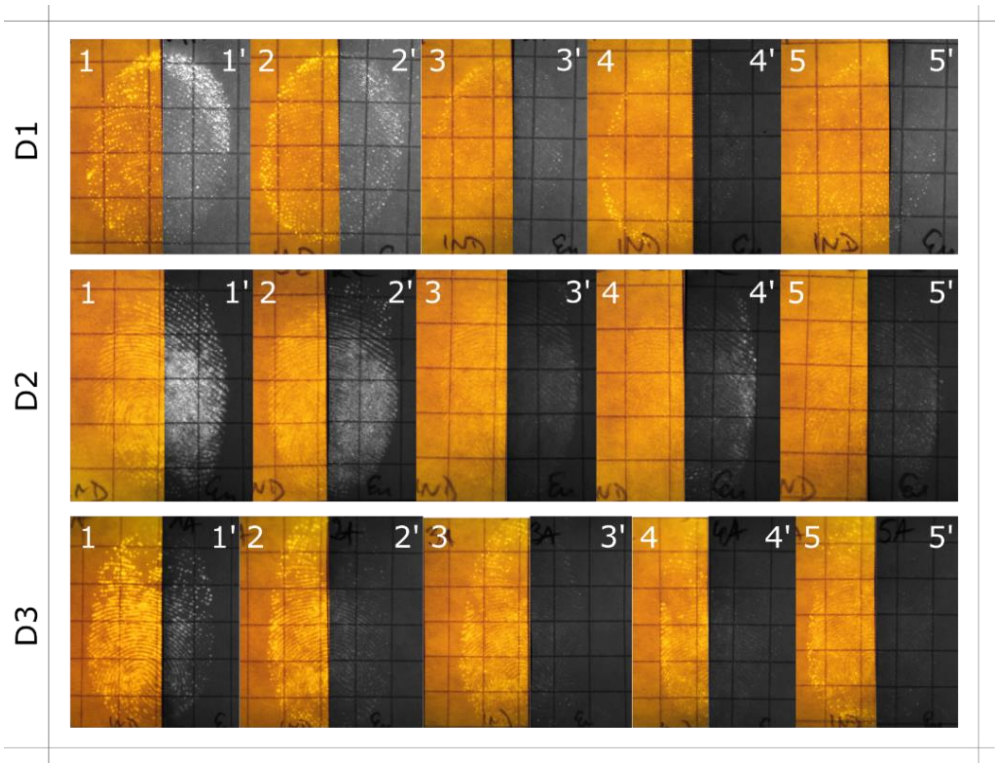

Figure 4.23 Depletion series on paper by different donors D1, D2 and D3, developed with 1,2-indanedione formulation (1-5) and $Eu(TTA)_3(H_2O)_2$ complex (1'-5')

4.4 Conclusions

A detailed investigation of the interaction between the $Eu(TTA)_3(H_2O)_2$ complex and oleic acid, L-serine and squalene, as LFM components representatives, showed the potential of this lanthanide β-diketonate complex for the development of the fingermarks on paper substrates with the use of time-gated imaging.

The complex was obtained in the synthesis from the europium (III) chloride hexahydrate and 2-thenoyltrifluoroacetone under the basic environment. The spectrofluorimetric measurements confirmed the presence of large Stokes shift, narrow emission band and high intensity due to the TTA ligand influence.

The detailed analysis of the interactions between europium complex and LFM constituents showed that the replacement of water molecules in the complex with one of the LFM components did not affect any shift of the maximum excitation and emission peaks, whereas it did affect the changes in the luminescence intensity depending on the molar concentration of LMF compounds. Moreover, the luminescence lifetime measurements showed that the presence of oleic acid or squalene ligand in the reaction mixture significantly increased the luminescence decay time on both glass and paper surfaces, whereas the presence of L-serine influenced this parameter only on paper substrate.

The DRIFT analysis, as well as NMR spectroscopy measurements, was performed to characterise the $Eu(TTA)_3(H_2O)_2$ complex behaviour in the presence of LFM components. The results from both analyses confirmed the formation of the new europium complex with oleic acid. Also, ^{1}H NMR and ^{13}C NMR demonstrated the occurrence of possible interactions with L-serine, whereas no specific interaction between the europium complex and squalene have been noticed. It has been shown that the interactions between the europium complex and LFM constituents affected the luminescence lifetime, which is increasing locally on the fingermark ridges. This phenomena enabled the fingermark enhancement using time-gated imaging, with no need for selective deposition of the developing agent and eliminating the background interferences. The parameters of time-gated imaging have been optimised to obtain the highest contrast. The series of images have been taken in the time-gated mode changing the delay-to-shutter parameter in the range of 0 to 2000 µs. For each image, the histograms have been prepared with the extracted values of fingermark and background intensity. The best contrast, calculated with the Weber formula, was obtained for the delay-to-shutter time equal to 800 µs.

The luminescent $Eu(TTA)_3(H_2O)_2$ complex was deposited on various paper samples via spray-coating with the methanol solution. What makes this method advantageous is that the complex interacted selectively with LFM components and that the products of this reaction possessed long-lived luminescence, which allowed the luminescence of the fingermark to be distinguished from the luminescence of the background. In order to improve the quality of fingermark ridges, the concentration of the europium complex methanol solution was optimised to 50 mg mL^{-1}. A series of depleted natural fingermarks of several donors deposited on paper-based substrates have also been efficiently developed with europium complex solution. The europium complex indicated a high sensitivity, resulting in good fingermark contrast for most of the depleted deposits. The fingermark contrast quality has been further evaluating by comparing the fingermark enhancement with $Eu(TTA)_3(H_2O)_2$ complex and benchmark methods such as ninhydrin or

1,2-indanedione. The results indicated that the europium complex developed fingermarks with a much better quality of the ridges and significantly higher contrast than ninhydrin treatment. However, in the case of 1,2-indanedione treatment, this developing agent has shown the same quality of fingermark contrast as the europium complex did. Also, the potential of the europium complex was demonstrated for the fingermarks exposed to the water environment. In aqueous conditions, both ninhydrin and 1,2-indanedione treatment resulted in no fingermarks enhancement due to the lack of amino acids in fingermark residue, whereas $Eu(TTA)_3(H_2O)_2$ complex was able to develop superior contrast of fingermarks because the interaction of developing agent took place with the sebaceous fraction of LFM components.

In conclusion, the $Eu(TTA)_3(H_2O)_2$ complex has a great potential to develop latent fingermarks deposited on luminescent, patterned and also wetted paper-based substrates in the time-gated imaging process. The proposed method of development not only improved the quality of the fingermark contrast but also demonstrate the simplicity of developing agent application, eliminating the heating process necessary in benchmark methods.

4.5 References

[1] A. A. Frick, P. Fritz, and S. W. Lewis, “Chemical methods for the detection of latent fingermarks,” in *Forensic Chemistry Fundamentals and Applications*, J. Siegel, Ed. Wiley Blackwell, 2016.

[2] D. A. Wilkinson and J. E. Watkin, “Europium aryl-B-diketone complexes as fluorescent dyes for the detection of cyanoacrylate developed fingerprints on human skin,” vol. 60, pp. 67–79, 1993.

[3] D. Wilkinson, “A one-step fluorescent detection method for lipid fingerprints; Eu(TTA)3·2TOPO,” *Forensic Sci. Int.*, vol. 99, no. 1, pp. 5–23, Jan. 1999, doi: 10.1016/S0379-0738(98)00176-5.

[4] J. P. Caldwell, W. Henderson, and N. D. Kim, “Luminescent visualization of latent fingerprints by direct reaction with a lanthanide shift reagent,” *J. Forensic Sci.*, vol. 46, no. 6, pp. 1332–1341, 2001.

[5] A. V. S. Lourenço *et al.*, “Luminescent material based on the $[Eu(TTA)_3(H_2O)_2]$ complex incorporated into modified silica particles for biological applications.,” *J. Inorg. Biochem.*, vol. 123, pp. 11–7, 2013, doi: 10.1016/j.jinorgbio.2013.02.006.

[6] S. I. Weissman, “Intramolecular energy transfer the fluorescence of complexes of Europium,” *J. Chem. Phys.*, vol. 10, no. 4, pp. 214–217, 1942,

doi: 10.1063/1.1723709.

[7] Q. Liu, D. M. Wang, Y. Y. Li, M. Yan, Q. Wei, and B. Du, "Synthesis and luminescent properties of $Eu(TTA)_3 \cdot 3H2O$ nanocrystallines," *Luminescence*, vol. 25, no. 4, pp. 307–310, 2010, doi: 10.1002/bio.1150.

[8] N. B. D. Lima, A. I. S. Silva, V. F. C. Santos, S. M. C. Gonçalves, and A. M. Simas, "Europium complexes: choice of efficient synthetic routes from RM1 thermodynamic quantities as figures of merit," *RSC Adv.*, vol. 7, no. 34, pp. 20811–20823, Apr. 2017, doi: 10.1039/c7ra02019h.

[9] O. L. Malta *et al.*, "A theoretical analysis based on structural data obtained from a sparkle model," *J. Lumin. 75*, vol. 75, pp. 255–268, 1997.

[10] J. Kai, D. Fernandes Parra, and H. Felinto Brito, "Polymer matrix sensitizing effect on photoluminescence properties of Eu^{3+}-β-diketonate complex doped into poly-β-hydroxybutyrate (PHB) in film form," *J. Mater. Chem.*, vol. 18, pp. 4549–4554, 2008, doi: 10.1039/b808080a.

[11] J. Almog, A. A. Cantu, C. Champod, T. Kent, and C. Lennard, "Guidelines for the Assessment of Fingermark Detection Techniques," *J. Forensic Identif.*, vol. 64, no. 2, pp. 174–197, 2014.

[12] C. Marriott *et al.*, "Evaluation of fingermark detection sequences on paper substrates," *Forensic Sci. Int.*, vol. 236, pp. 30–37, 2014, doi: 10.1016/j.forsciint.2013.12.028.

[13] R. Jelly, E. L. T. Patton, C. Lennard, S. W. Lewis, and K. F. Lim, "The detection of latent fingermarks on porous surfaces using amino acid sensitive reagents: A review," *Anal. Chim. Acta*, vol. 652, no. 1–2, pp. 128–142, 2009, doi: 10.1016/j.aca.2009.06.023.

[14] C. Wallace-Kunkel, C. Lennard, M. Stoilovic, and C. Roux, "Optimisation and evaluation of 1,2-indanedione for use as a fingermark reagent and its application to real samples," *Forensic Sci. Int.*, vol. 168, no. 1, pp. 14–26, May 2007, doi: 10.1016/j.forsciint.2006.06.006.

[15] V. D'Elia, S. Materazzi, G. Iuliano, and L. Niola, "Evaluation and comparison of 1,2-indanedione and 1,8-diazafluoren-9-one solutions for the enhancement of latent fingerprints on porous surfaces," *Forensic Sci. Int.*, vol. 254, pp. 205–214, 2015, doi: 10.1016/j.forsciint.2015.07.036.

[16] B. Yamashita and M. French, "Latent Print Development," in *The Fingerprint Sourcebook*, H. J. Eric H., R. Laurie O., L. John H., B. Yamashita, and M. French, Eds. National Institute of Justice, 2011, pp. 7.1-7.67.

[17] H. L. Bandey, S. M. Bleay, V. J. Bowman, R. P. Downham, and V. G. Sears, *Fingermark Visualisation Manual*, First. Home Office Centre for Applied Science and Technology (CAST), 2014.

[18] J. R. Morris and G. C. Goode, "NFN - An Improved Ninhydrin Reagent for Detection of Latent Fingerprints," *Police Res. Bull.*, vol. 24, no. 24, pp. 45–53, 1974.

[19] O. Petrovskaia, B. M. Taylor, D. B. Hauze, P. J. Carroll, and M. M. Joullié, "Investigations of the Reaction Mechanisms of 1,2-Indanediones with Amino

Acids," doi: 10.1021/jo0105179.

[20] I. Mekkaoui Alaoui and J. Halamek, "Fluorescence of 1,2-Indanedione with Amino Acids Present in the Fingerprint Residue: Application in Gender Determination," *J. Forensic Sci.*, vol. 64, no. 5, pp. 1495–1499, 2019, doi: 10.1111/1556-4029.14025.

[21] S. Cadd, M. Islam, P. Manson, and S. Bleay, "Fingerprint composition and aging: A literature review," *Sci. Justice*, vol. 55, no. 4, pp. 219–238, 2015, doi: 10.1016/j.scijus.2015.02.004.

[22] A. Girod, R. Ramotowski, and C. Weyermann, "Composition of fingermark residue: A qualitative and quantitative review," *Forensic Science International*, vol. 223, no. 1–3. pp. 10–24, Nov. 30, 2012, doi: 10.1016/j.forsciint.2012.05.018.

[23] D. Ghosh and M. N. Luwang, "One-pot synthesis of 2-thenoyltrifluoroacetone surface functionalised SrF2:Eu3+ nanoparticles: Trace level detection of water," *RSC Adv.*, vol. 5, no. 58, pp. 47131–47139, May 2015, doi: 10.1039/c5ra08566g.

[24] G. L. Zhong and K. Z. Yang, "Luminescence enhancement effect of $Y(TTA)_3$Phen on europium(III) and intermolecular energy transfer in Langmuir-Blodgett films," *Langmuir*, vol. 14, no. 19, pp. 5502–5506, Sep. 1998, doi: 10.1021/la9711645.

[25] M. Zhang, X. Wei, B. Huang, and B. Long, "Luminescence Properties of $Eu(TTA)_3(H_2O)_2$ Doped with DNA-CTMA and Its Application in Fluorescent Inkjet Ink," *Adv. Graph. Commun. Media Technol.*, vol. 417, pp. 865–874, 2017, doi: 10.1007/978-981-10-3530-2.

[26] A. V. S. Lourenço *et al.*, "Luminescent material based on the $[Eu(TTA)_3(H_2O)_2]$ complex incorporated into modified silica particles for biological applications," *J. Inorg. Biochem.*, vol. 123, pp. 11–17, Jun. 2013, doi: 10.1016/j.jinorgbio.2013.02.006.

[27] B. B. J. Basu and N. Vasantharajan, "Temperature dependence of the luminescence lifetime of a europium complex immobilized in different polymer matrices," *J. Lumin.*, vol. 128, no. 10, pp. 1701–1708, Oct. 2008, doi: 10.1016/j.jlumin.2008.03.024.

[28] K. Binnemans, "Rare-earth beta-diketonates," in *Handbook on the Physics and Chemistry of Rare Earths*, vol. 35, no. 05, 2005, pp. 107–272.

[29] A. P. Duarte, M. Gressier, M. J. Menu, J. Dexpert-Ghys, J. M. A. Caiut, and S. J. L. Ribeiro, "Structural and luminescence properties of silica-based hybrids containing new silylated-diketonato europium(III) complex," *J. Phys. Chem. C*, vol. 116, no. 1, pp. 505–515, 2012, doi: 10.1021/jp210338t.

[30] M. L. P. Reddy, V. Divya, and R. Pavithran, "Visible-light sensitized luminescent europium(III)-β-diketonate complexes: Bioprobes for cellular imaging," *Dalt. Trans.*, vol. 42, no. 43, pp. 15249–15262, 2013, doi: 10.1039/c3dt52238e.

[31] A. I. S. Silva, N. B. D. Lima, A. M. Simas, and S. M. C. Gonçalves, "Europium

complexes: Luminescence boost by a single efficient antenna ligand," *ACS Omega*, vol. 2, no. 10, pp. 6786–6794, 2017, doi: 10.1021/acsomega.7b00647.

[32] O. L. theoretical analysis based on structural data obtained fro Malta *et al.*, "Spectroscopic properties of a new light-converting device Eu(thenoyltrifluoroacetonate)$_3$ 2(dibenzyl sulfoxide). A theoretical analysis based on structural data obtained from a sparkle model," *J. Lumin.*, vol. 75, no. 3, pp. 255–268, Oct. 1997, doi: 10.1016/S0022-2313(97)00107-5.

[33] J.-C. G. Bu and C. Piguet, "Taking advantage of luminescent lanthanide ions," *Chem. Soc. Rev.*, vol. 34, pp. 1048–1077, 2005, doi: 10.1039/b406082m.

[34] J. A. Stubenrauch, C. Mevissen, M. F. Schulte, S. Bochenek, M. Albrecht, and P. S. Subramanian, "Highly specific 'sensing' of tryptophan by a luminescent europium(III) complex," *Zeitschrift fur Naturforsch. - Sect. B J. Chem. Sci.*, vol. 71, no. 10, pp. 1025–1028, 2016, doi: 10.1515/znb-2016-0096.

[35] F. Söderlind, H. Pedersen, R. M. Petoral, P. O. Käll, and K. Uvdal, "Synthesis and characterisation of Gd_2O_3 nanocrystals functionalised by organic acids," *J. Colloid Interface Sci.*, vol. 288, no. 1, pp. 140–148, 2005, doi: 10.1016/j.jcis.2005.02.089.

[36] S. Ghosh, K. Das, K. Chakrabarti, and S. K. De, "Effect of oleic acid ligand on photophysical, photoconductive and magnetic properties of monodisperse SnO_2 quantum dots," *J. Chem. Soc. Dalt. Trans.*, vol. 42, no. 2, pp. 3434–3446, 2013, doi: 10.1039/c2dt31764h.

[37] F. J. Douglas, D. A. MacLaren, C. Renero-Lecuna, R. D. Peacock, R. Valiente, and M. Murrie, "Self-assembly of ultra-thin lanthanide oxide nanowires via surfactant-mediated imperfect oriented attachment of nanoparticles," *CrystEngComm*, vol. 14, no. 21, pp. 7110–7114, 2012, doi: 10.1039/c2ce25990g.

[38] S. Pawsey, K. Yach, J. Halla, and L. Reven, "Self-assembled monolayers of alkanoic acids: A solid-state NMR study," *Langmuir*, vol. 16, no. 7, pp. 3294–3303, 2000, doi: 10.1021/la991273e.

[39] S. Dasari and A. K. Patra, "Luminescent europium and terbium complexes of dipyridoquinoxaline and dipyridophenazine ligands as photosensitizing antennae: Structures and biological perspectives," *Dalt. Trans.*, vol. 44, no. 46, pp. 19844–19855, 2015, doi: 10.1039/c5dt02852c.

[40] S. K. Samanta, S. Sanyal, S. Samanta, and S. Ghosh, "Designing hydrophobic sheet protected Eu(III)-tetracycline complex using long chain unsaturated fatty acid: Efficient 'antenna effect' in aqueous medium," *J. Lumin.*, vol. 160, pp. 262–270, Apr. 2015, doi: 10.1016/j.jlumin.2014.12.017.

[41] B. Ortiz-Jaramillo, A. Kumcu, L. Platisa, and W. Philips, "Content-aware contrast ratio measure for images," *Signal Process. Image Commun.*, vol. 62, no. January 2018, pp. 51–63, 2018, doi: 10.1016/j.image.2017.12.007.

[42] D. G. Pelli and P. Bex, "Measuring contrast sensitivity," *Vision Res.*, vol. 90, pp. 10–14, 2013.

[43] O. P. Jasuja and G. Singh, “Development of latent fingermarks on thermal paper: Preliminary investigation into use of iodine fuming,” *Forensic Sci. Int.*, vol. 192, no. 1–3, pp. 10–16, 2009, doi: 10.1016/j.forsciint.2009.08.005.

[44] S. Stojkovikj, S. Oklevski, O. P. Jasuja, and M. Najdoski, “Visualization of latent fingermarks on thermal paper: A new method based on nitrogen dioxide treatment,” *Forensic Chem.*, vol. 17, no. November 2019, p. 100196, 2020, doi: 10.1016/j.forc.2019.100196.

Chapter 5 Summary and conclusions

This thesis aimed to develop an optical method of latent, natural fingermark visualisation on surfaces that cause difficulties in the imaging process because they are reflective, glossy, coloured, patterned or exhibit their own luminescence. In order to obtain an efficient forensic reagent that would selectively interact with the fingermark and which would have particular optical properties, the surface-modified silica particles as a luminophore carrier have been examined. Thiol-gold or lipophilic interactions and amide bond formation between modified silica particles and fingermark components have been investigated to be the most effective. Carboxyl or lipophilic moieties-functionalised silica particles provided the best results, selectively interacting with fingermark secretions. However, due to the additional number of carboxyl-modified silica particle suspension parameters demanding control during the development process, silica particles modified with phenyl groups and long hydrocarbon chains have been selected for further research.

Once the efficient silica surface modification was done, an attempt was made to luminophore encapsulation. Zinc oxide quantum dots encapsulated in the surface-modified silica structure were the first examined luminophore. The luminescent silica particles modified with lipophilic moieties possess optical properties such as visible blue emission when excited by the light of 365 nm wavelength and a long luminescence lifetime of ca 0.5 ms. These properties enabled this material to be applied as a development agent for time-gated fingermark visualisation. Zinc oxide QDs in silica matrix developed efficiently fingermarks deposited only on non-porous surfaces like glass, aluminium foil, beverage can, polypropylene foil, magazine cover paper, and the sticky side of adhesive tape. The sensitivity of the material was high, enabling the interactions with the fifth depletion of fingermark residue; however, this sensitivity was also donor-dependent. Fingermark secretions deposited on porous substrate diffuse into the paper structure, unlike the luminescent particles with a diameter range of 100 to 200 nm, which results in detection failure. It was determined that 1 % of modified silica particles with encapsulated zinc oxide QDs in water-ethanol solution was optimal to obtain the good fingermark enhancement. The use of a water-ethanol solution (97:3, v/v) allowed, firstly, avoiding the risk of airborne particles inhalation while applying the material to the fingermark, and secondly, using environmentally and user-friendly carrier solvent. Zinc oxide QDs in silica used for fingermark visualisation

with time-gated imaging performed more effectively or comparable to the benchmark methods such as Basic Violet 3 staining, SPR or luminescent powder dusting. Moreover, the application of the new luminescent material facilitated the visualisation of fingermark deposited on a substrate with a highly luminescent UV-active protected pattern.

The second investigated luminophore was silica-coated upconverting crystals further modified with lipophilic moieties. Hydrothermal synthesis and a solid-liquid thermal-decomposition process were used to obtain upconverting crystals. The crystals synthesised by the latter process have shown superior luminescence intensity and better affinity to fingermark secretions. The purpose of applying upconverting crystals to visualise the fingermark was to examine how effective these crystals would be to suppress the background interference during imaging of the fingermark samples. When the sample was illuminated with a near-infrared light of 980 nm wavelength, the crystals deposited on the fingermark ridges emitted green luminescence. Since most everyday-use objects that may bear a fingermark do not exhibit upconversion under infrared excitation, the use of crystals could prove to be very efficient in background interference elimination. Like zinc oxide QDs in silica particles, the upconverting particles were deposited on the fingermark in the form of water-ethanol suspension to avoid airborne particles inhalation and reduce the contact with toxic solvents. A variety of substrates such as paper, aluminium foil, beverage can, glass, sticky side of the adhesive tape, and several polymer substrates were explored to observe whether the upconverting particles could selectively interact with deposited fingermark and effectively visualise the fingermarks. Modified upconverting crystals obtained in the hydrothermal synthesis were able to develop fingermarks deposited only on glass and aluminium foil. Thus, the latter fingermark development experiments involved only SLTD-synthesised upconverting particles. The broad comparative assessment on 300 fingermark samples showed that fingermarks developed by the upconverting crystals have a lower potential to develop fingermarks on all considered surfaces and produce more background staining than the benchmark method of cyanoacrylate fuming followed by Rhodamine 6G staining. However, examining the multicoloured and highly luminescent surfaces of aluminium beverage cans as a substrate for fingermark visualisation, it was observed that upconverting crystals have a good potential to efficiently suppress the background interference, unlike cyanoacrylate fuming with Rhodamine 6G staining. Thus, further optimisation of the modified upconverting crystal method is needed.

The investigated luminophores such as zinc oxide QDs or upconverting crystals encapsulated in the silica structure proved to be effective in fingermark visualisation only on non-porous surfaces. On paper substrates, fingermark detection with these materials failed. Therefore, for porous surfaces, such as copy paper or notebook paper, the development potential of the europium β-diketonate complex was investigated. The $Eu(TTA)_3(H_2O)_2$ complex in methanol solution was distributed over the entire sample, which was further subjected to the time-gated imaging. It was observed that the complex in contact with fingermark components such as oleic acid, L-serine and squalene generated *in situ* new compounds, which had longer luminescence lifetimes than the initial europium complex deposited beyond the fingermark ridges. Therefore, it was possible to visualise fingermarks within the time-gated imaging methods eliminating the background interferences and without the need for selectivity of the developing agent. The replacement of water molecules in the europium complex with the investigated fingermark components did not influence the excitation and emission maximum peak shift. In contrast, it affects the luminescence intensity changes depending on the molar concentration of considered fingermark components. The NMR and DRIFT measurements confirmed the generation of a new europium complex with oleic acid and exhibited some possible interactions between the europium complex and L-serine. Due to the long luminescence lifetime of ca. 150 μs of europium complex mixture with fingermark components, the delay-to-shutter parameter of time-gated imaging was possible to optimise. For the delay-to-shutter parameters ranging from 0 to 2000 μs and using the Weber formula for contrast calculation, the highest image contrast was obtained for the delay-to-shutter time equal to 800 μs. Compared to the benchmark ninhydrin detection method, the use of $Eu(TTA)_3(H_2O)_2$ complex resulted in fingermarks developed with better quality and higher contrast. The use of 1,2-indanedione, in turn, developed fingermarks with comparable quality to the europium complex. Whereas the europium complex exhibited superior results when applied to the fingermark paper samples exposed to water. Both ninhydrin and 1,2-indanedione resulted in no fingermark detection due to the lack of amino acids eluted from the fingermark residue. Europium complex enhanced wetted fingermarks with sufficient quality and image contrast due to the interactions with the sebaceous fraction of the fingermark residue, which is resistant to water elution.

In conclusion, the presented work succeeded in achieving the aims established at the beginning. Indeed, none of the developed fingermark methods for fingermark enhancement is universal for both porous and non-porous surfaces, but

due to how the fingermark secretions interact with the surface of deposition, proposing a general method of fingermark development is very difficult. While the luminophores encapsulated in the silica structure failed to visualise fingermark on porous surfaces with time-gated imaging, the europium β-diketonate complex managed to interact with fingermark secretion yielding high-quality and good-contrast fingermark images. Both these methods have a great potential to develop fingermarks on luminescent, colourful, reflective or patterned surfaces in the time-gated imaging process. It is worth noting that all fingermarks used in this research were natural, not sebum-charged and highly toxic organic carrier solvents for fingermark development were eliminated.

The concepts of fingermark development introduced in this thesis have the potential to broaden and further develop the visualisation process. Apart from the forensic application, the developed luminescent materials and the methodology of imaging could also be used in bioimaging and medical imaging.

List of publications

Results presented in this thesis have been published in the following papers:

1. **Olszowska, I.**; Leśniewski, A.; Kelm, A.; Pieta, I. S.; Siejca, A.; Niedziółka-Jönsson, J.; Zinc oxide quantum dots embedded in hydrophobic silica particles for latent fingermarks visualisation based on time-gated luminescence measurements. *Methods and Applications in Fluorescence*, **2020**, *8 (2)*, 025001
2. **Olszowska-Łoś, I.**; Ratajczyk, T.; Pieta, I. S.; Siejca, A.; Niedziółka-Jönsson, J.; Leśniewski, A.; *In Situ* Interactions of $Eu(TTA)_3(H_2O)_2$ with Latent Fingermark Components – A Time-Gated Visualization of Latent Fingermarks on Paper. *Analytical Chemistry*, **2020**, *92*, 15671-15678

Other paper published during PhD studies:

1. **Olszowska, I.**; Deacon, P.; Lindsay, M.; Leśniewski, A.; Niedziółka-Jönsson, J.; Farrugia, K.; An alternative carrier solvent for fingermark enhancement reagents. *Forensic Science International*, **2018**, *284*, 53-64

Institute of Physical Chemistry
Polish Academy of Sciences

Kasprzaka 44/52
01-224 Warsaw, Poland

www.ichf.edu.pl